MALTOOLIGOSACCHARIDE CHEMOSENSATION BY INTESTINAL ENTEROENDOCRINE L-CELLS REGULATES THE ENDOGENOUS RELEASE OF GUT HORMONES AND CONTRIBUTES TO WEIGHT MANAGEMENT IN VIVO

by

Marwa Mohamed Mohamed El-Hindawy

A Dissertation

Submitted to the Faculty of Purdue University

In Partial Fulfillment of the Requirements for the degree of

Doctor of Philosophy

Department of Food Science

West Lafayette, Indiana

December 2018

THE PURDUE UNIVERSITY GRADUATE SCHOOL
STATEMENT OF DISSERTATION APPROVAL

Dr. Bruce R. Hamaker, Chair
Department of Food Science

Dr. Kee-Hong Kim
Department of Food Science

Dr. Buford L Nichols Jr, M.D.
Baylor College of Medicine

Dr. Kimberly Kinzig
Department of Psychological Sciences

Dr. Mario Ferruzzi
Department of Food Science and Nutrition

Approved by:

Dr. Arun Bhunia
Head of the Departmental Graduate Program

To my lovely parents,

Mrs. Nadia Atwa Abdelwahab and Dr. Mohamed Mohamed ElHindawy,

The most precious gift God has ever given me

ACKNOWLEDGMENTS

Any achievements or success I may have, especially but not limited to my graduate school experience, are due to opportunities and gifts that God has given me. I first want to acknowledge His grace, mercy, and guiding hand in my life. All praise belongs to Allah, Lord of all Worlds.

I express sincere appreciation for Dr. Bruce R. Hamaker, my advisor and mentor throughout the journey of my PhD studies. I am grateful for taking me on as his student, for his patience, guidance, and encouragement, and for his counsel and understanding through this learning process. I also wish to thank all Hamaker Lab members, past and present, for their friendship, help and encouragement. I am grateful for the comradery and cooperation I have experienced in the Hamaker lab.

I acknowledge and thank members of my graduate committee, Dr. Mario Ferruzzi, Dr. Buford L Nichols, Kee-Hong Kim and Dr. Kimberly Kinzig, for their guidance and assistance throughout the pursuit of my Ph.D.

Very Special thanks for Dr. Choon Young Kim at the department of Food and Nutrition, Yeungnam University for her great support and help during my studies even after being apart in south Korea. I would like to extend my special sincere appreciation to Prof. Dr. Michael Gribskov at Purdue biological science department for graciously offering and providing his analytical assistance to my research. Special thanks go to Carol Dowell, the training coordinator at Purdue laboratory animal program for her great helping in the animal studies and her kindness and support.

I also express gratitude for friends from the Hamaker lab, Jongbin Lim, Fang Fang, Thaisa Jungles, Nuseybe Bulut, Leigh Schmidt. I would like to thank all my lab mates and friends who spent several hours helping me during animal euthanasia and necropsy especially Maha Usama, Sarah Corwin, Anna Hayes, Thaisa Jungles, Nuseybe Bulut and Jongbin Lim.

I gratefully acknowledge my parents, Dr. Mohamed Mohamed El-Hindawy and Mrs. Nadia Atwa Abdelwahab, for the solid foundation and meaningful opportunities they provided to help me become who I am today.

.

TABLE OF CONTENTS

LIST OF TABLES

LIST OF FIGURES

LIST OF ABBREVIATIONS

Abbreviation	Term
(ct) MGAM	Carboxyl-terminus maltase-glucoamylase
(nt) MGAM	Amino-terminus maltase-glucoamylase
7TM	Seven-transmembrane
AgRP	Agouti-related peptide
CART	Cocaine-and amphetamine-regulated transcript
CaSR	Calcium-sensing receptor
CCK	Cholecystokinin
Ccl	Capacitance
CTRs	Calcitonin receptors
DAVID	Database for Annotation, Visualization and Integrated Discovery
DEXA	Dual-energy X-ray absorptiometry
DMEM	Dulbecco’s Modified Eagle’s Medium
DPBS	Dulbecco's phosphate-buffered saline
Epac	Exchange protein activated by cAMP
FBS	Fetal bovine serum
FFAR 2	Free-fatty-acid receptor 2
FFAR 3	Free-fatty acid receptor 3
GAPDH	Glyceraldehyde-3-phosphate dehydrogenase
GI	Glycemic index
GI	Gastrointestinal

GIP	Glucose-dependent insulinotropic peptide
GIP	Gastric inhibitory peptide
GLP-1	Glucagon like peptide-1
GLP-2	Glucagon like peptide-2
GLUT 2	Glucose transporter 2
GLUT 4	Glucose transporter 4
GO	Gene ontology
GOPOD	Glucose oxidase/peroxidase
GPCR	G-protein coupled receptor
GPR119	G-protein coupled receptor 119
GPR93	G-protein coupled receptor 93
GPRC6A	G-protein coupled receptor family C group 6 subtype A
GRP	Gastrin-releasing peptide
GRPP	Glicentin-related pancreatic polypeptide
GRPR	Gastrin-releasing peptide receptor
HDL	High-density lipoproteins
HEPES	2-[4-(2-hydroxyethyl) piperazin-1-yl] ethane sulfonic acid
HPSEC	High-performance size-exclusion chromatograph
ICAM1	Intercellular adhesion molecule-1
IP-1	Intervening peptide-1
IP-2	Intervening peptide-2
KEGG	Kyoto Encyclopedia of Genes and Genomes
LCFA	Long-chain fatty acids

LC-MS/MS	Liquid Chromatograph Triple Quadrupole Mass Spectrometer
LDLPR	Low-density lipoprotein particle receptor
MAPK	Mitogen-activated protein kinase
MCH	Melanin-concentrating hormone
MGAM	Maltase-glucoamylase
MOS	Maltooligosaccharides
MRI	Magnetic resonance imaging
MS	Mass spectrometry
NCBI	National Center for Biotechnology Information
NEAA	Non-essential amino acids
NK1R	Neurokinin-1 receptor
NMB	Neuromedin B
NT	Neurotensin
NYP	Neuropeptide Y
OEA	Oleoylethanolamide
OXM	Oxyntomodulin
PACUC	Purdue animal care and use committee
PBS	Phosphate buffered saline
PC 2	Prohormone convertase 2
PC1/3	Prohormone convertase 1
PCA	Principle component analysis
PGS	Pregelatinized starch
PKA	Protein kinase A

POMC	Pro-opiomelanocortin
PYY	Peptide YY
qRT-PCR	Quantitative reverse transcription-polymerase chain reaction
RAMPs	Receptor activity–modifying proteins
RCS	Raw corn starch
RDS	Rapidly digestible starch
RIP	Rat insulin promoter
SCFA	Short chain fatty acids
SDS	Slowly digestible starch
SEM	Standard error of the mean
SGLT1	Sodium-glucose cotransporters
SI	Sucrase-isomaltase
STI	Sweet taste inhibitor
TEER	Trans-epithelial/-endothelial electrical resistance
TNFα	Tumor necrosis factor
TxNIP	Thioredoxin-interacting protein
USDA	United States Department of Agriculture
WCS	Waxy corn starch
WHO	World health organization

ABSTRACT

Author: El-Hindawy, Marwa, M. M. Ph.D.
Institution: Purdue University
Degree Received: December 2018
Title: Maltooligosaccharide Chemosensation By Intestinal Enteroendocrine L-Cells Regulates the Endogenous Release of Gut Hormones and Contributes to Weight Management *In Vivo*
Major Professor: Dr. Bruce R. Hamaker

As obesity has become one of the most prevalent metabolic diseases, and diabetes mellitus has become the seventh leading causes of death in the United States, alternative food/nutrition-based approaches to tackle obesity that are both efficacious and cost effective are in high demand. Since starch and its derived products are the principal dietary supply of glucose, strategies of using slowly digestible starch to achieve moderated glycemic response and prolonged glucose delivery, as well as to locationally digest starch into the ileum, have shown successful results such as moderation of insulinemia and reducing food intake in obese animals. An important regulator of appetite suppression is the neuroendocrine system of the gut-brain axis. Glucagon-like peptide-1 (GLP-1), oxyntomodulin (OXM), and peptide YY (PYY) are the main anorexigenic peptide products of the intestinal enterendocrine L-cells that regulate postprandial insulin levels as well as satiety signals. The stimulation of the enteroendocrine L-cells throughout the gastrointestinal tract through glucose, fatty acids and proteins has been extensively studied and confirmed. However, the stimulatory effect of complex dietary carbohydrates on L-cells is not described. In this dissertation, we investigated the *in vitro* intestinal cell chemosensation of L-cells to α-amylase starch digestion products, named maltooligosaccharides (MOS), and in the possible application of using slowly digestible starch delivery of MOS *in vivo*.

In Chapter II of this dissertation, we reported a significantly higher stimulatory effect of MOS on GLP-1 and OXM secretion compared to glucose in mouse and human L-cells, respectively.

Additionally, maltotriose enhanced the relative expression of the gastrointestinal peptide, cholecystokinin. Moreover, MOS exhibited protective effects on barrier function and monolayer integrity of intestinal epithelial cells.

In Chapters III and IV, we performed a multiomics approach where transcriptomic analysis and global protein profiling of mouse L-cells treated with different types of MOS showed that the carbohydrates exhibit their effects through the induction of exocytosis of GLP-1- or OXM-containing vesicles and not through a positive regulation of the proglucagon gene expression. It is suggested that MOS induce higher secretion, but not higher synthesis, of the proglucagon gene products. In addition, maltotriose treatment downregulated the relative expression of the glucotoxicity marker, thioredoxin-interacting protein, and upregulated the relative expression of tight junction proteins supporting a role of MOS in barrier function integrity.

Translating the *in vitro* findings into an *in vivo* application that is beneficial for human health required the use of controllable tool for the delivery of MOS throughout the small intestine for sensing by a higher number of L-cells. Slowly digestible starch (SDS), compared to rapidly digestible starch, provided such a tool. For this purpose, we used alginate-entrapped SDS microspheres that digest distally into the ileum to examine the role of SDS in the intervention and prevention of obesity in C57BL/6J diet-induced obese (DIO) and lean mice models.

Results showed that 20% SDS in low-fat diets significantly improved weight loss and food intake reduction in DIO mice converted to low-fat diet for 12 weeks. Similarly, 15% SDS in high-fat diets showed significant reduction in body fat percent and significant increase in lean body mass as well as considerable reduction in weight gain rate and food intake in lean mice fed on 45% of calories high-fat diet. Immunohistochemistry of small intestine of mice in both the intervention and prevention studies revealed an even and thorough distribution of GLP-1 positive L-cells.

Overall, this dissertation proposes several insights into L-cell sensation of dietary starch-degraded MOS delivered by the consumption of slowly digestible starch. MOS exhibit unique influences on L-cell sensitivity and gut hormone productivity. Future research investigating the mechanisms of intestinal sensing of MOS, as well as the development of bioactive carbohydrate structures that could preserve body weight and modulate glucose tolerance *in vivo* is needed to translate these findings into nutritional recommendations and food products beneficial for human health. The intricate role of dietary carbohydrates on gut physiological response, related to satiety and food intake could be a new approach for design of foods for health applications.

CHAPTER 1. LITERATURE REVIEW

1.1 Glycemic Carbohydrates and Metabolic Disorders

Obesity has become one of the most prevalent metabolic diseases all over the world. It has been reported that one third of both children and adult in the developed countries are obese [1]. Although common therapies for severe obesity is not showing enough proficiency, new approaches such as bariatric surgery have been reported as the current most effective treatment [2]. However, limitations related to the high cost and the mortality risk reserved this approach for only the morbidity obese individuals [2]. Therefore, alternative food/nutrition-based approaches to tackle obesity are required.

1.1.1 Glucogenesis, Glycemic Index and Glycemic Load

The process of starch hydrolysis to release free glucose molecules is called α-glucogenesis. It varies between different species but generally involve the 6 α-glucogenic enzymes (salivary and pancreatic α-amylases, and the four-different brush border α-glucosidases) [3]. The glycemic index (GI) is a measure of the speed of increasing blood glucose levels due to eating a meal or a specific type of food. Technically, glycemic index definition is “The incremental area under the blood glucose response curve of a specific portion of a test food expressed as a percent of the response to the same amount of carbohydrate from a standard food taken by the same subject”. In other words, the glycemic index measures how much one gram of glycemic carbohydrate increases the blood glucose level after consumption of the food, relative to consumption of pure glucose as the reference meal. Different kinds of food show different effects on blood glucose levels. Glucose has a glycemic index of 100 and each food has a comparative estimated number that could be higher or smaller [4].

The consumption of foods with high-glycemic index results in high and rapid raising in blood glucose levels. On the contrary, consumption of foods with low-glycemic index does not show this spike increase in blood glucose levels. Quick increases in glucose levels in the blood are potent signals to the pancreatic β-cells to boost insulin secretion. These high insulin levels will eventually cause a quick decrease in glucose levels in the blood a phenomenon called, hypoglycemia. On the contrary, consumption of foods with low-glycemic index results in lesser but more constant increases in blood glucose levels and lowers the insulin secretion of the pancreatic β-cells [5]. A drawback of the glycemic index is that it does not consider the amount of carbohydrate consumed by the subjects. It is instead compares the ability of foods containing equal carbohydrate amount to increase blood glucose. Therefore, a related index is the glycemic load. The glycemic load resolves this limitation by multiplying the glycemic index of the food under consideration by the actual carbohydrate content that is consumed and dived the total by 100 [6].

1.1.2 Glucogenesis and Obesity

After a high glycemic load diet, blood glucose and insulin levels increase more than they do after a low-glycemic load diet containing equivalent calories. This is known as postprandial hyperglycemia and hyperinsulinemia. This phenomenon promotes postprandial carbohydrate oxidation at the cost of fat oxidation, and as a result shifting fuel partitioning to induce body fat gain [7]. Because of the boost of insulin secretion, blood glucose falls lower than they do after a low glycemic load diet. This is consistent with studies revealed that utilization of low glycemic index foods increase satiety and decreased the following food intake as compared to high glycemic index foods [8]. Interestingly, data from six randomized weight loss experiments concluded that overweight or obese persons who were feeding low glycemic load diet showed greater weight loss than others on a comparison diet that had energy-restricted low-fat diet [9].

1.1.3 Glucogenesis and Type II Diabetes Mellitus

The recent national vital statistics report (2018) revealed diabetes mellitus as the seventh leading causes of death in the United States [10]. The rapid and high increase in blood glucose levels after a meal with high glycemic load, increases the insulin demand and secretion to an excessive level that contributes to the failure of the pancreatic β-cells [11]. Failure of β-cell function related to insulin-secreting can leads to irretrievable diabetes. This study and many others reported that high glycemic load diets are associated with high risk of developing type II diabetes [12], [13]. In addition, a study from the U.S. national data in the period between 1909 -1997 showed that the increased consumption of developed carbohydrates such as corn syrup is coupled with decreasing dietary fiber intake, has paralleled the increase in popularity of type II diabetes [14].

1.1.4 Glucogenesis and Cardiovascular Diseases

In combination with high blood glucose and insulin levels, high glycemic loads are associated with increased levels of serum triglyceride and decreased high-density lipoproteins (HDL) cholesterol. These two factors are strong risk factors for cardiovascular disease [15], [16]. High glycemic loads are also associated with increased levels of serum C-reactive protein. This marker is a sensitive predictor of systemic inflammation [17]. In addition, human studies showed that women with high dietary glycemic loads had a risk of developing coronary heart disease, that was twice as high as those with the lowest dietary glycemic loads [17].

1.1.5 Modulation of Glucogenesis by Managing Mucosal α-Glucosidases Activities

As described above, starchy high glycemic foods could be associated with many risk factors starting from overweight and obesity and ending to cardiovascular disease and diabetes. Therefore, controlling glucogenesis and lowering the dietary glycemic load is a very important goal that both

food scientists and nutritionists look forward. From the consumer side, many simple strategies for lowering glycemic load can be used including; decreasing the starchy foods consumption. One of the recent approaches that are applied for the treatment of type II diabetics is to control glucogenesis and blood glucose levels to produce low glycemic index pattern [18]. In this prospective, regulation of the glycemic load pattern and controlling blood glucose levels is not through choosing specific food type or manipulating it with the recent formulations seeking slow glucose delivery, such as slowly digestible starches. It is, however, dependent on the management of the starch digestion enzymatic system. Inhibition of α-glucosidases could be a promising approach for managing glucogenesis. Because sucrase-isomaltase (SI) and maltase-glucoamylase (MGAM) are implicated in glucose delivery from α-limit dextrins, regulation of the activity of individual mucosal α-glucosidase is one of the most successful approaches for controlling blood glucose levels. Latest studies showed that individual mucosal α-glucosidases can be inhibited to different extent by using inhibitor such as acarbose [19] and plant phenolic compounds [20] as well as polyphenols. These findings suggest the possibility to control individual α-glucosidase activities by a toggling mechanism with specific inhibitors [21].

1.2 α-amylase starch digestion products (Maltooligosaccharides (MOS))

1.2.1 Starch Digestion and MOS Delivery

Starch is the main carbohydrate storage compound of the human diet. Carbohydrates serves as the main energy source for producing glucose, providing 45-65% of overall calories. The process of starch digestion is a tightly organized system. Starch is digested first by α-amylase which cleaves the α-1,4 glycosidic linkages between glucosyl units. The degradation products, termed as the α-limit dextrins, are composed of maltose and other MOS with different structures features (size and both linear and branched oligomers) [22]. The overall amylolytic activity of both

salivary and pancreatic α-amylases results release of only 4% of free glucose monomer. Subsequently, MOS undergo additional hydrolysis to obtain glucose, the main energy source required by cells [23]. Digestion of MOS is completed in the small intestine by the action of the α-glucosidase enzymes SI and MGAM that are associated with the brush-border membrane of intestinal enterocytes. SI and MGAM cooperate together to hydrolyze MOS in the small intestine and liberate free glucose. Specific carboxyl-terminus (ct) MGAM and amino-terminus (nt) MGAM subunits show unique hydrolysis properties on different MOS; ctMGAM has higher hydrolytic activity than ntMGAM, for long MOS; while ntMGAM primarily hydrolyzes short MOS [24]. Both N-terminal subunits show isomaltase activity on α (1-6) linkages with ntSI having much higher activity than ntMGAM [25]. Liberated glucose units are transported into the enterocytes by specific transporters [26]. Although pancreatic α-amylase is generally thought of as the dominant enzyme in carbohydrate digestion [27], the α-glycosidases are the ultimate players for glucose liberation and their activity is critical to glycemic control, as evidenced by the study of Nichols *et al.*, 2009 showing a decrease of 40% glucose absorption for MGAM null mice compared to the wild-type control [28]. The mucosal α-glycosidases, and their control, are thus critical for the health outcome of dietary glycemic carbohydrates.

1.2.2 Biological Activities of MOS

Because hydrolytic activity applied to MOS in the proximal small intestine suggests its complete hydrolysis to glucose by the duodenum, no attention has been given to MOS as bioactive carbohydrate molecules. Recent reports showed that MOS confer biological effects in lymphocytes and neutrocytes [29],[30]. In addition, an immunomodulatory effect of MOS was observed at the cell-cell interface of the JEG-3 trophoblasts where maltotriose and maltotetraose have been shown to inhibit IL-2 release by stimulated Jurkat lymphocytes [30]. MOS significantly reduced the

spontaneous motility of neutrophils when MOS-modified glass covers were used, suggesting an immunosuppressive potential of MOS [30]. Moreover, Uozumi *et al*., 2013 [31] designed bioactive formulation for neurokinin-1 receptor (NK1R) antagonism, where NK1R activation is involved in the development of inflammatory diseases, and had MOS as the active ingredient in the composition to achieve both safe application and good activity [31].

Moreover, maltotetraose was characterized by high performance liquid chromatography (HPLC) as the active component of bamboo stem extract that was capable of inhibiting tumor necrosis factor (TNFα)-induced expression of the intercellular adhesion molecule-1 (ICAM1) in the mouse MOVAS-1cell line. Since ICAM1 is tightly related to the development of atherosclerosis, maltotetraose was recommended as a dietary supplement that could delay the onset of cardiovascular diseases [32].

1.2.3 MOS Sensing by the Intestinal Epithelium

Chegeni *et al*. 2018, reported for the first-time maltose sensing by intestinal enterocytes [33]. Maltose induces the formation of higher molecular weight SI species in Caco-2 monolayers which are quickly sorted into the enterocyte brush-border [34], [33]. This sensing ability of enterocytes to respond to carbohydrates was observed with non-digestible oligosaccharides on both enterocytes and enteroendocrine cells. In addition, it was reported that the transepithelial/endothelial electrical resistance (TEER) values of Caco-2 monolayer treated with maltose for 12 h were comparable to those treated with glucose indicating maltose implication in higher tight junction barrier value [35].

The current knowledge of the carbohydrate sensation mechanism indicates that it is a complex process, which include nutrient transport, nutrient metabolite as well as cell membrane-bound receptors. One of the sugar sensors is the glucose transporter 2 (GLUT2) which facilitate

glucose transport from the enterocyte basolateral side to the blood stream [56]. Another group of G-protein coupled receptors, specifically in the enteroendocrine cells, were observed to sense sugars [36]. These receptors are known as sweet taste receptor as they have a binding affinity to sucrose and different artificial sweeteners [37]. It was reported that sweet taste receptor can stimulate absorptive enterocyte sodium-glucose cotransporters (SGLT1) expression mediated by glucose-dependent insulinotropic peptide (GIP) and glucagon-like peptide -1 (GLP-1) secretion [57]. Figure 1.1 represent the different receptors identified to sense macronutrients in the gastrointestinal tract.[38]. Mace *et al*., 2007 stated that the sweet taste receptor heterodimer coupled with the G-protein (α-gustducin) can sense sugar molecules independently of the SI expression [58]. Nevertheless, for the best of our knowledge, no receptor was reported in the literature for any of the starch α-amylase digestion products, such as maltose and maltotriose.

1.2.4 MOS Potentials in Gut Hormone Regulation

Glucose homeostasis is an important player in the metabolic processes related to obesity development and inhibition [39]. Alternative food/nutrition-based approaches of treatment that are both influential and cost effective are in high demand. As starch and its derived products are the principal dietary supply of glucose, investigation of their nutritional property involving rate and extent of digestion and absorption is important for this aspect of human health and may be important in other diet-related metabolic diseases such as type II diabetes. Little information is available regarding the correlation between complex carbohydrates (larger than glucose) and the release of gut hormones involved in the gut-brain axis and appetitive response. Izumi *et al*., 2010 reported that fructo-oligosaccharide (FOS) supplementation increased the expression of GLP-1- and GPR43-containing enteroendocrine L-cells in the large intestine [40]. In addition, Hasek *et al*., 2018 showed a suppression of the hypothalamic appetite-stimulating neuropeptide Y (NPY)

and Agouti-related peptide (AgRP) expression in obese rats fed slowly digestible starch that reached the ileum, and that this coincided with reduced food intake compared to rats fed a rapidly digestible starch Figure 1.2 [41]. This strategy of using slowly digestible carbohydrates to achieve prolonged glucose delivery to the body showed successful results in reducing food intake [41]. Use of slowly digestible glycemic carbohydrates is a possible way of achieving foods that moderate postprandial glycemic spikes from consumption of high glycemia-producing foods and provide prolonged delivery of glucose to the body [41]. Although the simplicity of the concept, there are a lot of challenges to effectively produce ingredients and foods that are mainly slowly digestible carbohydrate. The slow digestion of starch is expected to confer important health benefits related to reduce food intake and satiety induction. One of the important regulators of appetite suppression is the neuroendocrine system of the gut-brain axis [42]. The stimulation of L-cells, predominantly suggested to be located in the distal small intestine and colon, through fatty acids and proteins was extensively studied and confirmed [43],[44]. However, less information is available for the stimulation of L-cells by complex carbohydrates, larger than glucose.

1.3 Products of the Proglucagon Gene

The proglucagon gene (gcg) has been found to be expressed in different organs throughout mammalian bodies [45]. It is located on chromosome 37, 2q36 and expressed in the brain, pancreas and the gut to produce different proglucagon-derived peptides that exhibit both orexigenic and anorexigenic effects [45]. Expression of the gcg gene results in 160-amino acid peptide, proglucagon, that undergoes post-translation modification process to produce smaller peptides (Figure 1.3) [42]. The post translational modification process is tissue-specific and vary between different organs due to the differential expression of two splicing hormones known as prohormone convertase 1 /3 (PC1/3) and prohormone convertase 2 (PC2) [42]. In the pancreas, pancreatic

α-cells promote the splicing of the proglucagon into glicentin-related pancreatic polypeptide (GRPP), glucagon, intervening peptide-1 (IP-1) and major proglucagon fragment. In the intestine and the brain, the proglucagon peptide is spliced into glicentin, GLP-1, GLP-2 and intervening peptide-2 (IP-2) [45]. One of the important products of this process is the 30-amino acid hormonal peptide, GLP-1 [46] which is an important incretin hormone and strong appetitive suppressor [47]. In the intestine, glicentin could be further processed into oxyntomodulin (OXM) and GRPP [48].

1.4 L-cells Co-Localized Hormones

L-cells have been found to express the anorexigenic polypeptide YY (PYY) in the ileum and colon [49], [50]. In addition, studies indicated that GLP-1 is colocalized with Cholecystokinin (CCK), Neurotensin (NT) and PYY in the small and large intestine of mouse and human. On the other hand, it has been shown that GLP-1 colocalize with GIP in the proximal small intestine of mice, human, rats and pigs [50],[51]. Immunohistochemical analysis using fluorescence markers has facilitated the study of L-cell co-localized hormones. GLP-1 has been found to colocalized with CCK in the duodenum, with NT in the jejunum and with PYY in the ileum and colon [50], [52]. The colocalization of GLP-1 with GIP however was found to be limited to approximately 10% of L-cells throughout the gut [50].

1.5 The Ileal Brake

The mechanism by which distal small intestine (ileum) exposure to unabsorbed macronutrients inhibits upper gut function (i.e., ileal brake) and hypothalamic appetite control are not fully understood. Table 1.1 represent selected gastrointestinal and pancreatic peptides and their effect in regulating food intake [38]. The ileal wall peptides, GLP-1, OXM and PYY, are secreted from the enteroendocrine L-cells in the ileum and proximal colon and contribute to this mechanism

[45]. GLP-1 is secreted in response to nutrients after food intake and has multiple sites of action including the induction of neuronal activity in the central nervous system that regulates food intake and promotes satiety, stimulation of glucose-dependent insulin release from the pancreatic β-cells and causing of anti-hyperglycemic effect by slowing gastric emptying rate and reducing hepatic glucose productivity by inhibiting glucagon release (Figure 1.4) [45],[46],[53],[54]. OXM is another peptide that is produced by alternative splicing of the proglucagon gene. It is a 37-amino acid peptide hormone that had been shown to suppress appetite [55]. PYY is a 36-amino acid gastrointestinal peptide. The majority of PYY is produced by the L-cells in the ileum and colon with smaller amounts produced in the duodenum, jejunum, or the stomach [56]. PYY plays critical role in the regulation of energy homoeostasis, inhibition of gastric emptying, and reduction of food intake by acting on the NPY receptors in the hypothalamic central appetite circuit [56].

Previous studies showed that suppression of the hypothalamic neuropeptide expression in rats fed slowly digestible starch was concurrent with increased satiety and lower food intake compared to rats fed rapid digestible starch (Figure 1.2) [41]. This finding suggests that complex carbohydrates arriving the ileum can induce physiological effects. It is not clear, however, whether it is α-amylase degradation products, MOS, or glucose itself, or even fermentation products, short chain fatty acids, that cause these effects. Cell culture systems provide a unique tool to investigate each of these products independently as well as to compare their physiological effects.

1.6 Hypothesis

We hypothesize that ileal L-cells are significantly stimulated by large structures of carbohydrates delivered from slowly digestible starches arriving to distal gastrointestinal tract. The stimulated cells release specific gut hormones that are working through the gut-brain axis for reduced appetitive response. Intestinal L-cells are expected to exhibit different responses of gut

hormone secretion and signaling pathway proteins with different carbohydrate structures. In the current study, we are investigating intestinal chemosensation of mouse and human L-cell models to different MOS structure. The investigation is including the secretion assays of the major gut hormones released from L-cells (GLP-1, PYY and OXM). In addition, we are investigating the global changes in the cellular transcriptome and the proteome to reveal all the possible signaling pathways involved in the sensation process and its relation to glucose homeostasis. Finally, we examine the current hypothesis in an *in vivo* animal model using a tool of slowly digestible starch (SDS) delivery. SDS materials are hypothesized to efficiently deliver MOS to larger number of L-cells throughout the small intestine allowing for harnessing the endogenous release of gut hormones. Both obese and lean animal models are used to test the efficiency of SDS in the intervension and prevension of obesity. Understanding the ileal brake mechanisms and hypothalamic appetite control specifically related to their dietary triggers will establish a new relationship between carbohydrate digestion and body response. Bioactive carbohydrates can be designed to confer physiological outcomes related to type II diabetes treatment and obesity reduction. A model for the proposed outcomes is represented in Figure 1.5.

1.7 Significance

The secretion of GLP-1 and PYY was found to be reduced in both obese and type II diabetes patients, and is increased in bariatric surgery patients, making them reasonable targets for innovative treatments of these diseases [57]. Clinical approaches for modulating GLP-1 levels include the administration of the hormone or its mimetics, whereas intravenous administration of PYY is the most common [53],[56]. The issue of safety as well as potential side effects of these drugs and other anti-obesity therapies raises the question of whether functional foods can stimulate the endogenous secretion of these peptides and promote similar response as the orally

administrated drugs. Table 1.2 summaries potential gut peptide targets for obesity treatment and their mechanism of action [44]. Recent studies demonstrated that short chain fatty acids which are a gut microbiota product of fermentation of non-digestible carbohydrates activate the enteroendocrine free fatty acid receptors (FFAR2 and FFAR3) and promote the secretion of GLP-1 and PYY [58]. It was also shown that continuous ingestion of highly fermentable resistant starch, but not the less fermentable cellulose, leads to considerable increase in GLP-1 and PYY levels [59]. It was reported that intestinal enterocytes sense starch α-amylase digestion products, or maltooligosaccharides, to mobilize and activate the brush border α-glucosidase enzymes for glucose production [34]. Therefore, the current studies are investigating another route to activate the endogenous release of gut hormones based on starch digestion products that can reach the ileum where L-cells are suggested to be more abundant. Glucose was previously shown to trigger GLP-1 release in murine (GLUTage) [60] and human (NCI-H716) [61] L-cell lines. Studies have shown that lipids and fatty acids induce higher levels of GLP-1 [43], but scarce information is available regarding the effect of lipids on PYY secretion [34]. A recent study reported a reciprocal regulation effect between GLP-1 and the glucose transporter SGLT-1 and suggests that its activity is the driving force for glucose-stimulated GLP-1 secretion [43]. Moreover, GLUT2 and the calcium-sensing receptor (CasR) regulate L-cells activities in response to nutrients and non-nutrients stimuli [62].

1.8 Innovation

The Dietary Guidelines for Americans 2015-2020 (USDA) recommended dietary carbohydrates to provide 45-65% of the total caloric intake [63]. However, a large extent of variation occurs as a result of the large variability of carbohydrate quality including digestion, sustainability and absorption [64], [65]. Chronic consumption of high glycemic carbohydrates is

known to be associated with a large number of metabolic disorders and can eventually leads to detrimental health outcomes [5] through stresses on glucose homeostasis controls, promoting advanced glycation end product formation, favoring energy storage by hexosamine pathway, and other mechanisms [66]. This is mainly relevant in diabetic, and pre-diabetic, individuals where control of blood glucose levels is problematic. In contrast, glucose delivered in a slow rate was found to be associated with healthy influences and correlated to reduced risk factors for chronic diseases [67]. One of our key questions in carbohydrate nutrition is potential strategies to reduce glucose release rate in favor of human health. Therefore, we seek in this study to gain more fundamental and mechanistic understanding of a new aspect of carbohydrate quality, carbohydrate-gut interactions and exploring the carbohydrate chemosensation process of the intestinal cells in both *in vitro* and *in vivo* models. This knowledge will be the foundation for developing innovative technique for glycemic control.

1.9 References

[1] T. Kelly, W. Yang, C. S. Chen, K. Reynolds, and J. He, "Global burden of obesity in 2005 and projections to 2030," *Int. J. Obes.*, 2008.

[2] K. A. Elder and B. M. Wolfe, "Bariatric Surgery: A Review of Procedures and Outcomes," *Gastroenterology*, vol. 132, no. 6, pp. 2253–2271, May 2007.

[3] R. Quezada-Calvillo *et al.*, "Contribution of Mucosal Maltase-Glucoamylase Activities to Mouse Small Intestinal Starch α-Glucogenesis," *J. Nutr.*, vol. 137, no. 7, pp. 1725–1733, Jul. 2007.

[4] "Glycemic Index Testing | Glycemic | Glycemic Research Institute | Glycemic Index | Glycemic Load." [Online]. Available: http://www.glycemic.com/glycemicindex-loaddefined.htm. [Accessed: 31-Oct-2018].

[5] D. S. Ludwig, "The glycemic index: physiological mechanisms relating to obesity, diabetes, and cardiovascular disease.," *JAMA*, vol. 287, no. 18, pp. 2414–23, May 2002.

[6] S. Liu, J. E. Manson, J. E. Buring, M. J. Stampfer, W. C. Willett, and P. M. Ridker,

"Relation between a diet with a high glycemic load and plasma concentrations of high-sensitivity C-reactive protein in middle-aged women," *Am. J. Clin. Nutr.*, vol. 75, no. 3, pp. 492–498, Mar. 2002.

[7] J. C. Brand-Miller, S. H. A. Holt, D. B. Pawlak, and J. McMillan, "Glycemic index and obesity.," *Am. J. Clin. Nutr.*, vol. 76, no. 1, p. 281S–5S, Jul. 2002.

[8] D. S. Ludwig, "Dietary glycemic index and the regulation of body weight.," *Lipids*, vol. 38, no. 2, pp. 117–21, Feb. 2003.

[9] D. Thomas, E. J. Elliott, and L. Baur, "Low glycaemic index or low glycaemic load diets for overweight and obesity," *Cochrane Database Syst. Rev.*, no. 3, p. CD005105, Jul. 2007.

[10] J. Xu, S. L. Murphy, K. D. Kochanek, B. Bastian, and E. Arias, "National Vital Statistics Reports Volume 67, Number 5 July 26, 2018, Deaths: Final Data for 2016," 2018.

[11] W. Willett, J. Manson, and S. Liu, "Glycemic index, glycemic load, and risk of type 2 diabetes.," *Am. J. Clin. Nutr.*, vol. 76, no. 1, p. 274S–80S, Jul. 2002.

[12] J. Salmerón, J. E. Manson, M. J. Stampfer, G. A. Colditz, A. L. Wing, and W. C. Willett, "Dietary fiber, glycemic load, and risk of non-insulin-dependent diabetes mellitus in women.," *JAMA*, vol. 277, no. 6, pp. 472–7, Feb. 1997.

[13] R. Villegas *et al.*, "Prospective Study of Dietary Carbohydrates, Glycemic Index, Glycemic Load, and Incidence of Type 2 Diabetes Mellitus in Middle-aged Chinese Women," *Arch. Intern. Med.*, vol. 167, no. 21, p. 2310, Nov. 2007.

[14] L. S. Gross, L. Li, E. S. Ford, and S. Liu, "Increased consumption of refined carbohydrates and the epidemic of type 2 diabetes in the United States: an ecologic assessment," *Am. J. Clin. Nutr.*, vol. 79, no. 5, pp. 774–779, May 2004.

[15] S. Liu *et al.*, "Dietary glycemic load assessed by food-frequency questionnaire in relation to plasma high-density-lipoprotein cholesterol and fasting plasma triacylglycerols in postmenopausal women," *Am. J. Clin. Nutr.*, vol. 73, no. 3, pp. 560–566, Mar. 2001.

[16] E. S. Ford and S. Liu, "Glycemic Index and Serum High-Density Lipoprotein Cholesterol Concentration Among US Adults," *Arch. Intern. Med.*, vol. 161, no. 4, p. 572, Feb. 2001.

[17] S. Liu *et al.*, "A prospective study of dietary glycemic load, carbohydrate intake, and risk of coronary heart disease in US women," *Am. J. Clin. Nutr.*, vol. 71, no. 6, pp. 1455–1461, Jun. 2000.

[18] J. M. Chehade and A. D. Mooradian, “A Rational Approach to Drug Therapy of Type 2 Diabetes Mellitus,” *Drugs*, vol. 60, no. 1, pp. 95–113, Jul. 2000.

[19] P. Hollander, “Safety Profile of Acarbose, an α-Glucosidase Inhibitor,” *Drugs*, vol. 44, no. Supplement 3, pp. 47–53, 1992.

[20] H. Rasouli, S. M.-B. Hosseini-Ghazvini, H. Adibi, and R. Khodarahmi, “Differential α-amylase/α-glucosidase inhibitory activities of plant-derived phenolic compounds: a virtual screening perspective for the treatment of obesity and diabetes,” *Food Funct.*, vol. 8, no. 5, pp. 1942–1954, May 2017.

[21] K. Jones *et al.*, “Mapping the intestinal alpha-glucogenic enzyme specificities of starch digesting maltase-glucoamylase and sucrase-isomaltase,” *Bioorg. Med. Chem.*, vol. 19, no. 13, pp. 3929–3934, Jul. 2011.

[22] M. H. Stipanuk and M. A. Caudill, *Biochemical, Physiological, and Molecular Aspects of Human Nutrition, 3rd Edition - 9781437709599*. .

[23] C. Yook and J. F. Robyt, “Reactions of alpha amylases with starch granules in aqueous suspension giving products in solution and in a minimum amount of water giving products inside the granule.,” *Carbohydr. Res.*, vol. 337, no. 12, pp. 1113–7, Jun. 2002.

[24] R. Quezada-Calvillo *et al.*, “Luminal Starch Substrate ‘Brake’ on Maltase-Glucoamylase Activity Is Located within the Glucoamylase Subunit,” *J. Nutr.*, vol. 138, no. 4, pp. 685–692, Apr. 2008.

[25] L. Sim, C. Willemsma, S. Mohan, H. Y. Naim, B. M. Pinto, and D. R. Rose, “Structural Basis for Substrate Selectivity in Human Maltase-Glucoamylase and Sucrase-Isomaltase N-terminal Domains,” *J. Biol. Chem.*, vol. 285, no. 23, pp. 17763–17770, Jun. 2010.

[26] I. S. Wood and P. Trayhurn, “Glucose transporters (GLUT and SGLT): expanded families of sugar transport proteins,” *Br. J. Nutr.*, vol. 89, no. 01, p. 3, Jan. 2003.

[27] H. N. Englyst, S. M. Kingman, and J. H. Cummings, “Classification and measurement of nutritionally important starch fractions.,” *Eur. J. Clin. Nutr.*, vol. 46 Suppl 2, pp. S33-50, Oct. 1992.

[28] B. L. Nichols *et al.*, “Mucosal maltase-glucoamylase plays a crucial role in starch digestion and prandial glucose homeostasis of mice.,” *J. Nutr.*, vol. 139, no. 4, pp. 684–90, Apr. 2009.

[29] E. J. Bland, T. Keshavarz, and C. Bucke, “The influence of small oligosaccharides on the immune system,” *Carbohydr. Res.*, vol. 339, no. 10, pp. 1673–1678, Jul. 2004.

[30] A. Zhu, R. Romero, J.-B. Huang, A. Clark, and H. R. Petty, "Maltooligosaccharides from JEG-3 Trophoblast-Like Cells Exhibit Immunoregulatory Properties," *Am. J. Reprod. Immunol.*, vol. 65, no. 1, pp. 54–64, Jan. 2011.

[31] M. Uozumi, T.; Morishita, S.; Tanaka, Y.; Yumoto, "NKl receptor antagonist composition.," Patent No.: US 8,426,386 B2, 2013.

[32] S. Y. Shin, Y. J. Jung, Y. Yong, H. J. Cho, Y. Lim, and Y. H. Lee, "Inhibition of PDGF-induced migration and TNF-α-induced ICAM-1 expression by maltotetraose from bamboo stem extract (BSE) in mouse vascular smooth muscle cells," *Mol. Nutr. Food Res.*, vol. 60, no. 9, pp. 2086–2097, Sep. 2016.

[33] M. Chegeni, M. Amiri, B. L. Nichols, H. Y. Naim, and B. R. Hamaker, "Dietary starch breakdown product sensing [1] M. Chegeni, M. Amiri, B. L. Nichols, H. Y. Naim, and B. R. Hamaker, 'Dietary starch breakdown product sensing mobilizes and apically activates α-glucosidases in small intestinal enterocytes,' FASEB J., vol. 32," *FASEB J.*, vol. 32, no. 7, pp. 3903–3911, Jul. 2018.

[34] M.-W. Cheng *et al.*, "Different sucrose-isomaltase response of Caco-2 cells to glucose and maltose suggests dietary maltose sensing.," *J. Clin. Biochem. Nutr.*, vol. 54, no. 1, pp. 55–60, Jan. 2014.

[35] M. Chegeni, "Dietary carbohydrates influence the structure and function of the intestinal alpha-glucosidases." 2016.

[36] J. B. Furness, L. R. Rivera, H.-J. Cho, D. M. Bravo, and B. Callaghan, "The gut as a sensory organ," *Nat. Rev. Gastroenterol. Hepatol.*, vol. 1010, no. 1212, pp. 729–740, Sep. 2013.

[37] A. A. Lee and C. Owyang, "Sugars, Sweet Taste Receptors, and Brain Responses.," *Nutrients*, vol. 9, no. 7, Jun. 2017.

[38] D. E. Cummings and J. Overduin, "Gastrointestinal regulation of food intake," *J. Clin. Invest.*, vol. 117, 2007.

[39] F. M. Gribble, C. L. Meek, and F. Reimann, "Targeted intestinal delivery of incretin secretagogues-towards new diabetes and obesity therapies," 2018.

[40] I. Kaji, S.-I. Karaki, R. Tanaka, and A. Kuwahara, "Fructo-Oligosaccharide (FOS) Supplementation Increases Enteroendocrine L Cells Containing GLP-1 and SCFA Receptor GPR43 (Ffa2) in the Large Intestine," 2010.

[41] L. Y. Hasek *et al.*, "Dietary Slowly Digestible Starch Triggers the Gut-Brain Axis in Obese

Rats with Accompanied Reduced Food Intake," *Mol. Nutr. Food Res.*, vol. 62, no. 5, p. 1700117, Mar. 2018.

[42] N. J. W. Albrechtsen, R. E. Kuhre, C. F. Deacon, and J. J. Holst, "Targeting the intestinal L-cell for obesity and type 2 diabetes treatment," *Expert Rev. Endocrinol. Metab.*, vol. 9, no. 1, pp. 61–72, Jan. 2014.

[43] G. Tolhurst *et al.*, "Short-Chain Fatty Acids Stimulate Glucagon-Like Peptide-1 Secretion via the G-Protein-Coupled Receptor FFAR2," *Diabetes*, vol. 61, pp. 364–371, 2012.

[44] E. Spreckley and K. G. Murphy, "The L-cell in nutritional sensing and the regulation of appetite," *Front. Nutr.*, vol. 2, p. 23, 2015.

[45] J. J. Holst, "The Physiology of Glucagon-like Peptide 1," *Physiol. Rev.*, vol. 87, no. 4, pp. 1409–1439, Oct. 2007.

[46] D. A. Stoffers *et al.*, "Insulinotropic glucagon-like peptide 1 agonists stimulate expression of homeodomain protein IDX-1 and increase islet size in mouse pancreas.," *Diabetes*, vol. 49, no. 5, pp. 741–8, May 2000.

[47] L. L. Baggio and D. J. Drucker, "Biology of Incretins: GLP-1 and GIP," *Gastroenterology*, vol. 132, no. 6, pp. 2131–2157, May 2007.

[48] F. G. A. Baldissera, J. J. Holst, S. Knuhtsen, L. Hilsted, and O. V. Nielsen, "Oxyntomodulin (glicentin-(33–69)): pharmacokinetics, binding to liver cell membranes, effects on isolated perfused pig pancreas, and secretion from isolated perfused lower small intestine of pigs," *Regul. Pept.*, vol. 21, no. 1–2, pp. 151–166, May 1988.

[49] K. L. Egerod *et al.*, "A Major Lineage of Enteroendocrine Cells Coexpress CCK, Secretin, GIP, GLP-1, PYY, and Neurotensin but Not Somatostatin," *Endocrinology*, vol. 153, no. 12, pp. 5782–5795, Dec. 2012.

[50] A. M. Habib *et al.*, "Overlap of Endocrine Hormone Expression in the Mouse Intestine Revealed by Transcriptional Profiling and Flow Cytometry," *Endocrinology*, vol. 153, no. 7, pp. 3054–3065, Jul. 2012.

[51] A. M. Habib, P. Richards, G. J. Rogers, F. Reimann, and F. M. Gribble, "Co-localisation and secretion of glucagon-like peptide 1 and peptide YY from primary cultured human L cells," *Diabetologia*, vol. 56, no. 6, pp. 1413–1416, Jun. 2013.

[52] J. Pedersen *et al.*, "Glucose metabolism is altered after loss of L cells and α-cells but not influenced by loss of K cells," *Am. J. Physiol. Metab.*, vol. 304, no. 1, pp. E60–E73, Jan.

2013.

[53] K. Dungan and J. B. Buse, “Glucagon-Like Peptide 1-Based Therapies for Type 2 Diabetes: A Focus on Exenatide,” *Clin. Diabetes*, vol. 23, no. 2, pp. 56–62, Apr. 2005.

[54] G. E. Lim and P. L. Brubaker, “Glucagon-Like Peptide 1 Secretion by the L-Cell: The View From Within,” *Diabetes*, vol. 55, no. Supplement 2, pp. S70–S77, Dec. 2006.

[55] A. Pocai, “Action and therapeutic potential of oxyntomodulin,” *Mol. Metab.*, vol. 3, no. 3, pp. 241–251, Jun. 2014.

[56] K. V. Hand *et al.*, “Examining acute and chronic effects of short- and long-chain fatty acids on peptide YY (PYY) gene expression, cellular storage and secretion in STC-1 cells,” *Eur. J. Nutr.*, vol. 52, no. 4, pp. 1303–1313, Jun. 2013.

[57] S. Zac-Varghese, A. De Silva, and S. R. Bloom, “Translational studies on PYY as a novel target in obesity,” *Curr. Opin. Pharmacol.*, vol. 11, pp. 582–585, 2011.

[58] I. Kaji, S.-I. Karaki, and A. Kuwahara, “Short-Chain Fatty Acid Receptor and Its Contribution to Glucagon-Like Peptide-1 Release,” *Digestion*, vol. 89, pp. 31–36, 2014.

[59] J. Zhou *et al.*, “Dietary resistant starch upregulates total GLP-1 and PYY in a sustained day-long manner through fermentation in rodents.,” *Am. J. Physiol. Endocrinol. Metab.*, vol. 295, no. 5, pp. E1160-6, Nov. 2008.

[60] H.-J. Jang *et al.*, “Gut-expressed gustducin and taste receptors regulate secretion of glucagon-like peptide-1.,” *Proc. Natl. Acad. Sci. U. S. A.*, vol. 104, no. 38, pp. 15069–74, Sep. 2007.

[61] R. Pais, F. M. Gribble, and F. Reimann, “Stimulation of incretin secreting cells.,” *Ther. Adv. Endocrinol. Metab.*, vol. 7, no. 1, pp. 24–42, Feb. 2016.

[62] R. F. Margolskee *et al.*, “T1R3 and gustducin in gut sense sugars to regulate expression of Na-glucose cotransporter 1,” 2007.

[63] Office of Disease Prevention and Health Promotion, “2015-2020 Dietary Guidelines for Americans,” 2015.

[64] D. J. Jenkins *et al.*, “Glycemic index of foods: a physiological basis for carbohydrate exchange,” *Am. J. Clin. Nutr.*, vol. 34, no. 3, pp. 362–366, Mar. 1981.

[65] K. N. Englyst, S. Vinoy, H. N. Englyst, and V. Lang, “Glycaemic index of cereal products explained by their content of rapidly and slowly available glucose,” *Br. J. Nutr.*, vol. 89, no. 03, p. 329, Mar. 2003.

[66] M. Brownlee, “Biochemistry and molecular cell biology of diabetic complications,” *Nature*, vol. 414, no. 6865, pp. 813–820, Dec. 2001.

[67] D. J. A. Jenkins *et al.*, “Glycemic index: overview of implications in health and disease.,” *Am. J. Clin. Nutr.*, vol. 76, no. 1, p. 266S–73S, Jul. 2002.

[68] C. L. Dakin *et al.*, “Oxyntomodulin Inhibits Food Intake in the Rat,” *Endocrinology*, vol. 142, no. 10, pp. 4244–4250, Oct. 2001.

[69] K. Wynne *et al.*, “Oxyntomodulin increases energy expenditure in addition to decreasing energy intake in overweight and obese humans: a randomised controlled trial,” *Int. J. Obes.*, vol. 30, no. 12, pp. 1729–1736, Dec. 2006.

[70] T. E. ADRIAN, G. R. SAGOR, A. P. SAVAGE, A. J. BACARESE-HAMILTON, G. M. HALL, and S. R. BLOOM, “Peptide YY Kinetics and Effects on Blood Pressure and Circulating Pancreatic and Gastrointestinal Hormones and Metabolites in Man,” *J. Clin. Endocrinol. Metab.*, vol. 63, no. 4, pp. 803–807, Oct. 1986.

[71] S. A. Hawley, M. A. Selbert, E. G. Goldstein, A. M. Edelman, D. Carling, and D. G. Hardie, “5’-AMP activates the AMP-activated protein kinase cascade, and Ca2+/calmodulin activates the calmodulin-dependent protein kinase I cascade, via three independent mechanisms.,” *J. Biol. Chem.*, vol. 270, no. 45, pp. 27186–91, Nov. 1995.

[72] F. M. Gribble *et al.*, “Glutamine potently stimulates glucagon-like peptide-1 secretion from GLUTag cells,” *Diabetologia*, vol. 47, pp. 1592–1601, 2004.

[73] P. Nicklin *et al.*, “Bidirectional Transport of Amino Acids Regulates mTOR and Autophagy,” *Cell*, vol. 136, pp. 521–534.

[74] C. Clemmensen *et al.*, “Oral l -Arginine Stimulates GLP-1 Secretion to Improve Glucose Tolerance in Male Mice,” *Endocrinology*, vol. 154, no. 11, pp. 3978–3983, Nov. 2013.

[75] S. Joshi, I. R. Tough, and H. M. Cox, “Endogenous PYY and GLP-1 mediate l-glutamine responses in intestinal mucosa.,” *Br. J. Pharmacol.*, vol. 170, no. 5, pp. 1092–101, Nov. 2013.

[76] S. Choi, M. Lee, A. L. Shiu, J. Yo, G. Halldén, and G. W. Aponte, “GPR93 activation by protein hydrolysate induces CCK transcription and secretion in STC-1 cells,” 2007.

[77] P. Wellendorph and H. Bräuner-Osborne, “Molecular basis for amino acid sensing by family C G-protein-coupled receptors.,” *Br. J. Pharmacol.*, vol. 156, no. 6, pp. 869–84, Mar. 2009.

[78] P. Wellendorph *et al.*, “Deorphanization of GPRC6A: A Promiscuous L-Amino Acid Receptor with Preference for Basic Amino Acids □ S,” 2005.

[79] F. Reimann, A. M. Habib, G. Tolhurst, H. E. Parker, G. J. Rogers, and F. M. Gribble, “Glucose sensing in L cells: a primary cell study.,” *Cell Metab.*, vol. 8, no. 6, pp. 532–9, Dec. 2008.

[80] C. Cherbut *et al.*, “Short-chain fatty acids modify colonic motility through nerves and polypeptide YY release in the rat.,” *Am. J. Physiol.*, vol. 275, no. 6 Pt 1, pp. G1415-22, Dec. 1998.

[81] A. Psichas *et al.*, “The short chain fatty acid propionate stimulates GLP-1 and PYY secretion via free fatty acid receptor 2 in rodents,” *Int. J. Obes.*, vol. 39, no. 3, pp. 424–429, Mar. 2015.

[82] A. Hirasawa *et al.*, “Free fatty acids regulate gut incretin glucagon-like peptide-1 secretion through GPR120,” *Nat. Med.*, vol. 11, no. 1, pp. 90–94, Jan. 2005.

[83] S. Edfalk, P. Steneberg, and H. Edlund, “Gpr40 Is Expressed in Enteroendocrine Cells and Mediates Free Fatty Acid Stimulation of Incretin Secretion,” 2280.

[84] V. M. Stone *et al.*, “GPR120 (FFAR4) is preferentially expressed in pancreatic delta cells and regulates somatostatin secretion from murine islets of Langerhans,” *Diabetologia*, vol. 57, no. 6, pp. 1182–1191, Jun. 2014.

Table 1.1. Gastrointestinal and pancreatic hormones regulating food intake (anorexigenic and orexigenic) through the brain. (Source: Adapted from Cummings and Overduin, 2007) [38].

Peptide	Main Site of Synthesis	Receptors Mediating feeding effects	Sites of Actions			Effect on Food Intake
			Hypothalamus	Hindbrain	Vagus Nerve	
CCK	Proximal intestinal I-cells	CCK1R	X	X	X	Reduction
GLP-1	Distal-intestinal L-cells	GLP1R	UD	UD	X	Reduction
OXM	Distal-intestinal L-cells	GLP1R and others	X			Reduction
PYY $_{3-35}$	Distal-intestinal L-cells	Y2R	X		X	Reduction
Enterostatin	Exocrine Pancreas	F1-ATPase β subunit			X	Reduction
APO AVI	Intestinal epithelial cells	Unknown	X		X	Reduction
PP	Pancreatic F cells	Y4R, Y5R		X	X	Reduction
Amylin	Pancreatic β-cells	CTRs, RAMPs	X	X		Reduction
GRP and NMB	Gastric myenteric neurons	GRPR		X	X	Reduction
Gastric leptin	Gastric chief and P cells	Leptin receptor	UL	UL	X	Reduction
Ghrelin	Gastric X/A-like cells	Ghrelin receptor	X	X	X	Induction

CTRs: calcitonin receptors; RAMPs: receptor activity–modifying proteins; GRP: gastrin-releasing peptide; NMB: neuromedin B; GRPR: GRP receptor. X= Interacting with the specified sites. UD = undetermined. UL = unlikely to be interacting in these sites.

Table 1.2 Summary of potential targets for the treatment of obesity and their mechanisms. (Source: Spreckley and Murphy, 2015) [44].

Potential targets	Mechanism	Reference
Oxyntomodulin	GLP-1 and glucagon receptor agonism	[68], [69]
Peptide YY	Y2R agonism modulates central anorectic pathways and influences ileal brake	[44], [70]
Dietary supplementation with glutamine and l-arginine	Ingested glutamine and l-arginine potentiate the release of GLP-1 and PYY, via activation of AMPK and mTOR	[71], [72], [73], [74]
Calcium-sensing receptor	Activation by specific L-amino acids stimulates the secretion of GLP-1 and PYY	[75]
G-protein coupled receptor 93	Protein hydrolyzates stimulate the release of CCK	[76]
G-protein coupled receptor, class C, group 6, subtype A	Activation by specific L-amino acids stimulates the secretion of GLP-1	[77],[78]
Sodium-glucose transporter 1	Transport of ingested glucose into enterocytes stimulates the secretion of GLP-1	[79]
Free fatty acid receptor 2 and 3	Activation by short-chain fatty acids may stimulate the secretion of GLP-1 and PYY and inhibit gastrointestinal motility	[80], [43], [81]
Free fatty acid receptor 1 and 4	Activation by medium and long-chain fatty acids stimulates the secretion of GLP-1	[82], [83], [84]

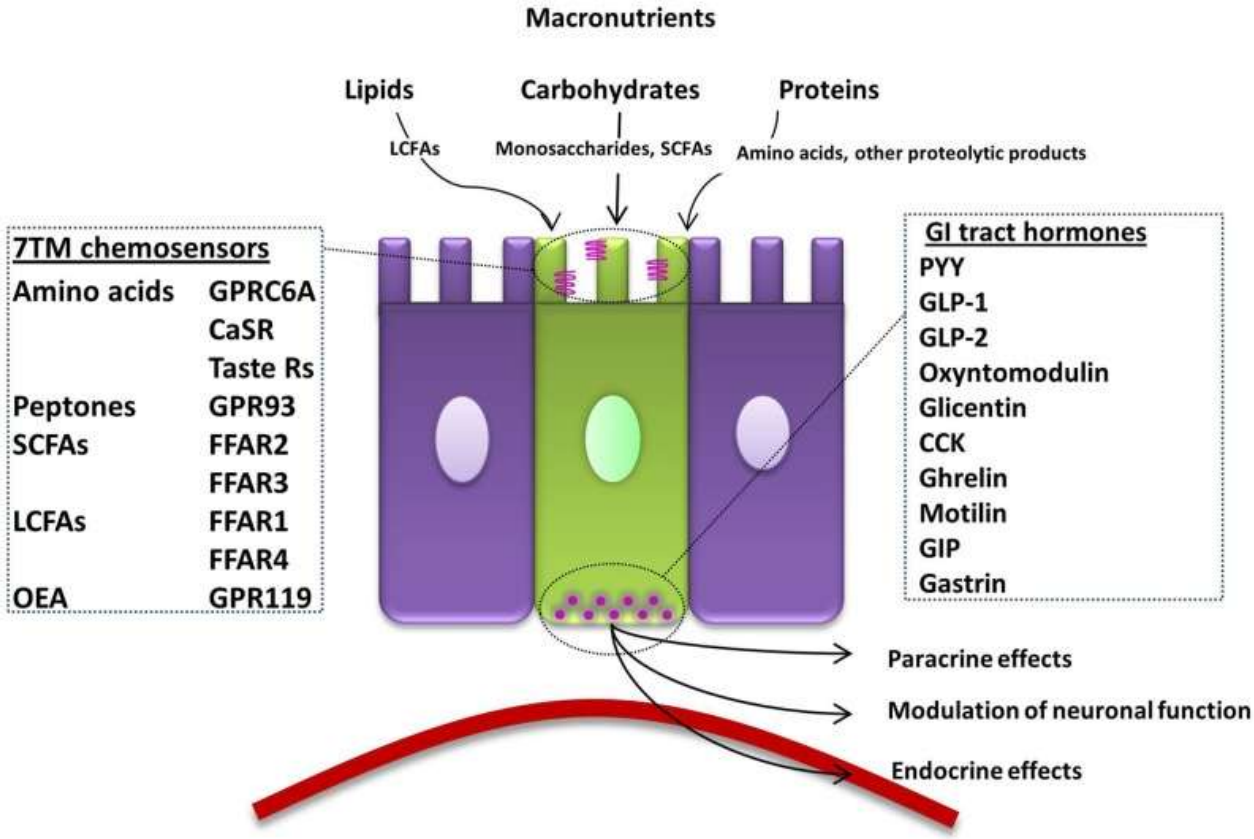

Figure 1.1 Intestinal chemosensation of dietary macronutrients by enteroendocrine cells through 7-transmembrane chemosensors. LCFA; long-chain fatty acids, 7TM; seven-transmembrane, CaSR; calcium-sensing receptor, GPRC6A; G-protein coupled receptor family C group 6 subtype A, GPR93; G-protein coupled receptor 93, SCFA; short-chain fatty acids, FFAR; free-fatty-acid receptor, OEA; oleoylethanolamide, GPR119; G-protein coupled receptor 119, GI; gastrointestinal, PYY; peptide YY, GLP; glucagon-like peptide, CCK; cholecystokinin, GIP; gastric inhibitory peptide. Source: Spreckley and Murphy, 2015 [44].

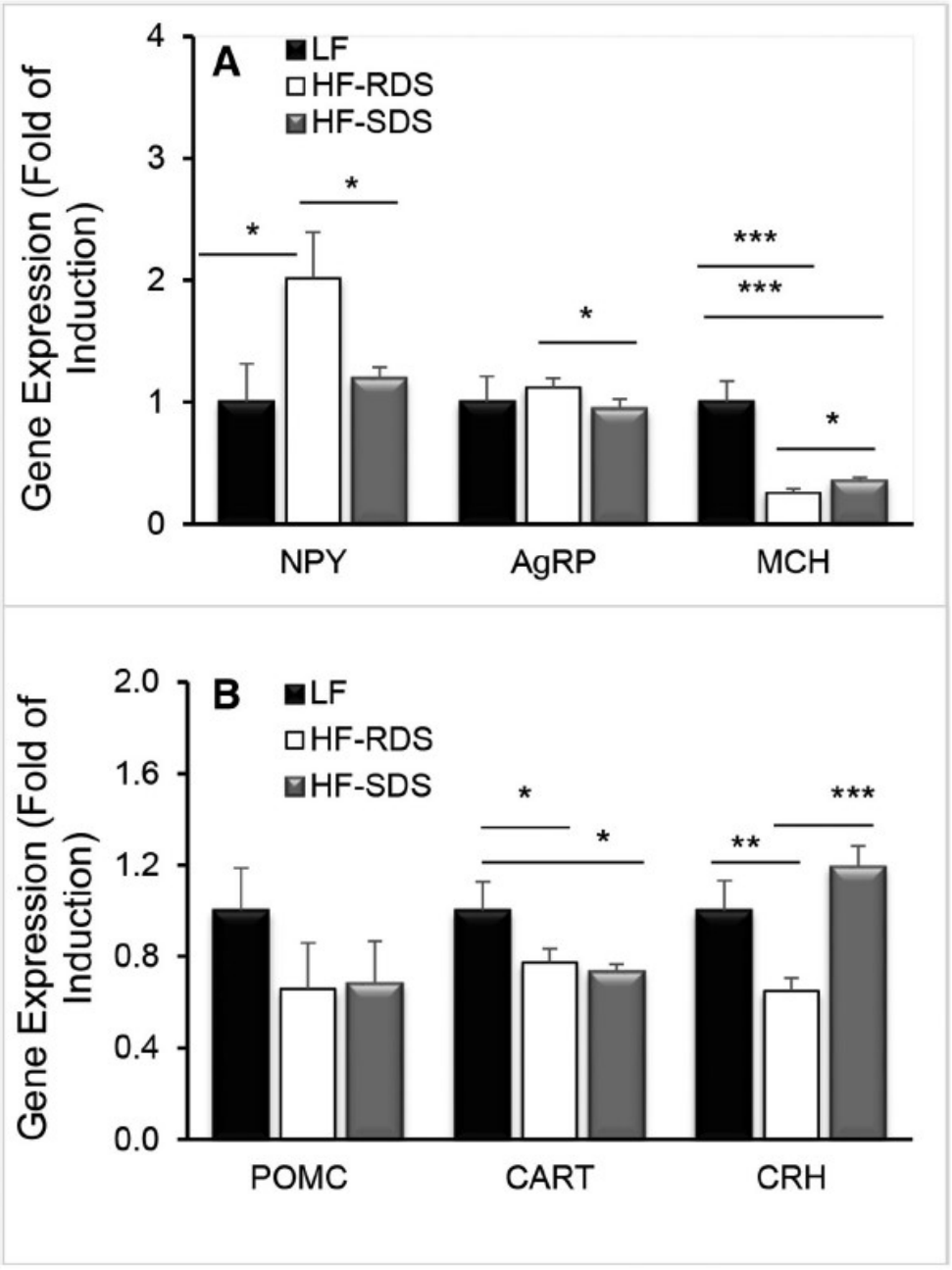

Figure 1.2 Gene expression of three orexigenic neuropeptides Y (NPY), agouti-related peptide (AgRP), and melanin-concentrating hormone (MCH) and three anorexigenic neuropeptides: proopiomelanocortin (POMC), cocaine-and amphetamine-regulated transcript (CART), and corticotropin-releasing hormone (CRH) in the hypothalamus of rats fed the low-fat control diet, high-fat diet with rapidly digestible starch (RDS), and high-fat diet with slowly digestible starch (SDS) after 12 weeks of feeding. Source: Hasek *et al*., 2018 [41].

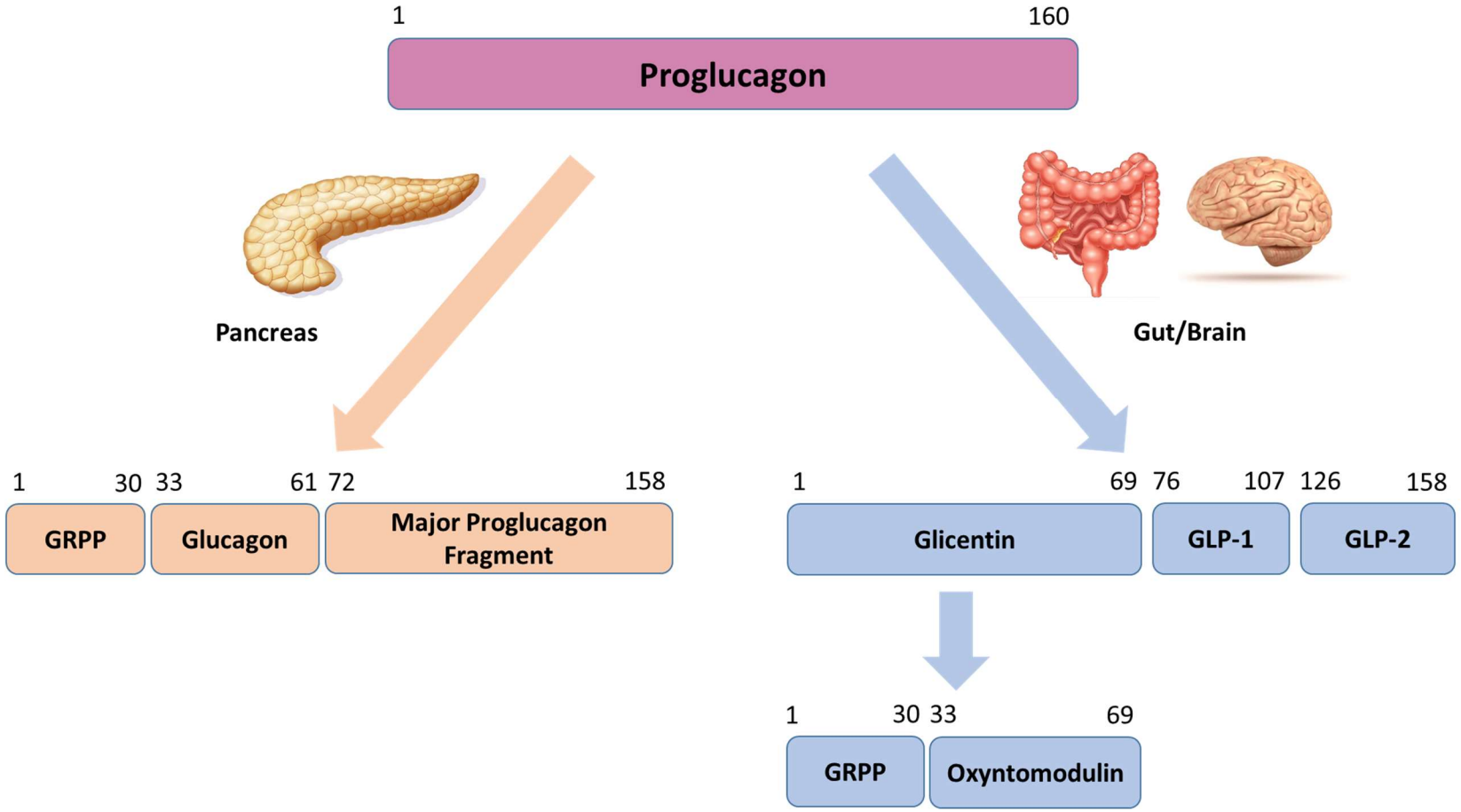

Figure 1.3 Post-translational processing of the proglucagon peptide is different in the pancreas from the gut and brain. The numbers indicate amino acid positions in the 160-amino acid proglucagon peptide. GRPP, glicentin-related pancreatic polypeptide; GLP-1, glucagon like peptide-1; GLP- 2, glucagon like peptide-2. Adapted from Holst, 2007 [45].

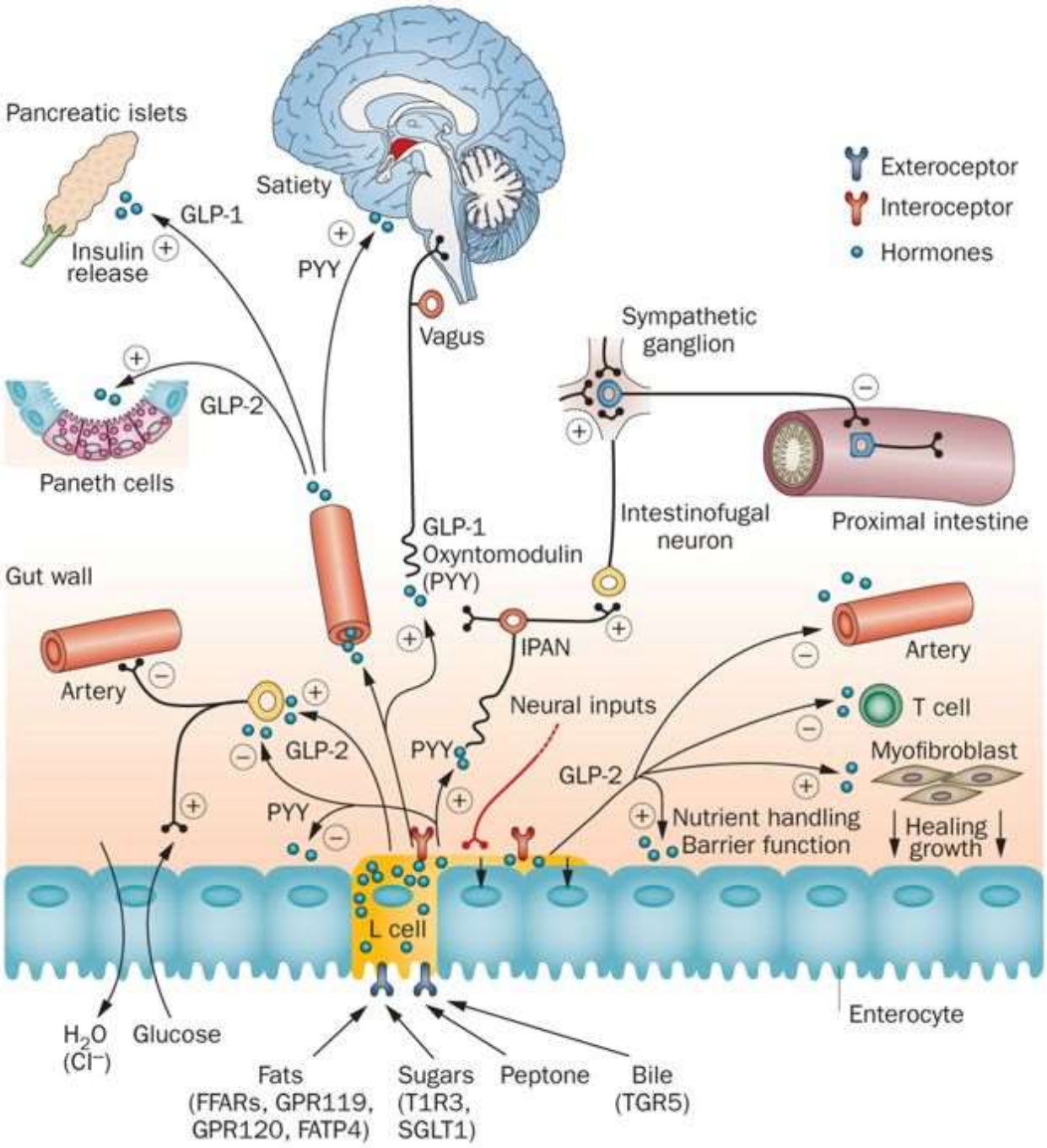

Figure 1.4 Multiple sensors and effectors in postprandial GLP-1 and PYY regulation pathways for energy homeostasis control. Source: Furness *et al*., 2013 [36].

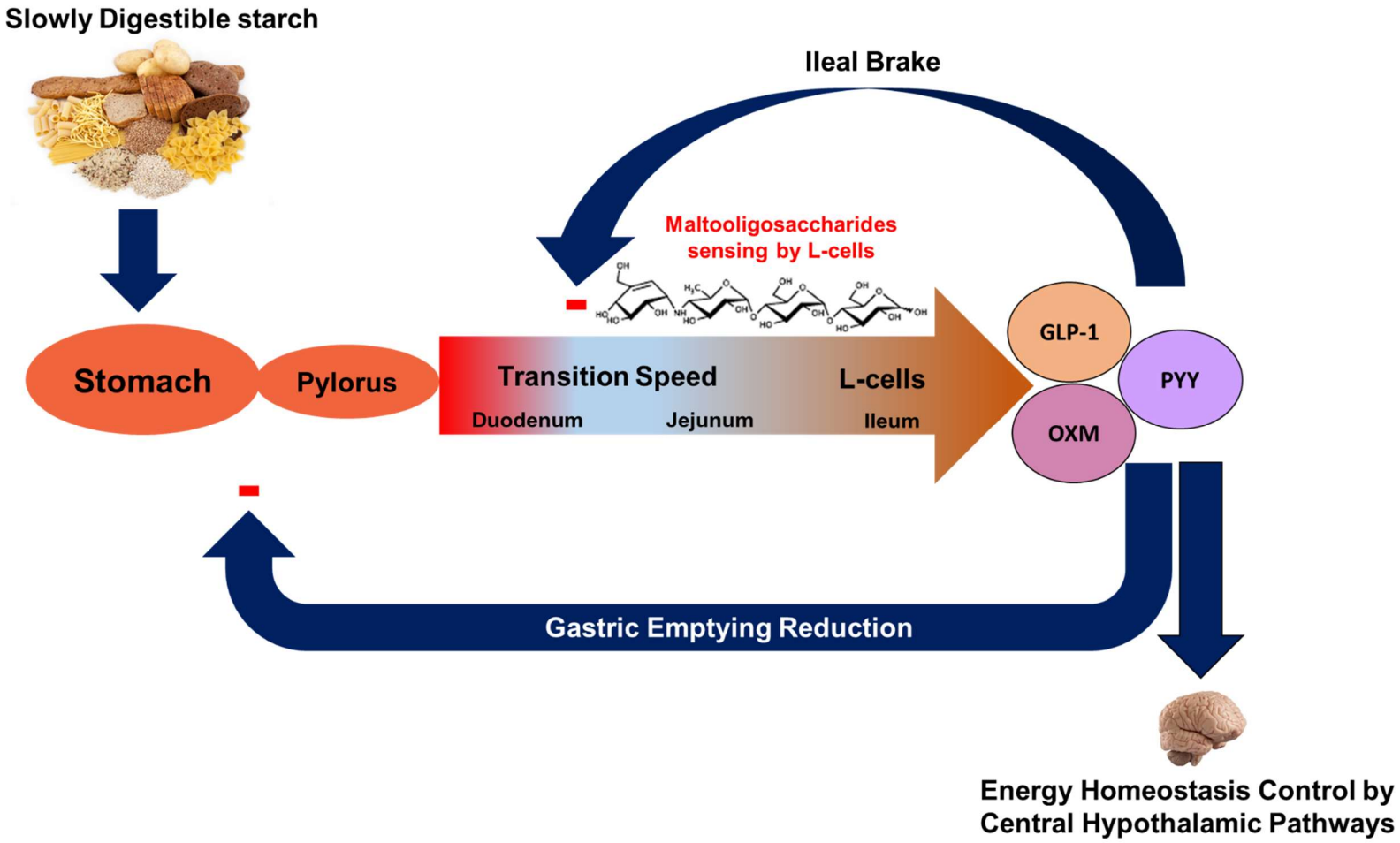

Figure 1.5 Proposed model for the beneficial outcomes of distal delivery of maltooligosaccharides (MOS) through the consumption of slowly digestible starch. Intestinal chemosensation of MOS triggers the release of L-cell major peptides GLP-1, OXM and PYY. The released peptides are involved in the reduction of gastric emptying, ileal brake and hypothalamic downregulation of satiety.

CHAPTER 2. MALTOOLIGOSACCHARIDES, REPRESENTING DIGESTED STARCH PRODUCTS, AS ACTIVATORS FOR GUT HORMONES CONTROLLING APPETITE

2.1 Abstract

As obesity became one of the most prevalent metabolic diseases, efficacious and cost-effective food/nutrition-based approaches are in high demand. One of the important regulators of appetite suppression is the neuroendocrine system of the gut-brain axis. The stimulation of L-cells, predominantly located in the distal small intestine (ileum) and colon, through fatty acids, proteins and simple sugars has been extensively studied and confirmed. However, the stimulation influences of complex dietary carbohydrates on L-cells is not fully described or even known. Recent studies showed that suppressed expression of the hypothalamic neuropeptide NPY in rats fed slowly digestible starch was concurrent with increased satiety and lower food intake compared to rats fed rapid digestible starch. This finding suggests that complex carbohydrates arriving to the ileum and through triggering L-cells promote these physiological effects. It was not clear, however, what carbohydrate type activates L-cells, whether it is starch digested α-amylase degradation products, or maltooligosaccharides (MOS, consisting linear and branched molecules), or glucose itself, or even bacterial fermentation products (short chain fatty acids). Here, we show for the first time that intestinal L-cells exhibit increased response of anorexigenic gut peptide secretion with MOS structures. Murine (STC-1) and the human (NCI-H716) enteroendocrine L-cells were used. Glucagon-like peptide-1 (GLP-1) secretion was higher in STC-1 cells treated with MOS compared to glucose or propionate. Increasing the degree of polymerization of the MOS, from maltose to maltopentaose, incrementally increased GLP-1 secretion. Maltotriose and maltopentaose showed over 2-fold increase in GLP-1 levels (1.33 ± 0.29 and 1.38 ± 0.22 ρM/μg

protein respectively) compared to glucose (0.74 ± 0.15 ρM/μg protein) or propionate (0.45 ± 0.11 ρM/μg protein). We indicate that this effect was due to the structure/size of the molecules and not due to accumulating glucose content, as there was absence of any digestion ability of the cells to breakdown MOS into glucose. MOS also increased oxyntomodulin (OXM) levels in the human enteroendocrine cells, and maltotriose promoted more than 2-fold increase in OXM release compared to glucose. In addition, the relative mRNA expression of the gastrointestinal peptide, cholecystokinin, in cells treated with maltotriose was highly enhanced compared to those treated with glucose. Moreover, MOS exhibited improved trans-epithelial electrical resistance in the enterocyte model, Caco-2, suggesting improved monolayer integrity. Our results reveal that MOS exhibits a unique effect on L-cell sensitivity and gut hormone productivity. The use of dietary carbohydrates to achieve a gut physiological response that relates to satiety and food intake could be a new approach for food for health applications. This could be achieved by triggering L-cells using starch digested α-amylase degradation products. It is conceivable that bioactive MOS could be designed to confer physiological outcomes relevant to obesity reduction and type II diabetes treatment.

2.2 Introduction

A number of investigations have focused on glucose as a dietary stimulator of GLP-1 secretion [1], [2], [3], [4]. Glucose had been shown to stimulate GLP-1 release in different *in vitro* models, including enteroendocrine cell lines [5], [6], [7] and primary intestinal cell culture systems [8] as well as *in vivo* models, such as mouse and human [9]. Although well-defined in the *in vitro* models, it is not well-characterized how much luminal glucose levels are required for *in vivo* L-cell stimulus to release GLP-1. Concentrations ranging from 5 to 1000 mM have been reported to cause GLP-1 release from the perfused ileum [10], [11], [12]. Different mechanisms have been suggested

to elucidate the stimulation effect of carbohydrates, primarily glucose, on GLP-1 secretion from L-cells. One of the common explanations is the electrogenic uptake of glucose through sodium-glucose transporter 1 (SGLT-1) [13], [14]. Gribble *et al*., 2003 illustrated that the mechanism underlying glucose sensing by the intestinal L-cells include the electrogenic SGLT-1 as an obligatory requirement. SGLT-1 facilitates the passage of one glucose molecule and two sodium ion (Na+) into the cells. The Na+ influx depolarizes the cell plasma membrane which, in turn, stimulates the opening of voltage sensitive calcium channels and exocytosis of GLP-1-containing secretory vesicles [14]. The hypothesis is consistent with the impairment of glucose-dependent GLP-1 release observed in isolated perfused rat small intestine that was depleted of luminal sodium chloride [4]. In addition, the use of the SGLT1 inhibitor, phloridzin, has been shown to completely abolish glucose-dependent GLP-1 release in rats [4] and mice [15] when administrated with glucose. Moreover, it was shown that sugars and sugar mimetics such as 2-deoxy-D-glucose and N-acetyl-D-glucosamine, that are not substrates to SGLT-1 nor are absorbed through fructose transporters, do not stimulate L-cells for GLP-1 release [12].

On the other hand, another proposed mechanism for glucose stimulation of GLP-1 release relay on the sensing machinery of sugars by sweet taste receptors [8], [16]. One of the pioneering studies that investigated carbohydrate sensing by intestinal L-cells is the study of Shima *et al*., 1990. The study investigated the structure-activity relationship of different sugars and its role in stimulating the secretion of GLP-1 in ileal loops of dogs [10]. Infusion of 139 mM different sugars (D-glucose, D-galactose, D-glucuronic acid, 3-0-methyl-D-glucose, maltose, sucrose and maltitol) into the intestinal lumen cause a significant increase on plasma GLP-1. However, the infusion did not affect plasma GLP-1 in the case of D-fructose, D-fucose, D-mannose, D-xylose and lactose [10]. This was in contrary to data suggesting that fructose induces a sodium-independent release

of GLP-1 in perfused rat ileum [12]. Importantly, this study for the first time (as the best of our knowledge) suggested that intestinal cells harbor a specific glucose sensor that could, upon stimulation, facilitate the release of the proglucagon gene products. This assumption is in agreement with the knowledge that intracellular metabolism or removal of carbohydrate from the intestinal cells is not required for GLP-1 release [12]. Molecules such as methyl-α- D-glucoside, which is not a substrate of the basolateral glucose transporter, and 3-O-methyl-D-glucose, which is not metabolized within intestinal cells, are still strong activators for GLP-1 release [12]. The positive response obtained from other sugars than glucose for GLP-1 release was explained by the suggestion that glucose has specific steric requirements and can be triggered by any sugar that provide these molecular requirements [10]. Shima *et al*., 1990 stated that GLP-1 release was stimulated with sugars containing electron density near C (6), an equatorial hydroxyl at C (2), and an axial hydroxyl at C (1). These features imply a sensor binding or recognition of the sugar [10]. Cani *et al*., 2007 reported that GLP-1 release was promoted in rats fed diet supplemented with 10 g oligofructose/100 g diet for 4 weeks compared to rats fed standard diets [17]. In addition, they showed two-fold increase in the number of cells expressing GLP-1 using immunohistochemistry [17].

The knowledge that SGLT-1 inhibition or its gene knockout improved GLP-1 and peptide YY (PYY) levels but completely eliminated glucose-dependent insulinotropic peptide (GIP) secretion in *in vivo* models [18] argues against the existence of an apical glucose sensing receptor in the GIP-secreting K cells [18]. In this instance, glucose accumulation in the lumen should be stimulating the proposed sensing receptor toward increased secretion. It could be claimed that SGLT-1 might transport glucose across the epithelium where it is then sensed by basolateral sweet taste receptor. A similar mechanism was previously described for the detection of bile acids by the

TGR5 receptor. However, the incretin secretion from mixed primary epithelial cultures, which gives complete access to both sides of an enteroendocrine cell, was also eliminated by SGLT-1 inhibition and was not responsive to artificial sweeteners [19],[8]. It was suggested that sweet taste receptor expression is sensitive to culture conditions [20]. Another elucidation for the impaired incretin secretion observed in mice with impaired taste receptor pathway activity could be that the well-recognized taste receptor dependent increase in SGLT-1 expression and glucose absorption [21] are also altered in these mice, and that this could result in a reduction in SGLT-1 expression in L-cells.

The secretion of GLP-1 and PYY was found to be reduced in both obese and type II diabetes patients, and is increased in bariatric surgery patients, making them reasonable targets for innovative treatments of these diseases [22]. Clinical approaches for modulating GLP-1 levels include the administration of the hormone or its mimetics, whereas intravenous administration of PYY is the most common [23], [24], [25] and [26]. The issue of safety as well as potential side effects of these and other anti-obesity therapies raises the question of whether functional foods can stimulate the endogenous secretion of these peptides and promote similar response as the orally administrated drugs. Recent studies demonstrated that short chain fatty acids (SCFAs) which are a gut microbiota product of fermentation of non-digestible carbohydrates activate the enteroendocrine free fatty acid receptors (FFAR2 and FFAR3) and promote the secretion of GLP-1 and PYY [27]. It was also shown that continuous ingestion of highly fermentable resistant starch, but not the less fermentable cellulose, leads to considerable increase in GLP-1 and PYY levels [28]. It is reported that intestinal enterocytes sense starch α-amylase digestion products, or maltooligosaccharides, to mobilize and activate the brush border α-glucosidase enzymes for glucose production [11]. In addition, a previous study showed a suppression of the hypothalamic

appetite-stimulating neuropeptides Neuropeptide Y (NPY) and Agouti-related peptide (AgRP) expression in obese rats fed slowly digestible starch that reached the ileum, and that this coincided with reduced food intake compared to rats fed a rapidly digestible starch [29]. Here, we are investigating another route to activate the endogenous release of GLP-1 and PYY based on starch digestion products that can reach the ileum where L-cells are abundant. Glucose was previously shown to trigger GLP-1 release in murine (GLUTage) [16] and human (NCI-H716) [30] L-cell lines. In addition to the role of glucose (or maltooligosaccharides), studies have shown that lipids and fatty acids induce higher levels of GLP-1 [31], but scarce information is available regarding the effect of lipids on PYY secretion [25]. Here, we hypothesized that starch degradation products that arrive in the ileum activate L-cells to secrete GLP-1, OXM, and PYY to affect appetitive response.

2.3 Materials and Methods

2.3.1 Cell Lines

2.3.1.1 STC-1 Cell Line (ATCC® CRL-3254™)

The STC-1 cell line is an adherent intestinal neuroendocrine tumor cells which are isolated from a C57B1/6J mice at ages between 10 to 13 weeks. The cells are isolated from the invasive small intestinal neuroendocrine carcinoma of RIP1Tag2/Rip2pyST1 double transgenic mice [5]. Double transgenic mice are developed by mating a transgenic mouse harboring a hybrid gene linking the rat insulin promoter (RIP) to the polyoma small T (PyST) antigen with another transgenic mouse harboring RIP linked to SV40 early region (Tag). The process results in an off-spring harboring both transgenes (double transgenics) [32]. The resulted double transgenic mice were found to have frequent intestinal tumors along with pancreatic β-cell tumors. Gene expression studies suggested that the intestinal and pancreatic tumors arose as separate entities. The STC-1

cell line was first characterized to produce the hormone secretin. STC-1 cells were found to have epithelial-like morphology that allows the use of these cells as a useful model for neuroendocrine neoplasms of the gastrointestinal tract, and are a valuable tool for studying gut hormone secretin [33]. In addition, STC-1 cells are used in the investigation of endocrine cell differentiation [34], neuroendocrine carcinomas [35] and intestinal immune response [36].

2.3.1.2 NCI-H716 [H716] Cell Line (ATCC® CCL-251™)

The NCI-H716 cell line is a suspension of multicell aggregates and some adherent cells that represent intestinal colorectal adenocarcinoma-derived cells. The cells were isolated from the cecum of a 33-year-old Caucasian male and have epithelial morphology. The line was derived from cells present in ascites fluid obtained from the patient after treatment with 5-fluorouracil. Interestingly, NCI-H716 in contrast to other colorectal lines, contains cytoplasmic dense core granules characteristic of endocrine secretion [37].

2.3.1.3 Caco-2 Cell Line (ATCC® HTB-37™)

The Caco-2 cell line is adherent epithelial cells which were isolated from the colon of a 72-year-old Caucasian male. The cells were isolated from a colorectal adenocarcinoma and have an epithelial-like morphology. Upon reaching confluence, the cells express characteristics of enterocyte differentiation [38].

2.3.2 Cell Culture Procedure

STC-1: STC-1 cells (passage 34 to 37) were cultured according to the protocol described by the American Type Culture Collection (ATCC) (Rockville, MD). Cells were grown in Dulbecco's Modified Eagle's Medium (DMEM) (Corning, Lowell, MA) supplemented with 10% heat-inactivated fetal bovine serum (FBS) (Lonza, Walkersville, MD), 10 mM 2-[4-(2-

hydroxyethyl) piperazin-1-yl] ethane sulfonic acid (HEPES) (Thermo Fisher Scientific, Waltham, MA), 100 μM non-essential amino acids (NEAA) (Corning, Lowell, MA), 100 U/ml pencelline and 100 μg/ml streptomycine (Lonza, Walkersville, MD), and 50 μg/ml gentamycine (J R Scientific Inc., Woodland, CA). Cultures were retained in AutoFlow NU-4750 Water Jacket CO_2 incubator (Nuaire, Plymouth, MN) which provides 5% CO_2, 95% humidity and 37°C. NCI-H716: NCI-H716 cells were purchased and cultured according to the protocol described by ATCC (Rockville, MD). Cells were grown in RPMI-1640 medium (ATCC 30-2001) supplemented with 10% heat-inactivated FBS (Lonza, Walkersville, MD), 10 mM HEPES (Thermo Fisher Scientific, Waltham, MA), 100 μM NEAA (Corning, Lowell, MA), 100 U/ml pencelline and 100 μg/ml streptomycine (Lonza, Walkersville, MD) and 50 μg/ml gentamycine (J R Scientific Inc., Woodland, CA). Cultures were retained in an AutoFlow NU-4750 Water Jacket CO_2 incubator (Nuaire, Plymouth, MN) which provides 5% CO_2, 95% humidity, and 37°C. NCI-H716 cells grow in suspension until ready for seeding in cell culture 6-well plates. Before seeding, plates were precoated with Matrigel® basement membrane matrix (Corning Inc., Corning, NY) to facilitate cell adherence and attachment. Caco-2 (HTB-37): Caco-2 cell line at passage (passage 28 to 37) were purchased from the ATCC (Rockville, MD) and maintained according to standard protocols. Cells were grown in DMEM (Corning, Lowell, MA) containing 25 mM glucose (Sigma, St. Louis, MO) and supplemented with 10% heat-inactivated FBS, 100 unit/ml penicillin, 100 μg/ml streptomycin, 2 mM L-glutamine, 50 μg/ml gentamycin sulfate, 10 mM HEPES (Thermo Fisher Scientific, Waltham, MA), and 100 μM NEAA (Thermo Fisher Scientific, Waltham, MA). Cultures were retained in an AutoFlow NU-4750 Water Jacket CO_2 incubator (Nuaire, Plymouth, MN) which provides 5% CO_2, 95% humidity and 37°C. Cells were grown until 100% confluence and allowed to fully differentiate to form a monolayer before experiment [39].

2.3.3 Maltooligosaccharide Treatment

Upon reaching 80% confluence (within 48 h of culturing), cells were treated with the following carbohydrates for 2h: 25 mM glucose, 25 mM maltose, 25 mM maltotriose, 25 mM isomaltotriose, 25 mM maltotetraose, 25 mM maltopentaose and 25 mM sodium propionate (all from Sigma, St. Louis, MO). 25 mM 2-deoxyglucose (Sigma, St. Louis, MO) was used in some of the experiments as a negative control to GLP-1 and OXM secretion. Treatments were dissolved in Dulbecco's Phosphate-Buffered Saline (DPBS) containing calcium chloride and magnesium chloride (Sigma # 806544) and sterilized using Steriflip-GV Sterile Centrifuge Tube Top 0.22 µm filter (MilliporeSigma, Burlington, MA). A blank control was cells that were treated with pure DPBS vehicle without any solutes dissolved in it. After treatment incubation time, the supernatant media was collected rapidly into cold tubes containing DPPVI inhibitor and aprotinin (both from MilliporeSigma, Burlington, MA). The collected media was then centrifuged at 1500 rpm for 5 min at 4 ºC to remove any residual cells in the solution. The supernatant was then transferred rapidly into new tubes, flash-frozen into liquid nitrogen, and stored at -80 °C until analysis. The attached cells were rinsed twice with cold DPBS and rapidly treated with 500 µl of NP40 cell lysis buffer (Thermo Fisher Scientific, Waltham, MA) containing protease inhibitor (Sigma, St. Louis, MO), DPPVI inhibitor (MilliporeSigma, Burlington, MA) and phenylmethylsulfonyl fluoride (PMSF) (Sigma, St. Louis, MO). The lysate was left on ice for 30 min before centrifugation at 14,000 rpm for 10 min. The supernatant was then aliquoted and flash-frozen into liquid nitrogen until analysis.

2.3.4 Hormone Analysis

GLP-1 was measured in the culture media after cell incubation using the GLP-1 (Active) (Human, Rat, Mouse) ELISA kit (MilliporeSigma, Burlington, MA; Catalog # EGLP-35K).

Oxyntomodulin was measured in the culture media using the Oxyntomodulin (Human, Rat, Mouse) EIA Kit (Phoenix Pharmaceuticals, Burlingame, CA; Catalog # EK-028-22). PYY was measured in the culture media after cell incubation using the Mouse/Rat PYY ELISA kit (ALPCO, Macedon, NY; Catalog # 48-PYYRT-E01.). Cellular protein content was determined in cell lysate using Pierce™ BCA Protein Assay Kit (Thermo Fisher Scientific, Waltham, MA) and used to estimate total GLP-1 by ρM per µg cellular protein (ρM/µg protein).

2.3.5 Quantitative Realtime PCR

2.3.5.1 mRNA Isolation

All used equipment for RNA isolation was guaranteed to be RNAase-free by autoclaving at 121°C for 30 min, whipping with RNaseZap® RNase Decontamination Solution (Thermo Fisher Scientific, Waltham, MA), and rinsing with diethylpyrocarbonate, 0.1% v/v water (DEPC H_2O) (Sigma, St. Louis, MO). Treated cells were washed twice with DPBS and collected for cell lysis using RNeasy Mini Kit lysis buffer. Cell lysate was applied to a QIAshredder (Qiagen, Netherlands) for complete homogenization. Total RNA was extracted using a RNeasy Plus Mini Kit for cells/tissues (Qiagen, Netherlands; Catalog # 74134). RNA was collected in RNAase free water and isolated RNA was measured by Nanodrop (Thermo Fisher Scientific, Waltham, MA). RNA quality was confirmed by A260/A280 and A260/A230 ratios equal or higher than 2 (Thermo Scientific T042-technical bulletin).

2.3.5.2 cDNA Synthesis and qRT- PCR Analysis

Relative levels of the mRNA of proglucagon, PYY, CCK, prohormone convertase1/3 (PC1/3) and prohormone convertase 2 (PC 2) in STC-1 RNA were quantified by reverse transcription and Real-Time Quantitative Reverse Transcription PCR (qRT-PCR). TURBO DNA-free™ Kit (Thermo Fisher Scientific, Waltham, MA) was used for DNase treatment. cDNA

synthesis was done using High-Capacity cDNA Reverse Transcription Kit (Applied Biosystems, Foster City, CA). cDNA was diluted 5-fold with nuclease-free water before performing a qRT-PCR reaction using CFX Connect™ Real-Time PCR Detection System (BioRad, Hercules, CA). SYBR-green (BioRad, Hercules, CA) protocol was used with specific primers for each target gene. Primers were designed using the National Center for Biotechnology Information (NCBI) website that uses Primer-BLAST tool [40]. Primers for the internal genes (β-actin and GAPDH) were used. GenBank BLAST and global alignment algorithm were used to match primer sequences to their corresponding mouse full-length sequences. Sequence of the used primers (Sigma, St. Louis, MO) are represented in Table 2.1.

2.3.6 Trans-epithelial Electrical Resistance (TEER)

Caco-2 cells of passage #37 were seeded into the insert of 12-well trans-wells and cultured for 21 days as described in section 2.2.2 to confirm monolayer differentiation. After 21 days, barrier integrity of the Caco-2 monolayers was monitored by measuring TEER. Measurements were conducted before each experiment, using EMD Millicell ERS2 instrument (Millipore, Bedford, MA), to confirm full differentiation. Values between 500-600 ohm × cm2 were confirmed to be achieved before applying any experimental treatments. TEER of Caco-2 monolayers treated with 25 mM glucose, 25 mM maltose, 25 mM maltotriose and 25 mM maltotetraose were monitored using the cellZscope Original instrument. Cell inserts were transferred into the cellZscope wells and glucose, maltose, maltotriose and maltotetraose were added to glucose-free, sodium pyruvate-free DMEM buffer for 80 h where TEER and the capacitance (Ccl) were automatically measured every 2 h.

2.3.7 Statistical Analysis

Statistical analysis was conducted using SAS 9.4 (SAS Institute Inc., Cary, NC). We used generalized linear model with one-way analysis of variance (ANOVA) followed by pairwise comparison of treatments by Tukey's test. Statistical differences were evaluated at $p < 0.05$. Data shown represent average values and standard error of the mean (Mean ± SEM).

2.4 Results

One of the unique characteristics observed for STC-1 mouse cell line, is its strong ability to secrete GLP-1 under varying conditions [33]. The glucose-free DMEM culture media were found to be stimulator to STC-1 cells, and amino acids such as glutamine, valine, lysine and glycine have been reported to trigger GLP-1 release in STC-1 cells [33]. Therefore, choosing the vehicle buffer for dissolving treatments is an important factor. Figure 2.1 shows the effect of using different incubation buffers on GLP-1 concentration (ρmoles) [33]. We choose to use DPBS buffer as Phosphate-Buffered Saline (PBS) showed the higher difference in GLP-1 levels between control and nutrient treatments incubated for 3 h. From different independent experiments, we observed that $CaCl_2$ and $MgCl_2$ are required for the adherence and integrity of the cells during the treatment incubation periods. Therefore, we used DPBS supplemented with $CaCl_2$ and $MgCl_2$ as treatment vehicle for experiments with STC-1 and NCI-H716 cell lines. Figure 2.2 shows the total GLP-1 secreted from STC-1 cells at different incubation time points. We chose to incubate STC-1 cells for 2 h for the hormone secretion assays and for 90 minutes for the relative mRNA expression analysis to compromise between the significant response, observed at the longer time points, and the stress that may be applied to the cells with the glucose-free treatments.

2.4.1 GLP-1 Secretion From STC-1 Cell Line

STC-1 cells were able to release GLP-1 in the blank control vehicle, DPBS, (0.28 ± 0.05 ρM/μg protein; 42% compared to glucose). Although we did not detect an increase in GLP-1 release levels in cells treated with 25 mM maltose (0.77 ± 0.2 ρM/μg protein; 104.4 % compared to glucose), treatment with 25 mM of maltotriose or 25 mM of maltotetraose showed an average increase of released GLP-1 compared to glucose by 183.2 % and 185.7 % respectively. Treatment of 25 mM of maltopentaose (1.38 ± 0.2 ρM/μg protein) showed an average increase of 256.8% of released GLP-1 compared to glucose (0.74 ± 0.15 ρM/μg protein) (Figure 2.3). 2-Deoxy glucose has been used [30] as a negative control in GLP-1 release assays in cell culture systems, and here only 80.4 % (0.47 ± 0.13 ρM/μg protein) of GLP-1 secretion compared to glucose was observed. Sodium propionate (25 mM) showed similar GLP-1 release to the negative control, 2-deoxy glucose (0.45 ± 0.11 ρM/μg protein; 81.1 % compared to glucose).

2.4.2 STC-1 Cells and MOS Digestion

It was necessary to test if STC-1 cells have the capacity to digest maltooligosaccharides, as no information was available on STC-1 cell lines regarding whether they can express α-glucosidase enzymes to breakdown MOS into glucose for cell consumption. After 2 h incubation with maltose, maltotriose and sucrose, no glucose levels were observed in the culture media of cells treated with any of these three treatments (Figure 2.4).

2.4.3 The Involvement of Sweet Taste Receptor in STC-1 Stimulation

We used the mouse specific sweet taste inhibitor [41], [42], *p*-nitrophenyl α-D-glucopyranoside, to examine the potential role of STC-1 naturally-expressed sweet taste receptor [43] in the observed GLP-1 stimulation. Here we showed that sweet taste receptor inhibitor did not affect GLP-1 release by MOS. Contrary, the used sweet taste receptor inhibitor shows a slight

increase in the stimulation of GLP-1 release. Glucose (25 mM) with the addition of 20 μM of *p*-nitrophenyl α-D-glucopyranoside increased GLP-1 levels in the culture media by 131.5% compared to 25 mM glucose treatment alone (Figure 2.5). The addition effect was even higher with 25 mM maltose treatment where GLP-1 levels were increased by 182.7% compared to glucose in the presence of sweet taste receptor inhibitor. The addition of sweet taste receptor inhibitor to 25 mM maltotriose treatment increased GLP-1 levels from 183.2% compared to glucose in the case of maltotriose treatment alone to 220% compared to glucose in the case of maltotriose with 20 μM p-nitrophenyl α-D-glucopyranoside. Therefore, we suggest that the sweet taste receptor inhibitor did not affect GLP-1 release in STC-1 cells treated with MOS, but unexpectedly showed slight increase in GLP-1 release with all treatments including the glucose control.

2.4.4 Oxyntomodulin Secretion From NCI-H716 Cell Line

Oxyntomodulin (OXM) is another important product of the proglucagon gene that share the function, the location and the pancreatic β-cell binding receptor with GLP-1[44]. However, OXM is still hitherto neglected as important glucose- and appetite-regulating gut hormone [45]. Data of OXM release (ng/ml) from NCI-H716 human L-cell line with MOS are represented in Figure 2.6. Similar to the release of GLP-1 from the STC-1 mouse cells, NCI-H716 human cells released OXM in the blank control vehicle, DPBS, (1.9 ± 0.37 ng/ml). We observed a more than two-fold increase in the level of oxyntomodulin with the treatment of 25 mM maltotriose (8.4 ± 0.67 ng/ml) compared to glucose treated NCI-H716 cells (3.4 ± 0.28 ng/ml) (Figure 2.6). Also, treatment with 25 mM maltotetraose and 25 mM maltopentaose showed a stimulatory effect on oxyntomodulin release compared to glucose (5.7 ± 0.61 ng/ml and 4.4 ± 0.35 ng/ml, respectively). The increase observed in OXM release with maltotriose was statistically significant (at $\alpha = 0.05$)

compared to that of all other tested treatments. Maltose treatment did not show any increase in oxyntomodulin secretion over glucose (2.4 ± 0.62 ng/ml). Moreover, and similar to the observations in GLP-1 secretion assay, sodium propionate did not show an increase in oxyntomodulin level over glucose (3.5 ± 0.03 ng/ml). Instead, the stimulatory effects of glucose (3.4 ± 0.28 ng/ml) and sodium propionate (3.5 ± 0.03 ng/ml) were similar to that of the negative control 2-deoxy glucose (3.3 ± 0.2 ng/ml).

2.4.5 PYY Secretion From STC-1 Cell Line

Consistent with literature, peptide YY levels in most available L-cell lines were hard to be detected even though PYY is normally co-localized with GLP-1 in *in vivo* L-cells [46]. However, we were able to measure low levels of PYY in the cell culture media of STC-1 cells in picograms. Data of PYY release (ρg/ml) from STC-1 cells with maltose and maltotriose compared to propionate treatment are represented in Figure 2.7. The increase in PYY release with propionate treatment was statistically significant (at $\alpha = 0.05$) compared to all the other tested treatments. Interestingly, glucose did not show any stimulation effect on PYY release (12.8 ± 2.8 ρg/ml) over the vehicle control, and sodium propionate showed the highest stimulatory effect on PYY release in the culture media with a concentration of 43.7 ± 4.5 ρg/ml. The concentration of PYY in the culture media of the blank control vehicle, DPBS, treated cells was 16.9 ± 2.0 ρg/ml compared to 12.8 ± 2.8 ρg/ml in cells treated with 25 mM glucose. Contrary to this trend, 25 mM of maltose slightly increased the release of PYY to a concentration of 28.8 ± 5.3 ρg/ml, whereas maltotriose stimulated the release of PYY to a concentration of 17.3 ± 1.8 ρg/ml.

2.4.6 Relative mRNA Expression of Proglucagon, PYY and CCK genes in STC-1 Cells

Data of the relative expression of the proglucagon gene (the precursor of GLP-1 and OXM) in cells treated with 25 mM of glucose, maltose, maltotriose, maltotetraose and maltopentaose as

well as in STC-1 cells treated with the vehicle (DPBS) are represented in Figure 2.8. Relative expression was normalized to the housekeeping gene encoding glyceraldehyde 3-phosphate dehydrogenase (GAPDH). We couldn't detect a significant difference in the expression fold change between cells treated with DPBS, maltose, maltotriose and maltopentaose, although a slight increase was observed with maltose treatment in most of the biological replicates. Cells treated with glucose and maltotriose showed a significant reduction (at $\alpha = 0.05$) compared to other treatments in the relative expression of the proglucagon gene. Similarly, data of relative expression of the PYY gene (Figure 2.9) didn't show significant differences between any of the treatments. Another independent experiment was performed using the β-actin gene to normalize the proglucagon and PYY relative expression and didn't show any significant difference between STC-1 cells treated with glucose or maltotriose (Figure 2.10 (A and B)). However, cells treated with 25 mM maltotriose exhibited 5-fold increase in CCK expression over that of cells treated with 25 mM glucose (Figure 2.10 (C)).

2.4.7 Relative mRNA Expression of PC1/3 and PC2 in STC-1 Cells

The mRNA relative expression of the PC 1/3 and PC 2 genes was tested in STC-1 cells to investigate the involvement of the prohormone convertase family in the regulation in GLP-1 levels in this cell line by altering post-translational alternative spicing. Data of the mRNA relative expression of the PC 1/3 gene normalized to the relative expression of GAPDH and β-actin are represented in Figure 2.11 and Figure 2.12, respectively. The data didn't represent significant difference between the different treatments when normalized either to the GAPDH or to the β-actin housekeeping genes. Data of the mRNA relative expression of the PC 2 gene of cells treated with either 25 mM glucose or 25 mM maltotriose normalized to the relative expression of β-actin are

represented in Figure 2.13. Similarly, the data didn't represent significant difference between cells treated with glucose compared to cells treated with maltotriose.

2.4.8 Trans-epithelial Electrical Resistance (TEER)

The effect of maltose, maltotriose and maltotetraose treatment on the integrity of enterocyte monolayer was examined using the measurement of the trans-epithelial/-endothelial resistance (TEER) of Caco-2 differentiated monolayer cultured on trans-well inserts. Data of TEER and the capacitance (Ccl) values of Caco-2 monolayers incubated for 78 h with 25 mM glucose-containing DMEM compared to that of cells incubated with glucose-free DMEM are represented in Figure 2.14. As expected, the glucose-free DMEM b started to disrupt the monolayer integrity after 22 h recognized by the reduction in the TEER values ($\Omega.cm^2$) and the increase in the capacitance values ($\mu F/cm^2$) by 34 h. Cells treated with 25 mM maltose for 78 h didn't show differences from cells treated with the glucose control in the TEER values (Figure 2.15). However, cell treated with 25 mM maltotriose and 25 mM maltotetraose showed small, but detectable increase in the TEER values over the incubation time (Figure 2.16 and Figure 2.17).

2.5 Discussion and Conclusions

Although animal models used for gut hormone secretion studies can provide more relevant and physiologically representative sense of the broad biology of gut hormone release pathways, *in vitro* cell culture models provide more specific information about the direct and indirect effects of different nutrients or drugs on cell function. Enteroendocrine cell culture models also facilitate the investigation of the basic molecular mechanisms coupling stimulus to secretion [46]. Starting from around 1990, when three GLP-1 secreting cell lines were developed (GLUTag [6], STC-1 [47], and NCI-H716 [7]), many of the hypothesized mechanisms behind GLP-1 secretion and L-cell

response have been revealed. In the current study we used the STC-1 cell line, which was isolated from a mouse small intestine tumor, and NCI-H716 which is from ascites fluid of humans with colon tumors [32], [5], [48] to study L-cell response to dietary MOS.

We observed STC-1 cells to produce GLP-1 in high quantities and under different conditions. Even the composition of the recommended culture media (DMEM) was found to have a number of stimulators to GLP-1 release including the amino acids and proteins of the media. McCarthy *et al*., 2015, showed that different incubation buffers have high effect on GLP-1 release from STC-1 cell line as shown in Figure 2.1 [33]. DPBS was used in the current study for its mild effect on cells during incubation time and supplemented with $CaCl_2$ and $MgCl_2$ for the integrity of cell adhesion and attachment. We observed that the absence of calcium chloride and magnesium chloride during treatment incubation caused increased cell stress, detachment and death. However, these observations were eliminated by using DPBS buffer supplemented with $CaCl_2$ and $MgCl_2$. STC-1 cells were confirmed to not breakdown the provided MOS into glucose. This was an important factor that affects both cell viability and data interpretation, as the production of glucose would have favored cell viability and reduced cell stress and produced glucose would be a confounding factor to the sensing of carbohydrate structure by L-cells. The inability of STC-1 cells to produce glucose from MOS provided a good way to test the chemosensation hypothesis, and concurrently to limit treatment incubation time, as cells would not be provided required glucose. An incubation time of 2 hours was chosen for hormonal assays as suggested by McCarthy *et al*., 2015 [33] for optimal incubation time with monosaccharides. In addition, we chose an incubation time of 1.5 hour for mRNA expression experiments.

Here we report, for the first time, a sensing behavior in the STC-1 L-cells to carbohydrate structures larger than glucose and in a manner independent of SGLT1 co-transporter. As a possible

candidate for maltotriose and maltotetraose sensing, the sweet taste receptor was tested as a possible sensor, as has been described in early studies for small intestine enterocytes [49]. STC-1 cells have been reported to express the sweet taste receptor [43]. In an experiment where cells were co-incubated with 20 μM of *p*-nitrophenyl α-D-glucopyranoside, a well-described sweet taste inhibitor in mouse cells [42], GLP-1 secretion was conversely increased when exposed to glucose, maltose, and maltotriose. Thus, the sweet taste inhibitor did not prevent the stimulation effects of MOS.

The most common GLP-1 release hypothesis in enteroendocrine L-cells is sensing related to the SGLT1 co-transporter [14], [50], [51]. Shima *et al.*, 1990 was the first to report the possibility of carbohydrate sensing through a unique receptor that could recognize canonical molecular characteristics [10] to stimulate a signaling pathway that ends up with exocytosis of the GLP-1-included vesicle from the basolateral side of L-cells. However, in 2002 sweet taste receptors, that naturally exist in the oral cavity taste buds, was reported to be expressed in the small intestine as well as in the STC-1 cell line [52]. This fact suggested that the sweet taste receptor heterodimer expressed within the intestinal tract could be the mechanism for glucose-stimulated GLP-1 secretion. It was reported that, distal small intestine L-cells can express a T1R3-included receptor with a similar structure to sweet taste receptor which, upon glucose activation, facilitates the release of L-cell hormones [16], [53], [49]. Brown *et al*., 2009 and Gerspach *et al*., 2011 reported an important role of the sweet taste receptor in GLP-1 secretion [54], [55]. However, the results reported here are not interpretable with SGLT1 or the sweet taste receptor hypotheses of the glucose stimulatory effect on L-cell hormone release.

We hypothesize here, for the first time, of a new type of carbohydrate sensing mechanism that is independent from sweet taste receptor and that is affected by α-glucan structure size. The

observation that maltopentaose provided further higher release of GLP-1 compared to maltotriose and maltopentaose suggests that the effect appears to be due to the structure/size of the molecules and not due to accumulating glucose content, since we confirmed the absence of any digestion ability of the cells to breakdown these oligomers to glucose.

Remarkably, all MOS showed considerably stronger effect on GLP-1 release compared to sodium propionate. Short chain fatty acids (SCFA) (acetate, butyrate and propionate) had been identified as a strong activator of L-cells [56], [57]. The production of SCFA is mainly appears in the large intestine due to fiber fermentation by colon microbial community. The release of SCFA in the colon is an important regulator of energy and immunity in the body [58]. With the fact that the number of L-cells are increasing throughout the gastrointestinal tract and toward the distal intestine with the highest intensity in the distal small intestine [59], [60], [61], explains the importance of SCFA in L-cell stimulation. However, preliminary studies we conducted with the STC-1 system did not show strong triggering with acetate and butyrate. Propionate showed the highest response among SCFA. Therefore, we used propionate as a candidate of prospective SCFA effects. Our results are showing for the first time that specific types of starch digestion products, especially the larger structure with higher degree of polymerization, can be superior to SCFA in their effects on L-cells stimulation (Figure 2.3 and Figure 2.6). This raise the importance of sustainable and slow-digestible carbohydrates in providing beneficial physiological outcomes. A recent report showed a significant loss in OXM secretion in patients with type II diabetes, compared to 10-fold increase in blood OXM levels after gastric bypass surgery for those patients [62]. Although we couldn't detect measurable levels of OXM in the STC-1 cell line, we were able to show significant response of OXM in the human line, NCI-H716, after MOS treatment (Figure 2.6). These findings was consistent with a recent study indicated that the GluTag and NCI-H716

cell lines, but not STC-1 cell line, are the useful models for OXM stimulation studies [46]. The observed trend for OXM release was similar to that observed for GLP-1. Maltotriose, maltotetraose and maltopentaose showed higher statistically significant (at $\alpha = 0.05$) stimulation effect compared to glucose or propionate. Maltotriose showed the most statistically significant (at $\alpha = 0.05$) superior stimulation effect between the different MOS.

Interestingly, the ability of the used L-cell models to secret PYY was controversial. Geraedts *et al*., 2009 were the first to show that STC-1 cells can release PYY in response to short and long fatty acids [63]. On the other hand, Kuhre *et al*., 2016 reported that none of the available L-cell models can secrete PYY [46]. In the current study, we were able to detect PYY secretion in the STC-1 cell line, but not the NCI-H716, in low concentrations of picograms. Unlike the trend observed with GLP-1 and OXM peptides, the highest stimulator for PYY was sodium propionate (25 mM) followed by 25 mM of maltose. Our explanation of these results is that the used L-cell models could possess selective stimulatory mechanisms where larger MOS are highly stimulating toward GLP-1 (in case of STC-1 cells) and OXM (in case of NCI-H716 cells) whereas SCFA are highly stimulating toward PYY (in case of STC-1 cells). We recommend that unique stimulation ability of MOS on L-cells works toward the proglucagon gene products but not PYY. This suggestion is in accordance with a recent report of Larraufie *et al*., 2018 showing that propionate and butyrate dramatically augmented the expression of PYY but not the proglucagon gene in NCI-H716 and intestinal primary culture [56]. However, these results were observed only n the human-derived cells and the mouse-derived cells [56] which is the opposite to the findings of the current study.

To investigate whether the observed stimulation effects of MOS on GLP-1 release are mediated by positive regulation of the proglucagon gene (gcg) expression, we tested the mRNA

relative expression of the gcg gene in STC-1 cells treated with MOS compared to glucose and vehicle control. No statistically significant differences (at $\alpha = 0.05$) were observed between different treatments except for significant increase in gcg expression with maltose when compared to that of glucose and maltotetraose. Similarly, no statistically significant differences were observed in PYY expression with MOS treatment. Interestingly, STC-1 cells treated with maltotriose showed higher average relative gene expression of the CCK gene compared to cells treated with glucose, although not statistically significant at ($\alpha = 0.05$) with $P = 0.1105$.

As described in Chapter I, proglucagon undergo differential post-translational modification in the pancreas, the brain or the intestine through the act of the prohormone convertase 1/3 (PC1/3) and prohormone convertase 2 (PC 2) enzymes [64], [65]. As we didn't detect a significant or explainable trend in the relative expression of the proglucagon gene, we investigated the hypothesis that altering the post-translational modification processes could be the mechanism by which MOS enhance GLP-1 and OXM levels. However, no statistical differences were observed in the relative expression of PC 1/3 or PC 2 with MOS treatment. Putting these findings together strongly recommend that MOS exhibit their effects through the induction of exocytosis of GLP-1-containing vesicle and not through a positive regulation of the proglucagon gene expression. These data suggest that MOS induce higher secretion, but not higher synthesis, of the proglucagon gene products (mainly GLP-1 and OXM).

Finally, we examined the potential enhancing effects of MOS on intestinal barrier integrity and cell tight junctions. A better model for this purpose, is the Caco-2 cell line which provides, after proper differentiation on trans-wells, a monolayer that could be used to study barrier function, permeability and paracellular transport. Maltotriose and maltotetraose showed small but detectable improvement in TEER values throughout the 78 h of treatment. Although the treatment with

glucose-free DMEM alone started to cause monolayer disruption by 22 h which is an expected response due to the lack of energy or carbon source, cells treated with maltose, maltotriose or maltotetraose didn't show any indication of monolayer disruption measured by a reduction in the TEER values. This suggests that even with the insignificant improvement over cells treated with glucose, cells treated with MOS protected Caco-2 monolayer from disruption due to lack of glucose.

2.6 References

[1] R. M. Elliott, L. M. Morgan, J. A. Tredger, S. Deacon, J. Wright, and V. Marks, "Glucagon-like peptide-1 (7-36)amide and glucose-dependent insulinotropic polypeptide secretion in response to nutrient ingestion in man: acute post-prandial and 24-h secretion patterns.," *J. Endocrinol.*, vol. 138, no. 1, pp. 159–66, Jul. 1993.

[2] J. N. Roberge and P. L. Brubaker, "Secretion of proglucagon-derived peptides in response to intestinal luminal nutrients.," *Endocrinology*, vol. 128, no. 6, pp. 3169–74, Jun. 1991.

[3] S. H. Jacobsen *et al.*, "Changes in Gastrointestinal Hormone Responses, Insulin Sensitivity, and Beta-Cell Function Within 2 Weeks After Gastric Bypass in Non-diabetic Subjects," *Obes. Surg.*, vol. 22, no. 7, pp. 1084–1096, Jul. 2012.

[4] R. E. Kuhre, C. R. Frost, B. Svendsen, and J. J. Holst, "Molecular Mechanisms of Glucose-Stimulated GLP-1 Secretion From Perfused Rat Small Intestine," *Diabetes*, vol. 64, pp. 370–382, 2015.

[5] G. Rindi *et al.*, "Development of Neuroendocrine Tumors in the Gastrointestinal Tract of Transgenic Mice Heterogeneity of Hormone Expression," 1990.

[6] D. J. Drucker, T. Jin, S. L. Asa, T. A. Young, and P. L. Brubaker, "Activation of proglucagon gene transcription by protein kinase-A in a novel mouse enteroendocrine cell line.," *Mol. Endocrinol.*, vol. 8, no. 12, pp. 1646–1655, Dec. 1994.

[7] A. P. de Bruïne *et al.*, "NCI-H716 cells as a model for endocrine differentiation in colorectal cancer.," *Virchows Arch. B. Cell Pathol. Incl. Mol. Pathol.*, vol. 62, no. 5, pp. 311–20, 1992.

[8] F. Reimann, A. M. Habib, G. Tolhurst, H. E. Parker, G. J. Rogers, and F. M. Gribble, "Glucose sensing in L cells: a primary cell study.," *Cell Metab.*, vol. 8, no. 6, pp. 532–9, Dec. 2008.

[9] R. Pais, F. M. Gribble, and F. Reimann, "Stimulation of incretin secreting cells.," *Ther. Adv. Endocrinol. Metab.*, vol. 7, no. 1, pp. 24–42, Feb. 2016.

[10] K. Shima, T. Suda, K. Nishimoto, and S. Yoshimoto, "Relationship between molecular structures of sugars and their ability to stimulate the release of glucagon-like peptide-1 from canine ileal loops.," *Acta Endocrinol. (Copenh).*, vol. 123, no. 4, pp. 464–70, Oct. 1990.

[11] K. Sugiyama, H. Manaka, T. Kato, K. Yamatani, M. Tominaga, and H. Sasaki, "Stimulation of truncated glucagon-like peptide-1 release from the isolated perfused canine ileum by glucose absorption.," *Digestion*, vol. 55, no. 1, pp. 24–8, 1994.

[12] U. Ritzel, A. Fromme, M. Ottleben, U. Leonhardt, and G. Ramadori, "Release of glucagon-like peptide-1 (GLP-1) by carbohydrates in the perfused rat ileum," *Acta Diabetol.*, vol. 34, no. 1, pp. 18–21, Apr. 1997.

[13] E. M. Wright, "Renal Na(+)-glucose cotransporters," *Am. J. Physiol. Physiol.*, vol. 280, no. 1, pp. F10–F18, Jan. 2001.

[14] F. M. Gribble, L. Williams, A. K. Simpson, and F. Reimann, "A Novel Glucose-Sensing Mechanism Contributing to Glucagon-Like Peptide-1 Secretion From the GLUTag Cell Line," 2003.

[15] R. Moriya, T. Shirakura, J. Ito, S. Mashiko, and T. Seo, "Activation of sodium-glucose cotransporter 1 ameliorates hyperglycemia by mediating incretin secretion in mice," *Am J Physiol Endocrinol Metab*, vol. 297, pp. 1358–1365, 2009.

[16] R. F. Margolskee *et al.*, "T1R3 and gustducin in gut sense sugars to regulate expression of Na-glucose cotransporter 1," 2007.

[17] P. D. Cani, S. Hoste, Y. Guiot, and N. M. Delzenne, “Dietary non-digestible carbohydrates promote L-cell differentiation in the proximal colon of rats,” 2007.

[18] D. R. Powell *et al.*, “LX4211 Increases Serum Glucagon-Like Peptide 1 and Peptide YY Levels by Reducing Sodium/Glucose Cotransporter 1 (SGLT1)-Mediated Absorption of Intestinal Glucose,” *J. Pharmacol. Exp. Ther. J Pharmacol Exp Ther*, vol. 345, pp. 250–259, 2013.

[19] H. E. Parker *et al.*, “Predominant role of active versus facilitative glucose transport for glucagon-like peptide-1 secretion.”

[20] R. E. Kuhre *et al.*, “Fructose stimulates GLP-1 but not GIP secretion in mice, rats, and humans Effects of Fructose on Gut Hormone Secretion in Humans,” *Am J Physiol Gastrointest Liver Physiol*, vol. 306, pp. 622–630, 2014.

[21] H. D. Tamara Zietek, “Intestinal nutrient sensing and blood glucose control,” *Curr. Opin. Clin. Nutr. Metab. Care*, vol. 18, no. 4, pp. 381–388, Jul. 2015.

[22] S. Zac-Varghese, A. De Silva, and S. R. Bloom, “Translational studies on PYY as a novel target in obesity,” *Curr. Opin. Pharmacol.*, vol. 11, pp. 582–585, 2011.

[23] K. Dungan and J. B. Buse, “Glucagon-Like Peptide 1-Based Therapies for Type 2 Diabetes: A Focus on Exenatide,” *Clin. Diabetes*, vol. 23, no. 2, pp. 56–62, Apr. 2005.

[24] G. E. Lim and P. L. Brubaker, “Glucagon-Like Peptide 1 Secretion by the L-Cell: The View From Within,” *Diabetes*, vol. 55, no. Supplement 2, pp. S70–S77, Dec. 2006.

[25] K. V. Hand *et al.*, “Examining acute and chronic effects of short- and long-chain fatty acids on peptide YY (PYY) gene expression, cellular storage and secretion in STC-1 cells,” *Eur. J. Nutr.*, vol. 52, no. 4, pp. 1303–1313, Jun. 2013.

[26] S. Janssen and I. Depoortere, “Nutrient sensing in the gut: new roads to therapeutics?,” *Trends Endocrinol. Metab.*, vol. 24, pp. 92–100, 2013.

[27] J. Zhou *et al.*, “Dietary resistant starch upregulates total GLP-1 and PYY in a sustained day-long manner through fermentation in rodents.,” *Am. J. Physiol. Endocrinol. Metab.*, vol. 295, no. 5, pp. E1160-6, Nov. 2008.

[28] M.-W. Cheng *et al.*, “Different sucrose-isomaltase response of Caco-2 cells to glucose and maltose suggests dietary maltose sensing.,” *J. Clin. Biochem. Nutr.*, vol. 54, no. 1, pp. 55–60, Jan. 2014.

[29] L. Y. Hasek *et al.*, “Dietary Slowly Digestible Starch Triggers the Gut-Brain Axis in Obese Rats with Accompanied Reduced Food Intake,” *Mol. Nutr. Food Res.*, vol. 62, no. 5, p. 1700117, Mar. 2018.

[30] H.-J. Jang *et al.*, “Gut-expressed gustducin and taste receptors regulate secretion of glucagon-like peptide-1.,” *Proc. Natl. Acad. Sci. U. S. A.*, vol. 104, no. 38, pp. 15069–74, Sep. 2007.

[31] G. Tolhurst *et al.*, “Short-Chain Fatty Acids Stimulate Glucagon-Like Peptide-1 Secretion via the G-Protein-Coupled Receptor FFAR2,” *Diabetes*, vol. 61, pp. 364–371, 2012.

[32] S. G. N. Grant, I. Seidman, D. Hanahan, and V. L. Baiiteli’, “Early Invasiveness Characterizes Metastatic Carcinoid Tumors in Transgenic Mice1,” 1991.

[33] T. McCarthy, B. D. Green, D. Calderwood, A. Gillespie, J. F. Cryan, and L. Giblin, “STC-1 Cells,” in *The Impact of Food Bioactives on Health*, Cham: Springer International Publishing, 2015, pp. 211–220.

[34] C. Ratineau *et al.*, “Intestinal-type fibroblasts selectively influence proliferation rate and peptide synthesis in the murine entero-endocrine cell line STC-1,” *Differentiation*, vol. 62, no. 3, pp. 139–147, Dec. 1997.

[35] J. Bollard *et al.*, “Antitumor effect of everolimus in preclinical models of high-grade gastroenteropancreatic neuroendocrine carcinomas.,” *Neuroendocrinology*, vol. 97, no. 4, pp. 331–40, 2013.

[36] M. Palazzo *et al.*, “Activation of enteroendocrine cells via TLRs induces hormone, chemokine, and defensin secretion.,” *J. Immunol.*, vol. 178, no. 7, pp. 4296–303, Apr. 2007.

[37] J.-G. Park *et al.*, “Characteristics of Cell Lines Established from Human Colorectal Carcinoma1,” 1987.

[38] C. Jumarie and C. Malo, “Caco-2 cells cultured in serum-free medium as a model for the study of enterocytic differentiation in vitro,” *J. Cell. Physiol.*, vol. 149, no. 1, pp. 24–33, Oct. 1991.

[39] M. Le Gall, V. Tobin, E. Stolarczyk, V. Dalet, A. Leturque, and E. Brot-Laroche, “Sugar sensing by enterocytes combines polarity, membrane bound detectors and sugar metabolism,” *J. Cell. Physiol.*, vol. 213, no. 3, pp. 834–843, Dec. 2007.

[40] J. Ye, G. Coulouris, I. Zaretskaya, I. Cutcutache, S. Rozen, and T. L. Madden, “Primer-BLAST: A tool to design target-specific primers for polymerase chain reaction,” 2012.

[41] A. Niki, H. Niki, and T. Hashioka, “An inhibitor of sweet taste response inhibits glucose-induced insulin release,” 1989.

[42] V. Vlahopoulos and W. Jakinovich, “Antagonism of the gerbil’s sucrose taste response by p-nitrophenyl alpha-D-glucopyranoside and chloramphenicol.,” *J. Neurosci.*, vol. 6, no. 9, pp. 2611–5, Sep. 1986.

[43] I. Kojima and Y. Nakagawa, “The Role of the Sweet Taste Receptor in Enteroendocrine Cells and Pancreatic β-Cells.,” *Diabetes Metab. J.*, vol. 35, no. 5, pp. 451–7, Oct. 2011.

[44] F. G. A. Baldissera, J. J. Holst, S. Knuhtsen, L. Hilsted, and O. V. Nielsen, “Oxyntomodulin (glicentin-(33–69)): pharmacokinetics, binding to liver cell membranes, effects on isolated perfused pig pancreas, and secretion from isolated perfused lower small intestine of pigs,” *Regul. Pept.*, vol. 21, no. 1–2, pp. 151–166, May 1988.

[45] A. Pocai, “Action and therapeutic potential of oxyntomodulin,” *Mol. Metab.*, vol. 3, no. 3, pp. 241–251, Jun. 2014.

[46] R. E. Kuhre *et al.*, “Peptide production and secretion in GLUTag, NCI-H716, and STC-1 cells: a comparison to native L-cells,” *J. Mol. Endocrinol.*, vol. 56, no. 3, pp. 201–211, Apr. 2016.

[47] M. Cordier-Bussat *et al.*, “Peptones stimulate both the secretion of the incretin hormone glucagon-like peptide 1 and the transcription of the proglucagon gene.,” *Diabetes*, vol. 47, no. 7, pp. 1038–45, Jul. 1998.

[48] Y. C. Lee, S. L. Asa, and D. J. Drucker, “Glucagon gene 5’-flanking sequences direct expression of simian virus 40 large T antigen to the intestine, producing carcinoma of the large bowel in transgenic mice.,” *J. Biol. Chem.*, vol. 267, no. 15, pp. 10705–8, May 1992.

[49] J. B. Furness, L. R. Rivera, H.-J. Cho, D. M. Bravo, and B. Callaghan, “The gut as a sensory organ,” *Nat. Rev. Gastroenterol. Hepatol.*, vol. 1010, no. 1212, pp. 729–740, Sep. 2013.

[50] V. Gorboulev *et al.*, “Na(+)-D-glucose cotransporter SGLT1 is pivotal for intestinal glucose absorption and glucose-dependent incretin secretion.,” *Diabetes*, vol. 61, no. 1, pp. 187–96, Jan. 2012.

[51] H. Ogata *et al.*, “KATP channel as well as SGLT1 participates in GIP secretion in the diabetic state,” *J. Endocrinol.*, vol. 222, no. 2, pp. 191–200, Aug. 2014.

[52] S. V. Wu, N. Rozengurt, M. Yang, S. H. Young, J. Sinnett-Smith, and E. Rozengurt, “Expression of bitter taste receptors of the T2R family in the gastrointestinal tract and enteroendocrine STC-1 cells.,” *Proc. Natl. Acad. Sci. U. S. A.*, vol. 99, no. 4, pp. 2392–7, Feb. 2002.

[53] M. C. P. Geraedts *et al.*, “Transformation of postingestive glucose responses after deletion of sweet taste receptor subunits or gastric bypass surgery,” *Am. J. Physiol. Metab.*, vol. 303, no. 4, pp. E464–E474, Aug. 2012.

[54] R. J. Brown, M. Walter, and K. I. Rother, “Ingestion of Diet Soda Before a Glucose Load Augments Glucagon-Like Peptide-1 Secretion,” 2009.

[55] A. C. Gerspach, R. E. Steinert, L. Schönenberger, A. Graber-Maier, and C. Beglinger, “The role of the gut sweet taste receptor in regulating GLP-1, PYY, and CCK release in humans,” *Am J Physiol Endocrinol Metab*, vol. 301, pp. 317–325, 2011.

[56] P. Larraufie *et al.*, “SCFAs strongly stimulate PYY production in human enteroendocrine cells.,” *Sci. Rep.*, vol. 8, no. 1, p. 74, 2018.

[57] T. U. Greiner and F. Bäckhed, “Microbial regulation of GLP-1 and L-cell biology,” *Mol. Metab.*, vol. 5, no. 9, pp. 753–758, Sep. 2016.

[58] D. J. Morrison and T. Preston, “Formation of short chain fatty acids by the gut microbiota and their impact on human metabolism,” *Gut Microbes*, vol. 7, no. 3, p. 189, 2016.

[59] L. I. Larsson, J. Holst, R. Håkanson, and F. Sundler, “Distribution and properties of glucagon immunoreactivity in the digestive tract of various mammals: an immunohistochemical and immunochemical study.,” *Histochemistry*, vol. 44, no. 4, pp. 281–90, Sep. 1975.

[60] R. Eissele *et al.*, “Glucagon-like peptide-1 cells in the gastrointestinal tract and pancreas of rat, pig and man.,” *Eur. J. Clin. Invest.*, vol. 22, no. 4, pp. 283–91, Apr. 1992.

[61] E. Spreckley and K. G. Murphy, “The L-cell in nutritional sensing and the regulation of appetite,” *Front. Nutr.*, vol. 2, p. 23, 2015.

[62] N. J. Wewer Albrechtsen *et al.*, “Oxyntomodulin Identified as a Marker of Type 2 Diabetes and Gastric Bypass Surgery by Mass-spectrometry Based Profiling of Human Plasma,” *EBioMedicine*, vol. 7, pp. 112–120, May 2016.

[63] M. C. P. Geraedts, F. J. Troost, and W. H. M. Saris, “Peptide-YY Is Released by the Intestinal Cell Line STC-1,” *J. Food Sci.*, vol. 74, no. 2, pp. H79–H82, Mar. 2009.

[64] D. J. DRUCKER, J. PHILIPPE, and S. MOJSOV, “Proglucagon Gene Expression and Posttranslational Processing in a Hamster Islet Cell Line*,” *Endocrinology*, vol. 123, no. 4, pp. 1861–1867, Oct. 1988.

[65] S. Mojsov, G. Heinrich, I. B. Wilson, M. Ravazzola, L. Orci, and J. F. Habener, “Preproglucagon gene expression in pancreas and intestine diversifies at the level of post-translational processing.,” *J. Biol. Chem.*, vol. 261, no. 25, pp. 11880–9, Sep. 1986.

Table 2.1 RT-PCR primers and the sequences of forward and reverse primers.

Gene	(Forward) 5'-3'	(Reverse) 5'-3'
Proglucagon	GATCATTCCCAGCTTCCCAG	CTGGTAAAGGTCCCTTCAGC
PYY	AGCGGTATGGGAAAAGAGAAGTC	ACCACTGGTCCACACCTTCTG
CCK	GCA CTG CTA GCG CGA TAC ATC	CCA GGC TCT GCA GGT TCT TAA
PC1/3	AGGTGAAATTGCCATGCAAGCA	GGCCAGGGTTGAATCCAATTGA
PC 2	AATGGGAAGACGGTTGATGGGC	GCCGTCACAGTTGCAGTCATCG
GAPDH	TGCACCACCAACTGCTTAGC	GGCATGGACTGTGGTCATGAG
β-actin	CGGTTCCGATGCCCTGAGGCTCTT	CGTCACACTTCATGATGGAATTGA

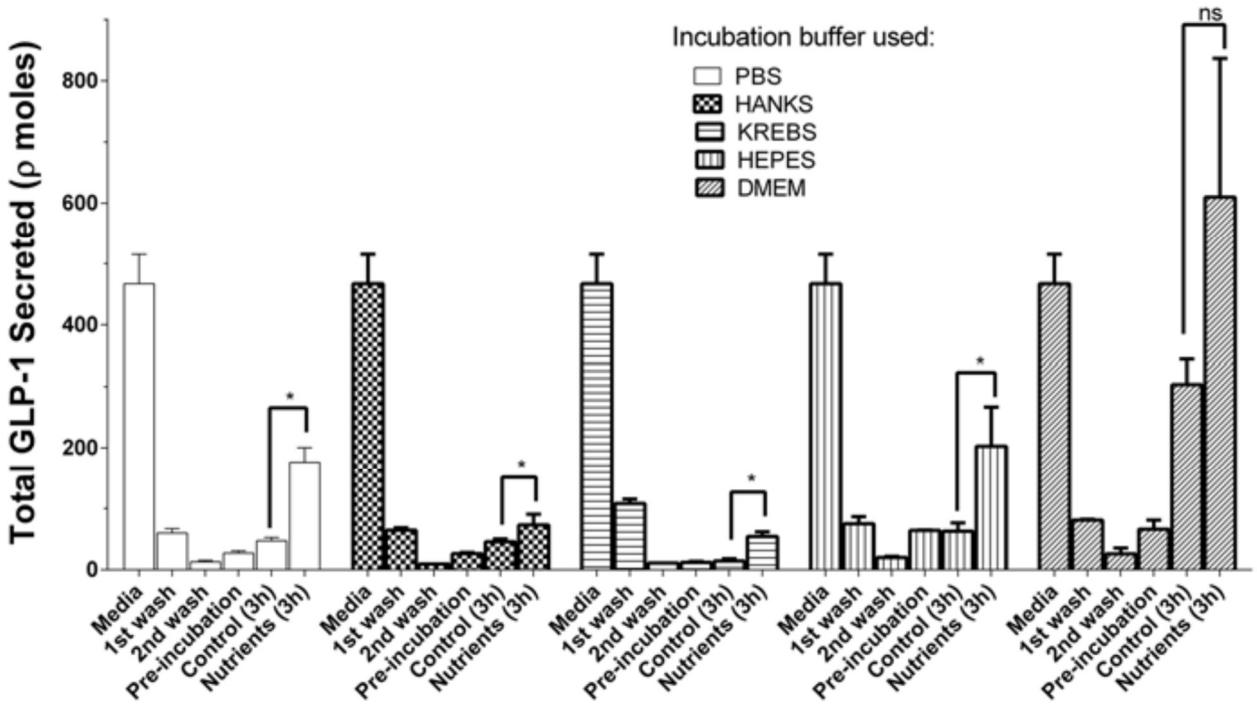

Figure 2.1 Effect of different incubation buffers on total GLP-1 levels secreted from the mouse endocrine L-cells (STC-1). Data are taken from McCarthy *et al*., 2015 [33]. Nutrient mixture is composed of 40 mM of each of the following; glutamine, valine, lysine, glycine, glucose and fructose. Nutrients were dissolved in Phosphate-Buffered Saline (PBS), Hank's Balanced Salt Solution (HANKS), Krebs-Ringer Bicarbonate Buffer (KREBS), 4-(2-hydroxyethyl)-1-piperazineethanesulfonic acid buffer (HEPES) or Dulbecco's Modified Eagle Medium (DMEM) (GlutaMAX, GIBCO, Paisley, UK). Buffer composition is as follows; PBS (136.9 mM NaCl, 2.7 mM KCl, 10.1 mM Na_2HPO_4, 1.8 mM KH_2PO_4), HANKS (136.9 mM NaCl, 5.4 mM KCl, 1.3 mM $CaCl_2$, 1 mM $MgSO_4$, 0.2 mM $NaHPO_4$, 0.4 mM KH_2PO_4, 4.2 mM $NaHCO_3$, 5.6 mM glucose), KREBS (118 mM NaCl, 4.7 mM KCl, 25 mM $NaHCO_3$, 1.25 mM $CaCl_2$, 1.2 mM $MgSO_4$, 1.2 mM KH_2PO_4, 11 mM glucose) and HEPES (140 mM NaCl, 4.5 mM KCl, 1.2 mM $CaCl_2$, 1.2 mM $MgCl_2$, 20 mM HEPES). STC-1 cells were incubated with buffers and media for 3h. Significant differences are indicated on the graph (*$P < 0.05$).

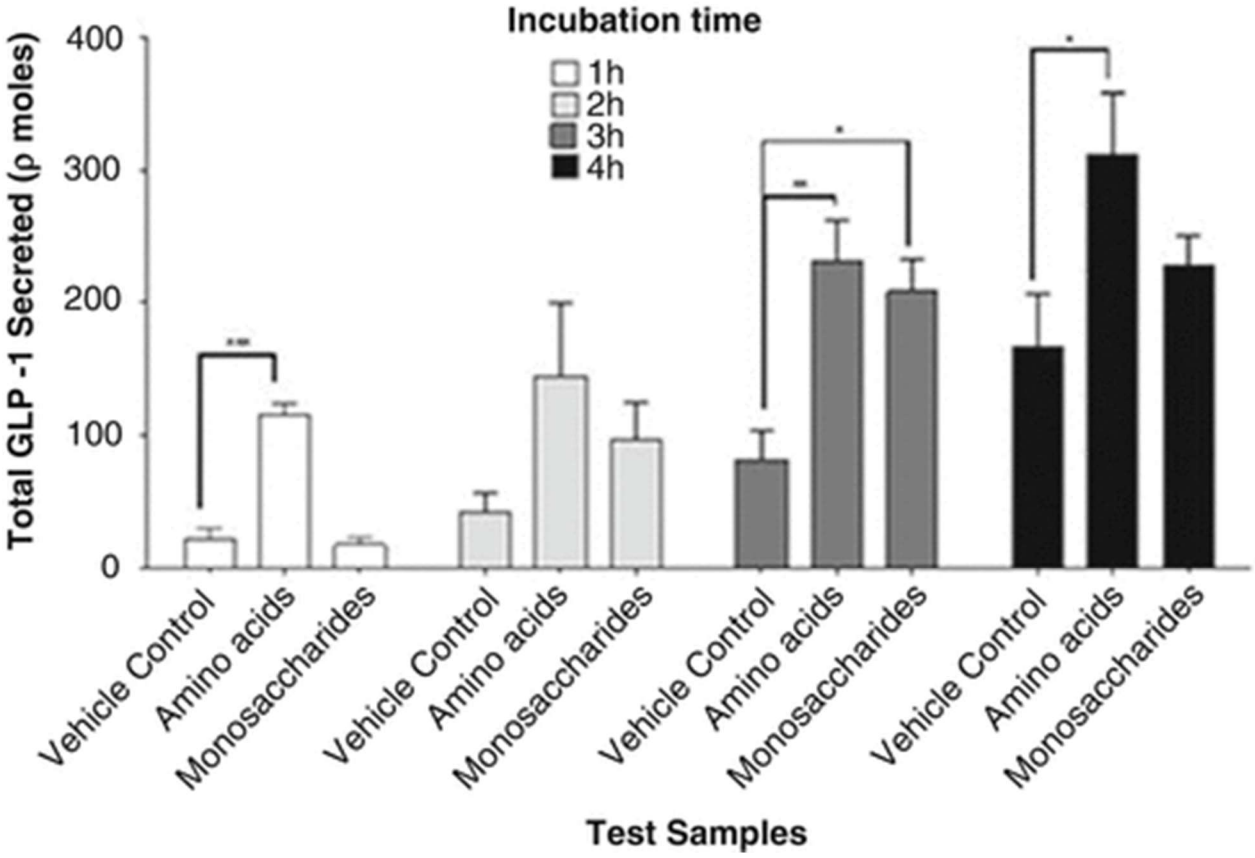

Figure 2.2 Total GLP-1 secreted from the mouse endocrine L-cell line (STC-1) at different incubation time points. Data are taken from McCarthy *et al*., 2015 [33]. STC-1 cells were triggered by amino acid solution composed of 40 mM of each of the following; glutamine, valine, lysine and glycine in HEPES buffer or monosaccharide solution composed of 40 mM glucose and 40 mM fructose in HEPES buffer. Data were statistically compared using the unpaired Student's t-test and significant differences to vehicle controls are indicated *$P < 0.05$, **$P < 0.01$ and ***$P < 0.001$.

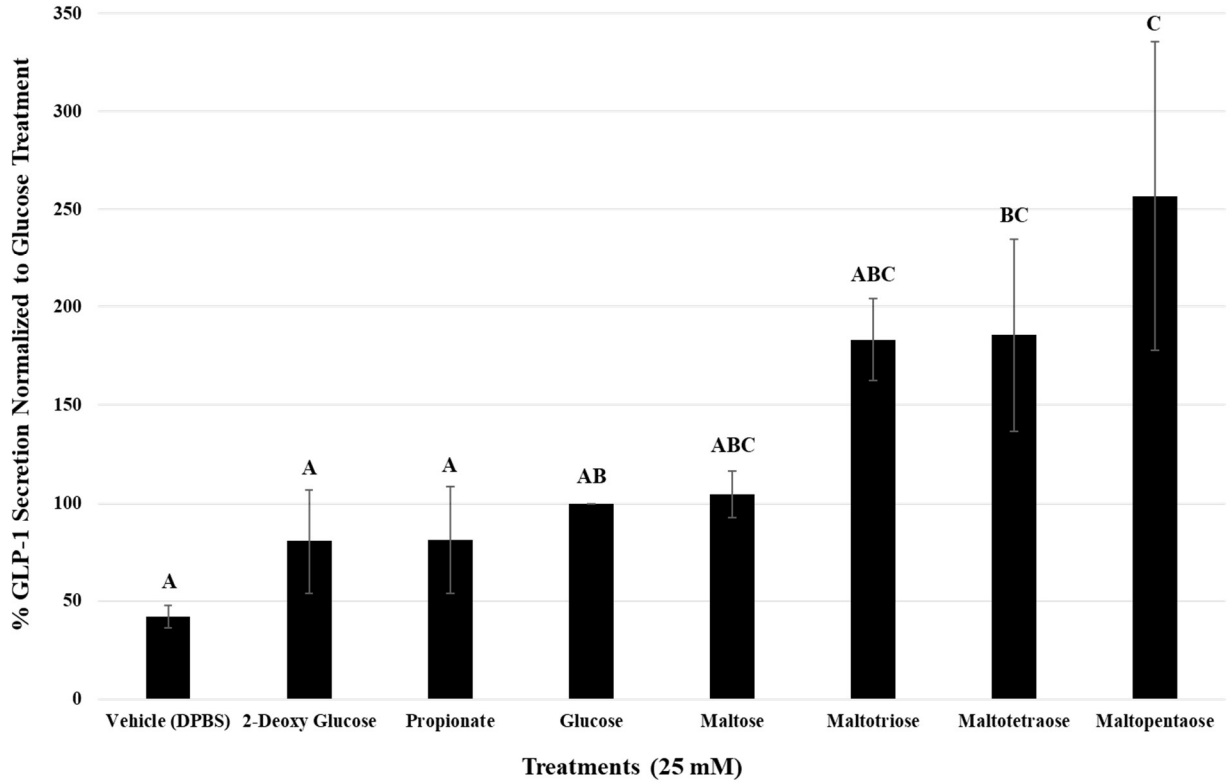

Figure 2.3 Maltooligosaccharides of DP 3-5 induced higher GLP-1 secretion in the mouse endocrine L-cells (STC-1) compared to glucose, maltose, 2-deoxy glucose and propionate. Values are the average of nine biological replicates from three independent experiments (n=9). Results are normalized to 100% with glucose treatment for better comparison. Bars represent standard error of the mean (Mean ± SEM). Vehicle represent the Dulbecco's Phosphate-Buffered Saline (DPBS) buffer solution used to dissolve treatments. Different letters denote statistically significant differences between treatments at α=0.05 based on Tukey's least squares means for treatment effect.

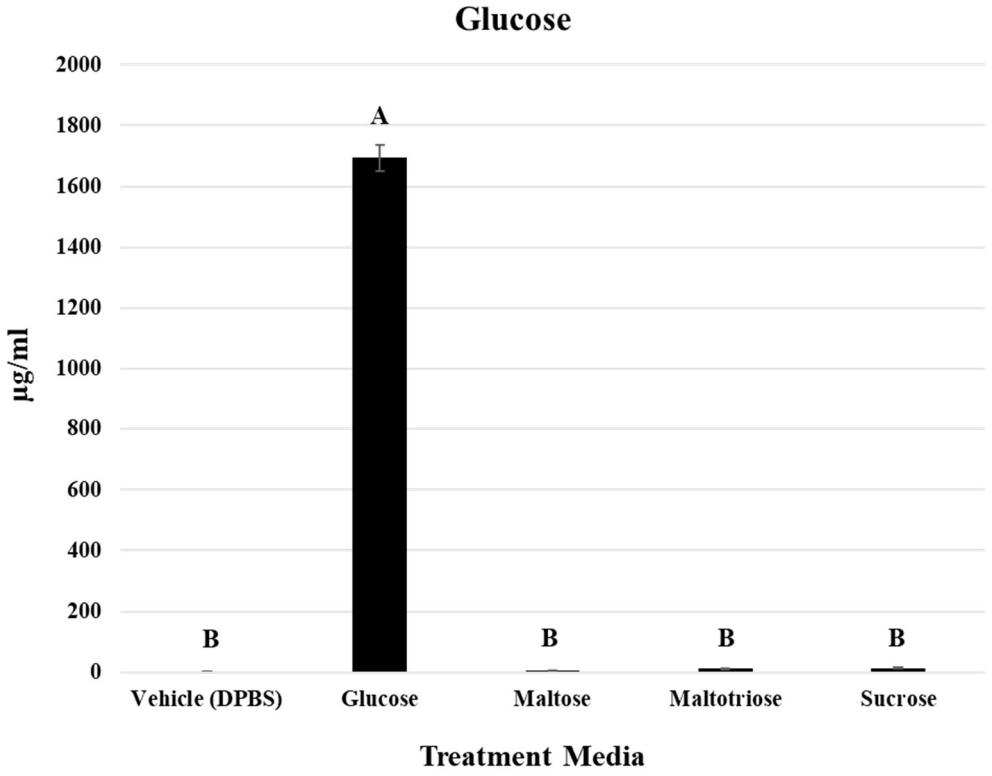

Figure 2.4 STC-1 cells do not digest maltose, maltotriose or sucrose into glucose units. Vehicle represent the Dulbecco's Phosphate-Buffered Saline (DPBS) buffer solution used to dissolve treatments. Values are the average of four biological replicates (n=4). Bars represent standard error of the mean (Mean ± SEM). Different letters denote statistically significant differences between treatments at α=0.05 based on Tukey's least squares means for treatment effect.

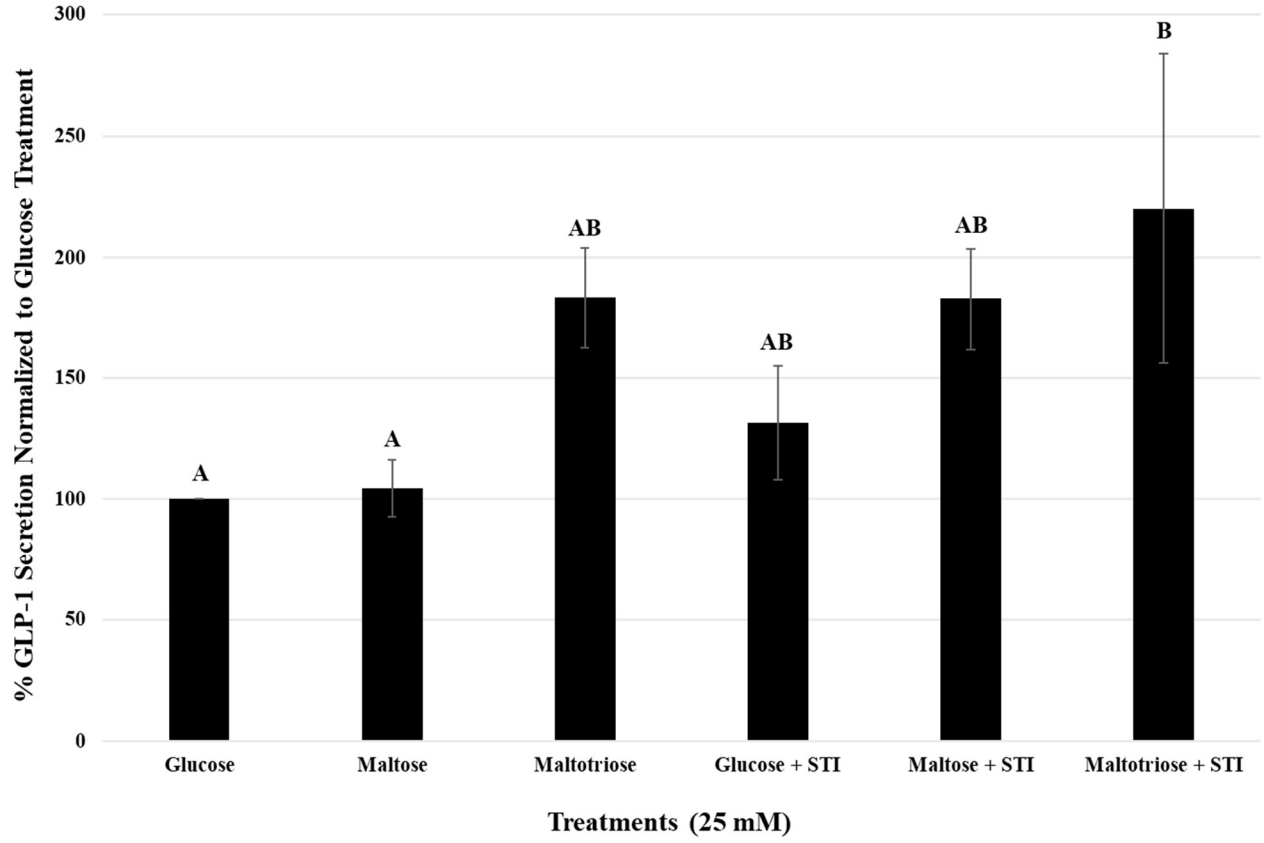

Figure 2.5 The stimulation effect of MOS on STC-1 cells to release GLP-1 is independent of the sweet taste receptor. STI: Sweet Taste Inhibitor to mouse cells (*p*-nitrophenyl α-D-glucopyranoside). Vehicle represent the Dulbecco's Phosphate-Buffered Saline (DPBS) buffer solution used to dissolve treatments. Values are the average of six biological replicates from two independent experiments (n=6). Results are normalized to 100% with glucose treatment for better comparison. Bars represent standard error of the mean (Mean ± SEM). Different letters denote statistically significant differences between treatments at α=0.05 based on Tukey's least squares means for treatment effect.

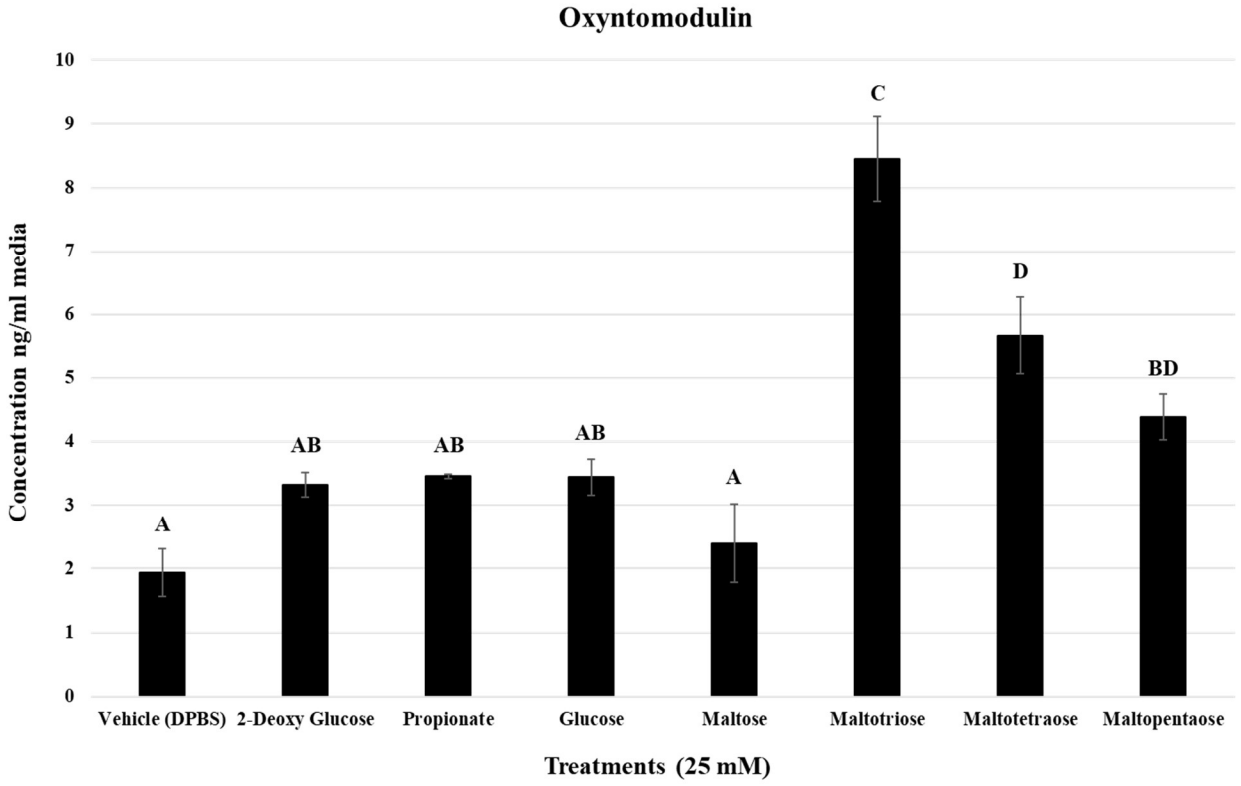

Figure 2.6 MOS of DP 3-5 promoted the human enteroendocrine L-cells (NCI-H716) toward higher secretion of oxyntomodulin. Values are the average of four biological replicates (n=4). Bars represent standard error of the mean (Mean ± SEM). Vehicle represent the Dulbecco's Phosphate-Buffered Saline (DPBS) buffer solution used to dissolve treatments. Different letters denote statistically significant differences between treatments at $\alpha=0.05$ based on Tukey's least squares means for treatment effect.

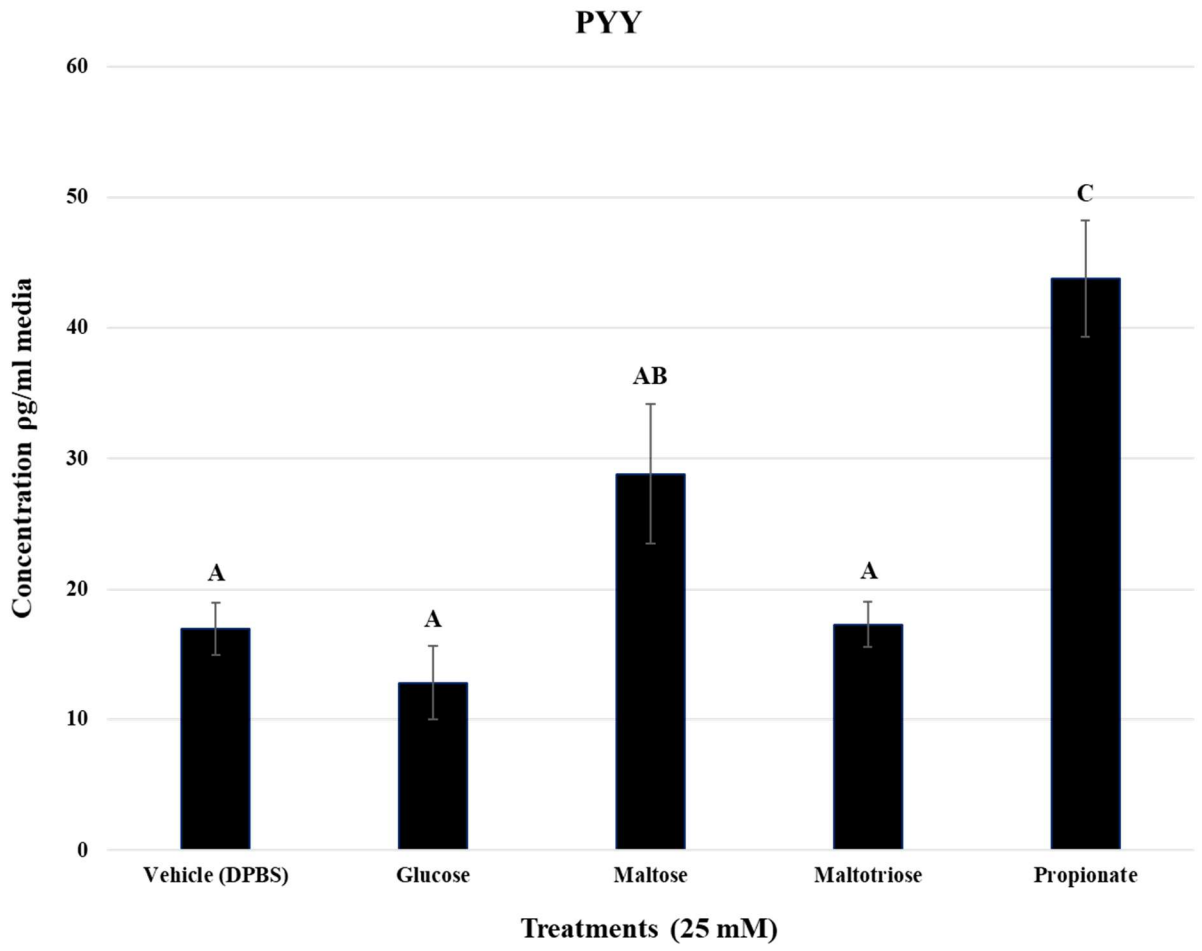

Figure 2.7 PYY concentration (ρg/ml) in cell culture media of STC-1 cells treated with MOS. Cells were treated with 25 mM glucose, 25 mM maltose, 25 mM maltotriose and 25 mM sodium propionate. Vehicle represent the Dulbecco's Phosphate-Buffered Saline (DPBS) buffer solution used to dissolve treatments. Values are the average of three biological replicates (n=3). Bars represent standard error of the mean (Mean ± SEM). Different letters denote statistically significant differences between treatments at α=0.05 based on Tukey's least squares means for treatment effect.

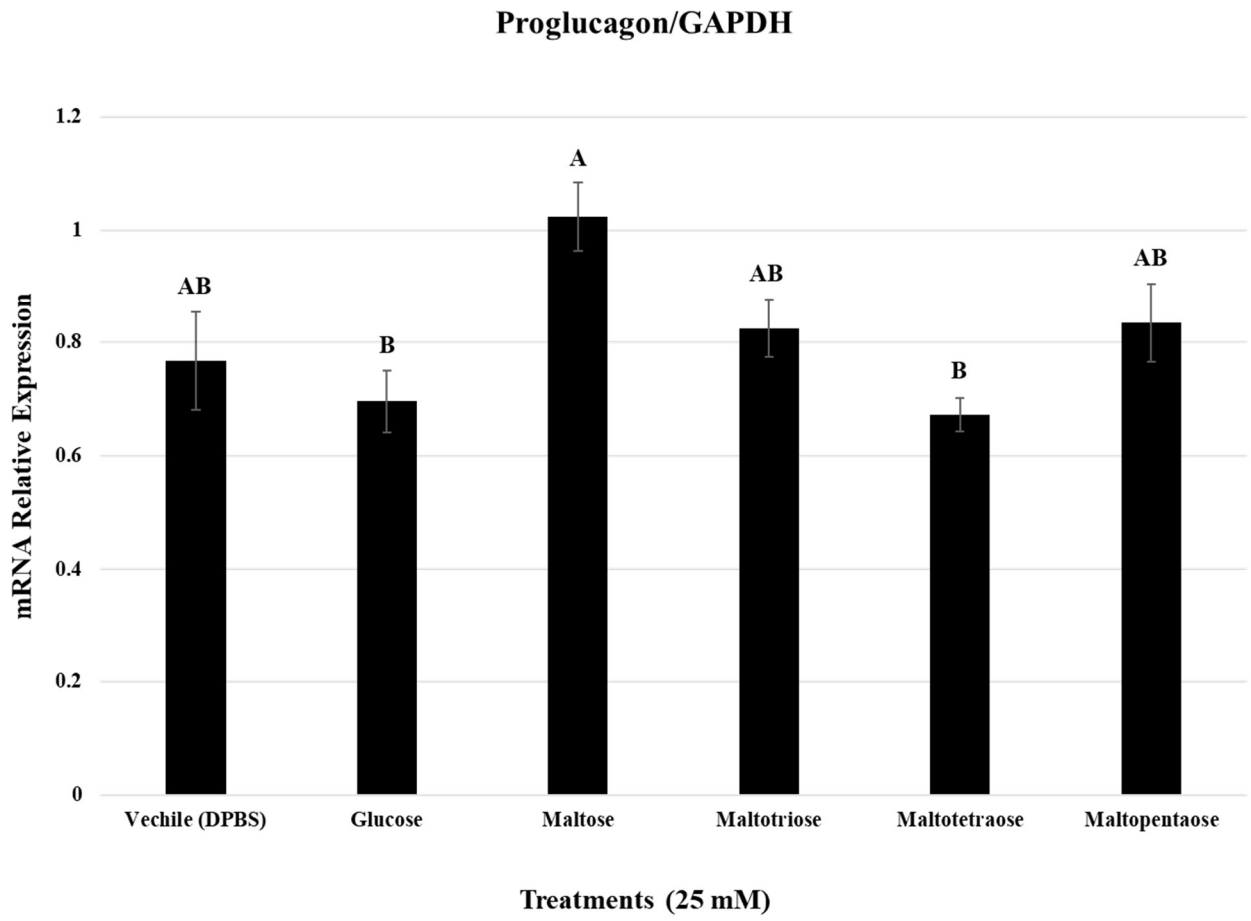

Figure 2.8 mRNA relative expression of the proglucagon gene in STC-1 cells treated with MOS. Cells were treated with 25 mM glucose, 25 mM maltose, 25 mM maltotriose, 25 mM maltotetraose and 25 mM maltopentaose for 90 minutes. Vehicle represent the Dulbecco's Phosphate-Buffered Saline (DPBS) buffer solution used to dissolve treatments. The mRNA relative expression was normalized to glyceraldehyde 3-phosphate dehydrogenase (GAPDH) expression. Values are the average of five biological replicates with 2 technical replicates for each biological replicate (n=5). Bars represent standard error of the mean (Mean ± SEM). Different letters denote statistically significant differences between treatments at α=0.05 based on Tukey's least squares means for treatment effect.

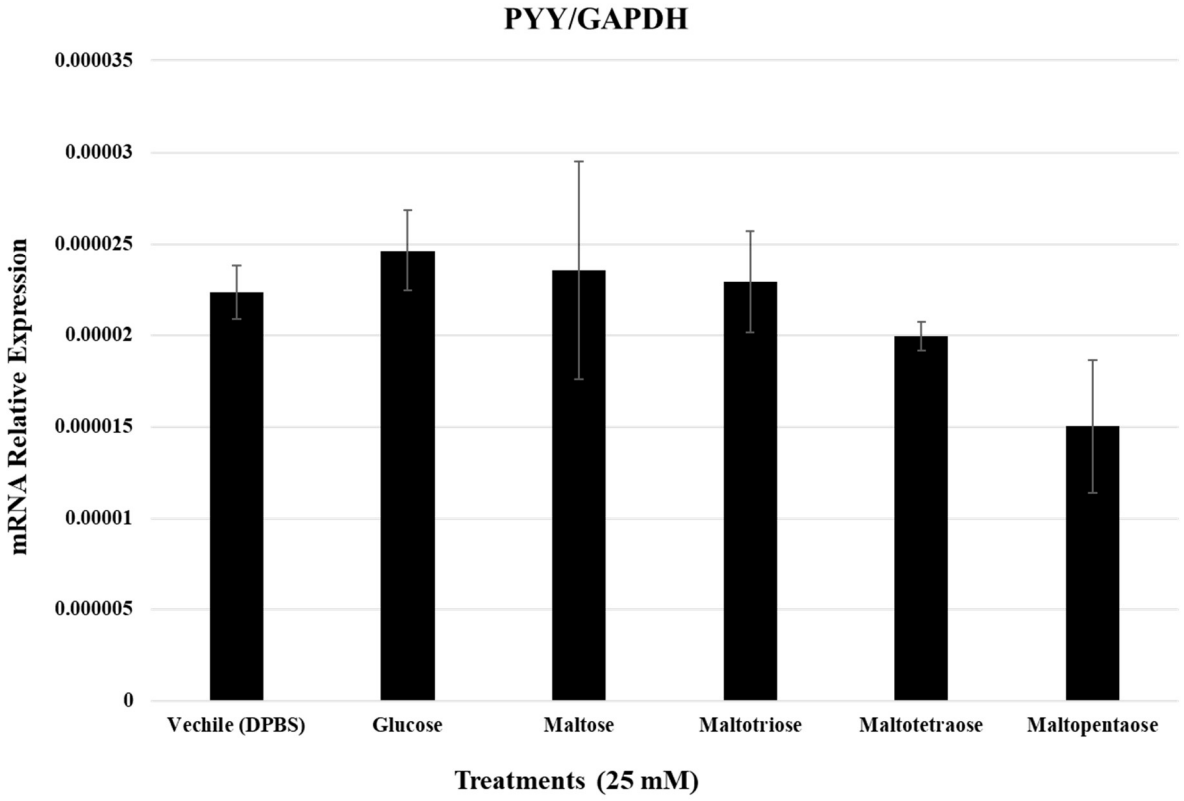

Figure 2.9 mRNA relative expression of the PYY gene in STC-1 cells treated with MOS. Cells were treated with 25 mM glucose, 25 mM maltose, 25 mM maltotriose, 25 mM maltotetraose and 25 mM maltopentaose for 90 minutes. Vehicle represent the Dulbecco's Phosphate-Buffered Saline (DPBS) buffer solution used to dissolve treatments. The mRNA relative expression was normalized to glyceraldehyde 3-phosphate dehydrogenase (GAPDH) expression. Values are the average of five biological replicates with 2 technical replicates for each biological replicate (n=5). Bars represent standard error of the mean (Mean ± SEM). Different letters denote statistically significant differences between treatments at α=0.05 based on Tukey's least squares means for treatment effect.

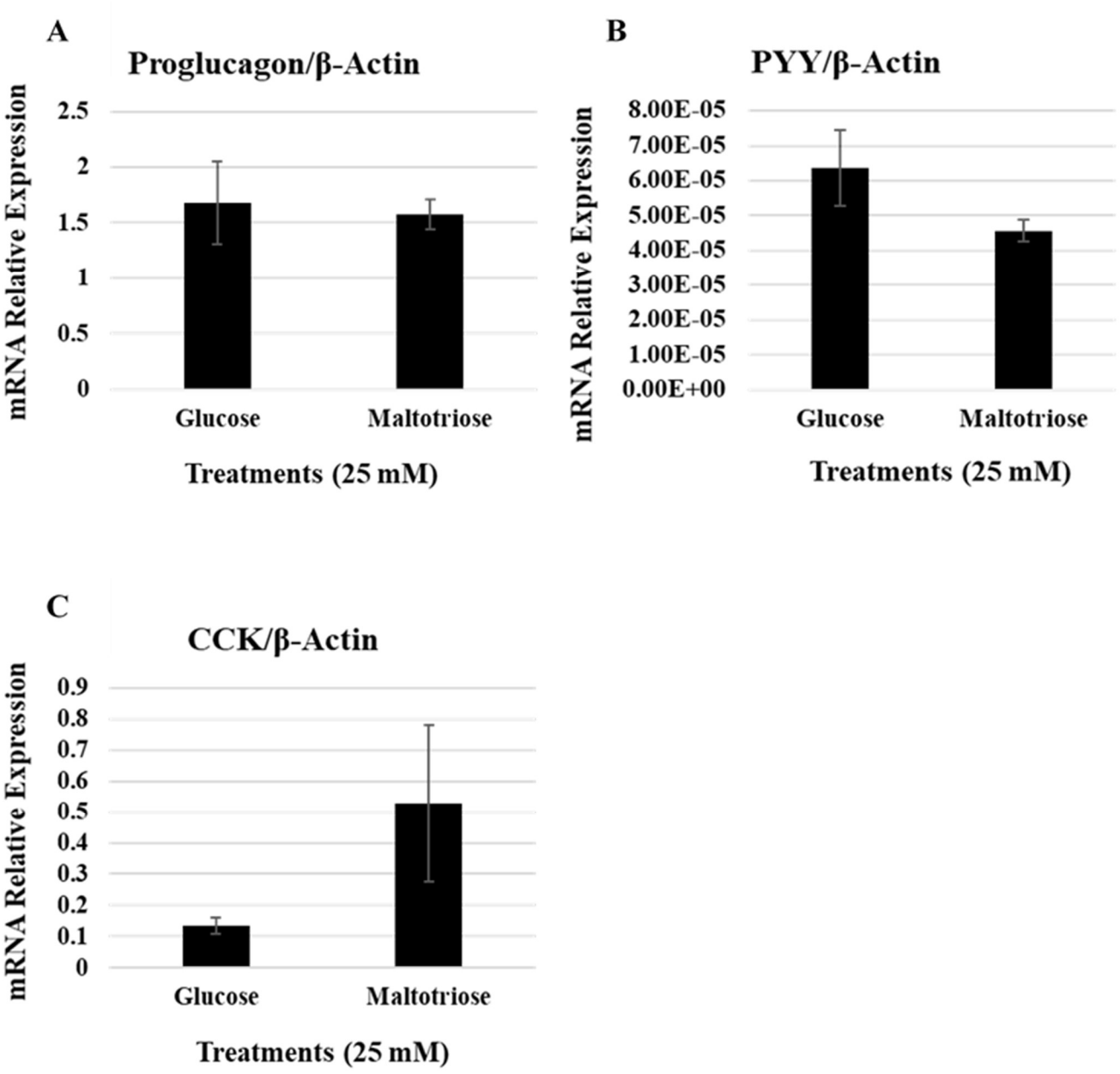

Figure 2. 10 mRNA relative expression of the proglucagon (A), PYY (B) and CCK (C) genes in STC-1 cells treated with maltotriose. Cells were treated with 25 mM glucose or 25 mM maltotriose for 90 minutes. The mRNA relative expression was normalized to β-Actin expression. Values are the average of four biological replicates with 2 technical replicates for each biological replicate (n=4). Bars represent standard error of the mean (Mean ± SEM). No statistically significant differences were observed between treatments at α=0.05 based on Tukey's least squares means for treatment effect.

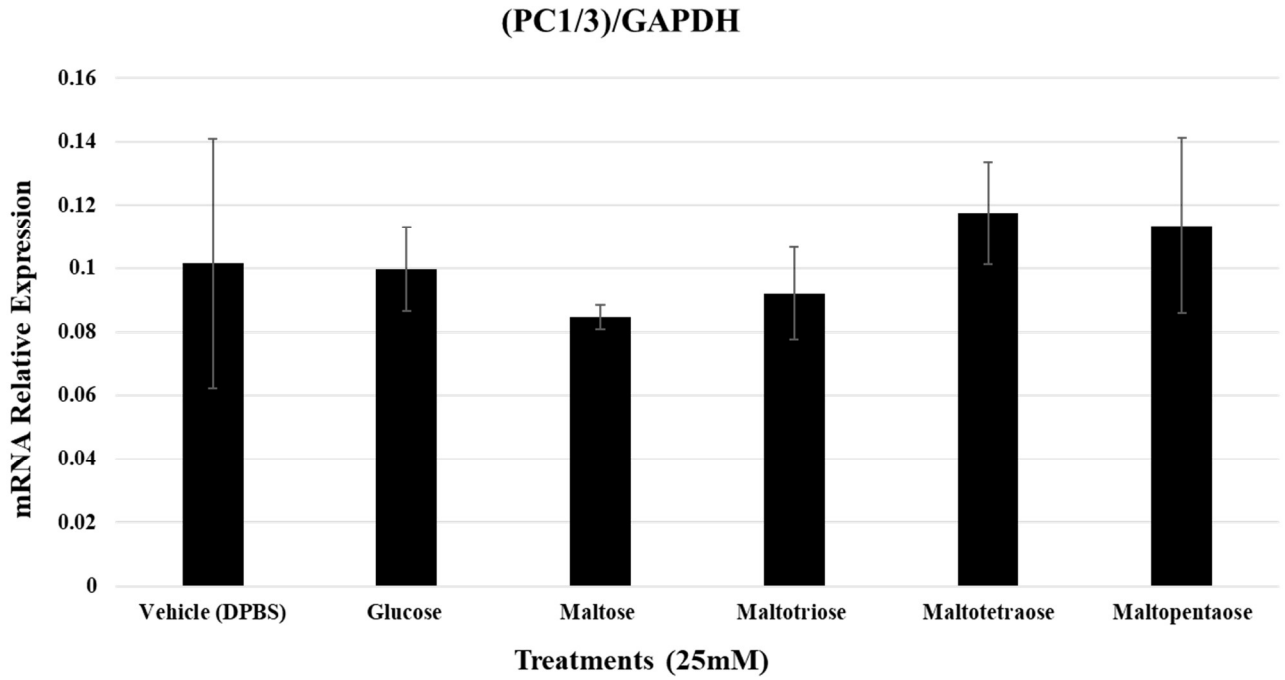

Figure 2.11 mRNA relative expression of the prohormone convertase1 (PC1/3) gene in STC-1 cells treated with MOS. Cells were treated with 25 mM glucose, 25 mM maltose, 25 mM maltotriose, 25 mM maltotetraose and 25 mM maltopentaose for 90 minutes. Vehicle represent the Dulbecco's Phosphate-Buffered Saline (DPBS) buffer solution used to dissolve treatments. The mRNA relative expression was normalized to glyceraldehyde 3-phosphate dehydrogenase (GAPDH) expression. Values are the average of five biological replicates with 2 technical replicates for each biological replicate (n=5). Bars represent standard error of the mean (Mean ± SEM). No statistically significant differences were observed between treatments at α=0.05 based on Tukey's least squares means for treatment effect.

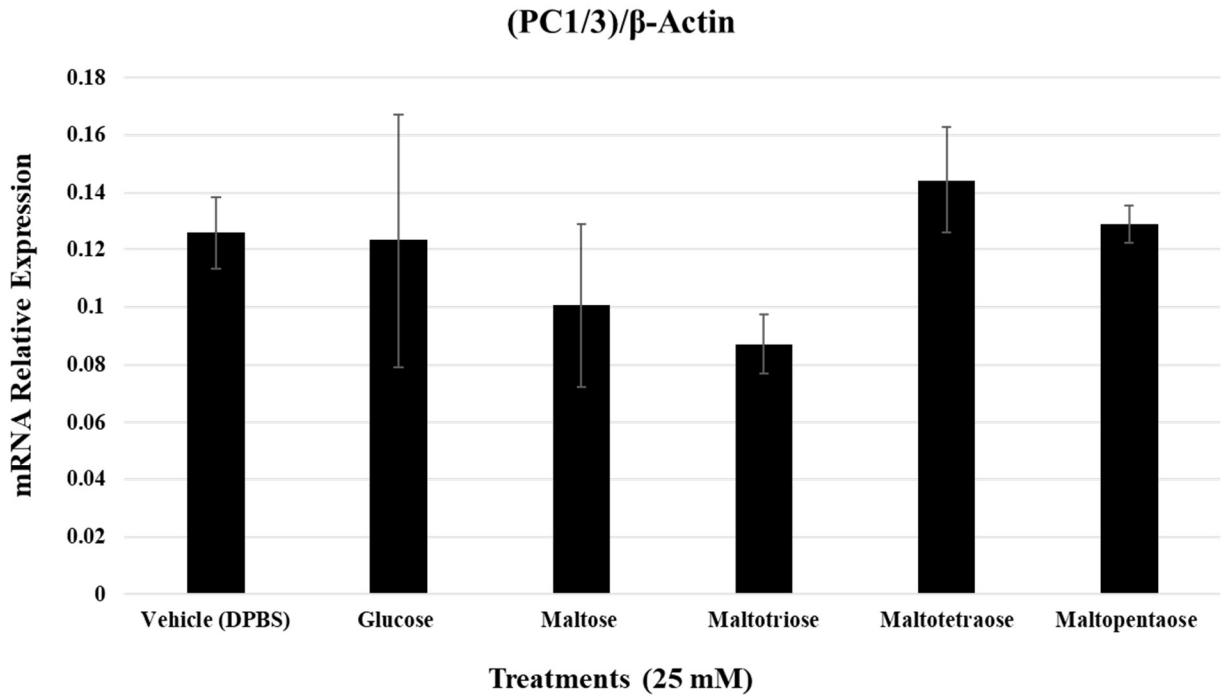

Figure 2.12 mRNA relative expression of the prohormone convertase1 (PC1/3) gene in STC-1 cells treated with MOS. Cells were treated with 25 mM glucose, 25 mM maltose, 25 mM maltotriose, 25 mM maltotetraose and 25 mM maltopentaose for 90 minutes. Vehicle represent the Dulbecco's Phosphate-Buffered Saline (DPBS) buffer solution used to dissolve treatments. The mRNA relative expression was normalized to β-Actin expression. Values are the average of five biological replicates with 2 technical replicates for each biological replicate (n=5). Bars represent standard error of the mean (Mean ± SEM). No statistically significant differences were observed between treatments at $\alpha=0.05$ based on Tukey's least squares means for treatment effect.

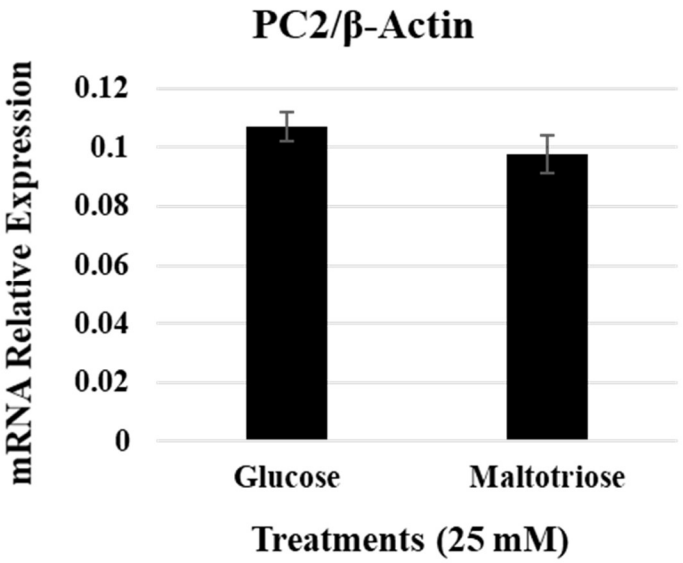

Figure 2.13 mRNA relative expression of the prohormone convertase2 (PC2) gene in STC-1 cells treated with maltotriose. Cells were treated with 25 mM glucose or 25 mM maltotriose for 90 minutes. The mRNA relative expression was normalized to β-Actin expression. Values are the average of four biological replicates with 2 technical replicates for each biological replicate (n=4). Bars represent standard error of the mean (Mean ± SEM). No statistically significant differences were observed between treatments at α=0.05 based on Tukey's least squares means for treatment effect.

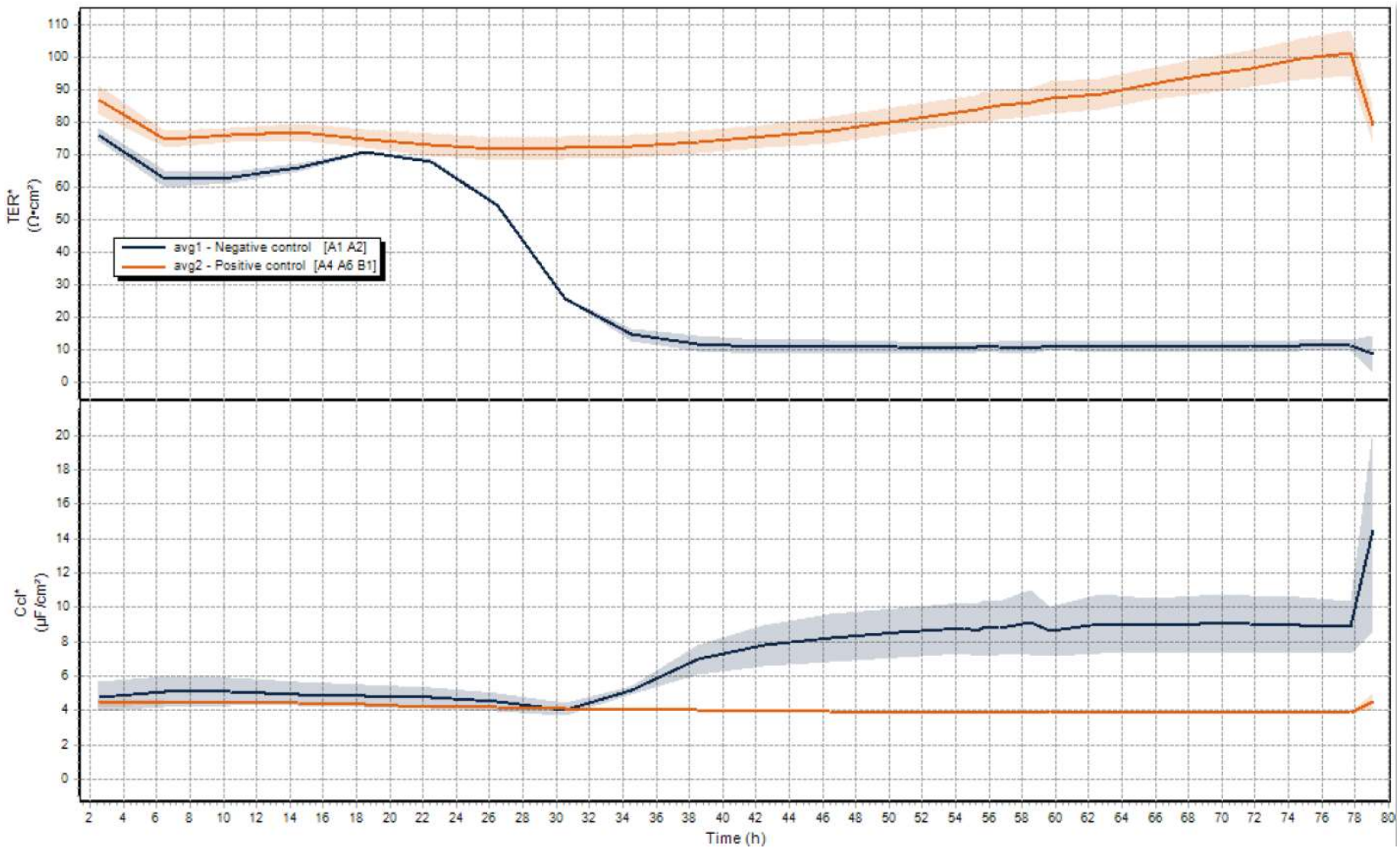

Figure 2.14 Trans-epithelial/-endothelial electrical resistance (TEER) and the capacitance (Ccl) of cultured Caco-2 monolayers incubated for 78 h with 25 mM glucose-containing DMEM media (orange) and glucose free DMEM media as negative control (blue). Values are the average of three biological replicates (n=3). Average means with error bars are displayed (Mean ± SEM).

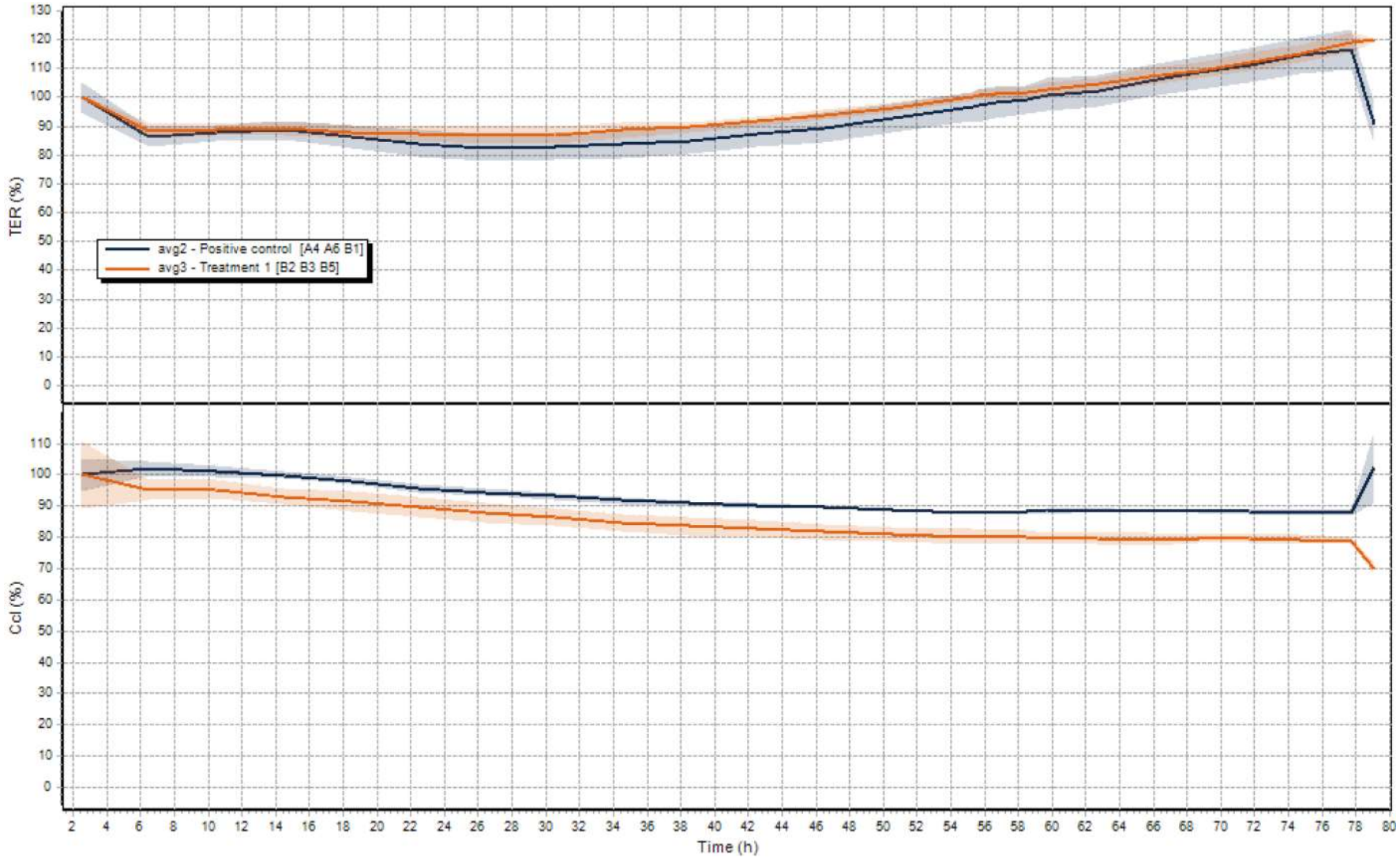

Figure 2.15 Trans-epithelial/-endothelial electrical resistance (TEER) and the capacitance (Ccl) of cultured Caco-2 monolayers incubated for 78 h with 25 mM glucose-containing DMEM media (blue) and 25 mM maltose-containing DMEM media (orange). Values are the average of three biological replicates (n=3). Results are normalized to 100% at time point 2h. Average means with error bars are displayed (Mean ± SEM).

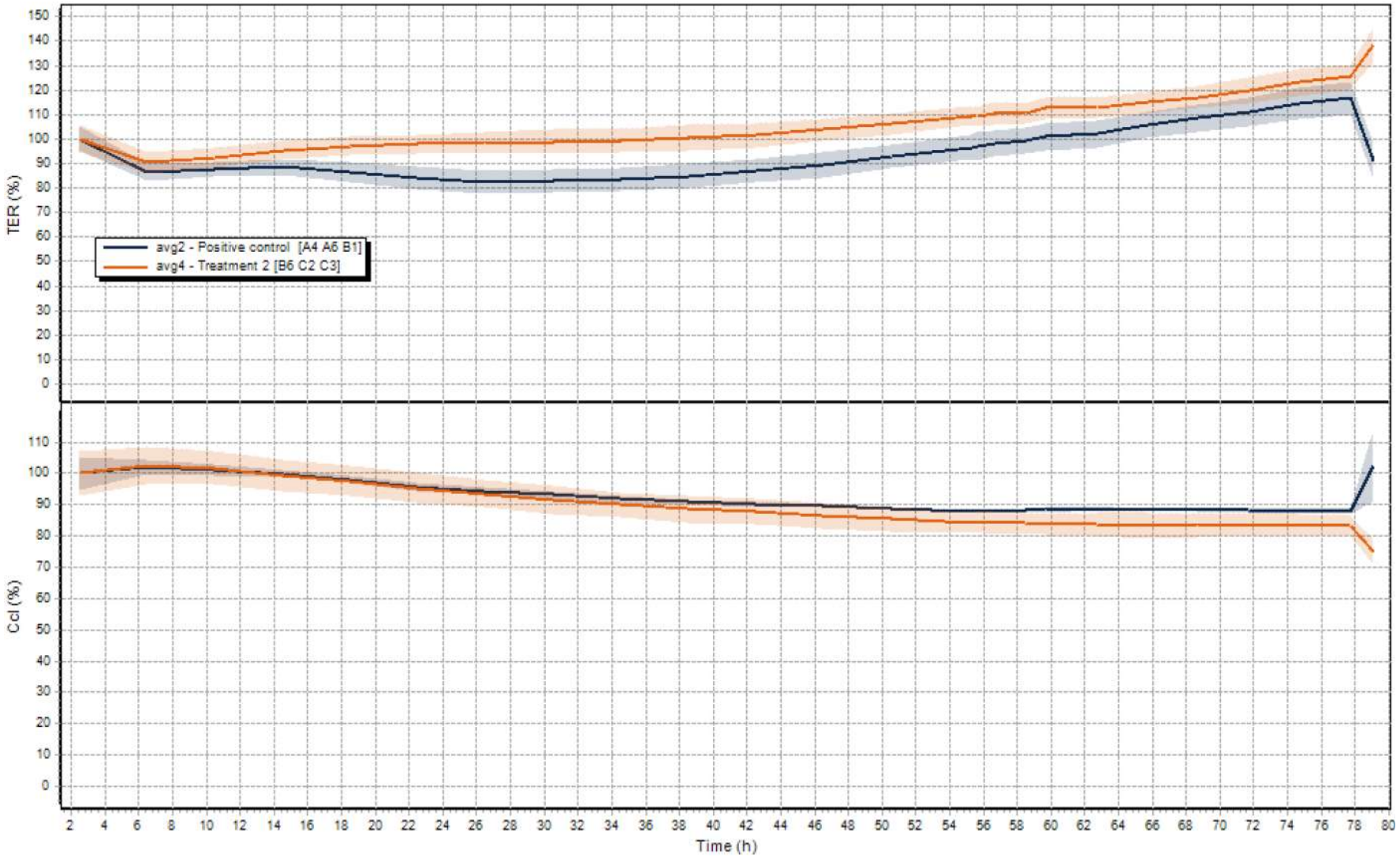

Figure 2.16 Trans-epithelial/-endothelial electrical resistance (TEER) and the capacitance (Ccl) of cultured Caco-2 monolayers incubated for 78 h with 25 mM glucose-containing DMEM media (blue) and 25 mM maltotriose-containing DMEM media (orange). Values are the average of three biological replicates (n=3). Results are normalized to 100% at time point 2h. Average means with error bars are displayed (Mean ± SEM).

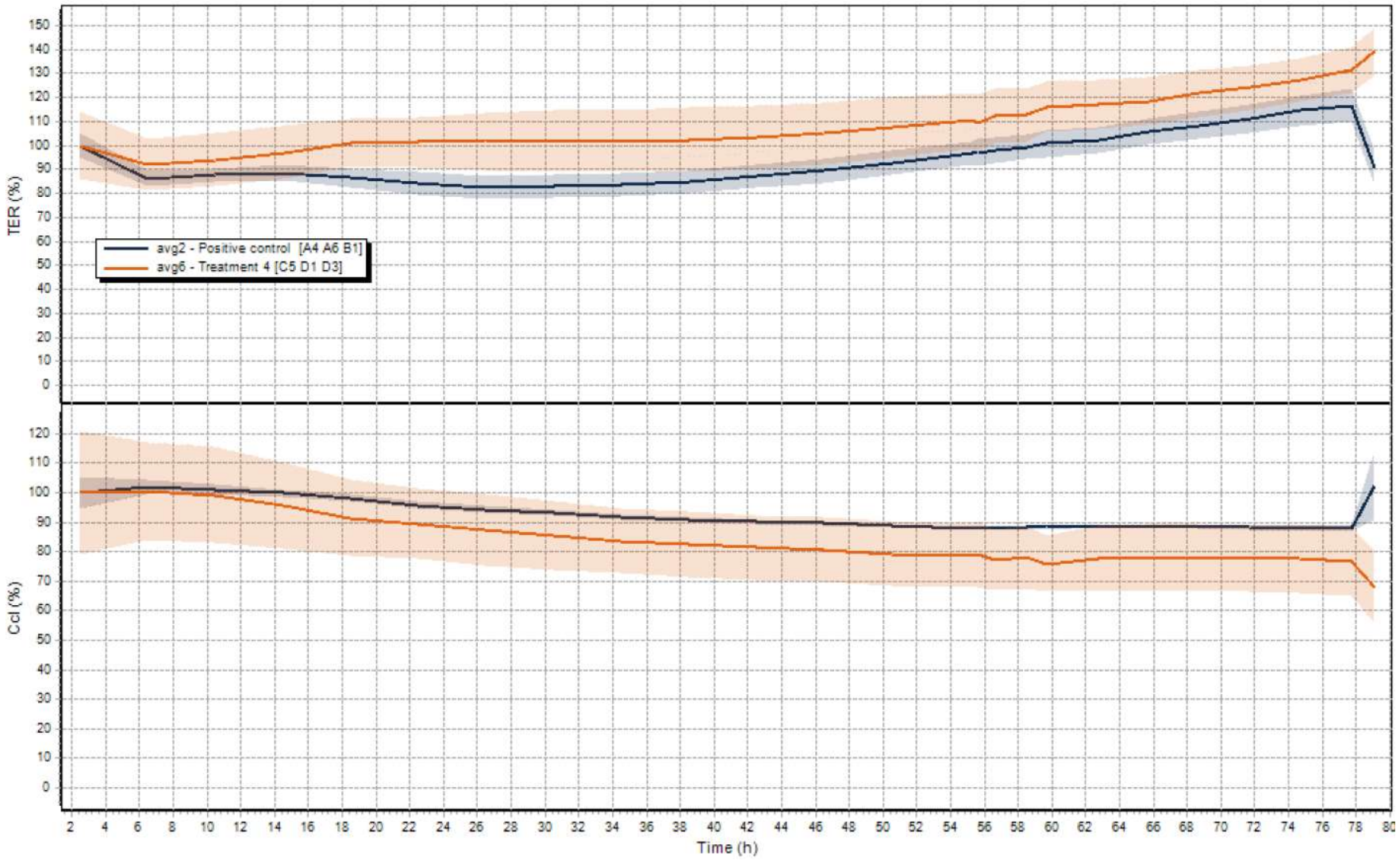

Figure 2.17 Trans-epithelial/-endothelial electrical resistance (TEER) and the capacitance (Ccl) of cultured Caco-2 monolayers incubated for 78 h with 25 mM glucose-containing DMEM media (blue) and 25 mM maltotetraose-containing DMEM media (orange). Values are the average of three biological replicates (n=3). Results are normalized to 100% at time point 2h. Average means with error bars are displayed (Mean ± SEM).

CHAPTER 3. TRANSCRIPTOME ANALYSIS OF DIFFERENTIALLY-EXPRESSED GENES IN INTESTINAL ENTEROENDOCRINE L-CELLS UNDER MALTOTRIOSE TREATMENT

3.1 Abstract

We observed stimulation effects of α-amylase degradation products of dietary starch, maltooigosaccharides (MOS), on the intestinal L-cell model (STC-1) to release higher levels of glucagon like peptide-1 and oxyntomodulin. In addition, we observed positive upregulation of the relative gene expression of the cholecystokinin gene but not the proglucagon or PYY genes using quantitative-real time PCR. In the current study global transcriptomic analysis of cells treated with maltotriose compared to cells treated with glucose was performed using RNA sequencing. Results revealed several putative target genes that may have a role in enteroendocrine L-cells in mediating the chemosensation and subsequent release of gut hormones, and barrier function, when exposed to MOS (and here maltotriose in particular). This is the first study that provides transcriptomic analysis to the STC-1 L-cell line and the first study that on transcriptomic analysis of cells treated with a carbohydrate that is exposed to them from the digestive process in the lumen of the small intestine. We identified several genes that are significantly upregulated with maltotriose treatment and are associated with signaling transduction pathways, cytoplasmic vesicle secretion, and cellular tight junctions. Maltotriose-treated cells showed significant reduction in the expression of the glucotoxicity marker, thioredoxin-interacting protein, as well as significant upregulation of genes encoding cell adhesion and tight junction proteins. On the other hand, the Wnt signaling pathway was enhanced in cells treated with glucose compared to those treated with maltotriose. The study provides a groundwork for further investigations to elucidate the potential beneficial outcomes that could be revealed by longer, sustainable, and distal delivery of α-amylase starch

degradation products by intestinal cells and the downstream roles of these outcomes to manage food intake and control obesity.

3.2 Introduction

Global transcriptome analysis of different cell types throughout the gastrointestinal tract lining could be a potent tool that helps to identify metabolic targets and pathways related to the food-gut interaction. Transcriptome analysis along with different bioinformatic tools and data processing provides an opportunity to simultaneously analyze a large number of target genes and identify the mechanisms of action after treatments [1]. RNA-sequencing provides several benefits over microarray since it prevents probe-specific hybridization of microarrays and has wide coverage. This facilitates the unprejudiced identification of novel transcripts and the detection of low-abundance transcripts [2]. RNA sequencing has been recently used to profile and evaluate different cell lines [3], [4], [5]. In addition, transcriptome profiling tools have been used to explain the mode of action of anti-obesity compounds *in vivo* [6], [7], [8]. The identification of changes in targeted genes and/or putative chemosensory receptors could help in the design of therapeutic strategies to treat and prevent obesity [9].

Glass *et al*., 2017 performed single cell RNA sequencing of preproglucagon-expressing cells isolated using flow cytometry from the upper small intestine of 3 GLU-Venus mice [10]. They identified three major GLP-1 secreting sub-populations that show overlapping in peptide secretion and their associated expression profiles of sensory receptors [10]. Sommer and Mostoslavsky, 2014 stated that the fatty acid-binding protein 5 was solely expressed in glucose-dependent insulinotropic peptide (GIP)-producing K cells and is required to keep suitable levels of circulating GIP, via antagonizing the endocannabinoids inhibitory effect [11]. They suggested the existence

of cell type-specific modulators of gut hormone release that can be targeted for obesity treatment and prevention [11].

As highlighted in the preceding chapters of this dissertation (Chapters I and III), obesity and its related metabolic disorders are progressively serious health problems. The role of the proglucagon gene products (Glucagon-Like peptide-1 (GLP-1) and Oxyntomodulin (OXM) and peptide YY (PYY) in obesity development and regression have been extensively studied in the last 45 years [12]. These peptides are released by L-cells that have been shown to locate in large numbers in the ileum. It was recently shown that, slowly digestible starch that digests into the ileum activated the gut-brain axis and resulted in lower food intake in diet-induced obese rats fed over 11-weeks [13]. The effect of α-amylase degradation products of starch on enteroendocrine L-cell function was shown to be effective in Chapter II on gut hormone secretion. We observed a unique stimulation effect of maltooligosaccharides (MOS) on L-cell models toward higher secretion of GLP-1 and OXM. However, mRNA relative expression of the proglucagon gene, did not show significant induction in its expression with MOS. On the other hand, detectable increase of mRNA relative expression of the cholecystokinin (CCK) gene has been observed with maltotriose treatment. Given the complexity of the pathways included in gut hormone synthesis and secretion, innovative tools are needed to understand the proposed sensing mechanisms of L-cells. RNA sequencing is one of such tools that could facilitate the identification of target proteins and pathways. Here, maltotriose, one of the stimulatory products for GLP-1 secretion in particular, was studied for its response at the level of the L-cells transcriptome. This investigation represents the first time to have the transcriptome of the L-cell model (STC-1) sequenced. The objective was to identify significant differentially expressed genes related to starch degradation product (i.e. maltotriose) treatment and to analyze its downstream protein products that may mediate or

facilitate the intestinal sensing mechanism of MOS by L-cells. The mouse-derived intestinal enteroendocrine tumor cells STC-1 were treated with glucose as a control and maltotriose as a treatment, and cellular RNA was sequenced for identification of differentially expressed genes. The objective was to examine the possible functional pathways that could be involved in the intestinal chemosensation of L-cells by maltotriose (which is one of the major α-amylase digestion products of starch) using RNA sequencing technique. The thinking was that this analysis could provide an elucidation of the underlying mechanisms whereby dietary α-amylase digestion products of starch promoted L-cell response and improved barrier function (Chapter II).

3.3 Materials and Methods

3.3.1 Cell Culture and Maltotriose Treatment

STC-1 cells at passage No. 34 were cultured according to the protocol described in Chapter II of this dissertation. Upon reaching 80% confluence (within 48 - 72 h), cells were exposed to the following treatments for 2 h (n=3): 25 mM glucose and 25 mM maltotriose, prepared as described before (Chapter II). Glucose and maltotriose were dissolved in Dulbecco's phosphate-buffered saline (DPBS) containing $CaCl_2$ and $MgCl_2$ (Sigma # 806544) and sterilized using a Steriflip-GV Sterile Centrifuge Tube Top 0.22 µm filter (MilliporeSigma, Burlington, MA).

3.3.2 RNA Isolation

After incubating cells for 2 h with treatment, cells were rinsed twice with DPBS, and lysed for RNA extraction using the lysis buffer of the RNA isolation kit containing an antifoaming reagent. Cellular RNA was extracted and purified using RNeasy Plus Mini Kit specific for cells/tissues (Qiagen, Netherlands; Catalog # 74134). RNA was collected in RNAase free water. Concentration and quality of the isolated RNA were measured by Nanodrop (Thermo Fisher

Scientific, Waltham, MA). RNA quality was confirmed by only using RNA samples that have A260/A280 and A260/A230 ratios equal or higher than 2 (Thermo Scientific T042-technical bulletin). RNA samples were then transferred to a RNAstable tube (Biomatrica, San Diego, CA) and allowed to dry for 2 h using a speed vacuum (Eppendorf, Hauppauge, NY). The dried RNA samples were then sent for sequencing at the core facility for genomics at the Shanghai Center for Plant Stress Biology (PSC) (Shanghai, China).

3.3.3 RNA Sequencing

Sequencing was performed using the TruSeq™ stranded MRNA LT kit by SciClone (SciClone, Foster City, CA). The used QC method was Agilent 2100 & Qubit. Information about sequencing details are shown in Table 3.1.

3.3.4 Quality Trimming and Adapter Removal

A summary of quality trimming and adaptor removal results is shown in Table 3.2. Trimmomatic v/0.36 was used for sequence cleaning using the following conditions: (1) Sequences matching Illumina Truseq adapters with a bit score greater than 5 (approximately equal to 8.6 perfect matches) at one end, or greater than 9 approximately equal to 15.5 perfect matches) in palindrome mode were trimmed off using an initial seed of 2 matching bases (ILLUMINACLIP:2:12:6); (2) Quality: Bases were removed from the ends of the reads until a base with error probability < 0.1 was found (LEADING:10 TRAILING:10) Reads were trimmed when a sliding window of five bases had error probability greater than 0.025 (SLIDINGWINDOW:5:16); (3) After adapter removal and quality trimming, reads shorter than 30 bases were dropped (MINLEN:30); (4) Only the paired reads were used in further analysis.

3.3.5 Mapping

Mapping to the *Mus musculus* reference genome (Mus_musculus.GRCm38, release 93) using BBMap v 37.93 (January 17, 2018), a splice aware aligner to confirm that reads are highly mappable to the *Mus musculus* genome. Mapping percentages are shown in Table 3.2 (R1 mapped, R2 mapped). This level of mapping is typical for mammalian RNA-Sequencing. Gene expression levels were quantified using Salmon, v0.10.2, using the --incompatPrior 1 option. Salmon results identified 112093 transcripts.

3.3.6 Differential Gene Expression

Differential gene expression was analyzed using DESeq2, v 1.20.0, running under R v 3.5.1. Read counts for the six samples were compared. No anomalies were noted as shown in Figure 3.1. Figure 3.2 provides an exploratory PCA analysis and volcano plot for the six samples of the two treatments used. Transcripts were pre-filtered to remove transcripts with very low counts. Prefiltering retained transcripts with normalized read counts > 50 summed over all six samples. This resulted in a list of 38615 transcripts with well-determined counts. Application of the standard normalization and differential expression estimation using DESEQ2 was successful: only 255 transcripts fell outside the modeling range of the analysis (padj=NA). Generally, these are transcripts whose measured counts are very low, and variable between samples. This analysis used the default target False Discovery Rate (FDR) of 0.1. The volcano plot shown in Figure 3.2 shows the distribution of adjusted *P*-value (padj is similar to FDR) and log2 fold change.

3.3.7 Functional Enrichment Analysis

Functional enrichment analysis was performed on the statistically significant genes using the Database for Annotation, Visualization and Integrated Discovery (DAVID) v6.8 and using the *Mus musculus* genome background. By submitting the official gene symbol of the 82 genes which

are upregulated in glucose, the database was able to recognize 79 genes in the mouse background. Similarly, the 99 genes which are upregulated with maltotriose treatment were submitted and the database recognized 98 genes in the mouse background.

3.4 Results

The gene expression profiling was performed using RNA-sequencing on the L-cell model (STC-1) and showed a number of significantly differentially expressed (SDE) genes (>4-fold change) in cells treated with 25 mM glucose compared to those treated with 25 mM maltotriose. Eighty-two common genes were consistently upregulated in glucose-treated samples. Gene ontology terms (GO) of these genes (79 genes identified by DAVID) are represented in Table 3.11, 3.12 and 3.13. In addition, ninety-nine genes were consistently upregulated in maltotriose-treated samples. GO terms of this group of genes (98 genes identified by DAVID) are represented in Table 3.15, 3.16 and 3.17. Further analysis of the common genes was performed by the Kyoto Encyclopedia of Genes and Genomes (KEGG) enrichment analysis. Data are shown in Table 3.14 and 3.18.

3.4.1 Pathways and Genes Upregulated by Glucose

The eighty-two genes that were upregulated in cells treated with glucose were identified as the genes that showed *p*adj value < 1e-01. From these, 48 genes were identified for transcripts with >4-fold (log2=+/-2) difference with *p*adj < 1e-01 (Table 3.3). In addition, 17 genes were identified for transcripts with >4-fold (log2=+/-2) difference with *p*adj < 1e-03 (Table 3.4) and 17 genes were identified for transcripts with >4-fold (log2=+/-2) difference with *p*adj < 1e-05 (Table 3.5). Gene names and description of differentially expressed genes upregulated in 25 mM glucose-treated STC-1 cells are represented in Table 3.9.

The most restricted adjusted *P*-value (*p*adj<1e-05) revealed 17 genes to be highly upregulated with 25 mM glucose compared to 25 mM maltotriose (Figure 3.4, Figure 3.5 and Figure 3.6). STC-1 cells treated with glucose showed a high increase in the expression levels of genes encoding oxidative stress marker, thirodoxin-interacting protein (Txnip1 and Txnip2), with *P*-value of 9.4E-49 and 7.3E-120, respectively (Table 3.5 and Figure 3.6). This result indicates an elevated oxidative stress and glucotoxicity in cells treated with glucose compared to those treated with maltotriose.

From the eighty-two SDE genes, GO terms were obtained for the 79 genes, identified by DAVID, which were upregulated with 25 mM glucose treatment. GO terms included information of the potential biological processes (Table 3.11), cellular compartments (Table 3.12), and molecular function (Table 3.13) of these genes. In addition, KEGG pathway analysis was performed for the prediction of pathways that may be enhanced with glucose treatment (Table 3.14). Functional enrichment analysis showed that genes that are significantly upregulated (with the highest restricted *P*-value) with glucose participate mainly in transcription regulation and cell differentiation (Table 3.11).

3.4.2 Pathways and Genes Upregulated by Maltotriose

The ninety-nine genes that were upregulated in cells treated with maltotriose were identified as the genes that showed *p*adj value < 1e-01. From these, 69 genes were identified for transcripts with >4-fold (log2=+/-2) difference with *p*adj < 1e-01 (Table 3.6). In addition, 21 genes were identified for transcripts with >4-fold (log2=+/-2) difference with *p*adj < 1e-03 (Table 3.7) and 9 genes were identified for transcripts with >4-fold (log2=+/-2) difference with *p*adj < 1e-05 (Table 3.8). Gene names and description of differentially expressed genes upregulated in 25 mM glucose-treated STC-1 cells are represented in Table 3.9. Gene names and description of

differentially expressed genes upregulated in 25 mM maltotriose-treated STC-1 cells are represented in Table 3.10. The most restricted adjusted *P*-value (*p*adj<1e-05) revealed 9 genes to be highly upregulated with 25 mM maltotriose compared to 25 mM glucose (Figure 3.7 and Figure 3.8). From the ninety-nine SDE genes, GO terms were obtained for the 98 genes, identified by DAVID, which were upregulated with 25 mM maltotriose treatment. GO terms included information of the potential biological processes (Table 3.15), cellular compartments (Table 3.16), and molecular function (Table 3.17) of these genes. In addition, KEGG pathway analysis was performed for the prediction of pathways that may be enhanced with maltotriose treatment (Table 3.18). Functional enrichment analysis showed that genes that are significantly upregulated (with the highest restricted *P*-value) with maltotriose participate mainly in transcription regulation (Table 3.15). Two genes were found to be involved in calcium ion regulated exocytosis (Table 3.15). Those are an important target for downstream analysis as the exocytosis of GLP-1-containng vesicles is regulated by the Ca^{+2} influx through Ca^{+2} channels [14]. Six genes out of the 98 recognized genes were found to be involved in cell adhesion (Table 3.15) and eight genes are involved in cell to cell connection (Table 3.16), contrary to only 4 genes upregulated in glucose treated cells (Table 3.12).

These findings are consistent with the previously found indication, in our group, of improved barrier function associated with maltotriose treatment on the Caco-2 monolayer [15], and the improved TEER values shown in Chapter II of this dissertation in cells treated with maltotriose and maltotetraose over 78 hours. Further analysis of the common genes was performed by the KEGG enrichment analysis. Common SDE genes upregulated by maltotriose are significantly involved in excitatory and glutamatergic synapse, Tables 3.15, 3.16 and 3.18. These findings may be part of the explanation to the stimulatory effect provided by MOS shown in

Chapter II. One of the mechanisms of SGLT-1 dependent stimulation of L-cells by glucose has been reported to rely on the presence of Na^+ ions [16]. The role of Na^+ is to depolarize the plasma membrane of L-cells to open the voltage sensitive calcium channels and finally promote exocytosis of GLP-1-containing vesicles [16]. In this context, data in Table 3.15 show an enhancement of calcium ion-regulated exocytosis processes in cells treated with maltotriose. Stimulating cell depolarization by maltotriose sensing could be the route through which GLP-1 secretion was enhanced.

3.5 Discussion and Conclusions

As thioredoxin-interacting protein (TxNIP) is considered to be a mediator in the cellular redox state and glucose homeostasis [17], the large increase in TxNIP transcripts observed in cells treated with glucose, compared to maltotriose (Table 3.5 and Figure 3.6), suggests a possible link between cellular redox state, glucotoxicity, and metabolism. TxNIP was previously identified by oligonucleotide microarray as the most upregulated gene in isolated human pancreatic islets treated with glucose [18]. In addition, glucose was found to induce a TxNIP-mediated apoptosis program in pancreatic β-cells [19] and is a critical regulator for normal glucose homeostasis in the liver [20].

Interestingly, GLP-1 and its mimetic, exendin-4, have been shown to diminish the expression level of TxNIP [21], [22]. This effect was explained as that GLP-1 stimulates protein kinase A (PKA) and exchange protein activated by cAMP (Epac) signaling pathways which, subsequently, promote proteasome-mediated TxNIP degradation [22]. Moreover, Yu and Jin, 2010 proposed that one of the beneficial effects of GLP-1 on pancreatic β-cells is its protective effect on reducing glucotoxicity [23]. An explanation of the observed upregulation of TxNIP in glucose-treated cells, compared to maltotriose-treated cells, could rely on the increased GLP-1 levels

secreted from maltotriose-treated cells that, in turn, could downregulate TxNIP degradation. On the other hand, the strong difference in TxNIP fold change could result from the absence of glucose in cells treated with maltotriose.

Performing the KEGG pathway analysis on genes upregulated with glucose treatment showed the enhancement of some KEGG annotated pathways, including adrenergic signaling because of the upregulation of Ppp2r1a, Ppp2r1b, Tpm1 and Adcy7 genes. Ppp2r1a and Ppp2r1b are the genes encoding the α- and β-isoforms of the serine/threonine-protein phosphatase 2A, which are two of the four major serine/threonine phosphatases and are implicated in the negative control of cell growth and division [24][25]. Tpm1 encodes the tropomyosin α-1 chain protein which is a member of the tropomyosin (Tm) family, a highly conserved actin-binding protein family. It was reported that Tm proteins regulate the calcium-dependent interaction of actin and myosin during muscle contraction. In addition, Tpm1 was shown to be involved in the cytoskeleton of non-muscle cells [26].

The Hippo signaling pathway was enhanced in cells treated with glucose likely through the upregulation of Ppp2r1a and Ppp2r1b genes described above, as well as the Dlg3 and Ctnnb1 genes. Dlg3 encodes the synapse-associated protein 102 which is a member of the membrane-associated guanylate kinase family. It is an important regulator of epithelial polarity and effectively organizes receptors involved in synapse as well as synapse downstream signaling pathways [27]. Ctnnb1 encodes a subunit of the adherens junctions complex required for epithelial cell integrity, cell growth, and adhesion between cells. In addition, the encoded protein was also found to be anchored in the actin cytoskeleton [28]. Is suggested that Ctnnb1 protein product play a critical role in transmitting the contact inhibition signal required for preventing excess cell division after the completion of the growth of the epithelial sheet. Mutations in the Ctnnb1 gene are correlated

with colorectal cancer [29], ovarian cancer [30], pilomatrixoma [31] and medulloblastoma [32]. Ctnnb1, Ppp2r1a, and Ppp2r1b genes are together suggested by the curated pathway analysis to be involved in the β-catenin phosphorylation cascade and catalysis pathways.

Besides its role as an adherens complex subunit, the Ctnnb1 gene product, β-catenin, has been identified as an important effector of the Wnt signaling pathway [33]. It was shown that a bipartite transcription factor complex of β-catenin and TCF7L2 effectors positively mediates the expression of the proglucagon gene in the mouse intestinal GLUTag and STC-1 cell lines [34], through the regulation of cAMP levels within the signaling cascade [35]. Here, we observed upregulation of one of the T cell transcription factors (TCF) with glucose treatment as well (Table 3.3), indicating a possible enhancement of the Wnt signaling pathway in cells treated with glucose. Adcy7 encodes the membrane-bound adenylyl cyclase type 7 enzyme which catalyzes the formation of cyclic AMP from ATP and could be inhibited by the presence of calcium ions [36]. The upregulation of Adcy7 in this study supports the enhancement of the adrenergic signaling and the Wnt pathway as the levels of cAMP have been shown to regulate the β-catenin/TCF7L2 complex formation [35]. The induction of the Wnt signaling pathway in cells treated with glucose and not in cells treated with maltotriose indicates that the expression of the proglucagon gene is positively regulation in glucose-treated cells and not in maltotriose-treated cells. These finding are consistent with relative gene expression data from Chapter II showing no induction in the proglucagon gene expression in cells treated with maltotriose and supporting the hypothesis that maltotriose stimulates the secretion, and not the synthesis (through transcription regulation), of the proglucagon gene products.

The KEGG pathway annotation suggests that the endocytosis pathway is enhanced in cells treated with maltotriose through the upregulation of the Sh3gl3, Dnajc6, Usp8 and Git2 genes.

Sh3gl3 is the gene encoding the Endophilin A3 protein, a member of the endophilin family which are important players in endocytosis. Endophilin A3 is suggested to have a role in transport through the formation of clathrin-coated vesicles from the plasma membrane [37]. Also, the Dnajc6 gene encodes the neuronal protein auxilin, which is also involved in the clathrin-mediated endocytosis pathway [38]. In addition, auxilin has been found to regulate cellular molecular chaperone activity by stimulating ATPase activity [39]. Moreover, the PI3K-Akt signaling pathway was enhanced in maltotriose-treated cells through the upregulation of the Itga3, Cdk2, Sgk3, and Jak1 genes. Furthermore, the glutamatergic synapse signaling pathway was enhanced through the upregulation of the Slc38a3, Dlg4, and Cacna1c genes. Some cancer pathways were enhanced through the upregulation of the Itga3, Cdk2, Arhgef11, and Jak1 genes. Curated annotation suggests the enhancement of genes of the Ub-specific processing proteases pathway Atxn7, Psmd13, Rnf146, Usp22, and Usp8 genes. Besides, genes encoding the curated SAGA-type complex subunits Atxn7, Usp22, and Taf6l, and the curated complex AP-type membrane coat adaptor complex subunits, Vps33b, Ap4b1, and Snap91 were upregulated.

3.6 References

[1] Z. Wang, M. Gerstein, and M. Snyder, “RNA-Seq: a revolutionary tool for transcriptomics.,” *Nat. Rev. Genet.*, vol. 10, no. 1, pp. 57–63, Jan. 2009.

[2] K.-H. Lin *et al.*, “RNA-seq transcriptome analysis of breast cancer cell lines under shikonin treatment OPEN.”

[3] E. Fasterius *et al.*, “A novel RNA sequencing data analysis method for cell line authentication.,” *PLoS One*, vol. 12, no. 2, p. e0171435, 2017.

[4] J. L. Harenza *et al.*, “Transcriptomic profiling of 39 commonly-used neuroblastoma cell lines,” *Sci. Data*, vol. 4, p. 170033, Mar. 2017.

[5] E. Fasterius and C. Al-Khalili Szigyarto, “Analysis of public RNA-sequencing data reveals biological consequences of genetic heterogeneity in cell line populations,” *Sci. Rep.*, vol. 8, no. 1, p. 11226, Dec. 2018.

[6] X. Wang, F. Liu, Y. Gao, C. Xue, R. W. Li, and Q. Tang, “Transcriptome analysis revealed anti-obesity effects of the Sodium Alginate in high-fat diet -induced obese mice,” *Int. J. Biol. Macromol.*, vol. 115, pp. 861–870, Aug. 2018.

[7] D. S. Kyung *et al.*, “Global transcriptome analysis identifies weight regain-induced activation of adaptive immune responses in white adipose tissue of mice,” *Int. J. Obes.*, vol. 42, no. 4, pp. 755–764, Apr. 2018.

[8] A. Ruifang Li, S. A. Grimm, D. Mav, B. Alex Merrick, D. Raftery, and P. A. Wade, “Transcriptome and DNA Methylome Analysis in a Mouse Model of Diet-Induced Obesity Predicts Increased Risk of Colorectal Cancer Data and Software Availability GSE85731 GSE100276,” 2018.

[9] L. J. A. Kogelman, S. Cirera, D. V Zhernakova, M. Fredholm, L. Franke, and H. N. Kadarmideen, “Identification of co-expression gene networks, regulatory genes and pathways for obesity based on adipose tissue RNA Sequencing in a porcine model.,” *BMC Med. Genomics*, vol. 7, p. 57, Sep. 2014.

[10] L. L. Glass *et al.*, “Single-cell RNA-sequencing reveals a distinct population of proglucagon-expressing cells specific to the mouse upper small intestine,” *Mol. Metab.*, vol. 6, no. 10, pp. 1296–1303, Oct. 2017.

[11] C. A. Sommer and G. Mostoslavsky, “RNA-Seq analysis of enteroendocrine cells reveals a role for FABP5 in the control of GIP secretion.,” *Mol. Endocrinol.*, vol. 28, no. 11, pp. 1855–65, Nov. 2014.

[12] R. Pais, F. M. Gribble, and F. Reimann, “Stimulation of incretin secreting cells.,” *Ther. Adv. Endocrinol. Metab.*, vol. 7, no. 1, pp. 24–42, Feb. 2016.

[13] L. Y. Hasek *et al.*, “Dietary Slowly Digestible Starch Triggers the Gut-Brain Axis in Obese Rats with Accompanied Reduced Food Intake,” *Mol. Nutr. Food Res.*, vol. 62, no. 5, p. 1700117, Mar. 2018.

[14] L. L. Baggio and D. J. Drucker, “Biology of Incretins: GLP-1 and GIP,” *Gastroenterology*, vol. 132, no. 6, pp. 2131–2157, May 2007.

[15] M. Chegeni, “Dietary carbohydrates influence the structure and function of the intestinal alpha-glucosidases.” 2016.

[16] F. M. Gribble, L. Williams, A. K. Simpson, and F. Reimann, “A Novel Glucose-Sensing Mechanism Contributing to Glucagon-Like Peptide-1 Secretion From the GLUTag Cell Line,” 2003.

[17] A. Shalev, “Minireview: Thioredoxin-Interacting Protein: Regulation and Function in the Pancreatic β-Cell,” *Mol. Endocrinol.*, vol. 28, no. 8, pp. 1211–1220, Aug. 2014.

[18] A. Shalev *et al.*, “Oligonucleotide Microarray Analysis of Intact Human Pancreatic Islets: Identification of Glucose-Responsive Genes and a Highly Regulated TGFβ Signaling Pathway,” *Endocrinology*, vol. 143, no. 9, pp. 3695–3695, Sep. 2002.

[19] A. H. Minn, C. Hafele, and A. Shalev, “Thioredoxin-Interacting Protein Is Stimulated by Glucose through a Carbohydrate Response Element and Induces β-Cell Apoptosis,” *Endocrinology*, vol. 146, no. 5, pp. 2397–2405, May 2005.

[20] W. A. Chutkow, P. Patwari, J. Yoshioka, and R. T. Lee, “Thioredoxin-interacting protein (Txnip) is a critical regulator of hepatic glucose production.,” *J. Biol. Chem.*, vol. 283, no. 4, pp. 2397–406, Jan. 2008.

[21] J. Chen, F. M. Couto, A. H. Minn, and A. Shalev, “Exenatide inhibits β-cell apoptosis by decreasing thioredoxin-interacting protein,” *Biochem. Biophys. Res. Commun.*, vol. 346, no. 3, pp. 1067–1074, Aug. 2006.

[22] W. Shao, Z. Yu, I. G. Fantus, and T. Jin, “Cyclic AMP signaling stimulates proteasome degradation of thioredoxin interacting protein (TxNIP) in pancreatic β-cells,” *Cell. Signal.*, vol. 22, no. 8, pp. 1240–1246, Aug. 2010.

[23] Z. Yu and T. Jin, “New insights into the role of cAMP in the production and function of the incretin hormone glucagon-like peptide-1 (GLP-1),” *Cell. Signal.*, vol. 22, no. 1, pp. 1–8, Jan. 2010.

[24] A. D. Everett, C. Xue, and T. Stoops, “Developmental expression of protein phosphatase 2A in the kidney.,” *J. Am. Soc. Nephrol.*, vol. 10, no. 8, pp. 1737–45, Aug. 1999.

[25] B. E. Baysal, J. E. Farr, J. R. Goss, B. Devlin, and C. W. Richard III, “Genomic organization and precise physical location of protein phosphatase 2A regulatory subunit A beta isoform gene on chromosome band 11q23,” *Gene*, vol. 217, no. 1–2, pp. 107–116, Sep. 1998.

[26] D. F. McKillop and M. A. Geeves, “Regulation of the interaction between actin and myosin subfragment 1: evidence for three states of the thin filament.,” *Biophys. J.*, vol. 65, no. 2, pp. 693–701, Aug. 1993.

[27] P. Tarpey *et al.*, “Mutations in the DLG3 gene cause nonsyndromic X-linked mental retardation.,” *Am. J. Hum. Genet.*, vol. 75, no. 2, pp. 318–24, Aug. 2004.

[28] K.-H. LIU, Y.-T. TSAI, S.-Y. CHIN, W.-R. LEE, Y.-C. CHEN, and S.-C. SHEN, “Hypoxia Stimulates the Epithelial–to–Mesenchymal Transition in Lung Cancer Cells Through Accumulation of Nuclear β-Catenin,” *Anticancer Res.*, vol. 38, no. 11, pp. 6299–6308, Nov. 2018.

[29] A. Kakkar, M. Rajeshwari, P. Sakthivel, M. C. Sharma, and S. C. Sharma, “Biphenotypic sinonasal sarcoma: A series of six cases with evaluation of role of β-catenin immunohistochemistry in differential diagnosis,” *Ann. Diagn. Pathol.*, vol. 33, pp. 6–10, Apr. 2018.

[30] H. Long *et al.*, “Prognostic significance of β-catenin expression in patients with ovarian cancer: A meta-analysis,” *Gene*, vol. 678, pp. 270–279, Dec. 2018.

[31] R. B. Cavalcante, C. F. W. Nonaka, H. B. de P. Santos, S. H. B. Rabenhorst, L. Pereira Pinto, and L. B. de Souza, “Assessment of CTNNB1 gene mutations and β-catenin immunoexpression in salivary gland pleomorphic adenomas and adenoid cystic carcinomas,” *Virchows Arch.*, vol. 472, no. 6, pp. 999–1005, Jun. 2018.

[32] M. Liu *et al.*, “Downregulation of Cancer Stemness by Novel Diterpenoid Ovatodiolide Inhibits Hepatic Cancer Stem Cell-Like Traits by Repressing Wnt/β-Catenin Signaling,” *Am. J. Chin. Med.*, vol. 46, no. 04, pp. 891–910, Jan. 2018.

[33] Y.-T. A. Chiang, W. Ip, T. Jin, and W.-P. Han, “The role of the Wnt signaling pathway in incretin hormone production and function,” 2012.

[34] Z. Ni, Y. Anini, X. Fang, G. Mills, P. L. Brubaker, and T. Jin, “Transcriptional activation of the proglucagon gene by lithium and beta-catenin in intestinal endocrine L cells.,” *J. Biol. Chem.*, vol. 278, no. 2, pp. 1380–7, Jan. 2003.

[35] T. Jin, I. George Fantus, and J. Sun, “Wnt and beyond Wnt: Multiple mechanisms control the transcriptional property of β-catenin,” *Cell. Signal.*, vol. 20, no. 10, pp. 1697–1704, Oct. 2008.

[36] K. Hellevuo, R. Berry, J. Sikela, and B. Tabakoff, “Localization of the gene for a novel human adenylyl cyclase (ADCY7) to chromosome 16,” *Hum. Genet.*, vol. 95, no. 2, pp. 197–200, Feb. 1995.

[37] A. C. Hughes, R. Errington, R. Fricker-Gates, and L. Jones, “Endophilin A3 forms filamentous structures that colocalise with microtubules but not with actin filaments,” *Mol. Brain Res.*, vol. 128, no. 2, pp. 182–192, Sep. 2004.

[38] Y.-I. Yim *et al.*, “Endocytosis and clathrin-uncoating defects at synapses of auxilin knockout mice.,” *Proc. Natl. Acad. Sci. U. S. A.*, vol. 107, no. 9, pp. 4412–7, Mar. 2010.

[39] K. Ohtsuka and M. Hata, “Mammalian HSP40/DNAJ homologs: cloning of novel cDNAs and a proposal for their classification and nomenclature.,” *Cell Stress Chaperones*, vol. 5, no. 2, pp. 98–112, Apr. 2000.

Table 3.1 Information about sequencing details.

Treatment (25 mM)	Data amount	Library size (bp)	Average size (bp)	QC method	QC passed	Library concentration	Volumes added to 5nmol/µl	TruSeq Adapter	Index sequence	Size
Glucose Rep# 1	4	173-697	311	Qubit	Y	10.6	27.9851	Index 14	AGTTCC	9,482G
Glucose Rep# 2	4	163-566	308	Qubit	Y	17.5	48.6529	Index 15	ATGTCA	7,803G
Glucose Rep# 3	4	170-800	337	Qubit	Y	8.74	20.577	Index 16	CCGTCC	9,987G
Maltotriose Rep #1	4	174-1121	352	Qubit	Y	11.1	25.6674	Index 18	GTCCGC	11,330G
Maltotriose Rep# 2	4	184-922	353	Qubit	Y	8.76	19.5599	Index 19	GTGAAA	12,438G
Maltotriose Rep# 3	4	177-591	339	Qubit	Y	15.4	38.2979	Index 20	GTGGCC	9,724G

Table 3.2 Trimmomatic and mapping summary.

	Glucose 1	Glucose 2	Glucose 3	Maltotriose 1	Maltotriose 2	Maltotriose 3
Raw	31,606,882	26,008,726	33,291,461	37,767,210	41,461,193	32,412,758
Cleaned	27,261,531	22,890,548	29,972,855	34,018,404	37,982,397	29,692,118
Remain	86.3%	88.0%	90.0%	90.1%	91.6%	91.6%
R1 mapped	97.3%	97.9%	97.9%	98.7%	97.3%	99.2%
R2 mapped	97.0%	97.5%	97.6%	98.3%	96.9%	98.9%
Salmon	81.5%	85.4%	85.1%	87.8%	81.5%	92.3%

Table 3.3 Differentially expressed genes (upregulated in 25 mM glucose- treated STC-1 cells) for transcripts with >4-fold (log2=+/-2) difference with ***p*adj < 1e-01**. padj: *P*-value adjusted; Glu1: 25 mM glucose Rep#1; Glu2: 25 mM glucose Rep#2; Glu3: 25 mM glucose Rep#3; Mt1: 25 mM maltotriose Rep#1; Mt2: 25 mM maltotriose Rep#2; Mt3: 25 mM maltotriose Rep#3.

Transcript	Gene name	Base mean	log2 Fold Change	padj	Glu1	Glu2	Glu3	Mt1	Mt2	Mt3
ENSMUST00000133454.7	Abcc1	55.9	-9.5	6.2E-02	39.2	0.0	296.3	0.0	0.0	0.0
ENSMUST00000098521.3	Adcy7	47.2	-9.2	7.2E-02	209.4	73.7	0.0	0.0	0.0	0.0
ENSMUST00000131556.1	Arfgef1	42.7	-9.1	8.7E-02	190.4	66.0	0.0	0.0	0.0	0.0
ENSMUST00000101695.8	Tfe3	41.3	-9.0	7.8E-02	170.2	0.0	77.6	0.0	0.0	0.0
ENSMUST00000018482.12	Tnip1	37.0	-8.9	9.4E-02	73.9	0.0	148.2	0.0	0.0	0.0
ENSMUST00000175645.7	Ppp2r1b	33.8	-8.7	5.3E-03	2.2	115.1	85.7	0.0	0.0	0.0
ENSMUST00000042964.12	Zfp189	30.7	-8.6	1.5E-02	57.1	1.3	126.0	0.0	0.0	0.0
ENSMUST00000205119.2	C2cd5	27.5	-8.4	3.0E-02	127.7	36.2	1.0	0.0	0.0	0.0
ENSMUST00000116237.2	1810043G02Rik	17.3	-7.8	6.8E-02	70.6	32.3	1.0	0.0	0.0	0.0
ENSMUST00000226718.1	Slc22a17	13.8	-7.4	4.3E-03	42.6	31.0	9.1	0.0	0.0	0.0
ENSMUST00000113684.7	Tpm1	13.7	-7.4	1.5E-02	38.1	38.8	5.0	0.0	0.0	0.0
ENSMUST00000108376.8	Myo18a	13.3	-7.4	2.5E-03	31.4	37.5	11.1	0.0	0.0	0.0
ENSMUST00000024650.11	1700010I14Rik	13.0	-7.4	2.5E-03	34.7	32.3	11.1	0.0	0.0	0.0
ENSMUST00000107475.8	Rara	12.8	-7.3	3.7E-03	37.0	29.7	10.1	0.0	0.0	0.0
ENSMUST00000184646.2	Lhx1	12.1	-7.3	7.5E-03	44.8	11.6	16.1	0.0	0.0	0.0
ENSMUST00000166744.7	Ppard	10.6	-7.1	2.4E-02	7.8	41.4	14.1	0.0	0.0	0.0
ENSMUST00000168334.7	Ncoa4	10.2	-7.0	1.6E-03	17.9	23.3	20.2	0.0	0.0	0.0
ENSMUST00000167992.7	Tusc3	35.5	-7.0	5.0E-02	1.1	90.5	119.9	0.0	1.6	0.0
ENSMUST00000229031.1	Micall1	9.8	-7.0	3.1E-03	21.3	14.2	23.2	0.0	0.0	0.0
ENSMUST00000202435.3	Tcf4	9.7	-6.9	8.1E-03	12.3	15.5	30.2	0.0	0.0	0.0
ENSMUST00000225401.1	Thoc7	9.4	-6.9	1.0E-02	14.6	29.7	12.1	0.0	0.0	0.0
ENSMUST00000129895.7	Plekhh3	9.0	-6.8	1.8E-02	29.1	15.5	9.1	0.0		0.0
ENSMUST00000120128.7	Adgrl3	8.8	-6.8	1.2E-02	10.1	25.9	17.1	0.0	0.0	0.0
ENSMUST00000146591.1	Tgfbr3	8.8	-6.8	3.0E-02	32.5	10.3	10.1	0.0	0.0	0.0
ENSMUST00000056107.10	Zfp677	8.6	-6.8	1.9E-02	20.2	23.3	8.1	0.0	0.0	0.0

Table 3.3 (Continued).

Transcript	Gene name	Base mean	log2 Fold Change	padj	Glu1	Glu2	Glu3	Mt1	Mt2	Mt3
ENSMUST00000148337.1	Slc25a36	8.1	-6.7	7.1E-02	32.5	10.3	6.0	0.0	0.0	0.0
ENSMUST00000227990.1	App	7.9	-6.6	1.0E-02	19.0	15.5	13.1	0.0	0.0	0.0
ENSMUST00000006754.13	Ubtf	7.2	-6.5	3.9E-02	10.1	23.3	10.1	0.0	0.0	0.0
ENSMUST00000132855.7	Wipf3	7.1	-6.5	2.8E-02	15.7	18.1	9.1	0.0	0.0	0.0
ENSMUST00000095045.8	St6galnac6	6.9	-6.4	5.9E-02	9.0	23.3	9.1	0.0	0.0	0.0
ENSMUST00000138111.7	Evi5	6.8	-6.4	6.8E-02	5.6	18.1	17.1	0.0	0.0	0.0
ENSMUST00000150636.7	Prpf40b	6.7	-6.4	5.9E-02	6.7	14.2	19.2	0.0	0.0	0.0
ENSMUST00000113736.8	Dlg3	6.3	-6.3	7.1E-02	13.4	6.5	18.1	0.0	0.0	0.0
ENSMUST00000137035.7	St3gal6	6.2	-6.3	5.0E-02	16.8	10.3	10.1	0.0	0.0	0.0
ENSMUST00000174253.1	Smarcd2	10.8	-6.1	1.2E-02	13.4	32.3	18.1	0.0	0.0	0.9
ENSMUST00000108484.7	Atp2a3	25.6	-5.3	8.8E-02	10.1	85.4	54.4	0.0	0.0	3.8
ENSMUST00000166119.7	Slc29a1	43.2	-5.1	2.9E-03	126.5	46.6	78.6	0.0	0.8	6.6
ENSMUST00000121049.7	Adgrb2	53.6	-4.6	6.5E-03	150.1	71.1	87.7	2.5	0.0	10.4
ENSMUST00000129448.1	Cyp51	36.8	-4.3	2.6E-02	122.1	64.7	23.2	4.2	6.4	0.0
ENSMUST00000140007.1	Pde3b	32.5	-4.1	9.8E-02	116.5	51.7	16.1	3.4	7.2	0.0
ENSMUST00000229413.1	Eif3d	132.6	-4.0	4.9E-02	309.1	207.0	231.8	0.0	29.7	18.0
ENSMUST00000170444.7	Upp1	36.5	-3.9	7.4E-02	59.4	104.8	41.3	3.4	0.0	10.4
ENSMUST00000229120.1	Pmm1	74.5	-3.4	8.1E-02	236.3	77.6	94.7	19.3	0.8	18.0
ENSMUST00000172247.7	Gstm5	105.7	-3.3	1.8E-03	389.7	99.6	86.7	14.2	20.0	23.7
ENSMUST00000216176.1	Cck	2725.0	-3.0	2.9E-02	9143.8	3136.6	2301.2	1071.9	409.6	286.7
ENSMUST00000061753.14	Wdfy4	27.9	-3.0	9.3E-02	29.1	40.1	79.6	12.6	4.0	1.9
ENSMUST00000149669.7	Wsb2	310.1	-2.5	6.0E-02	771.6	429.4	383.0	19.3	161.1	95.9
ENSMUST00000162044.7	Phf21b	85.1	-2.0	8.2E-02	123.2	93.1	190.5	25.1	58.5	19.9

Table 3.4 Differentially expressed genes (upregulated in 25 mM glucose- treated STC-1 cells) for transcripts with >4-fold (log2=+/-2) difference with ***p*adj < 1e-03**. padj: *P*-value adjusted; Glu1: 25 mM glucose Rep#1; Glu2: 25 mM glucose Rep#2; Glu3: 25 mM glucose Rep#3; Mt1: 25 mM maltotriose Rep#1; Mt2: 25 mM maltotriose Rep#2; Mt3: 25 mM maltotriose Rep#3.

Transcript	Gene name	Base mean	log2 Fold Change	padj	Glu1	Glu2	Glu3	Mt1	Mt2	Mt3
ENSMUST00000212660.1	Adgrg1	15.5	-21.7	2.8E-05	0.0	93.1	0.0	0.0	0.0	0.0
ENSMUST00000110175.8	Tbc1d31	14.4	-21.6	3.0E-05	0.0	86.7	0.0	0.0	0.0	0.0
ENSMUST00000132302.1	Smad5	14.2	-21.1	5.2E-05	0.0	85.4	0.0	0.0	0.0	0.0
ENSMUST00000206068.1	Bckdk	43.2	-9.1	4.8E-05	192.6	36.2	30.2	0.0	0.0	0.0
ENSMUST00000178791.2	Gm2058	30.8	-8.6	1.2E-05	109.7	37.5	37.3	0.0	0.0	0.0
ENSMUST00000145230.7	Adrm1	22.1	-8.1	1.8E-05	28.0	40.1	64.5	0.0	0.0	0.0
ENSMUST00000139946.7	Ash2l	21.6	-8.1	1.8E-05	41.4	60.8	27.2	0.0	0.0	0.0
ENSMUST00000229957.1	Pmm1	19.0	-7.9	2.9E-05	28.0	33.6	52.4	0.0	0.0	0.0
ENSMUST00000132719.1	Prkab2	18.3	-7.9	5.6E-05	41.4	22.0	46.4	0.0	0.0	0.0
ENSMUST00000232404.1	Pi4ka	16.5	-7.7	5.2E-05	35.8	38.8	24.2	0.0	0.0	0.0
ENSMUST00000124525.1	Kdm5a	16.1	-7.7	4.4E-05	37.0	33.6	26.2	0.0	0.0	0.0
ENSMUST00000139632.7	Gnpda2	14.4	-7.5	7.8E-05	26.9	31.0	28.2	0.0	0.0	0.0
ENSMUST00000038831.14	Hexdc	13.8	-7.4	7.3E-04	24.6	16.8	41.3	0.0	0.0	0.0
ENSMUST00000060807.11	Fam83h	44.3	-7.3	1.5E-04	47.0	175.9	41.3	0.0	1.6	0.0
ENSMUST00000147641.7	Zfp707	11.7	-7.2	4.7E-04	24.6	24.6	21.2	0.0	0.0	0.0
ENSMUST00000221279.1	Zfp934	11.7	-7.2	4.7E-04	24.6	23.3	22.2	0.0	0.0	0.0
ENSMUST00000179365.7	Snx10	122.0	-2.7	5.6E-05	295.6	121.6	214.7	47.8	25.7	26.6

Table 3.5 Differentially expressed genes (upregulated in 25 mM glucose- treated STC-1 cells) for transcripts with >4-fold (log2=+/-2) difference with ***p*adj < 1e-05**. padj: *P*-value adjusted; Glu1: 25 mM glucose Rep#1; Glu2: 25 mM glucose Rep#2; Glu3: 25 mM glucose Rep#3; Mt1: 25 mM maltotriose Rep#1; Mt2: 25 mM maltotriose Rep#2; Mt3: 25 mM maltotriose Rep#3.

Transcript	Gene name	Base mean	log2 Fold Change	padj	Glu1	Glu2	Glu3	Mt1	Mt2	Mt3
ENSMUST00000115520.7	Ica1	117.9	-10.5	3.8E-10	156.8	439.8	110.9	0.0	0.0	0.0
ENSMUST00000108448.7	Srr	70.9	-9.8	2.1E-09	104.1	232.8	88.7	0.0	0.0	0.0
ENSMUST00000202046.3	Uvssa	66.9	-9.7	5.7E-10	194.9	119.0	87.7	0.0	0.0	0.0
ENSMUST00000098585.3	E130208F15Rik	45.9	-9.2	6.2E-06	107.5	144.9	23.2	0.0	0.0	0.0
ENSMUST00000126633.1	Ctnnb1	43.3	-9.1	6.4E-06	153.4	80.2	26.2	0.0	0.0	0.0
ENSMUST00000225000.1	Ndst2	34.8	-8.8	3.4E-06	40.3	119.0	49.4	0.0	0.0	0.0
ENSMUST00000133726.7	Uqcc1	34.6	-8.8	9.7E-06	127.7	33.6	46.4	0.0	0.0	0.0
ENSMUST00000207832.1	Smarca2	25.0	-8.3	3.4E-06	32.5	58.2	59.5	0.0	0.0	0.0
ENSMUST00000100794.9	Myo18a	23.6	-8.2	5.4E-06	56.0	55.6	30.2	0.0	0.0	0.0
ENSMUST00000099934.10	Mical1	20.2	-8.0	4.4E-06	42.6	37.5	41.3	0.0	0.0	0.0
ENSMUST00000185656.6	Zfp287	94.9	-7.0	9.9E-13	150.1	222.5	192.5	4.2	0.0	0.0
ENSMUST00000147983.2	Ppp2r1a	68.1	-6.6	2.5E-06	178.1	148.7	77.6	4.2	0.0	0.0
ENSMUST00000172416.7	Ino80d	121.9	-6.3	1.2E-14	296.8	307.8	117.9	3.4	4.8	0.9
ENSMUST00000115791.9	Synj2	31.5	-5.7	3.4E-06	45.9	78.9	60.5	0.0	0.8	2.8
ENSMUST00000185265.1	Sumo1	99.1	-5.2	4.7E-06	166.9	196.6	214.7	0.0	4.8	11.4
ENSMUST00000049093.7	Txnip1	2777.8	-2.1	9.4E-49	4077.5	4688.7	4783.8	1025.0	893.0	1199.0
ENSMUST00000074519.12	Txnip2	2516.8	-2.1	7.3E-120	3900.5	4096.3	4168.9	885.0	1016.4	1033.8

Table 3.6 Differentially expressed genes (upregulated in 25 mM maltotriose- treated STC-1 cells) for transcripts with >4-fold (log2=+/-2) difference with ***p*adj < 1e-01**. padj: *P*-value adjusted; Glu1: 25 mM glucose Rep#1; Glu2: 25 mM glucose Rep#2; Glu3: 25 mM glucose Rep#3; Mt1: 25 mM maltotriose Rep#1; Mt2: 25 mM maltotriose Rep#2; Mt3: 25 mM maltotriose Rep#3.

Transcript	Gene name	Base mean	log2 Fold Change	padj	Glu1	Glu2	Glu3	Mt1	Mt2	Mt3
ENSMUST00000223880.1	Atxn7	59.4	2.1	1.8E-02	35.8	11.6	21.2	101.4	112.2	74.0
ENSMUST00000125521.7	Ncln	48.7	2.2	7.4E-02	19.0	15.5	18.1	51.1	48.1	140.5
ENSMUST00000106933.1	Dnajc6	156.0	2.4	1.5E-02	90.7	22.0	36.3	201.1	219.6	366.4
ENSMUST00000153287.7	Ucp2	17.9	3.4	8.7E-02	4.5	5.2	0.0	31.8	23.2	42.7
ENSMUST00000034281.12	6430548M08Rik	33.6	4.0	4.2E-02	0.0	10.3	2.0	87.2	52.9	49.4
ENSMUST00000231671.1	Yeats2	21.0	4.6	9.2E-02	0.0	5.2	0.0	39.4	57.7	23.7
ENSMUST00000129008.4	Mlxipl	30.2	4.7	1.2E-02	5.6	0.0	1.0	51.1	24.8	98.7
ENSMUST00000228971.1	Sgsm3	11.5	4.9	5.9E-02	0.0	0.0	2.0	21.0	14.4	31.3
ENSMUST00000208149.1	Rinl	12.9	5.1	5.8E-02	1.1	0.0	1.0	14.2	12.8	48.4
ENSMUST00000136167.7	Jak1	14.1	5.1	3.2E-02	0.0	2.6	0.0	18.4	24.8	38.9
ENSMUST00000172281.7	Gpaa1	55.1	5.3	1.9E-02	0.0	0.0	8.1	49.4	94.6	178.5
ENSMUST00000211811.1	Slc27a1	15.7	5.3	3.7E-02	0.0	2.6	0.0	46.9	29.7	15.2
ENSMUST00000144051.7	Rps8	122.7	5.3	5.4E-02	0.0	0.0	18.1	373.0	99.4	245.9
ENSMUST00000193932.5	Slc38a3	9.4	5.5	5.0E-02	0.0	0.0	1.0	28.5	14.4	12.3
ENSMUST00000202556.3	Slc5a6	67.8	5.6	2.1E-03	0.0	0.0	8.1	189.4	129.9	79.7
ENSMUST00000162406.1	Tmem163	40.2	5.7	9.5E-02	4.5	0.0	0.0	46.1	7.2	183.2
ENSMUST00000070418.8	Dclk1	11.3	5.8	1.2E-02	0.0	1.3	0.0	26.8	17.6	21.8
ENSMUST00000213199.1	1700017B05Rik	6.3	5.9	9.0E-02	0.0	0.0	0.0	17.6	8.0	12.3
ENSMUST00000132837.4	Mtmr1	6.7	6.0	4.7E-02	0.0	0.0	0.0	15.9	12.0	12.3
ENSMUST00000074783.11	Hmcn1	6.8	6.0	4.9E-02	0.0	0.0	0.0	15.9	10.4	14.2
ENSMUST00000133172.1	Mvp	7.1	6.1	6.6E-02	0.0	0.0	0.0	21.8	11.2	9.5
ENSMUST00000162201.1	Sertm1	7.2	6.1	7.4E-02	0.0	0.0	0.0	9.2	10.4	23.7
ENSMUST00000146044.7	Git2	7.4	6.1	8.3E-02	0.0	0.0	0.0	12.6	7.2	24.7
ENSMUST00000128254.7	Vps33b	7.5	6.2	6.1E-02	0.0	0.0	0.0	8.4	23.2	13.3
ENSMUST00000180268.1	Gm14596	7.5	6.2	3.8E-02	0.0	0.0	0.0	18.4	9.6	17.1

Table 3.6 (Continued).

Transcript	Gene name	Base mean	log2 Fold Change	padj	Glu1	Glu2	Glu3	Mt1	Mt2	Mt3
ENSMUST00000153492.7	Spg7	7.6	6.2	5.2E-02	0.0	0.0	0.0	8.4	15.2	21.8
ENSMUST00000177895.7	Sh3gl3	7.6	6.2	2.3E-02	0.0	0.0	0.0	17.6	13.6	14.2
ENSMUST00000037548.10	Rnf146	7.8	6.2	3.2E-02	0.0	0.0	0.0	10.1	17.6	19.0
ENSMUST00000202409.1	Poln	7.9	6.2	2.0E-02	0.0	0.0	0.0	18.4	12.8	16.1
ENSMUST00000177193.7	Traf7	8.0	6.3	6.1E-02	0.0	0.0	0.0	15.9	7.2	24.7
ENSMUST00000173525.1	Usp22	8.1	6.3	9.3E-02	0.0	0.0	0.0	9.2	8.0	31.3
ENSMUST00000152522.7	Pigt	8.1	6.3	7.7E-02	0.0	0.0	0.0	6.7	13.6	28.5
ENSMUST00000182713.1	Nktr	8.2	6.3	5.9E-02	0.0	0.0	0.0	19.3	23.2	6.6
ENSMUST00000212952.1	Csnk2a2	8.3	6.3	2.3E-02	0.0	0.0	0.0	10.9	16.8	21.8
ENSMUST00000212824.1	Nup93	8.8	6.4	1.3E-02	0.0	0.0	0.0	13.4	16.8	22.8
ENSMUST00000177424.1	Satb2	9.2	6.5	3.5E-02	0.0	0.0	0.0	26.0	21.6	7.6
ENSMUST00000142964.7	Mpg	18.4	6.5	3.5E-03	0.0	1.3	0.0	59.5	20.8	28.5
ENSMUST00000068992.7	Pcdh9	9.5	6.5	6.3E-03	0.0	0.0	0.0	15.9	20.0	20.9
ENSMUST00000147109.1	Mapk8ip3	9.6	6.5	1.3E-02	0.0	0.0	0.0	24.3	11.2	21.8
ENSMUST00000163586.8	Senp8	9.8	6.6	1.6E-02	0.0	0.0	0.0	31.0	14.4	13.3
ENSMUST00000178255.1	Gm7958	9.9	6.6	8.5E-03	0.0	0.0	0.0	21.8	12.8	24.7
ENSMUST00000224820.1	Zkscan3	10.0	6.6	3.7E-02	0.0	0.0	0.0	24.3	28.9	6.6
ENSMUST00000223033.1	Cast	10.1	6.6	4.4E-02	0.0	0.0	0.0	20.1	6.4	34.2
ENSMUST00000084843.9	Xntrpc	10.1	6.6	4.7E-03	0.0	0.0	0.0	16.8	19.2	24.7
ENSMUST00000150951.1	Ipo4	10.3	6.6	4.2E-02	0.0	0.0	0.0	40.2	12.0	9.5
ENSMUST00000020311.12	Micu1	10.5	6.6	1.6E-02	0.0	0.0	0.0	11.7	16.0	35.1
ENSMUST00000200377.4	Ap4b1	10.8	6.7	8.0E-02	0.0	0.0	0.0	15.1	44.9	4.7
ENSMUST00000188181.6	Cacna1c	11.3	6.8	3.4E-02	0.0	0.0	0.0	10.1	45.7	12.3
ENSMUST00000191823.5	Clasp1	11.5	6.8	1.1E-02	0.0	0.0	0.0	39.4	15.2	14.2
ENSMUST00000120375.7	Itga3	11.5	6.8	1.7E-02	0.0	0.0	0.0	39.4	9.6	19.9
ENSMUST00000178563.1	Mfsd4b4	11.8	6.8	1.2E-02	0.0	0.0	0.0	12.6	40.9	17.1
ENSMUST00000219983.1	Cdk2	11.8	6.8	3.2E-03	0.0	0.0	0.0	15.1	31.3	24.7

Table 3.6 (Continued).

Transcript	Gene name	Base mean	log2 Fold Change	padj	Glu1	Glu2	Glu3	Mt1	Mt2	Mt3
ENSMUST00000206117.1	Arhgap17	11.8	6.8	9.3E-02	0.0	0.0	0.0	52.8	14.4	3.8
ENSMUST00000212799.1	Adgrg1	12.2	6.9	3.9E-03	0.0	0.0	0.0	14.2	24.0	35.1
ENSMUST00000169828.7	Nfe2l1	12.6	6.9	8.7E-02	0.0	0.0	0.0	2.5	46.5	26.6
ENSMUST00000223025.1	Ptpdc1	12.7	6.9	7.4E-03	0.0	0.0	0.0	34.4	10.4	31.3
ENSMUST00000174663.7	Dtnb	13.1	7.0	5.3E-03	0.0	0.0	0.0	11.7	38.5	28.5
ENSMUST00000205930.1	Spns1	13.2	7.0	3.3E-03	0.0	0.0	0.0	13.4	29.7	36.1
ENSMUST00000123977.7	Pced1a	13.3	7.0	8.3E-03	0.0	0.0	0.0	15.9	48.9	15.2
ENSMUST00000155417.1	Dlat	13.6	7.0	8.2E-03	0.0	0.0	0.0	45.3	25.7	10.4
ENSMUST00000176425.1	Glmp	13.6	7.0	1.6E-03	0.0	0.0	0.0	26.8	16.8	38.0
ENSMUST00000018700.13	Dlg4	91.4	7.3	4.1E-02	2.2	1.3	0.0	339.4	205.2	0.0
ENSMUST00000191290.2	Snap91	16.7	7.3	7.7E-03	0.0	0.0	0.0	68.7	16.0	15.2
ENSMUST00000111297.9	Phf21a	17.3	7.4	3.7E-03	0.0	0.0	0.0	53.6	10.4	39.9
ENSMUST00000187987.1	Soat1	20.8	7.6	2.3E-03	0.0	0.0	0.0	12.6	34.5	77.8
ENSMUST00000020529.12	Ahsa2	32.1	8.3	3.3E-02	0.0	0.0	0.0	53.6	137.9	0.9
ENSMUST00000037489.14	Agpat1	39.1	8.6	1.4E-03	0.0	0.0	0.0	187.7	12.8	34.2
ENSMUST00000196141.4	Zgrf1	60.4	9.2	6.2E-02	0.0	0.0	0.0	240.5	121.8	0.0
ENSMUST00000135802.7	Kdm5a	61.2	9.2	6.6E-02	0.0	0.0	0.0	122.4	0.0	244.9

Table 3.7 Differentially expressed genes (upregulated in 25 mM maltotriose- treated STC-1 cells) for transcripts with >4-fold (log2=+/-2) difference with ***p*adj < 1e-03**. padj: *P*-value adjusted; Glu1: 25 mM glucose Rep#1; Glu2: 25 mM glucose Rep#2; Glu3: 25 mM glucose Rep#3; Mt1: 25 mM maltotriose Rep#1; Mt2: 25 mM maltotriose Rep#2; Mt3: 25 mM maltotriose Rep#3.

Transcript	Gene name	Base mean	log2 Fold Change	padj	Glu1	Glu2	Glu3	Mt1	Mt2	Mt3
ENSMUST00000224797.1	Actr8	71.9	2.2	1.5E-04	26.9	22.0	26.2	127.4	76.2	152.8
ENSMUST00000160244.7	Etv1	54.1	2.6	6.2E-04	9.0	12.9	23.2	98.9	65.7	114.9
ENSMUST00000163524.7	Tenm2	220.0	4.3	7.5E-05	47.0	11.6	6.0	189.4	476.2	589.5
ENSMUST00000113706.9	Trim39	21.3	5.8	8.3E-04	0.0	0.0	2.0	32.7	50.5	42.7
ENSMUST00000107744.1	Galnt12	53.9	5.9	6.6E-04	0.0	0.0	5.0	82.1	52.9	183.2
ENSMUST00000171265.7	Sgk3	38.6	6.0	5.3E-04	0.0	3.9	0.0	116.5	72.1	38.9
ENSMUST00000232072.1	Itgb1bp1	13.1	7.0	8.4E-04	0.0	0.0	0.0	33.5	22.4	22.8
ENSMUST00000163610.8	Psmd13	15.6	7.2	2.5E-04	0.0	0.0	0.0	40.2	25.7	27.5
ENSMUST00000138410.7	Grip1	16.0	7.3	4.2E-04	0.0	0.0	0.0	31.8	43.3	20.9
ENSMUST00000212015.1	Arhgef11	31.7	7.3	5.8E-05	0.0	0.0	1.0	91.4	40.9	57.0
ENSMUST00000137212.7	Snx10	16.8	7.3	7.5E-05	0.0	0.0	0.0	38.6	32.1	30.4
ENSMUST00000176140.7	Pou6f1	17.0	7.3	7.1E-04	0.0	0.0	0.0	26.8	20.8	54.1
ENSMUST00000139608.7	Rtel1	19.9	7.6	4.2E-04	0.0	0.0	0.0	38.6	61.7	19.0
ENSMUST00000106403.7	Kdm4a	20.4	7.6	5.8E-05	0.0	0.0	0.0	26.8	41.7	54.1
ENSMUST00000226415.1	Eif3e	21.6	7.7	1.8E-04	0.0	0.0	0.0	55.3	54.5	19.9
ENSMUST00000177056.7	Taf6l	21.8	7.7	2.9E-05	0.0	0.0	0.0	29.3	52.9	48.4
ENSMUST00000039998.10	Fbxo27	24.7	7.9	1.6E-05	0.0	0.0	0.0	56.2	31.3	60.8
ENSMUST00000200389.1	Pde5a	26.5	8.0	5.7E-05	0.0	0.0	0.0	57.0	24.0	77.8
ENSMUST00000036462.11	Fam214b	31.2	8.2	5.0E-04	0.0	0.0	0.0	59.5	13.6	113.9
ENSMUST00000002924.14	Tmem39a	33.7	8.3	1.8E-05	0.0	0.0	0.0	26.8	85.0	90.2
ENSMUST00000087258.9	Tro	47.5	8.8	8.1E-05	0.0	0.0	0.0	59.5	22.4	203.2

Table 3.8 Differentially expressed genes (upregulated in 25 mM maltotriose-treated STC-1 cells) for transcripts with >4-fold (log2=+/-2) difference with ***p*adj < 1e-05**. padj: *P*-value adjusted; Glu1: 25 mM glucose Rep#1; Glu2: 25 mM glucose Rep#2; Glu3: 25 mM glucose Rep#3; Mt1: 25 mM maltotriose Rep#1; Mt2: 25 mM maltotriose Rep#2; Mt3: 25 mM maltotriose Rep#3.

Transcript	Gene name	Base mean	log2 Fold Change	padj	Glu1	Glu2	Glu3	Mt1	Mt2	Mt3
ENSMUST00000170442.7	Usf2	34.6	5.5	1.4E-06	0.0	1.3	3.0	54.5	73.7	75.0
ENSMUST00000108318.2	Ints8	31.5	8.2	4.7E-06	0.0	0.0	0.0	38.6	60.1	90.2
ENSMUST00000168631.7	Pkp4	381.4	8.5	6.0E-11	1.1	0.0	5.0	1046.0	117.0	1119.2
ENSMUST00000110416.2	Usp8	46.5	8.8	5.5E-06	0.0	0.0	0.0	31.0	141.9	106.3
ENSMUST00000232523.1	Top3b	51.1	8.9	3.7E-06	0.0	0.0	0.0	182.7	85.0	38.9
ENSMUST00000173240.7	Dtnb	52.8	9.0	2.9E-07	0.0	0.0	0.0	85.5	172.3	58.9
ENSMUST00000109058.8	Gm14391	85.3	9.7	2.9E-07	0.0	0.0	0.0	321.8	52.1	137.6
ENSMUST00000168086.6	Jade1	109.8	10.0	2.5E-07	0.0	0.0	0.0	151.7	54.5	452.8
ENSMUST00000232239.1	Rcan1	140.3	10.4	9.9E-09	0.0	0.0	0.0	60.3	338.3	443.3

Table 3.9 Description of differentially expressed genes upregulated in 25 mM glucose-treated STC-1 cells.

Gene name	Description
Adgrg1	Adhesion G protein-coupled receptor G1 [Source:MGI Symbol;Acc:MGI:1340051]
Tbc1d31	TBC1 domain family, member 31 [Source:MGI Symbol;Acc:MGI:2684931]
Smad5	SMAD family member 5 [Source:MGI Symbol;Acc:MGI:1328787]
Ica1	Islet cell autoantigen 1 [Source:MGI Symbol;Acc:MGI:96391]
Srr	Serine racemase [Source:MGI Symbol;Acc:MGI:1351636]
Uvssa	UV stimulated scaffold protein A [Source:MGI Symbol;Acc:MGI:1918351]
Abcc1	ATP-binding cassette, sub-family C (CFTR/MRP), member 1 [Source:MGI Symbol;Acc:MGI:102676]
Adcy7	Adenylate cyclase 7 [Source:MGI Symbol;Acc:MGI:102891]
E130208F15Rik	RIKEN cDNA E130208F15 gene [Source:MGI Symbol;Acc:MGI:3767226]
Ctnnb1	Catenin (cadherin associated protein), beta 1 [Source:MGI Symbol;Acc:MGI:88276]
Bckdk	Branched chain ketoacid dehydrogenase kinase [Source:MGI Symbol;Acc:MGI:1276121]
Arfgef1	ADP-ribosylation factor guanine nucleotide-exchange factor 1(brefeldin A-inhibited) [Source:MGI Symbol;Acc:MGI:2442988]
Tfe3	Transcription factor E3 [Source:MGI Symbol;Acc:MGI:98511]
Tnip1	TNFAIP3 interacting protein 1 [Source:MGI Symbol;Acc:MGI:1926194]
Ndst2	N-deacetylase/N-sulfotransferase (heparan glucosaminyl) 2 [Source:MGI Symbol;Acc:MGI:97040]
Uqcc1	Ubiquinol-cytochrome c reductase complex assembly factor 1 [Source:MGI Symbol;Acc:MGI:1929472]
Ppp2r1b	Protein phosphatase 2, regulatory subunit A, beta [Source:MGI Symbol;Acc:MGI:1920949]
Gm2058	Predicted gene 2058 [Source:MGI Symbol;Acc:MGI:3805010]
Zfp189	Zinc finger protein 189 [Source:MGI Symbol;Acc:MGI:2444707]
C2cd5	C2 calcium-dependent domain containing 5 [Source:MGI Symbol;Acc:MGI:1921991]
Smarca2	SWI/SNF related, matrix associated, actin dependent regulator of chromatin [Source:MGI Symbol;Acc:MGI:99603]
Myo18a	Myosin XVIIIA [Source:MGI Symbol;Acc:MGI:2667185]
Adrm1	Adhesion regulating molecule 1 [Source:MGI Symbol;Acc:MGI:1929289]
Ash2l	ASH2 like histone lysine methyltransferase complex subunit [Source:MGI Symbol;Acc:MGI:1344416]
Mical1	Microtubule associated monooxygenase, calponin and LIM domain containing 1 [Source:MGI Symbol;Acc:MGI:2385847]
Pmm1	Phosphomannomutase 1 [Source:MGI Symbol;Acc:MGI:1353418]
Prkab2	Protein kinase, AMP-activated, beta 2 non-catalytic subunit [Source:MGI Symbol;Acc:MGI:1336185]

Table 3.9 (Continued).

Gene name	Description
1810043G02Rik	RIKEN cDNA 1810043G02 gene [Source:MGI Symbol;Acc:MGI:1915134]
Pi4ka	Phosphatidylinositol 4-kinase alpha [Source:MGI Symbol;Acc:MGI:2448506]
Kdm5a	Lysine (K)-specific demethylase 5A [Source:MGI Symbol;Acc:MGI:2136980]
Gnpda2	Glucosamine-6-phosphate deaminase 2 [Source:MGI Symbol;Acc:MGI:1915230]
Hexdc	Hexosaminidase (glycosyl hydrolase family 20, catalytic domain) containing [Source:MGI Symbol;Acc:MGI:3605542]
Slc22a17	Solute carrier family 22 (organic cation transporter), member 17 [Source:MGI Symbol;Acc:MGI:1926225]
Tpm1	Tropomyosin 1, alpha [Source:MGI Symbol;Acc:MGI:98809]
Myo18a	Myosin XVIIIA [Source:MGI Symbol;Acc:MGI:2667185]
1700010I14Rik	RIKEN cDNA 1700010I14 gene [Source:MGI Symbol;Acc:MGI:1914181]
Rara	Retinoic acid receptor, alpha [Source:MGI Symbol;Acc:MGI:97856]
Fam83h	Family with sequence similarity 83, member H [Source:MGI Symbol;Acc:MGI:2145900]
Lhx1	LIM homeobox protein 1 [Source:MGI Symbol;Acc:MGI:99783]
Zfp707	Zinc finger protein 707 [Source:MGI Symbol;Acc:MGI:1916270]
Zfp934	Zinc finger protein 934 [Source:MGI Symbol;Acc:MGI:1924367]
Ppard	Peroxisome proliferator activator receptor delta [Source:MGI Symbol;Acc:MGI:101884]
Zfp287	Zinc finger protein 287 [Source:MGI Symbol;Acc:MGI:2176561]
Ncoa4	Nuclear receptor coactivator 4 [Source:MGI Symbol;Acc:MGI:1350932]
Tusc3	Tumor suppressor candidate 3 [Source:MGI Symbol;Acc:MGI:1933134]
Micall1	Microtubule associated monooxygenase, calponin and LIM domain containing -like 1 [Source:MGI Symbol;Acc:MGI:105870]
Tcf4	Transcription factor 4 [Source:MGI Symbol;Acc:MGI:98506]
Thoc7	THO complex 7 [Source:MGI Symbol;Acc:MGI:1913481]
Plekhh3	Pleckstrin homology domain containing, family H (with MyTH4 domain) member 3 [Source:MGI Symbol;Acc:MGI:2384950]
Adgrl3	Adhesion G protein-coupled receptor L3 [Source:MGI Symbol;Acc:MGI:2441950]
Tgfbr3	Transforming growth factor, beta receptor III [Source:MGI Symbol;Acc:MGI:104637]
Zfp677	Zinc finger protein 677 [Source:MGI Symbol;Acc:MGI:3053207]
Slc25a36	Solute carrier family 25, member 36 [Source:MGI Symbol;Acc:MGI:1924909]
App	Amyloid beta (A4) precursor protein [Source:MGI Symbol;Acc:MGI:88059]

Table 3.9 (Continued).

Gene name	Description
Ppp2r1a	Protein phosphatase 2, regulatory subunit A, alpha [Source:MGI Symbol;Acc:MGI:1926334]
Ubtf	Upstream binding transcription factor, RNA polymerase I [Source:MGI Symbol;Acc:MGI:98512]
Wipf3	WAS/WASL interacting protein family, member 3 [Source:MGI Symbol;Acc:MGI:3044681]
St6galnac6	ST6 (α-N-acetyl-neuraminyl-2,3-beta-galactosyl-1,3)-N-acetylgalactosaminide α-2,6-sialyltransferase 6 [Source:MGI Symbol;Acc:MGI:1355316]
Evi5	Ecotropic viral integration site 5 [Source:MGI Symbol;Acc:MGI:104736]
Prpf40b	Pre-mRNA processing factor 40B [Source:MGI Symbol;Acc:MGI:1925583]
Dlg3	Discs large MAGUK scaffold protein 3 [Source:MGI Symbol;Acc:MGI:1888986]
St3gal6	ST3 beta-galactoside alpha-2,3-sialyltransferase 6 [Source:MGI Symbol;Acc:MGI:1888707]
Ino80d	INO80 complex subunit D [Source:MGI Symbol;Acc:MGI:3027003]
Smarcd2	SWI/SNF related, matrix associated, actin dependent regulator of chromatin, subfamily d, member 2 [Source:MGI Symbol;Acc:MGI:1933621]
Synj2	Synaptojanin 2 [Source:MGI Symbol;Acc:MGI:1201671]
Atp2a3	ATPase, Ca++ transporting, ubiquitous [Source:MGI Symbol;Acc:MGI:1194503]
Sumo1	Small ubiquitin-like modifier 1 [Source:MGI Symbol;Acc:MGI:1197010]
Slc29a1	Solute carrier family 29 (nucleoside transporters), member 1 [Source:MGI Symbol;Acc:MGI:1927073]
Adgrb2	Adhesion G protein-coupled receptor B2 [Source:MGI Symbol;Acc:MGI:2451244]
Cyp51	Cytochrome P450, family 51 [Source:MGI Symbol;Acc:MGI:106040]
Pde3b	Phosphodiesterase 3B, cGMP-inhibited [Source:MGI Symbol;Acc:MGI:1333863]
Eif3d	Eukaryotic translation initiation factor 3, subunit D [Source:MGI Symbol;Acc:MGI:1933181]
Upp1	Uridine phosphorylase 1 [Source:MGI Symbol;Acc:MGI:1097668]
Pmm1	Phosphomannomutase 1 [Source:MGI Symbol;Acc:MGI:1353418]
Gstm5	Glutathione S-transferase, mu 5 [Source:MGI Symbol;Acc:MGI:1309466]
Cck	Cholecystokinin [Source:MGI Symbol;Acc:MGI:88297]
Wdfy4	WD repeat and FYVE domain containing 4 [Source:MGI Symbol;Acc:MGI:3584510]
Snx10	Sorting nexin 10 [Source:MGI Symbol;Acc:MGI:1919232]
Wsb2	WD repeat and SOCS box-containing 2 [Source:MGI Symbol;Acc:MGI:2144041]
Txnip1	Thioredoxin interacting protein1 [Source:MGI Symbol;Acc:MGI:1889549]

Table 3.9 (Continued).

Gene name	Description
Txnip2	Thioredoxin interacting protein2 [Source:MGI Symbol;Acc:MGI:1889549]
Phf21b	PHD finger protein 21B [Source:MGI Symbol;Acc:MGI:2443812]

Table 3.10 Description of differentially expressed genes upregulated in 25 mM maltotriose-treated STC-1 cells.

Gene name	Description
Atxn7	Ataxin 7 [Source:MGI Symbol;Acc:MGI:2179277]
Ncln	Nicalin [Source:MGI Symbol;Acc:MGI:1926081]
Actr8	ARP8 actin-related protein 8 [Source:MGI Symbol;Acc:MGI:1860775]
Dnajc6	DnaJ heat shock protein family (Hsp40) member C6 [Source:MGI Symbol;Acc:MGI:1919935]
Etv1	Ets variant 1 [Source:MGI Symbol;Acc:MGI:99254]
Ucp2	Uncoupling protein 2 (mitochondrial, proton carrier) [Source:MGI Symbol;Acc:MGI:109354]
6430548M08Rik	RIKEN cDNA 6430548M08 gene [Source:MGI Symbol;Acc:MGI:2443793]
Tenm2	Teneurin transmembrane protein 2 [Source:MGI Symbol;Acc:MGI:1345184]
Yeats2	YEATS domain containing 2 [Source:MGI Symbol;Acc:MGI:2447762]
Mlxipl	MLX interacting protein-like [Source:MGI Symbol;Acc:MGI:1927999]
Sgsm3	Small G protein signaling modulator 3 [Source:MGI Symbol;Acc:MGI:1916329]
Rinl	Ras and Rab interactor-like [Source:MGI Symbol;Acc:MGI:2444024]
Jak1	Janus kinase 1 [Source:MGI Symbol;Acc:MGI:96628]
Gpaa1	GPI anchor attachment protein 1 [Source:MGI Symbol;Acc:MGI:1202392]
Slc27a1	Solute carrier family 27 (fatty acid transporter), member 1 [Source:MGI Symbol;Acc:MGI:1347098]
Rps8	Ribosomal protein S8 [Source:MGI Symbol;Acc:MGI:98166]
Slc38a3	Solute carrier family 38, member 3 [Source:MGI Symbol;Acc:MGI:1923507]
Usf2	Upstream transcription factor 2 [Source:MGI Symbol;Acc:MGI:99961]
Slc5a6	Solute carrier family 5 (sodium-dependent vitamin transporter), member 6 [Source:MGI Symbol;Acc:MGI:2660847]
Tmem163	Transmembrane protein 163 [Source:MGI Symbol;Acc:MGI:1919410]
Dclk1	Doublecortin-like kinase 1 [Source:MGI Symbol;Acc:MGI:1330861]
Trim39	Tripartite motif-containing 39 [Source:MGI Symbol;Acc:MGI:1890659]
Galnt12	Polypeptide N-acetylgalactosaminyltransferase 12 [Source:MGI Symbol;Acc:MGI:2444664]
1700017B05Rik	RIKEN cDNA 1700017B05 gene [Source:MGI Symbol;Acc:MGI:1921461]
Sgk3	Serum/glucocorticoid regulated kinase 3 [Source:MGI Symbol;Acc:MGI:2182368]
Mtmr1	Myotubularin related protein 1 [Source:MGI Symbol;Acc:MGI:1858271]
Hmcn1	Hemicentin 1 [Source:MGI Symbol;Acc:MGI:2685047]

Table 3.10 (Continued).

Gene name	Description
Mvp	Major vault protein [Source:MGI Symbol;Acc:MGI:1925638]
Sertm1	Serine rich and transmembrane domain containing 1 [Source:MGI Symbol;Acc:MGI:3607715]
Git2	G protein-coupled receptor kinase-interactor 2 [Source:MGI Symbol;Acc:MGI:1347053]
Vps33b	Vacuolar protein sorting 33B [Source:MGI Symbol;Acc:MGI:2446237]
Gm14596	Predicted gene 14596 [Source:MGI Symbol;Acc:MGI:3705870]
Spg7	SPG7, paraplegin matrix AAA peptidase subunit [Source:MGI Symbol;Acc:MGI:2385906]
Sh3gl3	SH3-domain GRB2-like 3 [Source:MGI Symbol;Acc:MGI:700011]
Rnf146	Ring finger protein 146 [Source:MGI Symbol;Acc:MGI:1915281]
Poln	DNA polymerase N [Source:MGI Symbol;Acc:MGI:2675617]
Traf7	TNF receptor-associated factor 7 [Source:MGI Symbol;Acc:MGI:3042141]
Usp22	Ubiquitin specific peptidase 22 [Source:MGI Symbol;Acc:MGI:2144157]
Pigt	Phosphatidylinositol glycan anchor biosynthesis, class T [Source:MGI Symbol;Acc:MGI:1926178]
Nktr	Natural killer tumor recognition sequence [Source:MGI Symbol;Acc:MGI:97346]
Csnk2a2	Casein kinase 2, alpha prime polypeptide [Source:MGI Symbol;Acc:MGI:88547]
Nup93	Nucleoporin 93 [Source:MGI Symbol;Acc:MGI:1919055]
Satb2	Special AT-rich sequence binding protein 2 [Source:MGI Symbol;Acc:MGI:2679336]
Mpg	N-methylpurine-DNA glycosylase [Source:MGI Symbol;Acc:MGI:97073]
Pcdh9	Protocadherin 9 [Source:MGI Symbol;Acc:MGI:1306801]
Mapk8ip3	Mitogen-activated protein kinase 8 interacting protein 3 [Source:MGI Symbol;Acc:MGI:1353598]
Senp8	SUMO/sentrin specific peptidase 8 [Source:MGI Symbol;Acc:MGI:1918849]
Gm7958	Predicted gene 7958 [Source:MGI Symbol;Acc:MGI:3643207]
Zkscan3	Zinc finger with KRAB and SCAN domains 3 [Source:MGI Symbol;Acc:MGI:1919989]
Cast	Calpastatin [Source:MGI Symbol;Acc:MGI:1098236]
Xntrpc	Xndc1-transient receptor potential cation channel, subfamily C, member 2 [Source:MGI Symbol;Acc:MGI:5546370]
Ipo4	Importin 4 [Source:MGI Symbol;Acc:MGI:1923001]
Micu1	Mitochondrial calcium uptake 1 [Source:MGI Symbol;Acc:MGI:2384909]
Ap4b1	Adaptor-related protein complex AP-4, beta 1 [Source:MGI Symbol;Acc:MGI:1337130]

Table 3.10 (Continued).

Gene name	Description
Cacna1c	Calcium channel, voltage-dependent, L type, alpha 1C subunit [Source:MGI Symbol;Acc:MGI:103013]
Clasp1	CLIP associating protein 1 [Source:MGI Symbol;Acc:MGI:1923957]
Itga3	Integrin alpha 3 [Source:MGI Symbol;Acc:MGI:96602]
Mfsd4b4	Major facilitator superfamily domain containing 4B4 [Source:MGI Symbol;Acc:MGI:3035041]
Cdk2	Cyclin-dependent kinase 2 [Source:MGI Symbol;Acc:MGI:104772]
Arhgap17	Rho GTPase activating protein 17 [Source:MGI Symbol;Acc:MGI:1917747]
Adgrg1	Adhesion G protein-coupled receptor G1 [Source:MGI Symbol;Acc:MGI:1340051]
Nfe2l1	Nuclear factor, erythroid derived 2, -like 1 [Source:MGI Symbol;Acc:MGI:99421]
Ptpdc1	Protein tyrosine phosphatase domain containing 1 [Source:MGI Symbol;Acc:MGI:2145430]
Dtnb	Dystrobrevin, beta [Source:MGI Symbol;Acc:MGI:1203728]
Itgb1bp1	Integrin beta 1 binding protein 1 [Source:MGI Symbol;Acc:MGI:1306802]
Spns1	Spinster homolog 1 [Source:MGI Symbol;Acc:MGI:1920908]
Pced1a	PC-esterase domain containing 1A [Source:MGI Symbol;Acc:MGI:2442177]
Dlat	Dihydrolipoamide S-acetyltransferase (E2 of pyruvate dehydrogenase complex) [Source:MGI Symbol;Acc:MGI:2385311]
Glmp	Glycosylated lysosomal membrane protein [Source:MGI Symbol;Acc:MGI:1913318]
Psmd13	Proteasome (prosome, macropain) 26S subunit, non-ATPase, 13 [Source:MGI Symbol;Acc:MGI:1345192]
Grip1	Glutamate receptor interacting protein 1 [Source:MGI Symbol;Acc:MGI:1921303]
Arhgef11	Rho guanine nucleotide exchange factor (GEF) 11 [Source:MGI Symbol;Acc:MGI:2441869]
Dlg4	Discs large MAGUK scaffold protein 4 [Source:MGI Symbol;Acc:MGI:1277959]
Snap91	Synaptosomal-associated protein 91 [Source:MGI Symbol;Acc:MGI:109132]
Snx10	Sorting nexin 10 [Source:MGI Symbol;Acc:MGI:1919232]
Pou6f1	POU domain, class 6, transcription factor 1 [Source:MGI Symbol;Acc:MGI:102935]
Phf21a	PHD finger protein 21A [Source:MGI Symbol;Acc:MGI:2384756]
Rtel1	Regulator of telomere elongation helicase 1 [Source:MGI Symbol;Acc:MGI:2139369]
Kdm4a	Lysine (K)-specific demethylase 4A [Source:MGI Symbol;Acc:MGI:2446210]
Soat1	Sterol O-acyltransferase 1 [Source:MGI Symbol;Acc:MGI:104665]
Eif3e	Eukaryotic translation initiation factor 3, subunit E [Source:MGI Symbol;Acc:MGI:99257]

Table 3.10 (Continued).

Gene name	Description
Taf6l	TATA-box binding protein associated factor 6 like [Source:MGI Symbol;Acc:MGI:2444957]
Fbxo27	F-box protein 27 [Source:MGI Symbol;Acc:MGI:2685007]
Pde5a	Phosphodiesterase 5A, cGMP-specific [Source:MGI Symbol;Acc:MGI:2651499]
Fam214b	Family with sequence similarity 214, member B [Source:MGI Symbol;Acc:MGI:2441854]
Ints8	Integrator complex subunit 8 [Source:MGI Symbol;Acc:MGI:1919906]
Ahsa2	AHA1, activator of heat shock protein ATPase 2 [Source:MGI Symbol;Acc:MGI:1916133]
Tmem39a	Transmembrane protein 39a [Source:MGI Symbol;Acc:MGI:1915096]
Pkp4	Plakophilin 4 [Source:MGI Symbol;Acc:MGI:109281]
Agpat1	1-acylglycerol-3-phosphate O-acyltransferase 1 (lysophosphatidic acid acyltransferase, alpha) [Source:MGI Symbol;Acc:MGI:1932075]
Usp8	Ubiquitin specific peptidase 8 [Source:MGI Symbol;Acc:MGI:1934029]
Tro	Trophinin [Source:MGI Symbol;Acc:MGI:1928994]
Top3b	Topoisomerase (DNA) III beta [Source:MGI Symbol;Acc:MGI:1333803]
Dtnb	Dystrobrevin, beta [Source:MGI Symbol;Acc:MGI:1203728]
Zgrf1	Zinc finger, GRF-type containing 1 [Source:MGI Symbol;Acc:MGI:1918893]
Kdm5a	Lysine (K)-specific demethylase 5A [Source:MGI Symbol;Acc:MGI:2136980]
Gm14391	Predicted gene 14391 [Source:MGI Symbol;Acc:MGI:3709324]
Jade1	Jade family PHD finger 1 [Source:MGI Symbol;Acc:MGI:1925835]
Rcan1	Regulator of calcineurin 1 [Source:MGI Symbol;Acc:MGI:1890564]

Table 3.11 GO terms **(biological process)** for 79 recognized genes upregulated with glucose treatment.

Term	Count	%	*P*-Value	Benjamini
Regulation of transcription, DNA-templated	21	26.6	5.2E-4	1.8E-1
Transcription, DNA-templated	15	19.0	1.7E-2	7.7E-1
Positive regulation of transcription, DNA-templated	9	11.4	2.2E-3	4.3E-1
Positive regulation of transcription from RNA polymerase II promoter	9	11.4	4.7E-2	8.7E-1
Nervous system development	7	8.9	4.2E-3	5.4E-1
Cell differentiation	7	8.9	9.5E-2	9.0E-1
Positive regulation of cell proliferation	6	7.6	6.8E-2	8.9E-1
Cellular process	4	5.1	1.2E-4	8.7E-2
Endocytosis	4	5.1	3.7E-2	8.5E-1
Negative regulation of gene expression	4	5.1	9.2E-2	9.0E-1
Protein N-linked glycosylation via asparagine	3	3.8	6.9E-3	6.5E-1
Regulation of insulin secretion	3	3.8	1.5E-2	8.1E-1
Ureteric bud development	3	3.8	1.6E-2	7.8E-1
Positive regulation of cell adhesion	3	3.8	2.2E-2	7.8E-1
Protein complex assembly	3	3.8	2.9E-2	8.2E-1
Negative regulation of angiogenesis	3	3.8	3.4E-2	8.5E-1
Response to estrogen	3	3.8	3.7E-2	8.3E-1
Response to estradiol	3	3.8	6.3E-2	8.9E-1
Neuron migration	3	3.8	9.0E-2	9.1E-1
Oviduct development	2	2.5	1.2E-2	7.8E-1
Beta-catenin destruction complex disassembly	2	2.5	2.0E-2	7.8E-1
Ventricular compact myocardium morphogenesis	2	2.5	2.8E-2	8.3E-1
Chromatin-mediated maintenance of transcription	2	2.5	4.4E-2	8.6E-1
Layer formation in cerebral cortex	2	2.5	5.5E-2	9.0E-1
Positive regulation of extrinsic apoptotic signaling pathway in absence of ligand	2	2.5	5.9E-2	9.0E-1
Endoderm formation	2	2.5	6.3E-2	9.0E-1
Cardiac muscle cell proliferation	2	2.5	6.6E-2	9.0E-1
Regulation of osteoclast differentiation	2	2.5	6.6E-2	9.0E-1
Ganglioside biosynthetic process	2	2.5	7.0E-2	8.9E-1
Seminiferous tubule development	2	2.5	7.4E-2	8.9E-1
Response to vitamin A	2	2.5	7.4E-2	8.9E-1
Regulation of protein binding	2	2.5	8.1E-2	9.1E-1
Regulation of myelination	2	2.5	8.1E-2	9.1E-1
Anterior/posterior axis specification	2	2.5	8.5E-2	9.1E-1
Transcription elongation from RNA polymerase II promoter	2	2.5	8.5E-2	9.1E-1
Renal system development	2	2.5	8.9E-2	9.1E-1
Embryonic pattern specification	2	2.5	9.3E-2	9.0E-1

Table 3.12 Go terms **(cellular component)** for 79 recognized genes upregulated with glucose treatment.

Term	Count	%	*P*-Value	Benjamini
Cytoplasm	37	46.8	7.2E-3	7.3E-1
Nucleoplasm	13	16.5	6.2E-2	6.2E-1
Intracellular	12	15.2	3.9E-2	6.5E-1
Cytoskeleton	10	12.7	2.5E-2	6.9E-1
Golgi apparatus	9	11.4	8.3E-2	5.8E-1
Nuclear chromatin	5	6.3	1.1E-2	6.4E-1
Golgi membrane	5	6.3	6.8E-2	6.0E-1
Cell-cell junction	4	5.1	4.2E-2	6.2E-1
Basolateral plasma membrane	4	5.1	4.3E-2	5.5E-1
Membrane raft	4	5.1	7.9E-2	6.1E-1
Transcription factor complex	4	5.1	8.2E-2	6.0E-1
Dendritic shaft	3	3.8	2.3E-2	7.5E-1
Extrinsic component of membrane	3	3.8	4.2E-2	5.8E-1
Apical part of cell	3	3.8	7.1E-2	5.9E-1
Ruffle membrane	3	3.8	3.7E-2	6.8E-1
Fibrillar center	2	2.5	3.4E-2	7.1E-1
SWI/SNF complex	2	2.5	4.8E-2	5.6E-1
BAF-type complex	2	2.5	6.3E-2	6.0E-1

Table 3.13 Go terms **(molecular function)** for 79 recognized genes upregulated with glucose treatment.

Term	Count	%	*P*-Value	Benjamini
Protein binding	24	0.2	3.4E-2	6.9E-1
Metal ion binding	22	0.2	1.4E-2	4.9E-1
DNA binding	13	0.1	5.2E-2	7.1E-1
Transcription factor activity, sequence-specific DNA binding	12	0.1	5.7E-4	1.3E-1
Chromatin binding	6	0.1	3.5E-2	6.5E-1
Protein heterodimerization activity	6	0.1	5.0E-2	7.4E-1
Transcription regulatory region DNA binding	5	0.0	1.3E-2	5.4E-1
Enzyme binding	5	0.0	6.3E-2	7.5E-1
PDZ domain binding	4	0.0	1.0E-2	7.1E-1
Transcription coactivator activity	4	0.0	3.3E-2	7.3E-1
Ubiquitin protein ligase binding	4	0.0	9.9E-2	7.3E-1
Drug binding	3	0.0	7.1E-2	7.1E-1
SH3 domain binding	3	0.0	7.7E-2	6.9E-1
Rab GTPase binding	3	0.0	9.3E-2	7.4E-1
Actin filament binding	3	0.0	9.4E-2	7.2E-1
Euchromatin binding	2	0.0	1.2E-2	6.0E-1
Protein kinase B binding	2	0.0	6.4E-2	7.3E-1
Protein phosphatase type 2A regulator activity	2	0.0	6.8E-2	7.2E-1
Sialyl transferase activity	2	0.0	7.5E-2	7.1E-1

Table 3.14 KEGG pathway analysis for 79 recognized genes upregulated with glucose treatment.

Term	Count	%	*P*-Value	Benjamini
Metabolic pathways	10	0.1	8.3E-2	8.3E-1
Pathways in cancer	5	0.0	8.7E-2	7.8E-1
Adrenergic signaling in cardiomyocytes	4	0.0	2.6E-2	9.3E-1
Hippo signaling pathway	4	0.0	2.6E-2	7.4E-1
TGF-beta signaling pathway	3	0.0	5.1E-2	8.3E-1
Oocyte meiosis	3	0.0	8.0E-2	8.8E-1
Sphingolipid signaling pathway	3	0.0	9.8E-2	7.7E-1

Table 3.15 Go terms **(biological process)** for 98 recognized genes upregulated with maltotriose treatment.

Term	Count	%	*P*-Value	Benjamini
Regulation of transcription, DNA-templated	20	20.4	9.7E-3	9.9E-1
Transcription, DNA-templated	17	17.3	1.5E-2	9.4E-1
Negative regulation of transcription from RNA Polymerase II promoter	9	9.2	2.3E-2	8.7E-1
Positive regulation of transcription, DNA-templated	8	8.2	2.0E-2	9.3E-1
Protein transport	8	8.2	2.3E-2	8.3E-1
Cell cycle	8	8.2	2.7E-2	8.1E-1
Cell adhesion	6	6.1	8.1E-2	9.3E-1
Covalent chromatin modification	5	5.1	3.8E-2	8.3E-1
DNA repair	5	5.1	6.5E-2	9.0E-1
Endosome organization	3	3.1	1.0E-2	9.4E-1
Histone H3 acetylation	3	3.1	2.1E-2	9.0E-1
Forebrain development	3	3.1	6.3E-2	9.2E-1
Attachment of GPI anchor to protein	2	2.0	2.4E-2	8.0E-1
Regulation of clathrin-mediated endocytosis	2	2.0	2.8E-2	7.9E-1
Phosphatidic acid biosynthetic process	2	2.0	3.7E-2	8.5E-1
Short-term memory	2	2.0	6.0E-2	9.2E-1
Calcium ion regulated exocytosis	2	2.0	6.5E-2	9.1E-1
Histone deubiquitination	2	2.0	6.5E-2	9.1E-1
Negative regulation of cell cycle arrest	2	2.0	8.7E-2	9.3E-1

Table 3.16 Go terms **(cellular component)** for 98 recognized genes upregulated with maltotriose treatment.

Term	Count	%	*P*-Value	Benjamini
Nucleus	44	0.3	6.2E-4	1.1E-1
Membrane	43	0.3	2.4E-2	4.8E-1
Cytoplasm	42	0.3	1.6E-2	4.6E-1
Cytosol	15	0.1	3.5E-2	5.2E-1
Endoplasmic reticulum	12	0.1	4.2E-2	4.9E-1
Cytoplasmic vesicle	9	0.1	1.0E-2	3.8E-1
Cell junction	8	0.0	4.9E-2	4.9E-1
Synapse	7	0.0	3.0E-2	5.1E-1
Endosome	7	0.0	4.0E-2	5.1E-1
Cytoplasmic, membrane-bounded vesicle	6	0.0	6.8E-4	6.3E-2
Postsynaptic density	6	0.0	5.1E-3	2.7E-1
Growth cone	4	0.0	3.8E-2	5.2E-1
Postsynaptic membrane	4	0.0	8.4E-2	6.0E-1
Cell periphery	3	0.0	4.3E-2	4.7E-1
Early endosome membrane	3	0.0	6.2E-2	5.5E-1
Extrinsic component of endosome membrane	2	0.0	2.3E-2	5.2E-1
GPI-anchor transamidase complex	2	0.0	2.3E-2	5.2E-1
STAGA complex	2	0.0	6.3E-2	5.4E-1
Cell-cell contact zone	2	0.0	7.6E-2	5.8E-1
Nuclear periphery	2	0.0	8.9E-2	6.0E-1

Table 3.17 Go terms **(molecular functions)** for 98 recognized genes upregulated with maltotriose treatment.

Term	Count	%	*P*-Value	Benjamini
Protein binding	28	0.2	4.3E-2	9.6E-1
Zinc ion binding	12	0.1	1.4E-2	9.5E-1
Sequence-specific DNA binding	7	0.0	8.5E-2	8.8E-1
RNA polymerase II core promoter proximal region sequence-specific DNA binding	5	0.0	9.5E-2	8.9E-1
Protein transporter activity	3	0.0	4.6E-2	9.2E-1
Protein phosphatase binding	3	0.0	6.7E-2	9.2E-1
Protein tyrosine phosphatase activity	3	0.0	8.0E-2	9.0E-1
GPI-anchor transamidase activity	2	0.0	2.4E-2	9.3E-1
Receptor signaling complex scaffold activity	2	0.0	5.6E-2	9.2E-1
1-phosphatidylinositol binding	2	0.0	7.4E-2	9.1E-1

Table 3.18 KEGG pathway analysis for 98 recognized genes upregulated with maltotriose treatment.

Term	Count	%	*P*-Value	Benjamini
Herpes simplex infection	4	0.0	6.7E-2	1.0E0
Epstein-Barr virus infection	4	0.0	7.3E-2	9.7E-1
Glutamatergic synapse	3	0.0	9.5E-2	9.6E-1

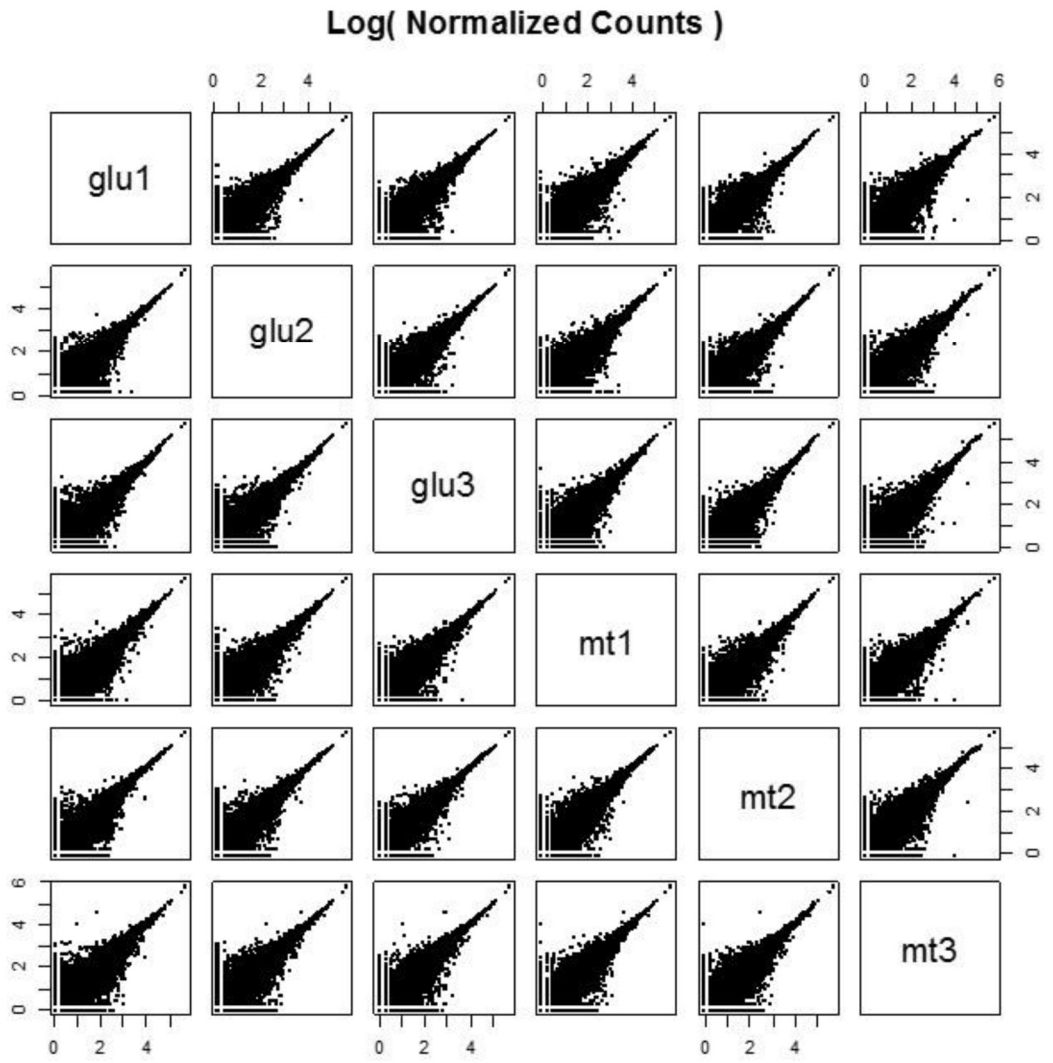

Figure 3.1 Comparison of normalized read counts. Glu1, glu2 and glu3 refer to the three biological replicates of cells treated with glucose. Mt1, mt2 and mt3 refer to three biological replicates of cells treated with maltotriose.

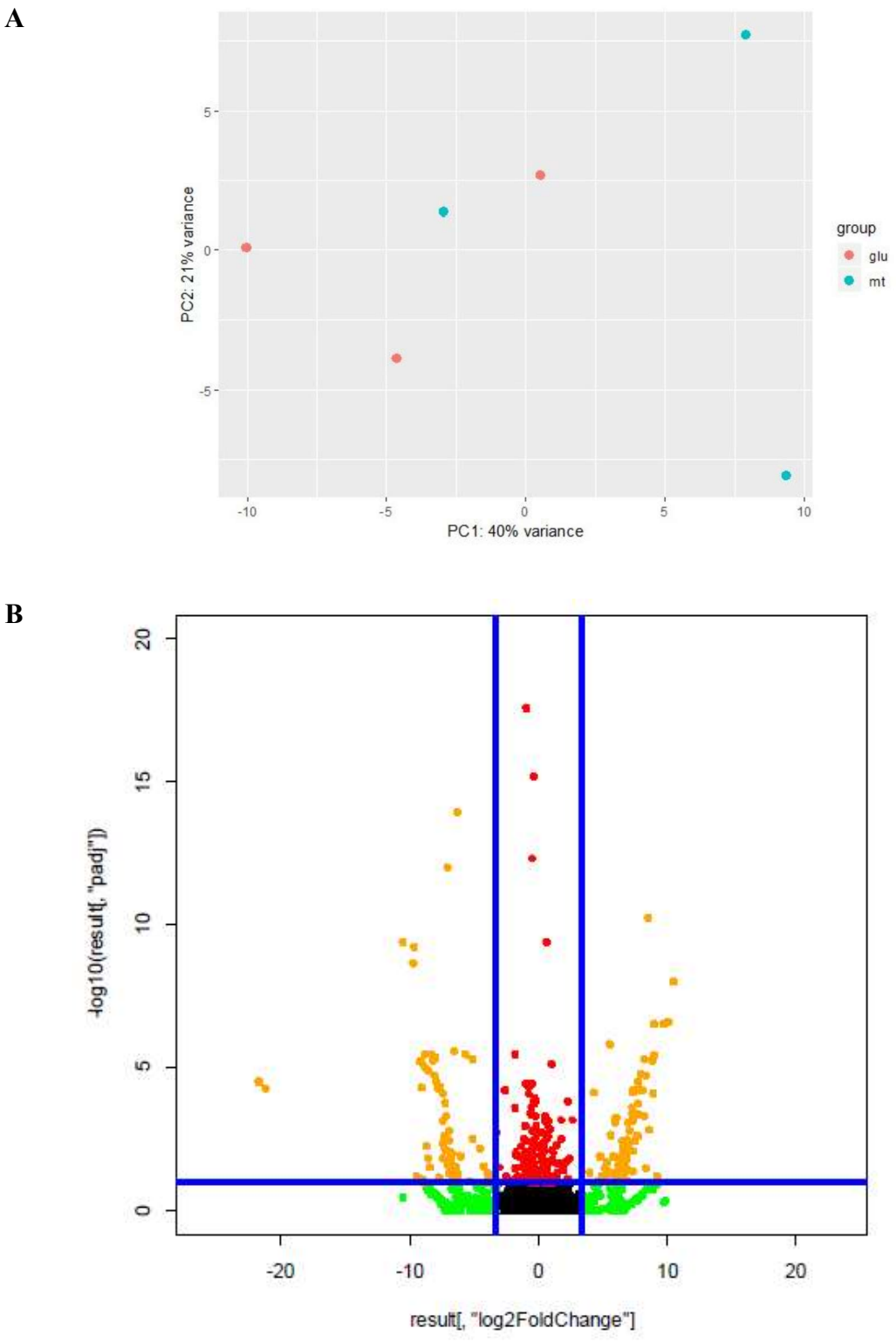

Figure 3.2 Exploratory PCA analysis (A) and volcano plot (B). glu: glucose; mt: maltose. Blue lines indicate log2 fold change = +/- 2 and adjusted *P*-value < 0.01.

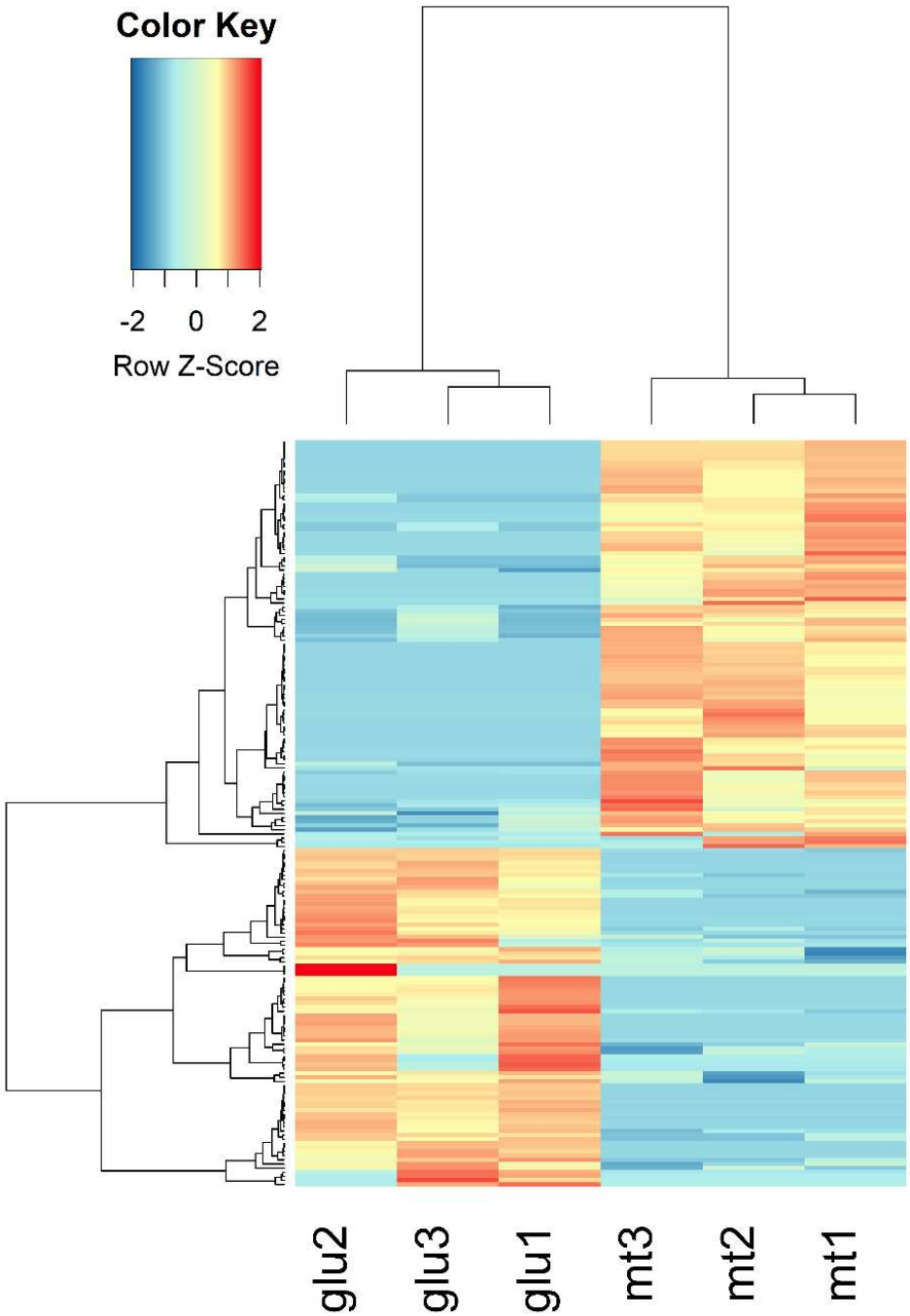

Figure 3.3 Heatmap of differentially expressed genes in different glucose- and maltotrisoe-treated STC-1 cells with log2 fold change replicates = +/- 2 and adjusted *P*-value < 0.01. Glu1, glu2 and glu3 refer to the three biological replicates of cells treated with glucose. Mt1, mt2 and mt3 refer to three biological replicates of cells treated with maltotriose. The order of gene names differentially expressed in glucose samples is the same as the order of gene names represented in Table 3.9. The order of gene names differentially expressed in maltotriose samples is the same as the order of gene names represented in Table 3.10.

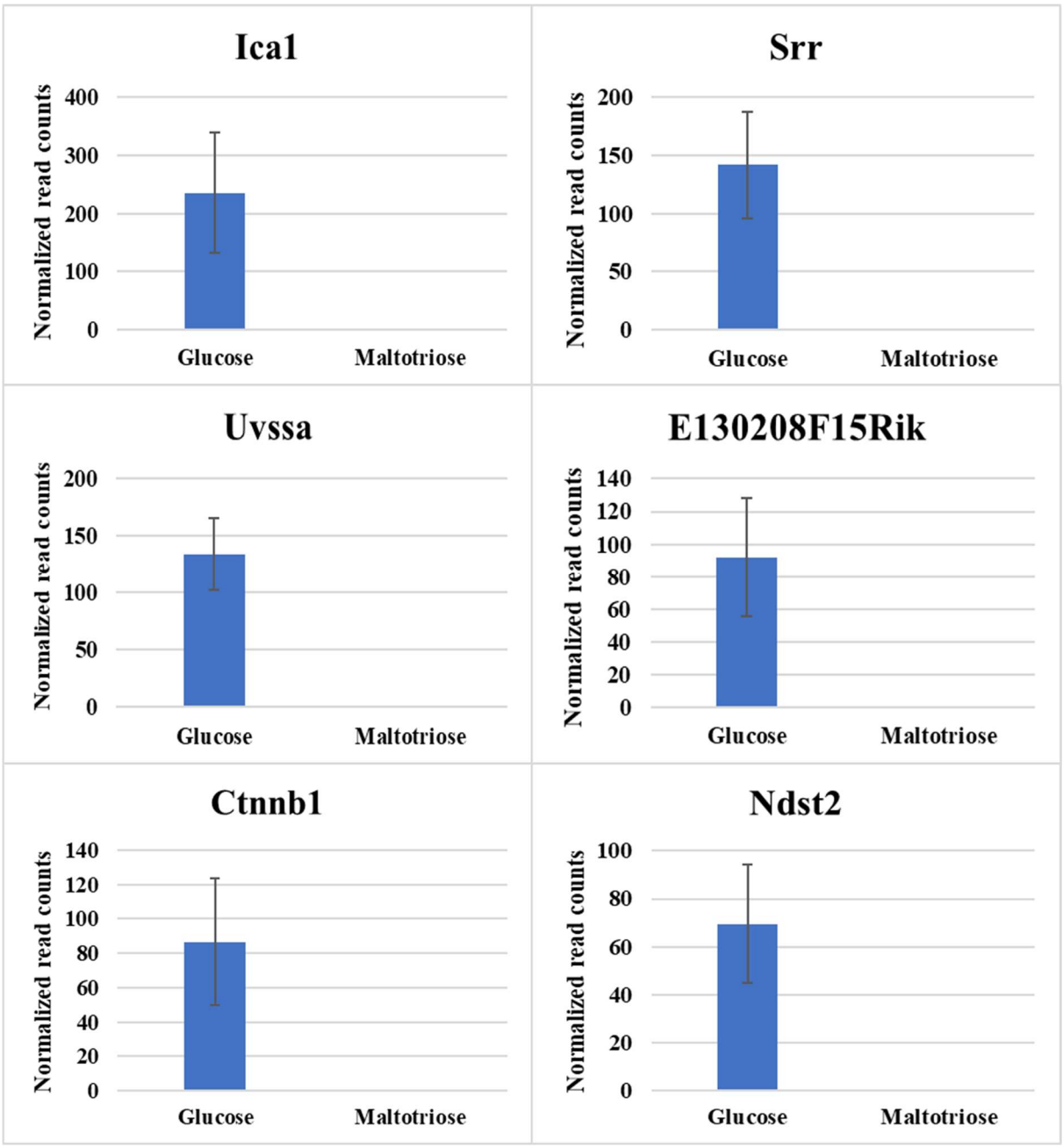

Figure 3.4 Normalized read counts of genes **upregulated with 25 mM glucose** compared to maltotriose treatment. Genes represented are the 17 genes resulted using the most restricted adjusted *P*-value **(*p*adj<1e-05)**. Ica1: islet cell autoantigen; Srr: serine racemase; Uvssa: UV stimulated scaffold protein A; E130208F15Rik: RIKEN cDNA E130208F15 gene; Ctnnb1: β-catenin1 (cadherin associated protein); Ndst2; N-deacetylase/N-sulfotransferase.

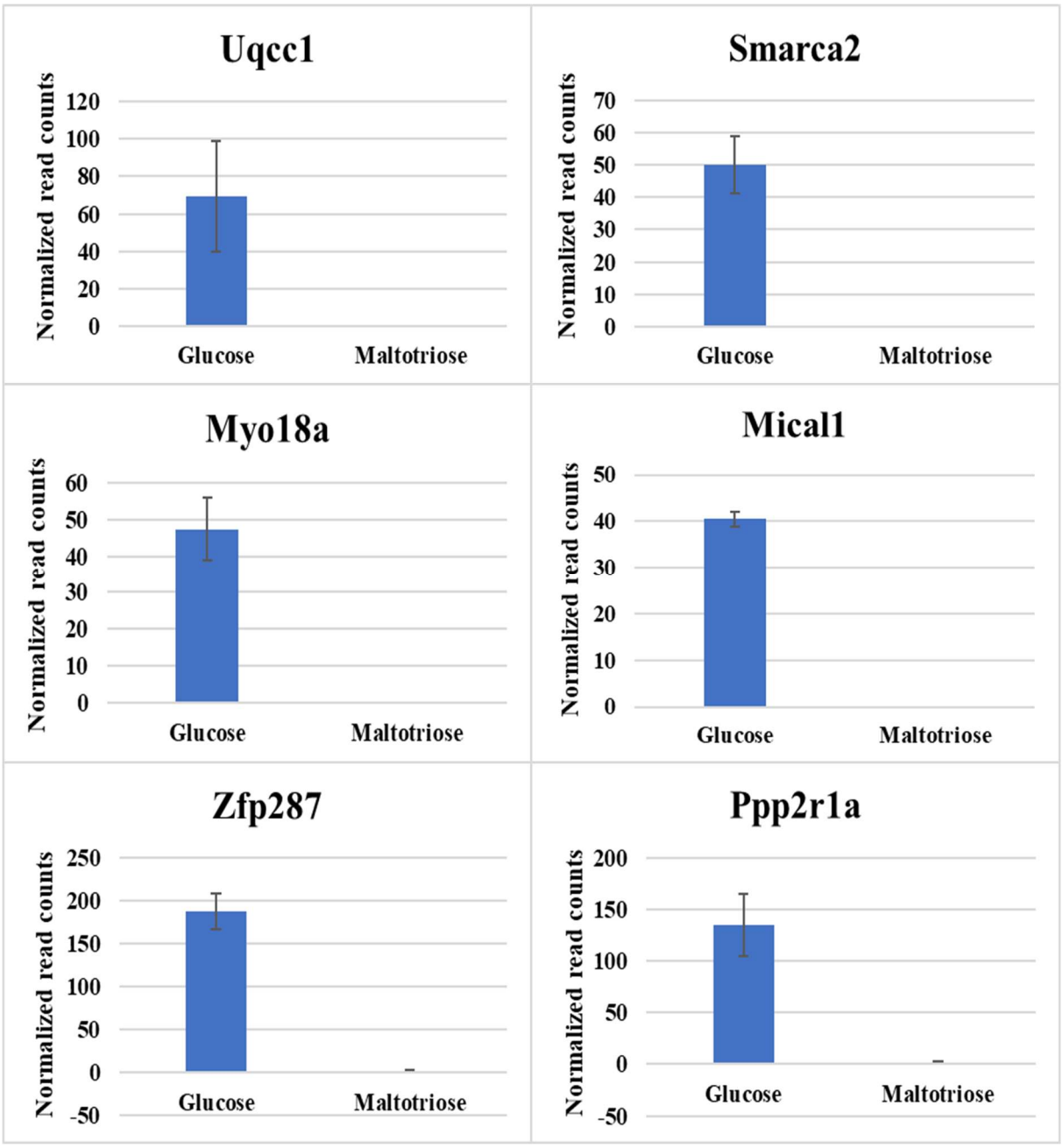

Figure 3.4 (Continued) Normalized read counts of genes **upregulated with 25 mM glucose** compared to maltotriose treatment. Genes represented are the 17 genes resulted using the most restricted adjusted *P*-value **(*padj*<1e-05)**. Uqcc1: ubiquinol-cytochrome c reductase complex assembly factor 1; Smarca2: SWI/SNF related; Myo18a: myosin XVIIIA; Mical1: microtubule associated monooxygenase; Zfp287: zinc finger protein 287; Ppp2r1a: protein phosphatase 2.

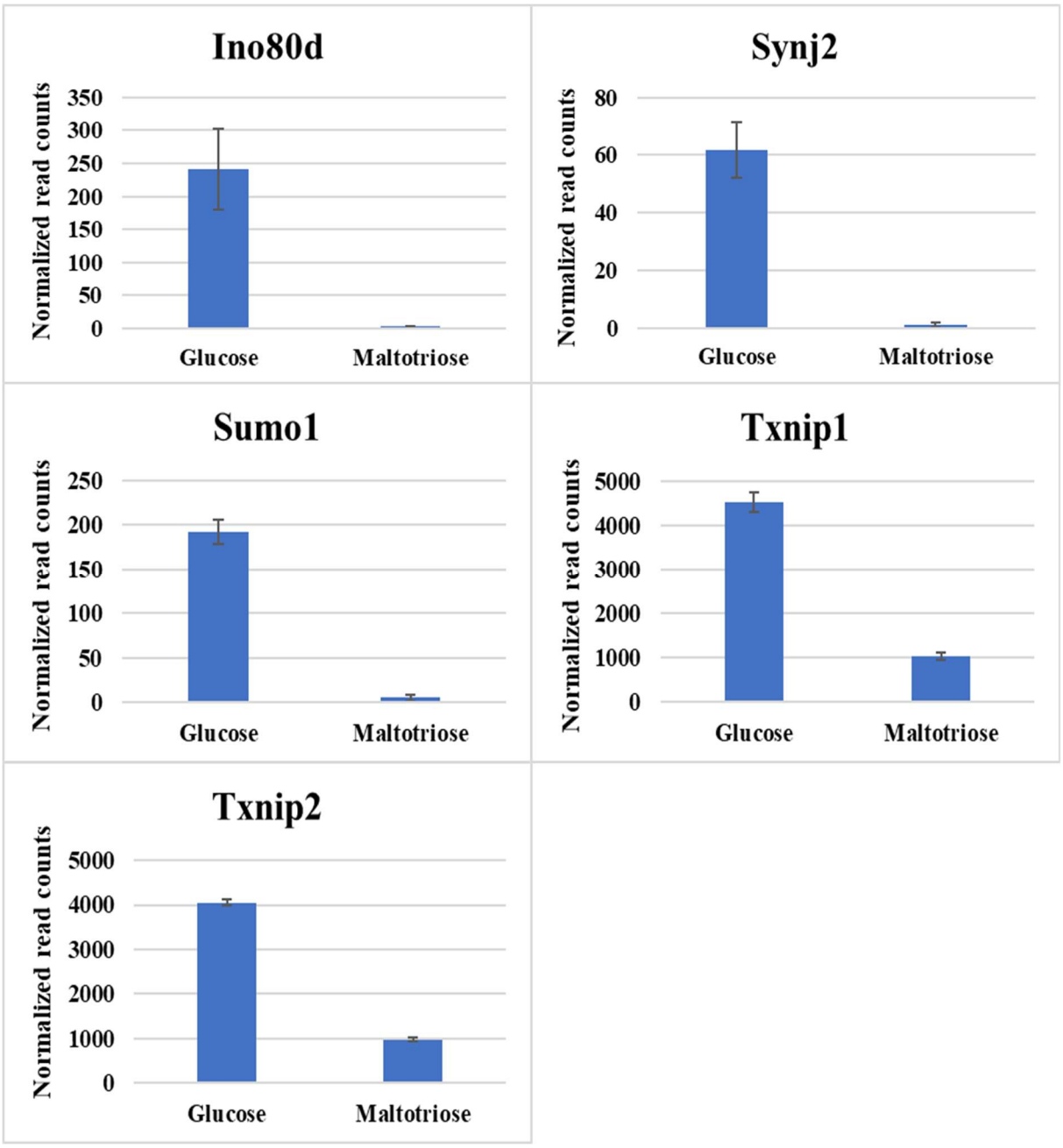

Figure 3.4 (Continued) Normalized read counts of genes **upregulated with 25 mM glucose** compared to maltotriose treatment. Genes represented are the 17 genes resulted using the most restricted adjusted *P*-value **(*p*adj<1e-05)**. Ino80d: INO80 complex subunit D; Synj2: synaptojanin 2; Sumo1: small ubiquitin-like modifier 1; Txnip1: thioredoxin interacting protein 1; Txnip2: thioredoxin interacting protein 2.

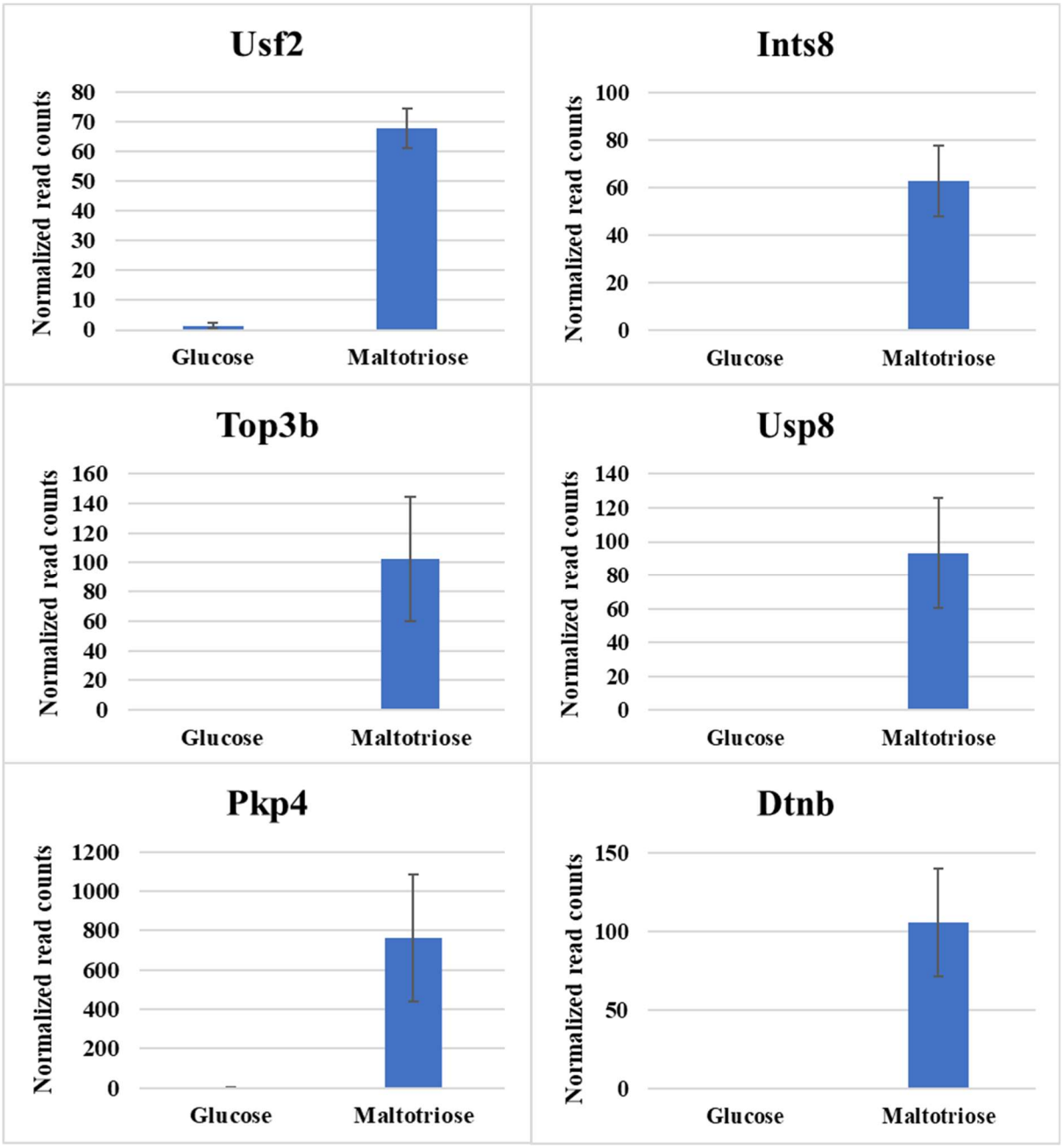

Figure 3.5 Normalized read counts of genes **upregulated with 25 mM maltotriose** compared to glucose treatment. Genes represented are the 9 genes resulted using the most restricted adjusted *P*-value **(*p*adj<1e-05)**. Usf2: upstream transcription factor 2; Ints8: integrator complex subunit 8; Top3b: topoisomerase (DNA) III β; Usp8: ubiquitin specific peptidase 8; Pkp4: plakophilin 4; Dtnb: β-dystrobrevin.

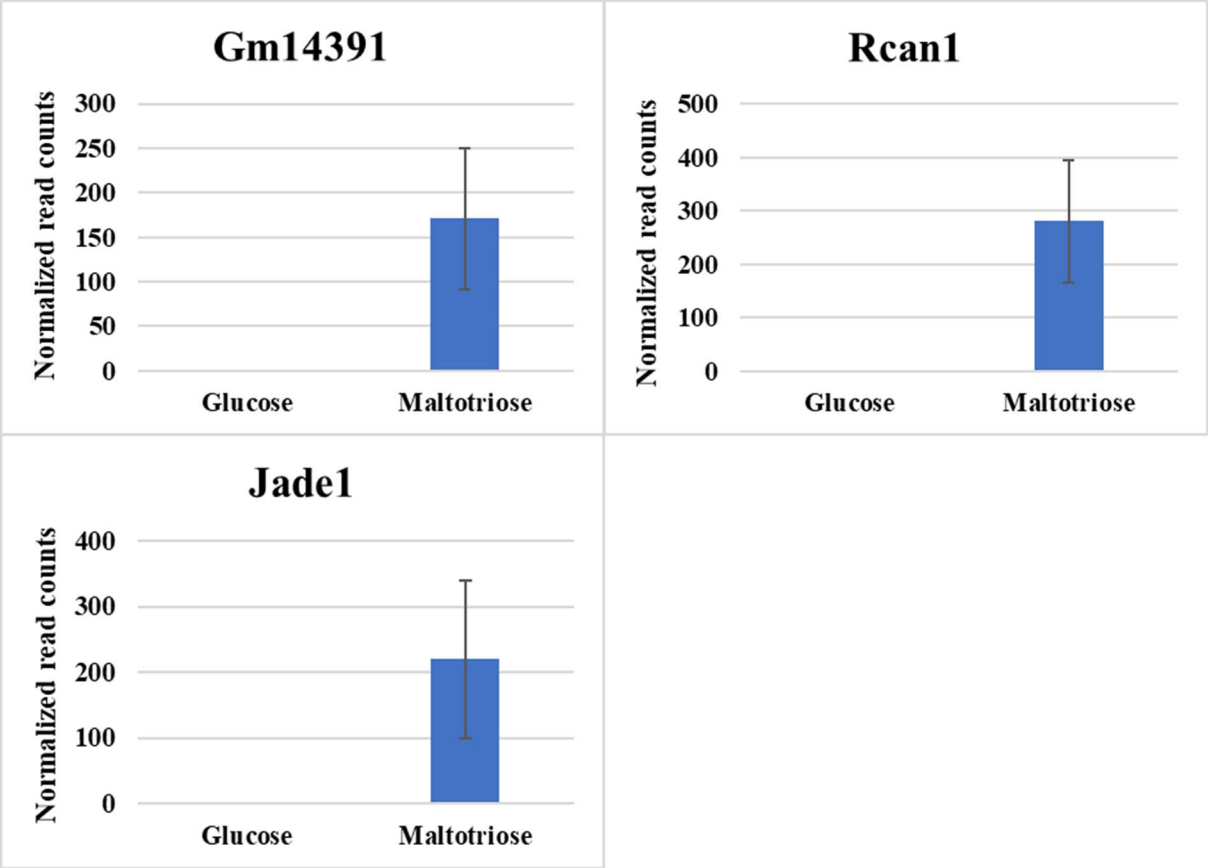

Figure 3.5 (Continued) Normalized read counts of genes **upregulated with 25 mM maltotriose** compared to glucose treatment. Genes represented are the 9 genes resulted using the most restricted adjusted *P*-value **(*p*adj<1e-05)**. Gm14391: predicted gene 14391; Rcan1: regulator of calcineurin 1; Jade1: jade family PHD finger 1.

CHAPTER 4. PROTEOMIC ANALYSIS OF MALTOOLIGOSACCHARIDES-TREATED L-CELLS

4.1 Abstract

Global proteomic analysis of mammalian cell lines representing intestinal endocrine cells can facilitate the identification and quantification of proteins in a broad and unbiased manner and highlight the cellular processes that are altered under different environmental conditions. The effect of complex carbohydrates such as the α-amylase starch digestion products, consisting of linear maltooligosaccharides (MOS) and branched limit-dextrins, on the intestinal cell proteome in general and on the intestinal enteroendocrine cells in particular is unknown. The identification of targeted proteins and/or putative chemosensory receptors could help in the understanding of the chemosensation mechanism of MOS by L-cells, as was shown to occur in Chapter II. The objective of the current study was to identify protein targets that mediate or facilitate the intestinal sensation of MOS by L-cells and downstream effects of hormone secretion and improved barrier function. The mouse-derived intestinal endocrine cell line, STC-1, was treated with linear (DP1 to DP4) and branched (DP3 and α-limit dextrins) MOS and global protein profiling was achieved by LC-MS/MS. Subsequent analysis revealed that MOS altered amounts of proteins that are associated with a number of cellular functions and pathways. Maltose treatment showed induction in α-mannosidase levels consistent with increase in α-glucosidase levels in the Caco-2 cell model. Levels of the proglucagon gene products (GLP-1 and OXM) were depleted in maltotetraose and isomaltotriose-treated cells supporting our hypothesis of secretion, and not synthesis enhancement. In addition, maltotriose boosted the integrin-mediated pathway indicating a possible target for an adhesion receptor for extracellular matrix sensation. As previously shown, the Wnt signaling pathway was enhanced in glucose-treated cells. This study provides a foundation proteome effect

for future studies to understand the sensing mechanisms in the intestinal lumen and the role of MOS in L-cell biology and metabolic disorders.

4.2 Introduction

Proteomic analysis includes the use of mass spectrometry (MS) to identify and quantify peptides. Over the past two decades, high throughput proteomic technologies have been developed to provide relatively rapid measurement of a large number of proteins from biological samples. Such tools can be employed both as a means of targeted measurement and as a discovery tool to detect global changes [1]. Effective proteomic researches should take into account the biological system as well as sensitivity and accuracy of the provided technology [1]. While proteomic studies can provide a wealth of data to identify mechanistic insights, thorough follow-up experiments using relevant models should be employed to draw the strongest conclusions [1]. By quantifying a large number of previously unexplored proteins, proteomics can be an effective hypothesis generating tool. Obesity has become one of the most prevalent metabolic disorders in both the developed and urbanized developing countries. Although the role of gut hormone balance and incretin effects on appetitive response and food intake is well-reported, no studies have investigated the importance of complex carbohydrates (larger than glucose) on gut hormone release or incretin effects. Most of the previous and current research in this area has focused on dietary fats and proteins as strong activators to the enteroendocrine cells of the gut. However, as we reported in the preceding chapters, we show a strong stimulation effect of maltooligosaccharides (the starch α-amylase digestion products) on mouse L-cells to secrete comparably high levels of GLP-1 and higher expression of CCK mRNA. The proteomic method was used here to better understand the mechanistic underpinnings behind this stimulation, as well

as potential therapeutic targets that could be used to harness the endogenous release of gut hormones by dietary high-quality carbohydrates.

4.3 Materials and Methods

4.3.1 Preparation of α-Limit Dextrins

4.3.1.1 α-Amylase Enzyme Preparation

Pancreatic α-amylase from porcine (Sigma, St. Louis, MO) was used to prepare α-limit dextrins. Powdered enzyme was weighed and dissolved in purified water at 10% concentration (w/v) and left at 4 ^{0}C for 2 h. The suspension was then centrifuged at 8000 rpm for 10 min at 4 ^{0}C and the supernatant was used for starch digestion.

4.3.1.2 Starch Digestion

α-Limit dextrins were prepared according to the method described by Lee and Hamaker, 2017 [2]. Waxy corn starch (WCS) (3% w/v) was gelatinized in purified water by boiling for 20 min. The gelatinized starch suspension was hydrolyzed by α-amylase at 37 ^{0}C for 24 h [3], and then the same amount of enzyme was added for another 24 h to produce fully α-amylolyzed WCS. The insolubilize residue was removed by centrifugation at 10,000 x g for 20 min. The clear supernatant was filtered through a 45 μm nylon filter. To remove α-amylase residue, the supernatant was filtered using an Amicon Ultra-15 centrifugal filter (regenerated cellulose 30,000 NMWL, UFC903008). The resulting solution was then freezed to -80 ^{0}C and freeze-dried using a VirTis benchtop K freeze dryer (SP Industries Inc, Hopkins, MI). for 72 h. The pure powder was resolubilized in purified water to prepare a 2% α-limit dextrin solution for chromatograph analysis. α-Limit dextrin solution (2%, 100 μl) was injected into a Superdex 30 column attached to a high-performance size-exclusion chromatograph (HPSEC, Agilent 1200 series, Santa Clara, CA). The

mobile phase was water and the sample running time was 60 min. The resulting HPSEC chromatogram of a 2% solution of the prepared α-limit dextrins is shown in Figure 4.1.

4.3.2 Cell culture and MOS Treatment

STC-1 cells at passage No. 37 were cultured according to the protocol described in Chapter II of this thesis. Upon reaching 80% confluence (within 48 h of culturing), cells were exposed to the following treatments for 200 min (n=4): 25 mM glucose, 25 mM maltose, 25 mM maltotriose, 25 mM isomaltotriose, 25 mM maltotetraose, and 2% α-limit dextrin (w/v). Carbohydrates were dissolved in phosphate buffered saline (PBS) containing calcium chloride and magnesium chloride (Sigma # 806544) and sterilized using Steriflip-GV Sterile Centrifuge Tube Top 0.22 µm filter. A blank control was cells that were treated with DPBS vehicle without any solutes dissolved in it. After incubation time, cells were rinsed twice with pure PBS, scraped, pelleted, flash-freezed in liquid nitrogen and stored at -80 ℃ until processing for proteomic analysis.

4.3.3 Digestion, Purification and Enrichment of Protein Samples for Mass Spectrometry

Digestion and purification of protein samples for mass spectrometry was performed at the Purdue Proteomics Facility according to the protocol of Hedrick et al., 2015. Ammonium bicarbonate buffer (100 mM) was used to resuspend the cell pellets before lysis in a barocycler (Barocycler NEP2320, Pressure Bioscience INC.). Protein content in the cell lysate was measured using the BCA method (Pierce Biotechnology, Rockford, lL). Enzymatic digestion with sequence grade Lys-C/Trypsin (Promega) was conducted in the barocycler. The pellet was then resuspended in a mixture of purified water (97%), acetonitrile (ACN) (3%), and formic acid (FA) (0.1%) prior to nano LC-MS/MS analysis.

4.3.4 LC-MS/MS Analysis

LC-MS/MS analysis was conducted using the nano Eksigent 425 HPLC system (Nano cHiPLC 200 µm x 0.5 mm ChromXP C18-CL 3 µm 120 Å trap column, and Nano cHiPLC 75 µm x 15 cm ChromXP C18-CL 5 µm 120 Å analytical column) coupled with the triple time-of-flight (TOF) 5600 plus detector (Sciex, Framingham, MA). Of note, the TripleTOF provides high resolving power, mass measurement accuracy, and acquisition rates [4]. Samples were then injected into the Triple TOF 5600 plus via the Nanospray III ion source using an emission tip from New Objective. Flow rate was set to 300 nL/min and a mobile phase of purified H_2O/0.1% FA (A) and ACN/0.1 % FA (B) was used. The 120 minutes method began with 95% A for 1 minute, followed by a gradient to 65% A over 90 minutes, then to 20% A in 2 minutes. 20% A was held for 5 min before returning to 95% A for the remainder of the method. Data was acquired by monitoring 50 precursor ions at 250 ms/scan.

Following mass spectrometry, the subsequent data output was analyzed using MaxQuant computational proteomics platform version 1.5.3.30 [5]. MaxQuant settings were as follows: initial precursor mass: 0.07 Da; fragment mass tolerance: 0.02; amino-acid minimum peptide length: 7; data analysis method: 'label-free quantification' (LFQ) checked and 'match between runs' interval set to one minute; randomized fasta databases; protein false discovery rate (FDR): 1%; enzymes: Trypsin/P and LysC; maximum missed cleavages: 2; maximum modifications per peptide: 3; fixed modifications: iodoethanol (C); and variable modifications: acetyl (Protein N-term) and Oxidation (M). The resulting output was compared both against a common contaminants database and the *Mus musculus* sequence database from Universal Protein Database (Uniprot) (retrieved 05-05-2016) [6],[7], [8]. An in-house script was used to determine LFQ intensity. Resulting values were then transformed using the log2(x) function. Results represented in this chapter are only for proteins showed log2 fold changer either > 0.5 or < -0.5.

4.3.5 Statistical Analysis

Analysis of variance (ANOVA) was used to identify differences between all treatment groups. However, in the analysis presented in this chapter, we used Student's T-test to determine statistical significance between paired treatments. For identification of associated pathways, statistical significance ($P < 0.05$) was determined by the associated software as the probability that x number of proteins in a list of the same size would be detected in the given pathway.

4.3.6 Data Analysis and Interpretation

Heat map and principle component analysis (PCA) plots were generated using InfernoRDN software. Identified proteins were categorized by molecular function or biological process gene ontology (GO) terms using Database for Annotation, Visualization and Integrated Discovery (DAVID) v. 6.8 and Uniprot [6], [7], [9]. Search Tool for the Retrieval of Interacting Genes/Proteins (STRING) v. 10.0 was also used to visualize protein interactions and additional GO term analysis [8]. Pathways were identified using Metacore (Clarivate Analytics), and Kyoto Encyclopedia of Genes and Genomes (KEGG) [10]. With the exception of Metacore, only protein names were used for analysis of functional classification and pathways.

4.4 Results

Summarized data of numbers of statistically differential proteins *P*-value (< 0.05) in STC-1 cells treated with 25 mM glucose compared to cells treated with vehicle blank (DPBS), 25 mM maltose, 25 mM maltotriose, 25 mM isomaltotriose, 25 mM maltotetraose and 2% α-limit dextrins are shown in Table 4.1. To test the possible effect of linear vs branched MOS on the sensation response by STC-1 cells, we identified statistically different proteins between cells treated with maltotriose compared to cells treated with isomaltotriose. Numbers of statistically differential

proteins *P*-value (< 0.05) in STC-1 cells treated with 25 mM isomaltotriose compared to cells treated with 25 mM maltotriose are shown in Table 4.2.

4.4.1 Proteins Affected by Different MOS Compared to Glucose

Gene ontology (GO) of statistically differential proteins downregulated (7 proteins; fold chain < - 0.5) and upregulated (15 protein; fold chain > 0.5) in STC-1 cells treated with 25 mM glucose compared to cells treated with the vehicle blank (DPBS) are presented in Table 4.3 and Table 4.4, respectively. The heatmap and PCA plot of differential proteins in glucose versus DPBS treatments are represented in Figure 4.4. Incubation of cells with DPBS buffer caused, as expected, increase in the levels of proteins involved in apoptosis programing (Bcl-2-like protein 1) and inflammation markers (amine oxidase) (Table 4.3). Glucose treatment enhanced the expression of Cadherin-2 which is an important regulator of the canonical Wnt signaling pathway and an important cell adhesion protein (Table 4.4). The Wnt signaling pathway has been reported to be involved in glucose homeostasis [11] through its effector TCF7L2 [12].

GO terms of statistically differential proteins downregulated (16 proteins; fold chain < - 0.5) and upregulated (9 protein; fold chain > 0.5) in STC-1 cells treated with 25 mM maltose compared to cells treated with the 25 mM glucose are presented in Tables 4.5 and 4.6, respectively. The heatmap and PCA plot of differential proteins in maltose versus glucose treatments are represented in Figure 4.5. We observed a reduction in the levels of the peroxiredoxin-6, a cellular redox regulator in maltose-treated cells. On the other hand, α-mannosidases were upregulated with maltose treatment. Consistent with this finding, our laboratory reported faster trafficking and maturation of α-glucosidase enzymes in Caco-2 cells treated with maltose [13]. In addition, the upregulation of the low-density lipoprotein particle receptor binding (LDLR) with maltose treatment suggests an enhancement of the Wnt signaling pathway [14].

GO terms of statistically differential proteins downregulated (2 proteins; fold chain < - 0.5) and upregulated (8 protein; fold chain > 0.5) in STC-1 cells treated with 25 mM maltotriose compared to cells treated with the 25 mM glucose are represented in Table 4.7 and Table 4.8, respectively. The heatmap and PCA plot of differential proteins in maltotriose versus glucose treatments are represented in Figure 4.6. An induction in the integrin-mediated signaling pathway was observed in cells treated with maltotriose (Table 4.8). Integrin proteins work as adhesion receptors for extracellular matrix proteins an ligands [15] and play a role in the signal transduction into cells and the subsequent cellular response [16]. GO terms of statistically differential proteins downregulated (13 proteins; fold chain < - 0.5) and upregulated (8 protein; fold chain > 0.5) in STC-1 cells treated with 25 mM isomaltotriose compared to cells treated with the 25 mM glucose are presented in Table 4.9 and Table 4.10, respectively. The heatmap and PCA plot of differential proteins in isomaltotriose versus glucose treatments are represented in Figure 4.7. Interestingly, a downregulation of the levels of the proglucagon protein products was observed in cells treated with isomaltotriose compared to glucose. Our explanation for this observation rely on our suggestion that MOS stimulate the secretion and not the synthesis of the proglucagon gene products (GLP-1 and OXM peptides). In this case, we expect a significant reduction of the cellular concentrations of these peptides that could be clearly observed in the proteomic data. The majority of the proteins upregulated with isomaltotriose treatments are involved in binding and RNA processing (Table 4.10). GO terms of statistically differential proteins downregulated (11 proteins; fold chain < - 0.5) and upregulated (6 protein; fold chain > 0.5) in STC-1 cells treated with 25 mM maltotetraose, compared to cells treated with the 25 mM glucose are presented in Tables 4.11 and 4.12. respectively. The heatmap and PCA plot of differential proteins in maltotetraose versus glucose treatments are represented in Figure 4.8. Similar to the observation in isomaltotriose-

treated cells, maltotetraose-treated cells had statistically significant lower levels of the cellular proglucagon protein. We think that this observation supports our hypothesis that high levels of GLP-1 and OXM are secreted into the media leaving lower concentrations inside the cells given the results observed in Chapter II where maltotetraose strongly stimulate GLP-1 release from STC-1 cells. GO terms of statistically differential proteins downregulated (5 proteins; fold chain < -0.5) and upregulated (17 protein; fold chain > 0.5) in STC-1 cells treated with 2% α-limit dextrins compared to cells treated with the 25 mM glucose are presented in Table 4.13 and Table 4.14, respectively. The heatmap and PCA plot of differential proteins in α-limit dextrins versus glucose treatments are represented in Figure 4.9. Most of the upregulated proteins were involving in RNA binding and transferase and dehydrogenase activities (Table 4.14).

4.4.2 Proteins Affected by Isomaltotriose (Branched) Compared to Maltotriose (Linear)

In an attempt to detect possible variation in the stimulation capacities of linear versus branched MOS, a Student's T-test was performed to compare protein regulation in cells treated with isomaltotriose (branched DP3) to cells treated with maltotriose (linear DP3). GO terms of statistically differential proteins downregulated (6 proteins; fold chain < - 0.5) and upregulated (2 protein; fold chain > 0.5) in STC-1 cells treated with 25 mM isomaltotriose compared to cells treated with the 25 mM maltotriose are presented in Tables 4.15 and 4.16, respectively. The heatmap and PCA plot are presented in Figure 4.10. Among the few differences observed, a significant downregulation was found in the glucagon protein in cells treated with isomaltotriose (Table 4.15) compared to cells treated with maltotriose. We explained in the previous section that the hypothesis of increased secretion, and not synthesis, of the proglucagon gene products (including GLP-1 and OXM) are consistent with depletion of these peptides inside the cells. Therefore, and although the secretion assay was not performed on isomaltotriose in Chapter II,

isomaltotriose appears to be a more potent stimulator on GLP-1 secretion of STC-1 cell line than maltotriose. Secretion assays are required for confirmation of this hypothesis. On the other hand, cells treated with isomaltotriose had higher levels of the transcription elongation factor SPT4-B and protein involved in serine-type endopeptidase activity (Table 4.16).

4.5 Discussion and Conclusions

Data from the current proteomic analysis provide a large number of target proteins that require further investigation to expand the current knowledge of carbohydrate chemosensation. In addition, more hypotheses could be drawn from the analysis of proteomic data. We performed pairwise comparison using Student's T-test to independently identify the group for proteins differentially altered after incubating STC-1 cells with glucose versus different MOS. We also examined the effect of incubating cells with a prepared product of starch digestion by α-amylase (α-limit dextrin). As a negative control, the vehicle, DPBS, was simultaneously incubated with cells. Data revealed that cells treated with DPBS showed the highest number of differentially altered proteins (306 proteins) at $P < 0.05$. Proteins that upregulated with glucose compared to DPBS involved mainly in RNA processing such as RNA binding and RNA splicing. The enhanced cadherin-2 levels in cells treated with glucose supporting previous indication that glucose is an important positive regulator of the mitogen-activated protein kinase (MAPK) cascade [17], synaptic vesicle clustering [18], cell adhesion [19] and Wnt signaling pathway [20] through its positive regulation of cadherin-2 [21]. As expected, cells incubated with DPBS showed high levels of stress markers and proteins involved in negative regulation of cell death, such as the anti-apoptotic regulator Bcl-2-like protein 1 [22].

Cells treated with maltose showed higher levels of proteins involved in RNA binding and α-mannosidase activity. In addition, the levels of a chaperone of the low-density lipoprotein particle receptor (LDLPR) was enhanced in cells treated with maltose. Interestingly, recent report indicated that maltose sensing by Caco-2 cells stimulate higher trafficking and maturation of the intestinal brush border membrane protein sucrase-isomaltase [13]. Here we observed that maltose stimulates an increase of LDLPR chaperone that play a role in protein localization to cell surface [23]. Therefore, we suggest that maltose is a unique stimulator to pathways involved in carbohydrate binding and metabolism.

Cells treated with maltotriose showed a number of differentially regulated proteins compared to cells treated with glucose. Most proteins increased with maltotriose treatment are involved in RNA processing pathways, including tRNA cytidylyltransferase activity, poly A binding and RNA splicing. Although these proteins are not directly associated with any of our hypotheses. These data indicate a high level of transcription regulation in the cells, with maltotriose treatment, that could be involved in regulating sensing pathways.

Significant downregulation in the levels of the proglucagon protein was observed in cells treated with isomaltotriose (Table 4.9) and cells treated with maltotetraose (Table 4.11) compared to glucose. Observation from Chapter II showed significant stimulation of GLP-1 secretion from STC-1 cell line with maltotriose and maltotetraose treatments. Since proteomic analysis monitors the protein levels inside the cells, these findings may indicate that, most of the GLP-1 peptides are secreted into the media leaving a lower GLP-1 concentration inside the cell.

4.6 References

[1] V. E. Hedrick, M. N. LaLand, E. S. Nakayasu, and L. N. Paul, “Digestion, Purification, and Enrichment of Protein Samples for Mass Spectrometry,” in *Current Protocols in Chemical Biology*, vol. 7, no. 3, Hoboken, NJ, USA: John Wiley & Sons, Inc., 2015, pp. 201–222.

[2] B.-H. Lee and B. R. Hamaker, “Number of branch points in α-limit dextrins impact glucose generation rates by mammalian mucosal α-glucosidases,” *Carbohydr. Polym.*, vol. 157, pp. 207–213, Feb. 2017.

[3] B.-H. Lee *et al.*, “Modulation of starch digestion for slow glucose release through "toggling" of activities of mucosal α-glucosidases.,” *J. Biol. Chem.*, vol. 287, no. 38, pp. 31929–38, Sep. 2012.

[4] G. L. Andrews, B. L. Simons, J. B. Young, A. M. Hawkridge, and D. C. Muddiman, “Performance characteristics of a new hybrid quadrupole time-of-flight tandem mass spectrometer (TripleTOF 5600).,” *Anal. Chem.*, vol. 83, no. 13, pp. 5442–6, Jul. 2011.

[5] J. Cox and M. Mann, “MaxQuant enables high peptide identification rates, individualized p.p.b.-range mass accuracies and proteome-wide protein quantification,” *Nat. Biotechnol.*, vol. 26, no. 12, pp. 1367–1372, Dec. 2008.

[6] D. W. Huang, B. T. Sherman, and R. A. Lempicki, “Systematic and integrative analysis of large gene lists using DAVID bioinformatics resources,” *Nat. Protoc.*, vol. 4, no. 1, pp. 44–57, Jan. 2009.

[7] T. U. UniProt Consortium, “UniProt: a hub for protein information.,” *Nucleic Acids Res.*, vol. 43, no. Database issue, pp. D204-12, Jan. 2015.

[8] D. Szklarczyk *et al.*, “STRING v10: protein-protein interaction networks, integrated over the tree of life.,” *Nucleic Acids Res.*, vol. 43, no. Database issue, pp. D447-52, Jan. 2015.

[9] D. W. Huang, B. T. Sherman, and R. A. Lempicki, “Bioinformatics enrichment tools: paths toward the comprehensive functional analysis of large gene lists.,” *Nucleic Acids Res.*, vol. 37, no. 1, pp. 1–13, Jan. 2009.

[10] M. Kanehisa, Y. Sato, M. Kawashima, M. Furumichi, and M. Tanabe, “KEGG as a reference resource for gene and protein annotation.,” *Nucleic Acids Res.*, vol. 44, no. D1, pp. D457-62, Jan. 2016.

[11] T. Jin, “Current Understanding on Role of the Wnt Signaling Pathway Effector TCF7L2 in Glucose Homeostasis,” *Endocr. Rev.*, vol. 37, no. 3, pp. 254–277, Jun. 2016.

[12] T. Jin, “Current Knowledge on the Role of Wnt Signaling Pathway in Glucose Homeostasis,” *Mol. Nutr. Diabetes*, pp. 357–369, Jan. 2016.

[13] M. Chegeni, M. Amiri, B. L. Nichols, H. Y. Naim, and B. R. Hamaker, “Dietary starch breakdown product sensing [1] M. Chegeni, M. Amiri, B. L. Nichols, H. Y. Naim, and B. R. Hamaker, ‘Dietary starch breakdown product sensing mobilizes and apically activates α-glucosidases in small intestinal enterocytes,’ FASEB J., vol. 32,” *FASEB J.*, vol. 32, no. 7, pp. 3903–3911, Jul. 2018.

[14] M. Borrell-Pagès, J. C. Romero, O. Juan-Babot, and L. Badimon, “Wnt pathway activation, cell migration, and lipid uptake is regulated by low-density lipoprotein receptor-related protein 5 in human macrophages,” *Eur. Heart J.*, vol. 32, no. 22, pp. 2841–2850, Nov. 2011.

[15] L. A. Cary, D. C. Han, and J. L. Guan, “Integrin-mediated signal transduction pathways.,” *Histol. Histopathol.*, vol. 14, no. 3, pp. 1001–9, 1999.

[16] D. S. Harburger and D. A. Calderwood, “Integrin signalling at a glance.,” *J. Cell Sci.*, vol. 122, no. Pt 2, pp. 159–63, Jan. 2009.

[17] W. ZHANG and H. T. LIU, “MAPK signal pathways in the regulation of cell proliferation in mammalian cells,” *Cell Res.*, vol. 12, no. 1, pp. 9–18, Mar. 2002.

[18] P. E. MacDonald, S. Obermüller, J. Vikman, J. Galvanovskis, P. Rorsman, and L. Eliasson, “Regulated Exocytosis and Kiss-and-Run of Synaptic-Like Microvesicles in INS-1 and Primary Rat β-Cells,” *Diabetes*, vol. 54, no. 3, pp. 736–743, Mar. 2005.

[19] T. Kaido, M. Yebra, V. Cirulli, and A. M. Montgomery, “Regulation of human beta-cell adhesion, motility, and insulin secretion by collagen IV and its receptor alpha1beta1.,” *J. Biol. Chem.*, vol. 279, no. 51, pp. 53762–9, Dec. 2004.

[20] S. Chouhan *et al.*, “Glucose induced activation of canonical Wnt signaling pathway in hepatocellular carcinoma is regulated by DKK4.,” *Sci. Rep.*, vol. 6, p. 27558, 2016.

[21] V. Cirulli, “Cadherins in islet β-cells: more than meets the eye.,” *Diabetes*, vol. 64, no. 3, pp. 709–11, Mar. 2015.

[22] J. M. Adams and S. Cory, “Life-or-death decisions by the Bcl-2 protein family,” *Trends Biochem. Sci.*, vol. 26, no. 1, pp. 61–66, Jan. 2001.

[23] J. Chen, C.-C. Liu, Q. Li, C. Nowak, G. Bu, and J. Wang, “Two structural and functional domains of MESD required for proper folding and trafficking of LRP5/6.,” *Structure*, vol. 19, no. 3, pp. 313–23, Mar. 2011.

Table 4.1 Number of statistically differential proteins *P*-value (< 0.05) in STC-1 cells treated with 25 mM glucose compared to cells treated with MOS. Data are the results of Student's T-test performed for paired groups comparation (n=4) between glucose and each of the following treatments: vehicle blank (DPBS), 25 mM maltose, 25 mM maltotriose, 25 mM isomaltotriose, 25 mM maltotetraose and 2% α-limit dextrins..

Treatment	**Total number of differential proteins *P*-value (< 0.0 5)**	**Upregulated compared to glucose (> 0. 5) fold change**	**Downregulated compared to glucose (-< 0. 5) fold change**
Vehicle (DPBS)	306	15	7
Maltose	130	9	16
Maltotriose	100	8	2
Isomaltotriose	280	8	13
Maltotetraose	86	6	11
α-Limit dextrins	90	17	5

Table 4.2 Number of statistically differential proteins *P*-value (< 0.05) in STC-1 cells treated with 25 mM isomaltotriose compared to cells treated with 25 mM maltotriose. Data are the results of Student's T-test performed for paired groups comparation (n=4).

Treatment	**Total number of differential proteins *P*-value (< 0.0 5)**	**Upregulated compared to maltotriose (> 0. 5) fold change**	**Downregulated compared to maltotriose (< - 0. 5) fold change**
Isomaltotriose	140	2	6

Table 4.3 Gene ontology (GO) terms of 7 statistically differential proteins downregulated (fold change < - 0.5) in STC-1 cells treated with 25 mM glucose compared cells treated with the vehicle blank (DPBS). ND = not detected.

Protein name	**Gene ontology (molecular function)**
Protein DEK	Chromatin binding; DNA binding; histone binding
Cytoskeleton-associated protein 5	ND
Amine oxidase [flavin-containing] B	Flavin adenine dinucleotide binding; primary amine oxidase activity; protein homodimerization activity
Bcl-2-like protein 1 (Fragment)	ND
Exportin-4	ND
Uracil phosphoribosyltransferase homolog	GTP binding; uridine kinase activity
LIM and SH3 protein 1; isoform CRA_b (Lasp1 protein)	Ion transmembrane transporter activity; metal ion binding
Protein name	**Gene ontology (biological process)**
Protein DEK	Chromatin remodeling; regulation of double-strand break repair; regulation of double-strand break repair via nonhomologous end joining
Cytoskeleton-associated protein 5	ND
Amine oxidase [flavin-containing] B	Negative regulation of serotonin secretion; neurotransmitter catabolic process; positive regulation of dopamine metabolic process; response to aluminum ion; response to corticosterone; response to ethanol; response to lipopolysaccharide; response to selenium ion
Bcl-2-like protein 1 (Fragment)	Apoptotic process; regulation of apoptotic process
Exportin-4	Positive regulation of protein export from nucleus
Uracil phosphoribosyltransferase homolog	Female pregnancy; lactation; pyrimidine nucleobase metabolic process; pyrimidine nucleoside salvage; response to insulin; UMP biosynthetic process
LIM and SH3 protein 1; isoform CRA_b (Lasp1 protein)	ND
Protein name	**Gene ontology (cellular component)**
Protein DEK	Contractile fiber; nucleus
Cytoskeleton-associated protein 5	ND
Amine oxidase [flavin-containing] B	Integral component of membrane; mitochondrial inner membrane; mitochondrial outer membrane; mitochondrion
Bcl-2-like protein 1 (Fragment)	ND

Table 4.3 (Continued)

Protein name	Gene ontology (cellular component) (Continued)
Exportin-4	Cytosol; nucleoplasm
Uracil phosphoribosyltransferase homolog	Cytosol; nucleus
LIM and SH3 protein 1; isoform CRA_b (Lasp1 protein)	Cortical actin cytoskeleton

Table 4.4 Gene ontology (GO) terms of 15 statistically differential proteins upregulated (fold change > 0.5) in STC-1 cells treated with 25 mM glucose compared cells treated with the vehicle blank (DPBS). ND = not detected.

Protein name	Gene ontology (molecular function)
MCG19223 (Protein LLP homolog)	Basal RNA polymerase II transcription machinery binding
CCA tRNA nucleotidyltransferase 1; mitochondrial (EC 2.7.7.72) (mitochondrial tRNA nucleotidyl transferase; CCA-adding) (mt CCA-adding enzyme) (mt tRNA CCA-diphosphorylase) (mt tRNA CCA-pyrophosphorylase) (mt tRNA adenylyltransferase)	ATP:3'-cytidine-cytidine-tRNA adenylyltransferase activity; ATP binding; CTP:3'-cytidine-tRNA cytidylyltransferase activity; CTP:tRNA cytidylyltransferase activity; tRNA binding; tRNA nucleotidyltransferase activit
Splicing factor; suppressor of white-apricot homolog (Splicing factor; arginine/serine-rich 8) (Suppressor of white apricot protein homolog)	RNA binding
Hnrpa3 protein	RNA binding
MKIAA0244 protein (Fragment)	
Heterogeneous nuclear ribonucleoproteins C1/C2 (Fragment)	RNA binding
Protein RRP5 homolog (Apoptosis-linked gene 4 protein) (Programmed cell death protein 11)	RNA binding; transcription factor binding
Small nuclear ribonucleoprotein Sm D1 (Sm-D1) (Sm-D autoantigen) (snRNP core protein D1)	RNA binding; U1 snRNP binding
Cadherin-2	Calcium ion binding; identical protein binding; protein kinase binding; protein phosphatase binding
Protein IWS1 homolog	ND
RNA binding motif protein; X chromosome; isoform CRA_b (RNA-binding motif protein; X chromosome)	RNA binding
Zinc finger protein 638	RNA binding; zinc ion binding
Scaffold attachment factor B1	RNA binding
Ferritin (Fragment)	Ferric iron binding
SAFB-like; transcription modulator (SAFB-like; transcription modulator; isoform CRA_d)	RNA binding
Protein name	**Gene ontology (biological process)**
MCG19223 (Protein LLP homolog)	Dendrite extension; positive regulation of dendritic spine development

Table 4.4 (Continued)

Protein name	Gene ontology (biological process) (Continued)
CCA tRNA nucleotidyltransferase 1; mitochondrial (EC 2.7.7.72) (mitochondrial tRNA nucleotidyl transferase; CCA-adding) (mt CCA-adding enzyme) (mt tRNA CCA-diphosphorylase) (mt tRNA CCA-pyrophosphorylase) (mt tRNA adenylyltransferase)	Mitochondrial tRNA 3'-end processing; tRNA 3'-terminal CCA addition; tRNA processing
Splicing factor; suppressor of white-apricot homolog (Splicing factor; arginine/serine-rich 8) (Suppressor of white apricot protein homolog)	Alternative mRNA splicing; mRNA 5'-splice site recognition; negative regulation of mRNA splicing; via spliceosome; regulation of transcription; DNA-templated; DNA-templated
Hnrpa3 protein	
MKIAA0244 protein (Fragment)	Transcription; DNA-templated
Heterogeneous nuclear ribonucleoproteins C1/C2 (Fragment)	ND
Protein RRP5 homolog (Apoptosis-linked gene 4 protein) (Programmed cell death protein 11)	Maturation of 5.8S rRNA from tricistronic rRNA transcript (SSU-rRNA; 5.8S rRNA; LSU-rRNA); maturation of SSU-rRNA from tricistronic rRNA transcript; mRNA processing
Small nuclear ribonucleoprotein Sm D1 (Sm-D1) (Sm-D autoantigen) (snRNP core protein D1)	Spliceosomal complex assembly; spliceosomal snRNP assembly
Cadherin-2	Blood vessel morphogenesis; brain morphogenesis; calcium-dependent cell-cell adhesion via plasma membrane cell adhesion molecules; cell migration; cerebral cortex development; heterophilic cell-cell adhesion via plasma membrane cell adhesion molecules; homeostasis of number of cells; homophilic cell adhesion via plasma membrane adhesion molecules; negative regulation of canonical Wnt signaling pathway; neuroepithelial cell differentiation; neuroligin clustering involved in postsynaptic membrane assembly; neuronal stem cell population maintenance; positive regulation of MAPK cascade and synaptic vesicle clustering; protein localization to plasma membrane; radial glial cell differentiation; regulation of oligodendrocyte progenitor proliferation; regulation of postsynaptic density protein 95 clustering; striated muscle cell differentiation

Table 4.4 (Continued)

Protein name	Gene ontology (biological process) (Continued)
Protein IWS1 homolog	ND
RNA binding motif protein; X chromosome; isoform CRA_b (RNA-binding motif protein; X chromosome)	ND
Zinc finger protein 638	RNA splicing
Scaffold attachment factor B1	Regulation of mRNA processing; regulation of transcription; DNA-templated
Ferritin (Fragment)	Cellular iron ion homeostasis; iron ion transport
SAFB-like; transcription modulator (SAFB-like; transcription modulator; isoform CRA_d)	
Protein name	**Gene ontology (cellular component)**
MCG19223 (Protein LLP homolog)	Nucleolus
CCA tRNA nucleotidyltransferase 1; mitochondrial (EC 2.7.7.72) (mitochondrial tRNA nucleotidyl transferase; CCA-adding) (mt CCA-adding enzyme) (mt tRNA CCA-diphosphorylase) (mt tRNA CCA-pyrophosphorylase) (mt tRNA adenylyltransferase)	Intracellular; mitochondrion
Splicing factor; suppressor of white-apricot homolog (Splicing factor; arginine/serine-rich 8) (Suppressor of white apricot protein homolog)	Nucleus
Hnrpa3 protein	ND
MKIAA0244 protein (Fragment)	ND
Heterogeneous nuclear ribonucleoproteins C1/C2 (Fragment)	ND
Protein RRP5 homolog (Apoptosis-linked gene 4 protein) (Programmed cell death protein 11)	Cytosol; nucleolus; nucleus; small-subunit processome
Small nuclear ribonucleoprotein Sm D1 (Sm-D1) (Sm-D autoantigen) (snRNP core protein D1)	Catalytic step 2 spliceosome; commitment complex; cytoplasm; cytosol; methylosome; nucleus; pICln-Sm protein complex; precatalytic spliceosome; prespliceosome; SMN-Sm protein complex; spliceosomal tri-snRNP complex; U12-type spliceosomal complex; U1 snRNP; U2 snRNP; U2-type catalytic step 2 spliceosome; U4 snRNP; U5 snRNP

Table 4.4 (Continued)

Protein name	Gene ontology (cellular component) (Continued)
Cadherin-2	Apical plasma membrane; basolateral plasma membrane; cell surface; fascia adherens; integral component of membrane; lamellipodium; plasma membrane raft; postsynaptic density; sarcolemma
Protein IWS1 homolog	Nucleus
RNA binding motif protein; X chromosome; isoform CRA_b (RNA-binding motif protein; X chromosome)	ND
Zinc finger protein 638	Nucleoplasm
Scaffold attachment factor B1	ND
Ferritin (Fragment)	Cell
SAFB-like; transcription modulator (SAFB-like; transcription modulator; isoform CRA_d)	Nuclear body

Table 4.5 Gene ontology (GO) terms of 16 statistically differential proteins downregulated (fold change < - 0.5) in STC-1 cells treated with 25 mM maltose compared to cells treated with 25 mM glucose. ND = not detected.

Protein name	**Gene ontology (molecular function)**
ATP-binding cassette sub-family F member 3	ATPase activity; ATP binding
Double-stranded RNA-binding protein Staufen homolog 1	RNA binding
N-alpha-acetyltransferase 10	ND
Peroxiredoxin-6	peroxiredoxin activity
Mitogen-activated protein kinase kinase kinase kinase 4	ATP binding; protein kinase activity
Adrenodoxin; mitochondrial (Fragment)	2 iron; 2 sulfur cluster binding; electron transfer activity
Protein DPCD	ND
Uncharacterized protein (Fragment)	Thiol-dependent ubiquitinyl hydrolase activity
RAC-beta serine/threonine-protein kinase	ATP binding; protein serine/threonine kinase activity
Deubiquitinating protein VCIP135	Thiol-dependent ubiquitin-specific protease activity
Oxysterol-binding protein-related protein 11	ND
Sin3 histone deacetylase corepressor complex component SDS3	Enzyme binding; histone deacetylase activity
Uncharacterized protein (Fragment)	Serine-type endopeptidase activity; serine-type exopeptidase activity
Uracil phosphoribosyltransferase homolog	GTP binding; uridine kinase activity
Ubiquitin-conjugating enzyme E2 C	ATP binding; transferase activity
Tuberin	GTPase activator activity
Protein name	**Gene ontology (biological process)**
ATP-binding cassette sub-family F member 3	Defense response to virus
Double-stranded RNA-binding protein Staufen homolog 1	ND
N-alpha-acetyltransferase 10	ND
Peroxiredoxin-6	Cell redox homeostasis
Mitogen-activated protein kinase kinase kinase kinase 4	ND
Adrenodoxin; mitochondrial (Fragment)	ND
Protein DPCD	Determination of left/right symmetry; epithelial cilium movement; flagellated sperm motility; lateral ventricle development; left/right pattern formation; spermatogenesis; third ventricle development; ventricular system development

Table 4.5 (Continued)

Protein name	Gene ontology (biological process) (Continued)
Uncharacterized protein (Fragment)	Protein deubiquitination; ubiquitin-dependent protein catabolic process
RAC-beta serine/threonine-protein kinase	Activation of GTPase activity; cellular response to high light intensity; glucose metabolic process; insulin receptor signaling pathway; intracellular protein transmembrane transport; peripheral nervous system myelin maintenance; positive regulation of glucose import in response to insulin stimulus; positive regulation of protein phosphorylation; positive regulation of protein targeting to membrane; positive regulation of vesicle fusion; protein kinase B signaling; protein localization to plasma membrane; retinal rod cell apoptotic process
Deubiquitinating protein VCIP135	Endoplasmic reticulum membrane fusion; Golgi reassembly; mitotic cell cycle; protein K11-linked deubiquitination; protein K48-linked deubiquitination; protein ubiquitination
Oxysterol-binding protein-related protein 11	ND
Sin3 histone deacetylase corepressor complex component SDS3	Negative regulation of transcription by RNA polymerase II; positive regulation of apoptotic process
Uncharacterized protein (Fragment)	ND
Uracil phosphoribosyltransferase homolog	Female pregnancy; lactation; pyrimidine nucleobase metabolic process; pyrimidine nucleoside salvage; response to insulin; UMP biosynthetic process
Ubiquitin-conjugating enzyme E2 C	ND
Tuberin	Negative regulation of TOR signaling; regulation of small GTPase mediated signal transduction
Protein name	**Gene ontology (cellular component)**
ATP-binding cassette sub-family F member 3	ND
Double-stranded RNA-binding protein Staufen homolog 1	ND
N-alpha-acetyltransferase 10	ND
Peroxiredoxin-6	Cell

Table 4.5 (Continued)

Protein name	Gene ontology (cellular component) (Continued)
Mitogen-activated protein kinase kinase kinase kinase 4	ND
Adrenodoxin; mitochondrial (Fragment)	ND
Protein DPCD	ND
Uncharacterized protein (Fragment)	ND
RAC-beta serine/threonine-protein kinase	Cell cortex; ruffle membrane
Deubiquitinating protein VCIP135	Cytoplasm
Oxysterol-binding protein-related protein 11	ND
Sin3 histone deacetylase corepressor complex component SDS3	Cytosol; nuclear body
Uncharacterized protein (Fragment)	ND
Uracil phosphoribosyltransferase homolog	Cytosol; nucleus
Ubiquitin-conjugating enzyme E2 C	ND
Tuberin	Nucleus; TSC1-TSC2 complex

Table 4.6 Gene ontology (GO) terms of 9 statistically differential proteins upregulated (fold change > 0.5) in STC-1 cells treated with 25 mM maltose compared to cells treated with 25 mM glucose. ND = not detected.

Protein name	**Gene ontology (molecular function)**
Predicted gene 5093	RNA binding; structural constituent of ribosome
CCA tRNA nucleotidyltransferase 1; mitochondrial (EC 2.7.7.72) (mitochondrial tRNA nucleotidyl transferase; CCA-adding) (mt CCA-adding enzyme) (mt tRNA CCA-diphosphorylase) (mt tRNA CCA-pyrophosphorylase) (mt tRNA adenylyltransferase)	ATP:3'-cytidine-cytidine-tRNA adenylyltransferase activity; ATP binding; CTP:3'-cytidine-tRNA cytidylyltransferase activity; CTP:tRNA cytidylyltransferase activity; tRNA binding; tRNA nucleotidyltransferase activity
Splicing factor; suppressor of white-apricot homolog (Splicing factor; arginine/serine-rich 8) (Suppressor of white apricot protein homolog)	RNA binding
DBF4-type zinc finger-containing protein 2 homolog	ND
Coiled-coil domain-containing protein 58	ND
LRP chaperone MESD (LDLR chaperone MESD) (Mesoderm development candidate 2) (Mesoderm development protein)	Identical protein binding; low-density lipoprotein particle receptor binding
Alpha-mannosidase (EC 3.2.1.-)	Alpha-mannosidase activity; carbohydrate binding; metal ion binding
BMS1 homolog; ribosome assembly protein (Yeast) (BMS1; ribosome biogenesis factor) (BMS1-like; ribosome assembly protein (Yeast))	GTPase activity; GTP binding; U3 snoRNA binding
Protein RRP5 homolog (Apoptosis-linked gene 4 protein) (Programmed cell death protein 11)	RNA binding; transcription factor binding
Protein name	**Gene ontology (biological process)**
Predicted gene 5093	Ribosomal large subunit assembly; translation
CCA tRNA nucleotidyltransferase 1; mitochondrial (EC 2.7.7.72) (mitochondrial tRNA nucleotidyl transferase; CCA-adding) (mt CCA-adding enzyme) (mt tRNA CCA-diphosphorylase) (mt tRNA CCA-pyrophosphorylase) (mt tRNA adenylyltransferase)	Mitochondrial tRNA 3'-end processing; tRNA 3'-terminal CCA addition; tRNA processing

Table 4.6 (Continued)

Protein name	Gene ontology (biological process) (Continued)
Splicing factor; suppressor of white-apricot homolog (Splicing factor; arginine/serine-rich 8) (Suppressor of white apricot protein homolog)	Alternative mRNA splicing; via spliceosome; mRNA 5'-splice site recognition; negative regulation of mRNA splicing; via spliceosome; regulation of transcription; DNA-templated; transcription; DNA-templated
DBF4-type zinc finger-containing protein 2 homolog	ND
Coiled-coil domain-containing protein 58	ND
LRP chaperone MESD (LDLR chaperone MESD) (Mesoderm development candidate 2) (Mesoderm development protein)	Mesoderm development; phagocytosis; positive regulation of skeletal muscle acetylcholine-gated channel clustering; protein folding; protein localization to cell surface; Wnt signaling pathway
Alpha-mannosidase (EC 3.2.1.-)	Mannose metabolic process
BMS1 homolog; ribosome assembly protein (Yeast) (BMS1; ribosome biogenesis factor) (BMS1-like; ribosome assembly protein (Yeast))	Endonucleolytic cleavage of tricistronic rRNA transcript (SSU-rRNA; 5.8S rRNA; LSU-rRNA); maturation of SSU-rRNA from tricistronic rRNA transcript (SSU-rRNA; 5.8S rRNA; LSU-rRNA)
Protein RRP5 homolog (Apoptosis-linked gene 4 protein) (Programmed cell death protein 11)	Maturation of 5.8S rRNA from tricistronic rRNA transcript (SSU-rRNA; 5.8S rRNA; LSU-rRNA); maturation of SSU-rRNA from tricistronic rRNA transcript (SSU-rRNA; 5.8S rRNA; LSU-rRNA); mRNA processing
Protein name	**Gene ontology (cellular component)**
Predicted gene 5093	Cytosolic large ribosomal subunit
CCA tRNA nucleotidyltransferase 1; mitochondrial (EC 2.7.7.72) (mitochondrial tRNA nucleotidyl transferase; CCA-adding) (mt tRNA CCA-diphosphorylase) (mt tRNA CCA-pyrophosphorylase) (mt tRNA adenylyltransferase)	Intracellular; mitochondrion
Splicing factor; suppressor of white-apricot homolog (Splicing factor; arginine/serine-rich 8)	Nucleus
DBF4-type zinc finger-containing protein 2 homolog	ND
Coiled-coil domain-containing protein 58	ND
LRP chaperone MESD (LDLR chaperone MESD) (Mesoderm development candidate 2) (Mesoderm development protein)	Endoplasmic reticulum; plasma membrane

Table 4.6 (Continued)

Protein name	Gene ontology (cellular component) (Continued)
Alpha-mannosidase (EC 3.2.1.-)	ND
BMS1 homolog; ribosome assembly protein (Yeast) (BMS1; ribosome biogenesis factor) (BMS1-like; ribosome assembly protein (Yeast))	90S preribosome; nucleolus; nucleus
Protein RRP5 homolog (Apoptosis-linked gene 4 protein) (Programmed cell death protein 11)	Cytosol; nucleolus; nucleus; small-subunit processome

Table 4.7 Gene ontology (GO) terms of 2 statistically differential proteins downregulated (fold change < - 0.5) in STC-1 cells treated with 25 mM maltotriose compared to cells treated with 25 mM glucose.

Protein name	**Gene ontology (molecular function)**
Spastic paraplegia 21 homolog (Human) (Spastic paraplegia 21 homolog (Human); isoform CRA_b)	CD4 receptor binding
Prolyl endopeptidase-like (PREPL)	Serine-type endopeptidase activity; Serine-type exopeptidase activity
Protein name	**Gene ontology (biological process)**
Spastic paraplegia 21 homolog (Human) (Spastic paraplegia 21 homolog (Human); isoform CRA_b)	Endomembrane system vesicle transportation
Prolyl endopeptidase-like (PREPL)	Proteolysis
Protein name	**Gene ontology (cellular component)**
Spastic paraplegia 21 homolog (Human) (Spastic paraplegia 21 homolog (Human); isoform CRA_b)	Cytosol; intracellular membrane-bounded organelle; trans-Golgi network transport vesicle; CD4 receptor binding
Prolyl endopeptidase-like (PREPL)	Serine-type endopeptidase activity; serine-type exopeptidase activity

Table 4.8 Gene ontology (GO) terms of 8 statistically differential proteins upregulated (fold change > 0.5) in STC-1 cells treated with 25 mM maltotriose compared to cells treated with 25 mM glucose. ND = not detected.

Protein name	Gene ontology (molecular function)
Predicted gene 5093	RNA binding; structural constituent of ribosome
CCA tRNA nucleotidyltransferase 1; mitochondrial (EC 2.7.7.72) (mitochondrial tRNA nucleotidyl transferase; CCA-adding) (mt CCA-adding enzyme) (mt tRNA CCA-diphosphorylase) (mt tRNA CCA-pyrophosphorylase) (mt tRNA adenylyltransferase)	ATP:3'-cytidine-cytidine-tRNA adenylyltransferase activity; ATP binding; CTP:3'-cytidine-tRNA cytidylyltransferase activity; CTP:tRNA cytidylyltransferase activity; tRNA binding; tRNA nucleotidyltransferase activity
Splicing factor; suppressor of white-apricot homolog (Splicing factor; arginine/serine-rich 8) (Suppressor of white apricot protein homolog)	RNA binding
fermitin family member 2(Fermt2)	Binding
heterogeneous nuclear ribonucleoprotein A3 Hnrpa3	RNA binding
Ferritin (Fragment)	Ferric iron binding
MKIAA0244 protein (Fragment)/ PHD finger protein 3(PHF3)	Zinc ion binding
Cleavage stimulation factor subunit 1 (CF-1 50 kDa subunit) (Cleavage stimulation factor 50 kDa subunit) (CSTF 50 kDa subunit) (CstF-50)	Poly(A) RNA binding
Protein name	**Gene ontology (biological process)**
Predicted gene 5093	Ribosomal large subunit assembly; translation
CCA tRNA nucleotidyltransferase 1; mitochondrial (EC 2.7.7.72) (mitochondrial tRNA nucleotidyl transferase; CCA-adding) (mt CCA-adding enzyme) (mt tRNA CCA-diphosphorylase) (mt tRNA CCA-pyrophosphorylase) (mt tRNA adenylyltransferase)	Mitochondrial tRNA 3'-end processing; tRNA 3'-terminal CCA addition; tRNA processing
Splicing factor; suppressor of white-apricot homolog (Splicing factor; arginine/serine-rich 8) (Suppressor of white apricot protein homolog)	Alternative mRNA splicing; via spliceosome; mRNA 5'-splice site recognition; negative regulation of mRNA splicing; via spliceosome; regulation of transcription; DNA-templated; transcription; DNA-templated
Fermitin family member 2 (Fermt2)	Integrin-mediated signaling pathway

Table 4.8 (Continued)

Protein name	**Gene ontology (biological process) (Continued)**
Heterogeneous nuclear ribonucleoprotein A3 Hnrpa3	RNA processing, nucleobase-containing compound transport, RNA metabolic process, mRNA metabolic process, RNA transport, mRNA transport, nucleic acid metabolic process,
Ferritin (Fragment)	Cellular iron ion homeostasis; iron ion transport
MKIAA0244 protein (Fragment)/ PHD finger protein 3(PHF3)	Transcription; DNA-templated
Cleavage stimulation factor subunit 1 (CF-1 50 kDa subunit) (Cleavage stimulation factor 50 kDa subunit) (CSTF 50 kDa subunit) (CstF-50)	mRNA processing
Protein name	**Gene ontology (cellular component)**
Predicted gene 5093	Cytosolic large ribosomal subunit
CCA tRNA nucleotidyltransferase 1; mitochondrial (EC 2.7.7.72) (mitochondrial tRNA nucleotidyl transferase; CCA-adding) (mt CCA-adding enzyme) (mt tRNA CCA-diphosphorylase) (mt tRNA CCA-pyrophosphorylase) (mt tRNA adenylyltransferase)	Intracellular; mitochondrion
Splicing factor; suppressor of white-apricot homolog (Splicing factor; arginine/serine-rich 8) (Suppressor of white apricot protein homolog)	Nucleus
Fermitin family member 2(Fermt2)	Cell, virion, membrane-enclosed lumen, macromolecular complex, organelle, organelle part, virion part, cell part,
heterogeneous nuclear ribonucleoprotein A3 Hnrpa3	Cell, virion, membrane-enclosed lumen, macromolecular complex, organelle, organelle part, virion part, cell part,
Ferritin (Fragment)	Cell
MKIAA0244 protein (Fragment)/ PHD finger protein 3(PHF3)	ND
Cleavage stimulation factor subunit 1 (CF-1 50 kDa subunit) (Cleavage stimulation factor 50 kDa subunit) (CSTF 50 kDa subunit) (CstF-50)	Cell, organelle, cell part

Table 4.9 Gene ontology (GO) terms of 13 statistically differential proteins downregulated (fold change < - 0.5) in STC-1 cells treated with 25 mM isomaltotriose compared to cells treated with 25 mM glucose. ND = not detected.

Protein name	Gene ontology (molecular function)
Methylthioribose-1-phosphate isomerase (M1Pi) (MTR-1-P isomerase) (EC 5.3.1.23) (S-methyl-5-thioribose-1-phosphate isomerase) (Translation initiation factor eIF-2B subunit alpha/beta/delta-like protein)	Identical protein binding; S-methyl-5-thioribose-1-phosphate isomerase activity
Proteasome subunit beta type (EC 3.4.25.1)	Threonine-type endopeptidase activity
Vbp1 protein (Fragment)	Binding
N-alpha-acetyltransferase 10	Catalytic activity, binding
Glucagon [Cleaved into: Glicentin; Glicentin-related polypeptide (GRPP); Oxyntomodulin (OXM) (OXY); Glucagon; Glucagon-like peptide 1 (GLP-1); Glucagon-like peptide 1(7-37) (GLP-1(7-37)); Glucagon-like peptide 1(7-36) (GLP-1(7-36)); Glucagon-like peptide 2 (GLP-2)]	Glucagon receptor binding; hormone activity; identical protein binding
Sorbitol dehydrogenase (EC 1.1.1.14) (L-iditol 2-dehydrogenase)	D-xylulose reductase activity; identical protein binding; L-iditol 2-dehydrogenase activity; NAD binding; zinc ion binding
Peptidyl-prolyl cis-trans isomerase (PPIase) (EC 5.2.1.8)	Peptidyl-prolyl cis-trans isomerase activity
Protein CutA	Binding
nudix (nucleoside diphosphate linked moiety X)-type motif 2(Nudt2)	Bis (5'-nucleosyl)-tetraphosphatase activity
Signal sequence receptor; delta; isoform CRA_b	ND
D-dopachrome decarboxylase	Catalytic activity
ER membrane protein complex subunit 1	ND
Cytokine receptor-like factor 3 (Cytokine receptor-like molecule 9) (CREME-9) (Cytokine receptor-related factor 4)	Identical protein binding
Protein name	**Gene ontology (biological process)**
Methylthioribose-1-phosphate isomerase (M1Pi) (MTR-1-P isomerase) (EC 5.3.1.23) (S-methyl-5-thioribose-1-phosphate isomerase) (Translation initiation factor eIF-2B subunit alpha/beta/delta-like protein)	L-methionine salvage from methylthioadenosine; L-methionine salvage from S-adenosylmethionine

Table 4.9 (Continued)

Protein name	Gene ontology (biological process) (Continued)
Proteasome subunit beta type (EC 3.4.25.1)	Immune system process; proteolysis involved in cellular protein catabolic process
Vbp1 protein (Fragment)	Protein folding
N-alpha-acetyltransferase 10	Metabolic process, cellular process
Glucagon [Cleaved into: Glicentin; Glicentin-related polypeptide (GRPP); Oxyntomodulin (OXM) (OXY); Glucagon; Glucagon-like peptide 1 (GLP-1); Glucagon-like peptide 1(7-37) (GLP-1(7-37)); Glucagon-like peptide 1(7-36) (GLP-1(7-36)); Glucagon-like peptide 2 (GLP-2)]	Adenylate cyclase-activating G-protein coupled receptor signaling pathway; adenylate cyclase-modulating G-protein coupled receptor signaling pathway; negative regulation of apoptotic process; negative regulation of appetite; negative regulation of execution phase of apoptosis; negative regulation of intrinsic apoptotic signaling pathway; positive regulation of calcium ion import; positive regulation of ERK1 and ERK2 cascade; positive regulation of gluconeogenesis by positive regulation of transcription from RNA polymerase II promoter; positive regulation of histone H3-K4 methylation; positive regulation of insulin secretion involved in cellular response to glucose stimulus; positive regulation of peptidyl-serine phosphorylation; positive regulation of peptidyl-threonine phosphorylation; positive regulation of protein binding; positive regulation of protein kinase activity; protein kinase A signaling; regulation of insulin secretion; response to starvation
Sorbitol dehydrogenase (EC 1.1.1.14) (L-iditol 2-dehydrogenase)	Flagellated sperm motility; fructose biosynthetic process; L-xylitol catabolic process; L-xylitol metabolic process; response to cadmium ion; response to copper ion; response to drug; response to hormone; response to nutrient levels; response to osmotic stress; sorbitol catabolic process; sorbitol metabolic process
Peptidyl-prolyl cis-trans isomerase (PPIase) (EC 5.2.1.8)	Neuron differentiation; protein folding
Protein CutA	Response to metal ion
nudix (nucleoside diphosphate linked moiety X)-type motif 2(Nudt2)	Single-organism cellular process
Signal sequence receptor; delta; isoform CRA_b	ND
D-dopachrome decarboxylase	Metabolic process, cellular process, single-organism process
ER membrane protein complex subunit 1	Cellular process

Table 4.9 (Continued)

Protein name	Gene ontology (biological process) (Continued)
Cytokine receptor-like factor 3 (Cytokine receptor-like molecule 9) (CREME-9) (Cytokine receptor-related factor 4)	G1/S transition of mitotic cell cycle; negative regulation of cell growth; positive regulation of cell cycle arrest; positive regulation of JAK-STAT cascade; positive regulation of transcription; DNA-templated; positive regulation of transcription by RNA polymerase II
Protein name	**Gene ontology (cellular component)**
Methylthioribose-1-phosphate isomerase (M1Pi) (MTR-1-P isomerase) (EC 5.3.1.23) (S-methyl-5-thioribose-1-phosphate isomerase) (Translation initiation factor eIF-2B subunit alpha/beta/delta-like protein)	Cytosol; fibrillar center; nucleoplasm
Proteasome subunit beta type (EC 3.4.25.1)	Cytoplasm; nucleus; proteasome core complex
Vbp1 protein (Fragment)	Prefoldin complex
N-alpha-acetyltransferase 10	ND
Glucagon [Cleaved into: Glicentin; Glicentin-related polypeptide (GRPP); Oxyntomodulin (OXM) (OXY); Glucagon; Glucagon-like peptide 1 (GLP-1); Glucagon-like peptide 1(7-37) (GLP-1(7-37)); Glucagon-like peptide 1(7-36) (GLP-1(7-36)); Glucagon-like peptide 2 (GLP-2)]	Cytoplasm; extracellular space; secretory granule lumen
Sorbitol dehydrogenase (EC 1.1.1.14) (L-iditol 2-dehydrogenase)	Extracellular exosome; membrane; mitochondrial membrane; mitochondrion; motile cilium
Peptidyl-prolyl cis-trans isomerase (PPIase) (EC 5.2.1.8)	Myelin sheath
Protein CutA	Extracellular region, membrane, organelle, extracellular region part
nudix (nucleoside diphosphate linked moiety X)-type motif 2(Nudt2)	Cell, organelle, cell part
Signal sequence receptor; delta; isoform CRA_b	Endoplasmic reticulum; integral component of membrane
D-dopachrome decarboxylase	Extracellular region, cell, organelle, extracellular region part, cell part
ER membrane protein complex subunit 1	ER membrane protein complex
Cytokine receptor-like factor 3 (Cytokine receptor-like molecule 9) (CREME-9) (Cytokine receptor-related factor 4)	Cytoplasm; cytosol; plasma membrane

Table 4.10 Gene ontology (GO) terms of 8 statistically differential proteins upregulated (fold change > 0.5) in STC-1 cells treated with 25 mM isomaltotriose compared to cells treated with 25 mM glucose. ND = not detected.

Protein name	Gene ontology (molecular function)
Predicted gene 5093	RNA binding; structural constituent of ribosome
Splicing factor; suppressor of white-apricot homolog (Splicing factor; arginine/serine-rich 8) (Suppressor of white apricot protein homolog)	RNA binding
fermitin family member 2	Binding
Ferritin (Fragment)	Ferric iron binding
Cleavage stimulation factor subunit 1 (CF-1 50 kDa subunit) (Cleavage stimulation factor 50 kDa subunit) (CSTF 50 kDa subunit) (CstF-50)	ND
MKIAA0244 protein (Fragment)	Binding
Neurabin-2 (Neurabin-II) (Protein phosphatase 1 regulatory subunit 9B) (Spinophilin)	Actin binding; actin filament binding; D2 dopamine receptor binding; ion channel binding; kinase binding; protein-containing complex binding; protein C-terminus binding; protein kinase activity; protein phosphatase 1 binding; protein phosphatase inhibitor activity
Methylenetetrahydrofolate dehydrogenase (NAD+ dependent)	Methylenetetrahydrofolate dehydrogenase (NADP+) activity
Protein name	**Gene ontology (biological process)**
Predicted gene 5093	Ribosomal large subunit assembly; translation
Splicing factor; suppressor of white-apricot homolog (Splicing factor; arginine/serine-rich 8) (Suppressor of white apricot protein homolog)	Alternative mRNA splicing; via spliceosome; mRNA 5'-splice site recognition; negative regulation of mRNA splicing; via spliceosome; regulation of transcription; DNA-templated; transcription; DNA-templated
fermitin family member 2	Integrin-mediated signaling pathway
Ferritin (Fragment)	Cellular iron ion homeostasis; iron ion transport
Cleavage stimulation factor subunit 1 (CF-1 50 kDa subunit) (Cleavage stimulation factor 50 kDa subunit) (CSTF 50 kDa subunit) (CstF-50)	mRNA processing
MKIAA0244 protein (Fragment)	Transcription; DNA-templated

Table 4.10 (Continued)

Protein name	Gene ontology (biological process) (Continued)
Neurabin-2 (Neurabin-II) (Protein phosphatase 1 regulatory subunit 9B) (Spinophilin)	Actin cytoskeleton organization; actin filament depolymerization; actin filament organization; aging; calcium-mediated signaling; cell migration; cellular response to epidermal growth factor stimulus; cellular response to estradiol stimulus; cellular response to morphine; cellular response to peptide; cerebral cortex development; dendrite development; developmental process involved in reproduction; filopodium assembly; hippocampus development; learning; male mating behavior; modulation of chemical synaptic transmission; negative regulation of cell growth; negative regulation of phosphoprotein phosphatase activity; positive regulation of cellular protein localization; positive regulation of protein localization to actin cortical patch; positive regulation of protein localization to plasma membrane; protein localization to actin cytoskeleton; protein localization to cell periphery; regulation of cell proliferation; regulation of opioid receptor signaling pathway; regulation of protein phosphorylation; reproductive system development; response to amphetamine; response to clozapine; response to immobilization stress; response to kainic acid; response to L-phenylalanine derivative; response to nicotine; response to prostaglandin E; response to steroid hormone
Methylenetetrahydrofolate dehydrogenase (NAD+ dependent)	ND
Protein name	**Gene ontology (cellular component)**
Predicted gene 5093	Cytosolic large ribosomal subunit
Splicing factor; suppressor of white-apricot homolog (Splicing factor; arginine/serine-rich 8) (Suppressor of white apricot protein homolog)	Nucleus
Fermitin family member 2	Cell, membrane, cell junction, membrane-enclosed lumen, macromolecular Complex, organelle, organelle part, membrane part, cell part, supramolecular fiber
Ferritin (Fragment)	Cell

Table 4.10 (Continued)

Protein name	Gene ontology (cellular component) (Continued)
Cleavage stimulation factor subunit 1 (CF-1 50 kDa subunit) (Cleavage stimulation factor 50 kDa subunit) (CSTF 50 kDa subunit) (CstF-50)	Nucleoplasm
MKIAA0244 protein (Fragment)	
Neurabin-2 (Neurabin-II) (Protein phosphatase 1 regulatory subunit 9B) (Spinophilin)	Actin cytoskeleton; adherens junction; cortical actin cytoskeleton; cytoplasm; cytoplasmic side of dendritic spine plasma membrane; dendritic spine; dendritic spine head; dendritic spine membrane; dendritic spine neck; filopodium; growth cone; lamellipodium; neuronal cell body; neuron projection; nucleoplasm; plasma membrane; postsynaptic density; ruffle membrane
methylenetetrahydrofolate dehydrogenase (NAD+ dependent)	Extracellular region, cell, organelle, extracellular region part, cell part

Table 4.11 Gene ontology (GO) terms of 11 statistically differential proteins downregulated (fold change < - 0.5) in STC-1 cells treated with 25 mM maltotetraose compared to cells treated with 25 mM glucose. ND = not detected.

Protein name	**Gene ontology (molecular function)**
DnaJ homolog subfamily C member 5 (Cysteine string protein) (CSP)	ATP-dependent protein binding
Delta-6 desaturase (EC 1.14.19.-) (Fragment)	Oxidoreductase activity
Glucagon [Cleaved into: Glicentin; Glicentin-related polypeptide (GRPP); Oxyntomodulin (OXM) (OXY); Glucagon; Glucagon-like peptide 1(7-37); Glucagon-like peptide 1(7-36); Glucagon-like peptide 2 (GLP-2)]	Glucagon receptor binding; hormone activity; identical protein binding
Dolichyl-diphosphooligosaccharide--protein glycosyltransferase 48 kDa subunit	Transferase activity; transferring glycosyl groups (Oligosaccharyl transferase 48 kDa subunit)
Dolichyl-diphosphooligosaccharide--protein glycosyltransferase subunit 1 (Fragment)	Dolichyl-diphosphooligosaccharide-protein glycotransferase activity
Protein max	Protein dimerization activity
Malectin	Carbohydrate binding; enzyme binding
Signal sequence receptor; delta; isoform CRA_b	ND
Sarm1 protein (Fragment)	Signaling adaptor activity
Zinc finger; MYND-type-containing 8	Lysine-acetylated histone binding; metal ion binding; methylated histone binding; protein N-terminus binding
Alpha-galactosidase (EC 3.2.1.-)	Alpha-galactosidase activity; galactoside binding; protein homodimerization activity; signaling receptor binding
Protein name	**Gene ontology (biological process)**
DnaJ homolog subfamily C member 5 (Cysteine string protein) (CSP)	Negative regulation of neuron apoptotic process
Delta-6 desaturase (EC 1.14.19.-) (Fragment)	Lipid metabolic process
Glucagon [Cleaved into: Glicentin; Glicentin-related polypeptide (GRPP); Oxyntomodulin (OXM) (OXY); Glucagon; Glucagon-like peptide 1(7-37); Glucagon-like peptide 1(7-36); Glucagon-like peptide 2 (GLP-2)]	Adenylate cyclase-activating G-protein coupled receptor signaling pathway; negative regulation of (apoptotic process, appetite and intrinsic apoptotic signaling pathway); positive regulation of (calcium ion import; ERK1 and ERK2 cascade; gluconeogenesis by positive regulation of transcription from RNA polymerase II promoter; histone H3-K4 methylation; insulin secretion

Table 4.11 (Continued)

Protein name	Gene ontology (biological process) (Continued)
Glucagon [Cleaved into: Glicentin; Glicentin-related polypeptide (GRPP); Oxyntomodulin (OXM) (OXY); Glucagon; Glucagon-like peptide 1(7-37); Glucagon-like peptide 1(7-36); Glucagon-like peptide 2 (GLP-2)]	involved in cellular response to glucose stimulus; peptidyl-serine phosphorylation; peptidyl-threonine phosphorylation; protein binding; protein kinase activity); protein kinase A signaling; regulation of insulin secretion; response to starvation
Dolichyl-diphosphooligosaccharide--protein glycosyltransferase 48 kDa subunit (Oligosaccharyl transferase 48 kDa subunit)	Protein N-linked glycosylation via asparagine
Dolichyl-diphosphooligosaccharide--protein glycosyltransferase subunit 1 (Fragment)	Protein glycosylation
Protein max	Metabolic process, cellular process, multicellular organismal process, developmental process, single-organism process, regulation of biological process, response to stimulus, biological regulation, cellular component organization or biogenesis
Malectin	Carbohydrate metabolic process
Signal sequence receptor; delta; isoform CRA_b	ND
Sarm1 protein (Fragment)	Negative regulation of MyD88-independent toll-like receptor signaling pathway; response to axon injury; signal transduction
Zinc finger; MYND-type-containing 8	Modulation of excitatory postsynaptic potential; negative regulation of cell migration; negative regulation of transcription from RNA polymerase II promoter by histone modification; positive regulation of dendritic spine development; positive regulation of dendritic spine maintenance; positive regulation of filopodium assembly; regulation of postsynaptic density protein 95 clustering
Alpha-galactosidase (EC 3.2.1.-)	Oligosaccharide metabolic process
Protein name	**Gene ontology (cellular component)**
DnaJ homolog subfamily C member 5 (Cysteine string protein) (CSP)	Anchored component of synaptic vesicle membrane; melanosome; plasma membrane; synaptic vesicle
Delta-6 desaturase (EC 1.14.19.-) (Fragment)	Integral component of membrane

Table 4.11 (Continued)

Protein name	Gene ontology (cellular component) (Continued)
Glucagon [Cleaved into: Glicentin; Glicentin-related polypeptide (GRPP); Oxyntomodulin (OXM) (OXY); Glucagon; Glucagon-like peptide 1(7-37); Glucagon-like peptide 1(7-36); Glucagon-like peptide 2 (GLP-2)]	Cytoplasm; extracellular space; secretory granule lumen
Dolichyl-diphosphooligosaccharide--protein glycosyltransferase 48 kDa subunit (Oligosaccharyl transferase 48 kDa subunit)	Endoplasmic reticulum membrane; integral component of membrane
Dolichyl-diphosphooligosaccharide--protein glycosyltransferase subunit 1 (Fragment)	Endoplasmic reticulum membrane; integral component of membrane
Protein max	MLL1 complex; RNA polymerase II transcription factor complex
Malectin	Endoplasmic reticulum; endoplasmic reticulum membrane; integral component of membrane
Signal sequence receptor; delta; isoform CRA_b	Endoplasmic reticulum; integral component of membrane
Sarm1 protein (Fragment)	Cell, membrane, cell junction, organelle, organelle part, membrane part, cell part, synapse, supramolecular fiber
Zinc finger; MYND-type-containing 8	Cytoplasm; dendritic shaft; dendritic spine; nucleus
Alpha-galactosidase (EC 3.2.1.-)	Extracellular region; Golgi apparatus; lysosome

Table 4.12 Gene ontology (GO) terms of 6 statistically differential proteins upregulated (fold change > 0.5) in STC-1 cells treated with 25 mM maltotetraose compared to cells treated with 25 mM glucose. ND = not detected.

Protein name	**Gene ontology (molecular function)**
Predicted gene 5093	RNA binding; structural constituent of ribosome
CCA tRNA nucleotidyltransferase 1; mitochondrial (EC 2.7.7.72) (mitochondrial tRNA nucleotidyl transferase; CCA-adding) (mt tRNA CCA-diphosphorylase) (mt tRNA CCA-pyrophosphorylase) (mt tRNA adenylyltransferase)	ATP:3'-cytidine-cytidine-tRNA adenylyltransferase activity; ATP binding; CTP:3'-cytidine-tRNA cytidylyltransferase activity; CTP:tRNA cytidylyltransferase activity; tRNA binding; tRNA nucleotidyltransferase activity
Uncharacterized protein	ND
Splicing factor; suppressor of white-apricot homolog (Splicing factor; arginine/serine-rich 8)	RNA binding
Gamma-aminobutyric acid receptor-associated protein-like 2 (GABA(A) receptor-associated protein-like 2) (Golgi-associated ATPase enhancer of 16 kDa) (GATE-16)	Ubiquitin protein ligase binding
MKIAA0244 protein (Fragment)	ND
Protein name	**Gene ontology (biological process)**
Predicted gene 5093	Ribosomal large subunit assembly; translation
CCA tRNA nucleotidyltransferase 1; mitochondrial (EC 2.7.7.72) (mitochondrial tRNA nucleotidyl transferase; CCA-adding) (mt tRNA CCA-diphosphorylase) (mt tRNA CCA-pyrophosphorylase) (mt tRNA adenylyltransferase)	Mitochondrial tRNA 3'-end processing; tRNA 3'-terminal CCA addition; tRNA processing
Uncharacterized protein	Integrin-mediated signaling pathway
Splicing factor; suppressor of white-apricot homolog (Splicing factor; arginine/serine-rich 8)	Alternative mRNA splicing; via spliceosome; mRNA 5'-splice site recognition; negative regulation of mRNA splicing; via spliceosome; regulation of transcription; DNA-templated; transcription; DNA-templated
Gamma-aminobutyric acid receptor-associated protein-like 2 (Golgi-associated ATPase enhancer of 16 kDa) (GATE-16)	Autophagosome assembly; autophagy of mitochondrion; cellular response to nitrogen starvation; intra-Golgi vesicle-mediated transport; negative regulation of proteasomal protein catabolic process; protein transport
MKIAA0244 protein (Fragment)	Transcription; DNA-templated

Table 4.12 (Continued)

Protein name	Gene ontology (cellular component)
Predicted gene 5093	Cytosolic large ribosomal subunit
CCA tRNA nucleotidyltransferase 1; mitochondrial (EC 2.7.7.72) (mitochondrial tRNA nucleotidyl transferase; CCA-adding) (mt tRNA CCA-diphosphorylase) (mt tRNA CCA-pyrophosphorylase) (mt tRNA adenylyltransferase)	Intracellular; mitochondrion
Uncharacterized protein	ND
Splicing factor; suppressor of white-apricot homolog (Splicing factor; arginine/serine-rich 8) (Suppressor of white apricot protein homolog)	Nucleus
Gamma-aminobutyric acid receptor-associated protein-like 2 (GABA(A) receptor-associated protein-like 2) (Golgi-associated ATPase enhancer of 16 kDa) (GATE-16)	Autophagosome; autophagosome membrane; cytoplasm; cytoplasmic vesicle; cytosol; Golgi apparatus; Golgi membrane; intracellular
MKIAA0244 protein (Fragment)	ND

Table 4.13 Gene ontology (GO) terms of 5 statistically differential proteins downregulated (fold change < - 0.5) in STC-1 cells treated with 2% α-limit dextrins compared to cells treated with 25 mM glucose. ND = not detected.

Protein name	Gene ontology (molecular function)
PIH1 domain-containing protein 1 (Nucleolar protein 17 homolog)	ATPase binding; histone binding; phosphoprotein binding; protein kinase binding; RNA polymerase I CORE element sequence-specific DNA binding
Bifunctional 3'-phosphoadenosine 5'-phosphosulfate synthase 2 (PAPS synthase 2) (Sulfurylase kinase 2) [Includes: Sulfate adenylyltransferase (EC 2.7.7.4) (ATP-sulfurylase) (Sulfate adenylate transferase) (SAT); Adenylyl-sulfate kinase (EC 2.7.1.25) (3'-phosphoadenosine-5'-phosphosulfate synthase) (APS kinase) (Adenosine-5'-phosphosulfate 3'-phosphotransferase)]	Adenylylsulfate kinase activity; ATP binding; nucleotidyltransferase activity; sulfate adenylyltransferase (ATP) activity
Deubiquitinating protein VCIP135	Thiol-dependent ubiquitin-specific protease activity
Transcriptional repressor p66 alpha	ND
Heparan sulfate 2-O-sulfotransferase 1 (2-O-sulfotransferase) (2-OST) (2OST) (EC 2.8.2.-)	Heparan sulfate 2-O-sulfotransferase activity
Protein name	**Gene ontology (biological process)**
PIH1 domain-containing protein 1 (Nucleolar protein 17 homolog)	Box C/D snoRNP assembly; chromatin remodeling; epithelial cell differentiation; establishment of protein localization to chromatin; negative regulation of cysteine-type endopeptidase activity involved in apoptotic signaling pathway; negative regulation of histone H3-K9 dimethylation; negative regulation of histone H3-K9 trimethylation; negative regulation of histone H4-K16 acetylation; positive regulation of glucose mediated signaling pathway; positive regulation of histone H3-K9 acetylation; positive regulation of histone H4 acetylation; positive regulation of protein complex assembly; positive regulation of protein serine/threonine kinase activity; positive regulation of TORC1 signaling; positive regulation of transcription of nucleolar large rRNA by RNA polymerase I; regulation of histone H3-K4 methylation; rRNA processing; snoRNA localization

Table 4.13 (Continued)

Protein name	Gene ontology (biological process) (Continued)
Bifunctional 3'-phosphoadenosine 5'-phosphosulfate synthase 2 (PAPS synthase 2) (Sulfurylase kinase 2) [Includes: Sulfate adenylyltransferase (EC 2.7.7.4) (ATP-sulfurylase) (Sulfate adenylate transferase) (SAT); Adenylyl-sulfate kinase (EC 2.7.1.25) (3'-phosphoadenosine-5'-phosphosulfate synthase) (APS kinase) (Adenosine-5'-phosphosulfate 3'-phosphotransferase)]	3'-phosphoadenosine 5'-phosphosulfate biosynthetic process; blood coagulation; bone development; sulfate assimilation
Deubiquitinating protein VCIP135	Endoplasmic reticulum membrane fusion; Golgi reassembly; mitotic cell cycle; protein K11-linked deubiquitination; protein K48-linked deubiquitination; protein ubiquitination
Transcriptional repressor p66 alpha	
Heparan sulfate 2-O-sulfotransferase 1 (2-O-sulfotransferase) (2-OST) (2OST) (EC 2.8.2.-)	Heparan sulfate proteoglycan biosynthetic process; polysaccharide chain biosynthetic process; heparin metabolic process; ureteric bud formation
Protein name	**Gene ontology (cellular component)**
PIH1 domain-containing protein 1 (Nucleolar protein 17 homolog)	Cytoplasm; nucleolus; nucleus; pre-snoRNP complex; R2TP complex
Bifunctional 3'-phosphoadenosine 5'-phosphosulfate synthase 2 (PAPS synthase 2) (Sulfurylase kinase 2) [Includes: Sulfate adenylyltransferase (EC 2.7.7.4) (ATP-sulfurylase) (Sulfate adenylate transferase) (SAT); Adenylyl-sulfate kinase (EC 2.7.1.25) (3'-phosphoadenosine-5'-phosphosulfate synthase) (APS kinase) (Adenosine-5'-phosphosulfate 3'-phosphotransferase)]	ND
Deubiquitinating protein VCIP135	Cytoplasm
Transcriptional repressor p66 alpha	ND
Heparan sulfate 2-O-sulfotransferase 1 (2-O-sulfotransferase) (2-OST) (2OST) (EC 2.8.2.-)	Golgi membrane; integral component of membrane

Table 4.14 Gene ontology (GO) terms of 17 statistically differential proteins upregulated (fold change > 0.5) in STC-1 cells treated with 2% α-limit dextrins compared to cells treated with 25 mM glucose. ND = not detected.

Protein name	Gene ontology (molecular function)
CCA tRNA nucleotidyltransferase 1; mitochondrial (EC 2.7.7.72) (mitochondrial tRNA nucleotidyl transferase; CCA-adding) (mt CCA-adding enzyme) (mt tRNA CCA-diphosphorylase) (mt tRNA CCA-pyrophosphorylase) (mt tRNA adenylyltransferase)	ATP:3'-cytidine-cytidine-tRNA adenylyltransferase activity; ATP binding; CTP:3'-cytidine-tRNA cytidylyltransferase activity; CTP:tRNA cytidylyltransferase activity; tRNA binding; tRNA nucleotidyltransferase activity
Splicing factor; suppressor of white-apricot homolog (Splicing factor; arginine/serine-rich 8) (Suppressor of white apricot protein homolog)	RNA binding
Uncharacterized protein	ND
Hnrpa3 protein	RNA binding
Propionyl-Coenzyme A carboxylase; alpha polypeptide; isoform CRA_b	ATP binding; enzyme binding; ligase activity; metal ion binding
Complement component 1 Q subcomponent-binding protein; mitochondrial (Complement component 1; q subcomponent binding protein; isoform CRA_b) (p32-RACK)	Adrenergic receptor binding; complement component C1q binding; hyaluronic acid binding; kininogen binding; protein kinase C binding; transcription corepressor activity; transcription factor binding
GrpE protein homolog 1; mitochondrial (Mt-GrpE#1)	Adenyl-nucleotide exchange factor activity; ATPase activator activity; ATPase binding; chaperone binding; protein homodimerization activity; unfolded protein binding
3-hydroxyisobutyrate dehydrogenase; mitochondrial (HIBADH) (EC 1.1.1.31)	3-hydroxyisobutyrate dehydrogenase activity; NAD binding; NADP binding
Isoleucine--tRNA ligase; mitochondrial (EC 6.1.1.5) (Isoleucyl-tRNA synthetase) (IleRS)	Aminoacyl-tRNA editing activity; ATP binding; isoleucine-tRNA ligase activity; tRNA binding
Ogdhl protein (Oxoglutarate dehydrogenase-like)	Oxoglutarate dehydrogenase (succinyl-transferring) activity; thiamine pyrophosphate binding
Stress-70 protein; mitochondrial (75 kDa glucose-regulated protein) (GRP-75) (Heat shock 70 kDa protein 9) (Mortalin) (Peptide-binding protein 74) (PBP74) (p66 MOT)	ATP binding; chaperone binding; enzyme binding; fibroblast growth factor binding; heat shock protein binding; ubiquitin protein ligase binding; unfolded protein binding

Table 4.14 (Continued)

Protein name	Gene ontology (molecular function) (Continue)
Pyruvate dehydrogenase protein X component; mitochondrial (Dihydrolipoamide dehydrogenase-binding protein of pyruvate dehydrogenase complex) (Lipoyl-containing pyruvate dehydrogenase complex component X)	Pyruvate dehydrogenase (NAD+) activity; transferase activity; transferring acyl groups
2-oxoglutarate dehydrogenase; mitochondrial (EC 1.2.4.2) (2-oxoglutarate dehydrogenase complex component E1) (OGDC-E1) (Alpha-ketoglutarate dehydrogenase)	Chaperone binding; heat shock protein binding; metal ion binding; oxoglutarate dehydrogenase (NAD+) activity; oxoglutarate dehydrogenase (succinyl-transferring) activity; thiamine pyrophosphate binding
MCG16685; isoform CRA_d (Pre-mRNA-splicing regulator WTAP)	ND
Carnitine O-acetyltransferase	Transferase activity; transferring acyl groups
60 kDa heat shock protein; mitochondrial (EC 3.6.4.9) (60 kDa chaperonin) (Chaperonin 60) (CPN60) (HSP-65) (Heat shock protein 60) (HSP-60) (Hsp60) (Mitochondrial matrix protein P1)	Apolipoprotein A-I binding; apolipoprotein binding; ATP binding; chaperone binding; double-stranded RNA binding; enzyme binding; high-density lipoprotein particle binding; hydrolase activity; insulin binding; lipopolysaccharide binding; modification-dependent protein binding; p53 binding; protease binding; protein binding involved in protein folding; protein-containing complex binding; protein heterodimerization activity; ubiquitin protein ligase binding
Pyruvate dehydrogenase E1 component subunit beta; mitochondrial (PDHE1-B) (EC 1.2.4.1)	Pyruvate dehydrogenase (acetyl-transferring) activity; pyruvate dehydrogenase (NAD+) activity; pyruvate dehydrogenase activity
Protein name	**Gene ontology (biological process)**
CCA tRNA nucleotidyltransferase 1; mitochondrial (EC 2.7.7.72) (mitochondrial tRNA nucleotidyl transferase; CCA-adding) (mt CCA-adding enzyme) (mt tRNA CCA-diphosphorylase) (mt tRNA CCA-pyrophosphorylase) (mt tRNA adenylyltransferase)	Mitochondrial tRNA 3'-end processing; tRNA 3'-terminal CCA addition; tRNA processing
Splicing factor; suppressor of white-apricot homolog (Splicing factor; arginine/serine-rich 8) (Suppressor of white apricot protein homolog)	Alternative mRNA splicing; via spliceosome; mRNA 5'-splice site recognition; negative regulation of mRNA splicing; via spliceosome; regulation of transcription; DNA-templated; transcription; DNA-templated

Table 4.14 (Continued)

Protein name	Gene ontology (biological process) (Continued)
Uncharacterized protein	Integrin-mediated signaling pathway
Hnrpa3 protein	ND
Propionyl-Coenzyme A carboxylase; alpha polypeptide; isoform CRA_b	ND
Complement component 1 Q subcomponent-binding protein; mitochondrial (Complement component 1; q subcomponent binding protein; isoform CRA_b) (p32-RACK)	Mature ribosome assembly; negative regulation of interferon-gamma production; negative regulation of interleukin-12 production; negative regulation of MDA-5 signaling pathway; negative regulation of mRNA splicing; via spliceosome; negative regulation of RIG-I signaling pathway; negative regulation of transcription by RNA polymerase II; phosphatidylinositol 3-kinase signaling; positive regulation of (apoptotic process; dendritic cell chemotaxis; neutrophil chemotaxis; protein kinase B signaling; substrate adhesion-dependent cell spreading; trophoblast cell migration); regulation of complement activation
GrpE protein homolog 1; mitochondrial (Mt-GrpE#1)	protein folding; protein import into mitochondrial matrix
3-hydroxyisobutyrate dehydrogenase; mitochondrial (HIBADH) (EC 1.1.1.31)	Valine catabolic process
Isoleucine--tRNA ligase; mitochondrial (EC 6.1.1.5) (Isoleucyl-tRNA synthetase) (IleRS)	Isoleucyl-tRNA aminoacylation
Ogdhl protein (Oxoglutarate dehydrogenase-like)	Tricarboxylic acid cycle
Stress-70 protein; mitochondrial (75 kDa glucose-regulated protein) (GRP-75) (Heat shock 70 kDa protein 9) (Mortalin) (Peptide-binding protein 74) (PBP74) (p66 MOT)	Erythrocyte differentiation; iron-sulfur cluster assembly; negative regulation of cell death; negative regulation of erythrocyte differentiation; negative regulation of hematopoietic stem cell differentiation; negative regulation of hemopoiesis; protein autophosphorylation; protein export from nucleus; protein folding; regulation of erythrocyte differentiation
Pyruvate dehydrogenase protein X component; mitochondrial (Dihydrolipoamide dehydrogenase-binding protein of pyruvate dehydrogenase complex) (Lipoyl-containing pyruvate dehydrogenase complex component X)	Mitochondrial acetyl-CoA biosynthetic process from pyruvate

Table 4.14 (Continued)

Protein name	Gene ontology (biological process) (Continued)
2-oxoglutarate dehydrogenase; mitochondrial (EC 1.2.4.2) (2-oxoglutarate dehydrogenase complex component E1) (OGDC-E1) (Alpha-ketoglutarate dehydrogenase)	2-oxoglutarate metabolic process; cerebellar cortex development; generation of precursor metabolites and energy; glycolytic process; hippocampus development; histone succinylation; NADH metabolic process; olfactory bulb mitral cell layer development; pyramidal neuron development; striatum development; succinyl-CoA metabolic process; tangential migration from the subventricular zone to the olfactory bulb; thalamus development; tricarboxylic acid cycle
MCG16685; isoform CRA_d (Pre-mRNA-splicing regulator WTAP)	mRNA methylation; regulation of alternative mRNA splicing; via spliceosome
Carnitine O-acetyltransferase	ND
60 kDa heat shock protein; mitochondrial (EC 3.6.4.9) (60 kDa chaperonin) (Chaperonin 60) (CPN60) (HSP-65) (Heat shock protein 60) (HSP-60) (Hsp60) (Mitochondrial matrix protein P1)	'De novo' protein folding; activation of cysteine-type endopeptidase activity involved in apoptotic process; apoptotic mitochondrial changes; B cell activation; B cell cytokine production; B cell proliferation; cellular response to heat; chaperone-mediated protein folding; interaction with symbiont; isotype switching to IgG isotypes; MyD88-dependent toll-like receptor signaling pathway; negative regulation of (apoptotic process; neuron apoptotic process; reactive oxygen species biosynthetic process); positive regulation of (apoptotic process; inflammatory response; interferon-alpha production; interferon-gamma production; interleukin-10 production; interleukin-12 production; interleukin-6 production; interleukin-6 secretion; macrophage activation; T cell activation; T cell mediated immune response to tumor cell; tumor necrosis factor secretion); protein import into mitochondrial intermembrane space; protein stabilization; response to activity; response to ATP; response to cocaine; response to cold; response to estrogen; response to glucocorticoid; response to hydrogen peroxide; response to hypoxia; response to ischemia; response to lipopolysaccharide; response to unfolded protein; T cell activation
Pyruvate dehydrogenase E1 component subunit beta; mitochondrial (PDHE1-B) (EC 1.2.4.1)	Acetyl-CoA biosynthetic process from pyruvate; glucose metabolic process; mitochondrial acetyl-CoA biosynthetic process from pyruvate; tricarboxylic acid cycle

Table 4.14 (Continued)

Protein name	Gene ontology (cellular component)
CCA tRNA nucleotidyltransferase 1; mitochondrial (EC 2.7.7.72) (mitochondrial tRNA nucleotidyl transferase; CCA-adding) (mt CCA-adding enzyme) (mt tRNA CCA-diphosphorylase) (mt tRNA CCA-pyrophosphorylase) (mt tRNA adenylyltransferase)	Intracellular; mitochondrion
Splicing factor; suppressor of white-apricot homolog (Splicing factor; arginine/serine-rich 8) (Suppressor of white apricot protein homolog)	Nucleus
Uncharacterized protein	ND
Hnrpa3 protein	ND
Propionyl-Coenzyme A carboxylase; alpha polypeptide; isoform CRA_b	ND
Complement component 1 Q subcomponent-binding protein; mitochondrial (Complement component 1; q subcomponent binding protein; isoform CRA_b) (p32-RACK)	Cell surface; cytosol; extracellular space; GABA-ergic synapse; glutamatergic synapse; mitochondrial matrix; nucleus; plasma membrane; presynaptic active zone
GrpE protein homolog 1; mitochondrial (Mt-GrpE#1)	Mitochondrial matrix; mitochondrion; nucleus; presequence translocase-associated import motor
3-hydroxyisobutyrate dehydrogenase; mitochondrial (HIBADH) (EC 1.1.1.31)	Mitochondrion
Isoleucine--tRNA ligase; mitochondrial (EC 6.1.1.5) (Isoleucyl-tRNA synthetase) (IleRS)	Cytosol; mitochondrial matrix; mitochondrion
Ogdhl protein (Oxoglutarate dehydrogenase-like)	ND
Stress-70 protein; mitochondrial (75 kDa glucose-regulated protein) (GRP-75) (Heat shock 70 kDa protein 9) (Mortalin) (Peptide-binding protein 74) (PBP74) (p66 MOT)	Cytoplasm; mitochondrial matrix; mitochondrial nucleoid; mitochondrion; myelin sheath; nucleolus
Pyruvate dehydrogenase protein X component; mitochondrial (Dihydrolipoamide dehydrogenase-binding protein of pyruvate dehydrogenase complex) (Lipoyl-containing pyruvate dehydrogenase complex component X)	Mitochondrial matrix; mitochondrion; pyruvate dehydrogenase complex

Table 4.14 (Continued)

Protein name	Gene ontology (cellular component) (Continued)
2-oxoglutarate dehydrogenase; mitochondrial (EC 1.2.4.2) (2-oxoglutarate dehydrogenase complex component E1) (OGDC-E1) (Alpha-ketoglutarate dehydrogenase)	Mitochondrial matrix; mitochondrial membrane; mitochondrion; nucleus; oxoglutarate dehydrogenase complex
MCG16685; isoform CRA_d (Pre-mRNA-splicing regulator WTAP)	Nuclear membrane; nuclear speck; RNA N6-methyladenosine methyltransferase complex
Carnitine O-acetyltransferase	ND
60 kDa heat shock protein; mitochondrial (EC 3.6.4.9) (60 kDa chaperonin) (Chaperonin 60) (CPN60) (HSP-65) (Heat shock protein 60) (HSP-60) (Hsp60) (Mitochondrial matrix protein P1)	Cell surface; clathrin-coated pit; coated vesicle; cytoplasm; cytosol; early endosome; extracellular exosome; extracellular space; Golgi apparatus; intracellular membrane-bounded organelle; lipopolysaccharide receptor complex; membrane; membrane raft; mitochondrial crista; mitochondrial inner membrane; mitochondrial matrix; mitochondrion; myelin sheath; peroxisomal matrix; plasma membrane; protein-containing complex; rough endoplasmic reticulum; secretory granule; zymogen granule
Pyruvate dehydrogenase E1 component subunit beta; mitochondrial (PDHE1-B) (EC 1.2.4.1)	Mitochondrial matrix; mitochondrion; nucleoplasm; pyruvate dehydrogenase complex

Table 4.15 Gene ontology (GO) terms of 6 statistically differential proteins downregulated (fold change < - 0.5) in STC-1 cells treated with 25 mM isomaltotriose compared to cells treated with 25 mM maltotriose. ND = not detected.

Protein name	Gene ontology (molecular function)
DCN1-like protein 5 (DCUN1 domain-containing protein 5) (Defective in cullin neddylation protein 1-like protein 5)	Cullin family protein binding; ubiquitin conjugating enzyme binding; ubiquitin-like protein binding
Glucagon [Cleaved into: Glicentin; Glicentin-related polypeptide (GRPP); Oxyntomodulin (OXM) (OXY); Glucagon; Glucagon-like peptide 1(7-37) (GLP-1(7-37)); Glucagon-like peptide 1(7-36) (GLP-1(7-36)); Glucagon-like peptide 2 (GLP-2)]	Glucagon receptor binding; hormone activity; identical protein binding
Protein kinase; AMP-activated; beta 1 non-catalytic subunit; isoform CRA_b	AMP-activated protein kinase activity; protein kinase binding
Tubulin alpha chain	GTPase activity; GTP binding; structural constituent of cytoskeleton
ER membrane protein complex subunit 1	ND
Cytokine receptor-like factor 3 (Cytokine receptor-like molecule 9) (CREME-9) (Cytokine receptor-related factor 4)	Identical protein binding
Protein name	**Gene ontology (biological process)**
DCN1-like protein 5 (DCUN1 domain-containing protein 5) (Defective in cullin neddylation protein 1-like protein 5)	Positive regulation of ubiquitin-protein transferase activity; protein neddylation
Glucagon [Cleaved into: Glicentin; Glicentin-related polypeptide (GRPP); Oxyntomodulin (OXM) (OXY); Glucagon; Glucagon-like peptide 1(7-37) (GLP-1(7-37)); Glucagon-like peptide 1(7-36) (GLP-1(7-36)); Glucagon-like peptide 2 (GLP-2)]	Adenylate cyclase-activating G-protein coupled receptor signaling pathway; adenylate cyclase-modulating G-protein coupled receptor signaling pathway; negative regulation of apoptotic process; negative regulation of appetite; negative regulation of execution phase of apoptosis; negative regulation of intrinsic apoptotic signaling pathway; positive regulation of (calcium ion import; ERK1 and ERK2 cascade; gluconeogenesis by positive regulation of transcription from RNA polymerase II promoter; histone H3-K4 methylation; insulin secretion involved in cellular response to glucose stimulus; peptidyl-serine phosphorylation; peptidyl-threonine phosphorylation; protein binding; protein kinase activity); protein kinase A signaling; regulation of insulin secretion; response to starvation

Table 4.15 (Continued)

Protein name	Gene ontology (biological process) (Continued)
Protein kinase; AMP-activated; beta 1 non-catalytic subunit; isoform CRA_b	Nail development; positive regulation of cold-induced thermogenesis; positive regulation of gene expression; protein heterooligomerization; regulation of catalytic activity
Tubulin alpha chain	Microtubule-based process
ER membrane protein complex subunit 1	ND
Cytokine receptor-like factor 3 (Cytokine receptor-like molecule 9) (CREME-9) (Cytokine receptor-related factor 4)	G1/S transition of mitotic cell cycle; negative regulation of cell growth; positive regulation of cell cycle arrest; positive regulation of JAK-STAT cascade; positive regulation of transcription; DNA-templated; positive regulation of transcription by RNA polymerase II
Protein name	**Gene ontology (cellular component)**
DCN1-like protein 5 (DCUN1 domain-containing protein 5) (Defective in cullin neddylation protein 1-like protein 5)	Ubiquitin ligase complex
Glucagon [Cleaved into: Glicentin; Glicentin-related polypeptide (GRPP); Oxyntomodulin (OXM) (OXY); Glucagon; Glucagon-like peptide 1(7-37) (GLP-1(7-37)); Glucagon-like peptide 1(7-36) (GLP-1(7-36)); Glucagon-like peptide 2 (GLP-2)]	Cytoplasm; extracellular space; secretory granule lumen
Protein kinase; AMP-activated; beta 1 non-catalytic subunit; isoform CRA_b	Nucleotide-activated protein kinase complex; nucleus
Tubulin alpha chain	Cytoplasmic microtubule
ER membrane protein complex subunit 1	ER membrane protein complex
Cytokine receptor-like factor 3 (Cytokine receptor-like molecule 9) (CREME-9) (Cytokine receptor-related factor 4)	Cytoplasm; cytosol; plasma membrane

Table 4.16 Gene ontology (GO) terms of 2 statistically differential proteins upregulated (fold change > 0.5) in STC-1 cells treated with 25 mM isomaltotriose compared to cells treated with 25 mM maltotriose. ND = not detected.

Protein name	**Gene ontology (molecular function)**
Transcription elongation factor SPT4-B (DRB sensitivity-inducing factor small subunit 2) (DSIF small subunit 2) (Transcription elongation factor SPT4 2)	DNA-binding transcription factor activity; RNA polymerase II complex binding; single-stranded RNA binding; zinc ion binding
Uncharacterized protein (Fragment)	Serine-type endopeptidase activity; serine-type exopeptidase activity
Protein name	**Gene ontology (biological process)**
Transcription elongation factor SPT4-B (DRB sensitivity-inducing factor small subunit 2) (DSIF small subunit 2) (Transcription elongation factor SPT4 2)	Chromatin organization; mRNA processing; positive regulation of DNA-templated transcription; elongation; regulation of transcription elongation from RNA polymerase II promoter; transcription; DNA-templated
Uncharacterized protein (Fragment)	ND
Protein name	**Gene ontology (cellular component)**
Transcription elongation factor SPT4-B (DRB sensitivity-inducing factor small subunit 2) (DSIF small subunit 2) (Transcription elongation factor SPT4 2)	DSIF complex
Uncharacterized protein (Fragment)	ND

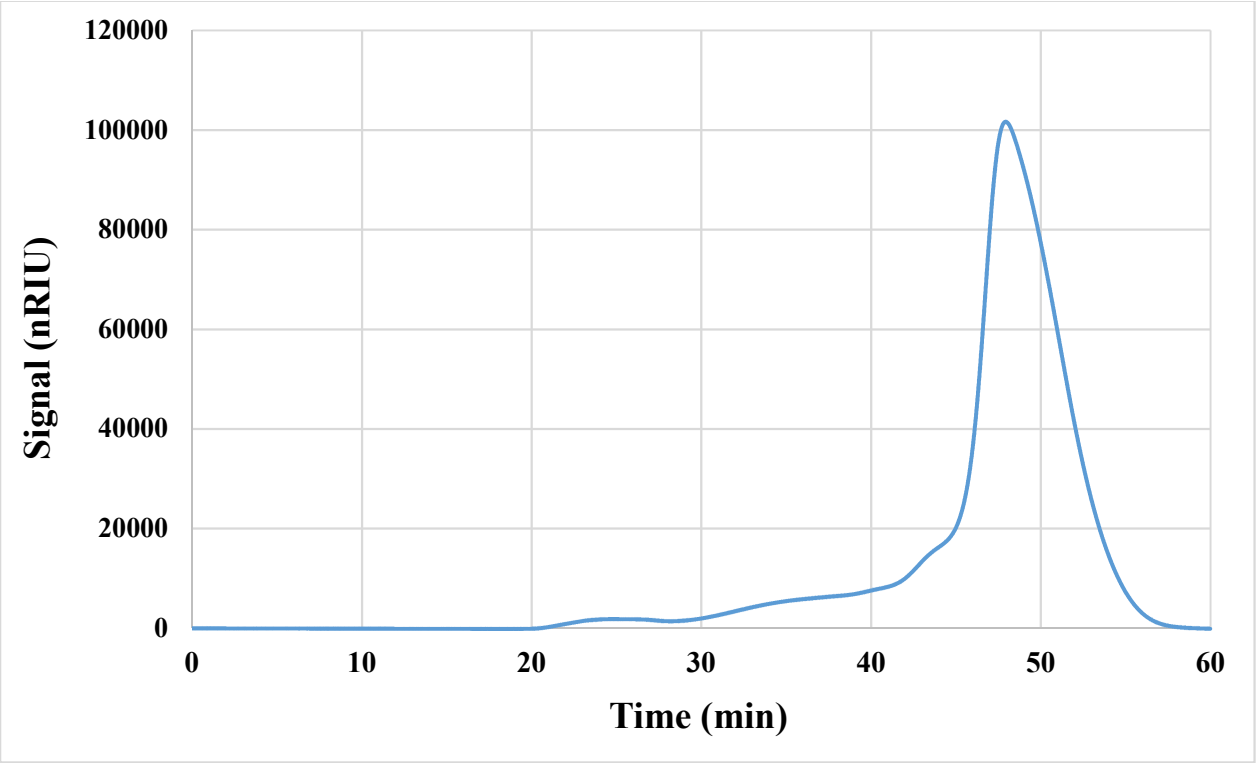

Figure 4.1 HPSEC chromatogram of 2% Solution of α-limit dextrins.

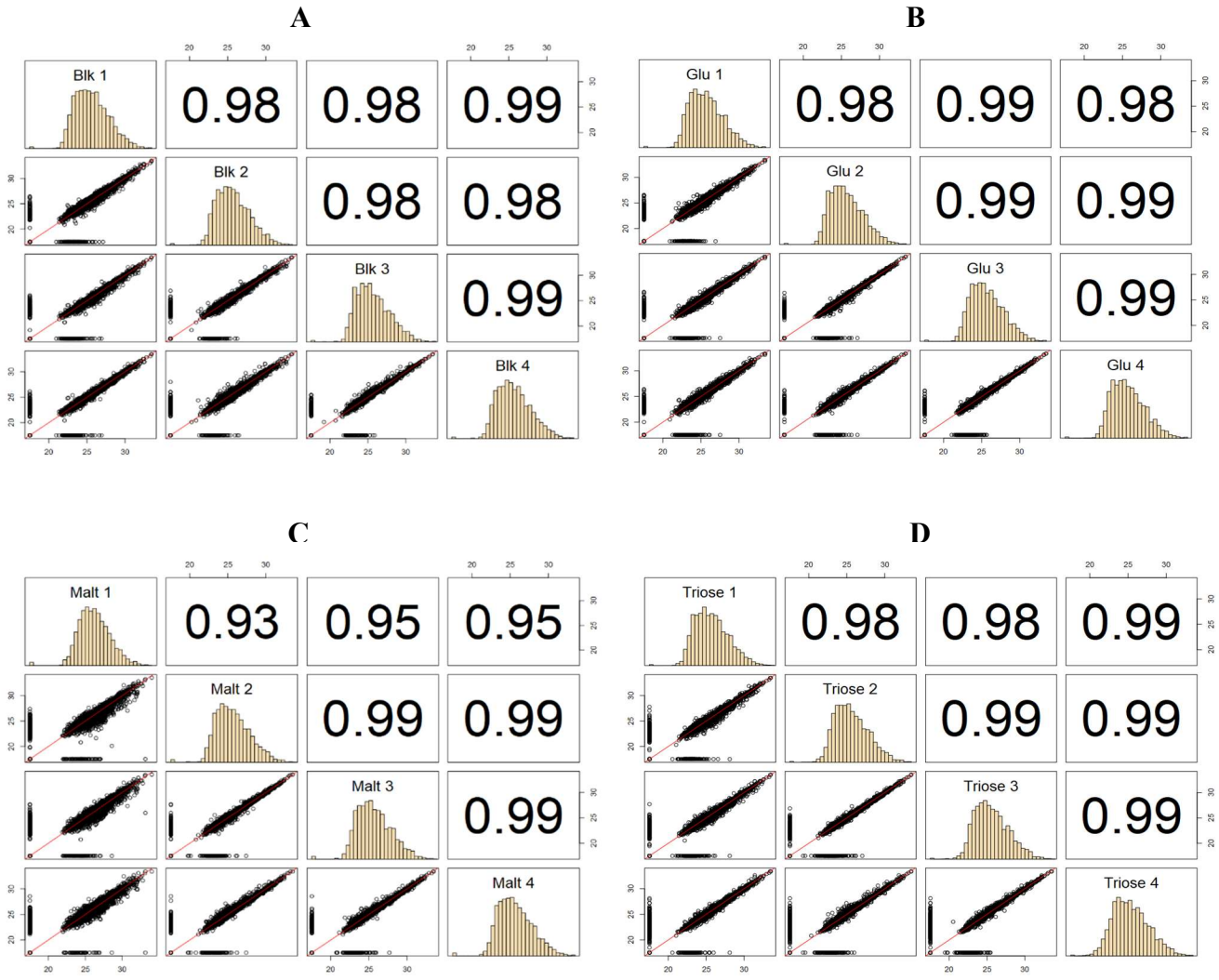

Figure 4.2 Comparison of normalized read count and correlation for each treatment biological replicates. A: vehicle (PBS- treated); B: glucose-treated; C: maltose-treated; D: maltotriose-treated.

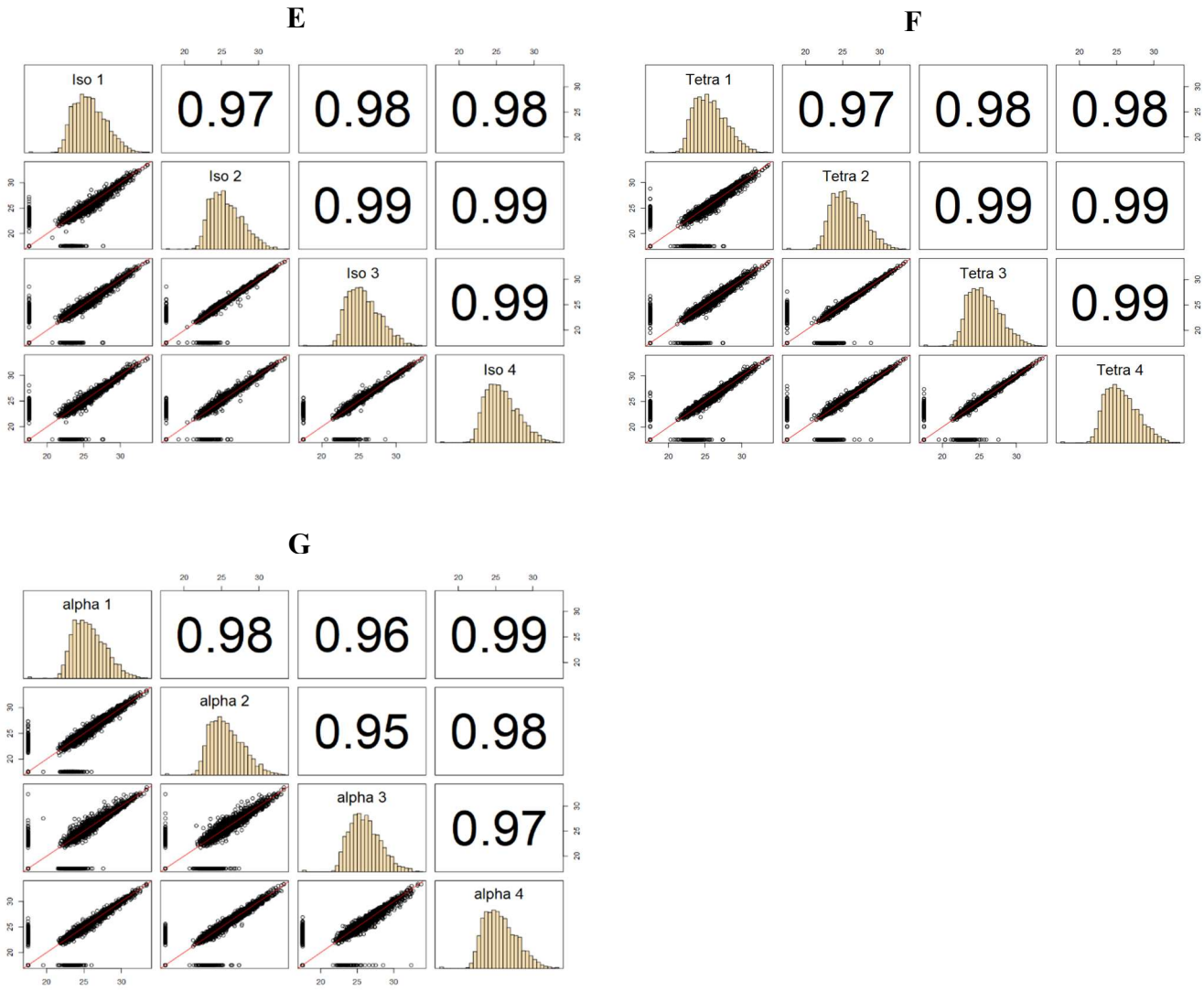

Figure 4.2 (Continued) Comparison of normalized read count and correlation for each treatment biological replicates. E: isomaltotriose-treated; F: maltotetraose-treated; G: α-limit dextrins-treated.

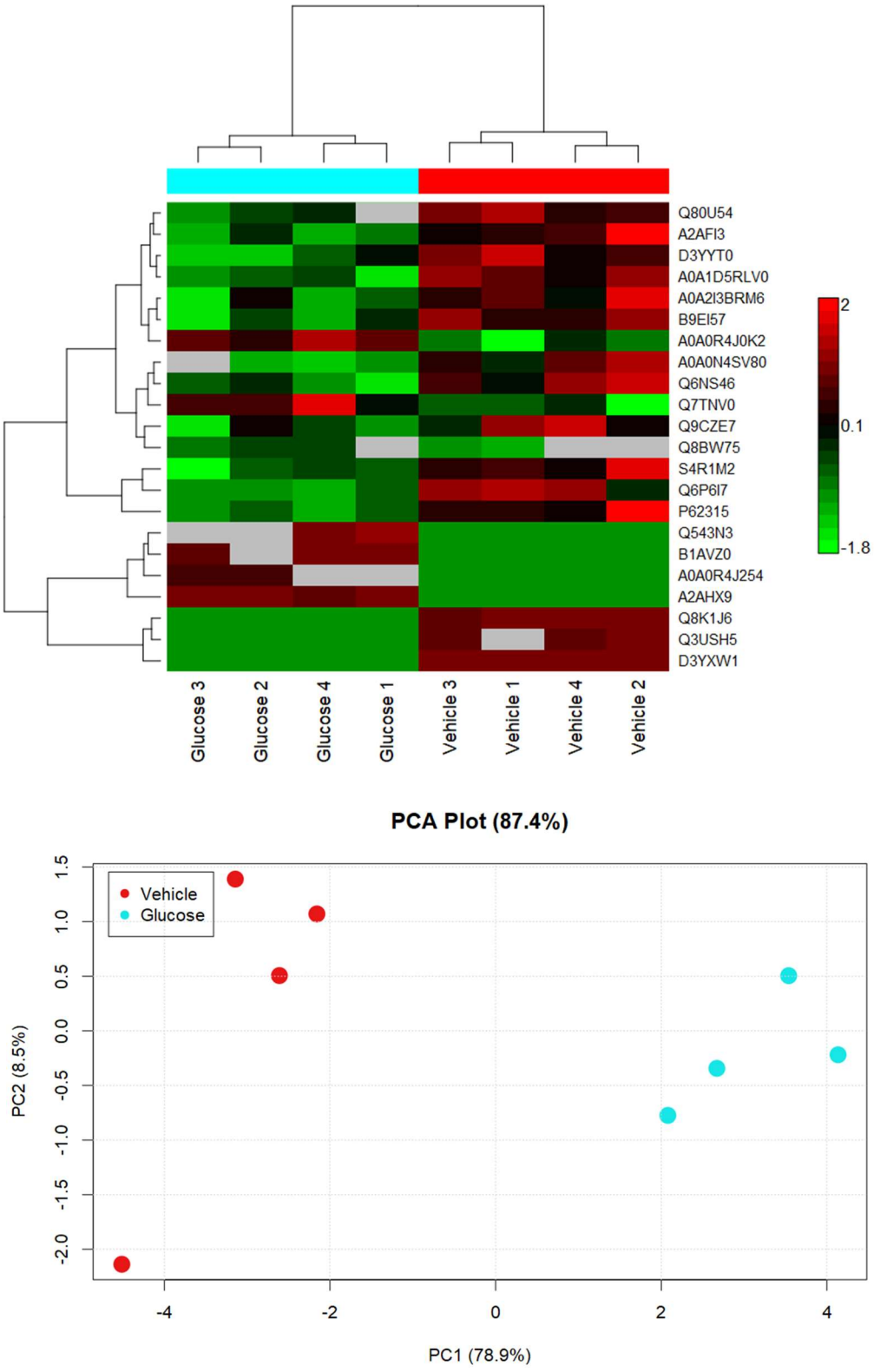

Figure 4.3 Heat map and PCA plot of identified proteins downregulated (< -0.5) fold change and upregulated (> 0.5) fold change in STC-1 cells treated with 25 mM glucose compared to STC-1 cells incubated with the dissolving vehicle buffer (DPBS).

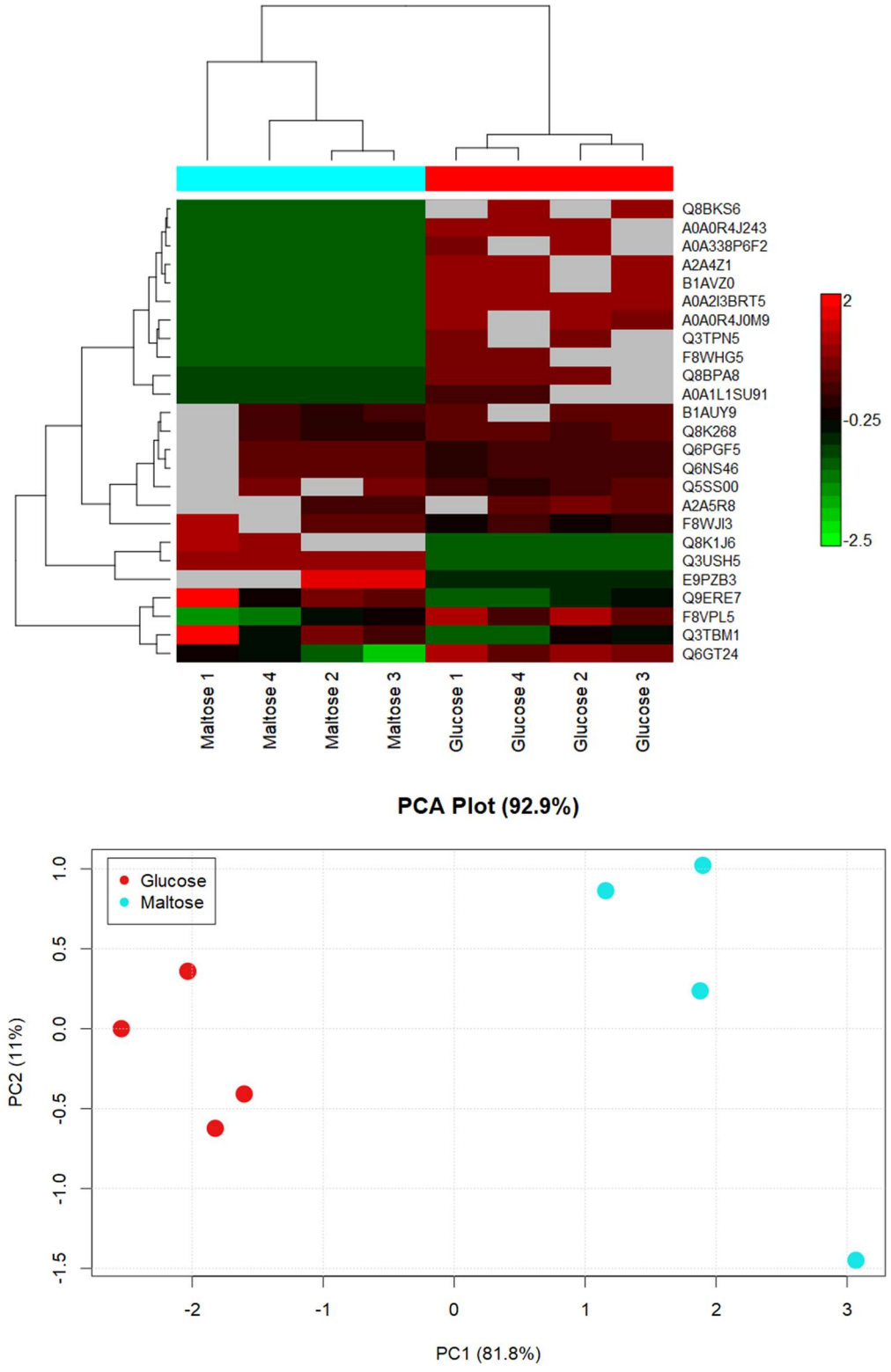

Figure 4.4 Heat map and PCA plot of identified proteins downregulated (< - 0.5) fold change and upregulated (> 0.5) fold change in STC-1 cells treated with 25 mM glucose compared to STC-1 cells treated with 25 mM maltose.

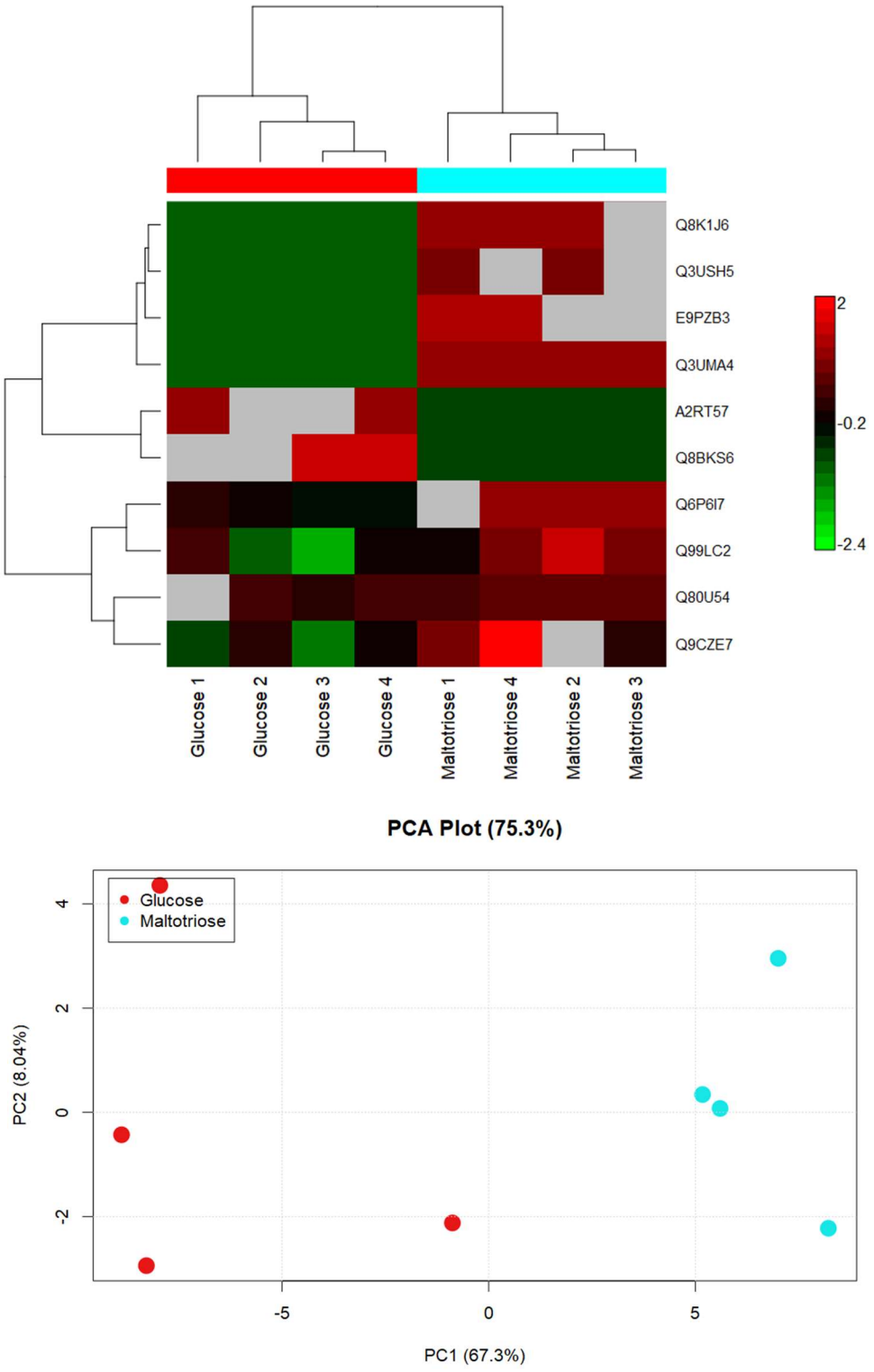

Figure 4.5 Heat map and PCA plot of identified proteins downregulated (< - 0.5) fold change and upregulated (> 0.5) fold change in STC-1 cells treated with 25 mM glucose compared to STC-1 cells treated with 25 mM maltotriose.

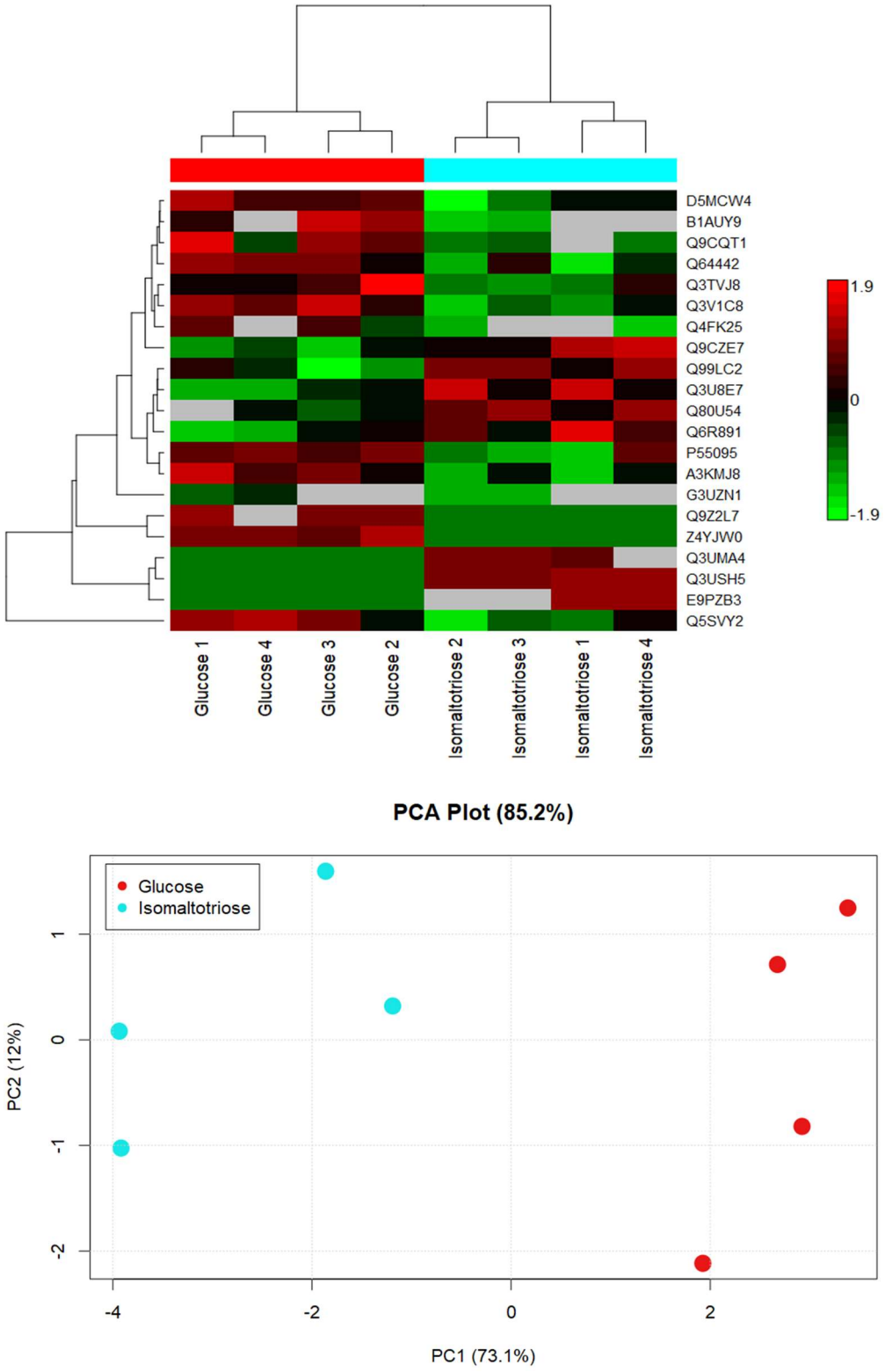

Figure 4.6 Heat map and PCA plot of identified proteins downregulated (< - 0.5) fold change and upregulated (> 0.5) fold change in STC-1 cells treated with 25 mM glucose compared to STC-1 cells treated with 25 mM isomaltotriose.

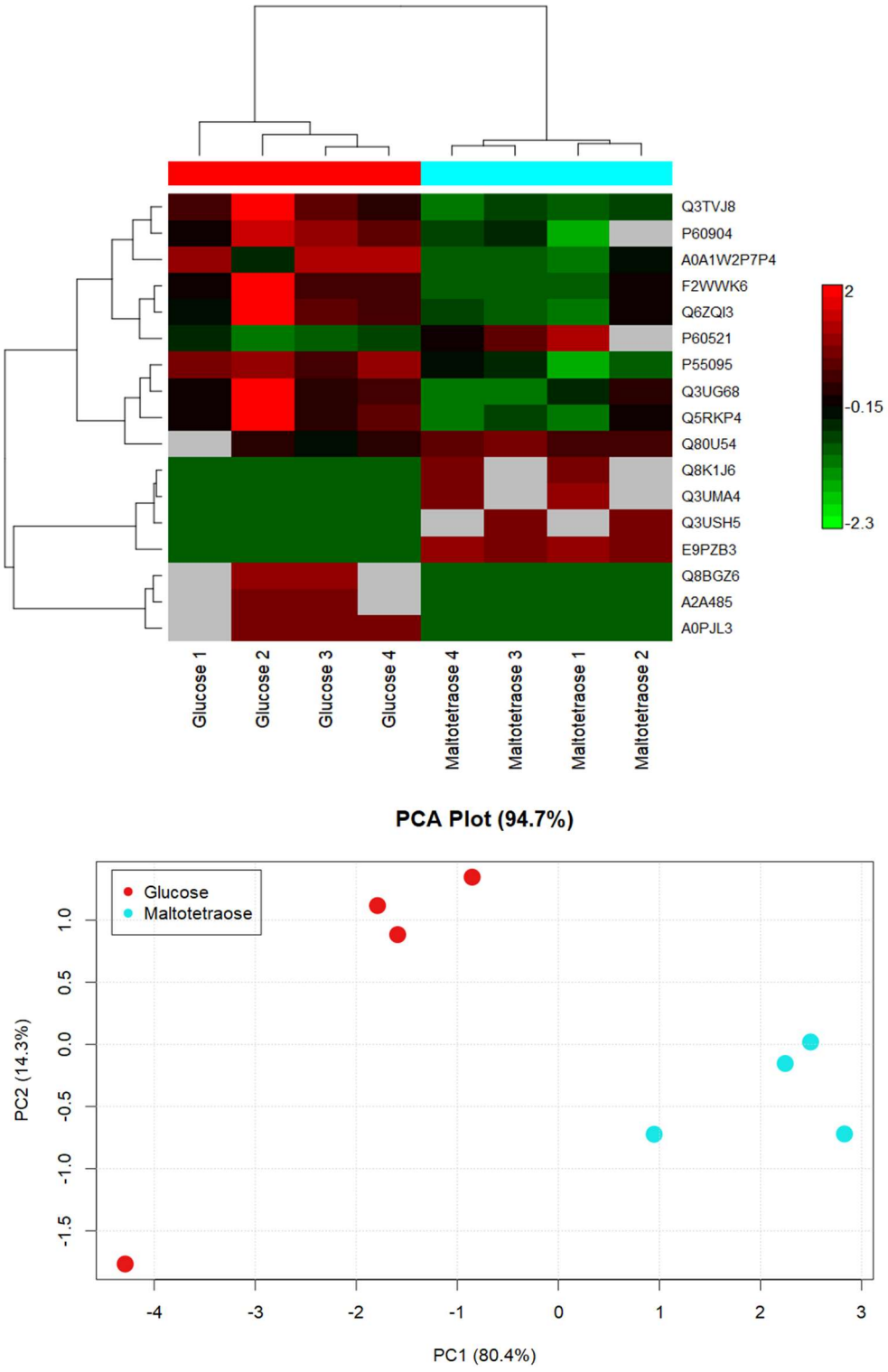

Figure 4.7 Heat map and PCA plot of identified proteins downregulated (< - 0.5) fold change and upregulated (> 0.5) fold change in STC-1 cells treated with 25 mM glucose compared to STC-1 cells treated with 25 mM maltotetraose.

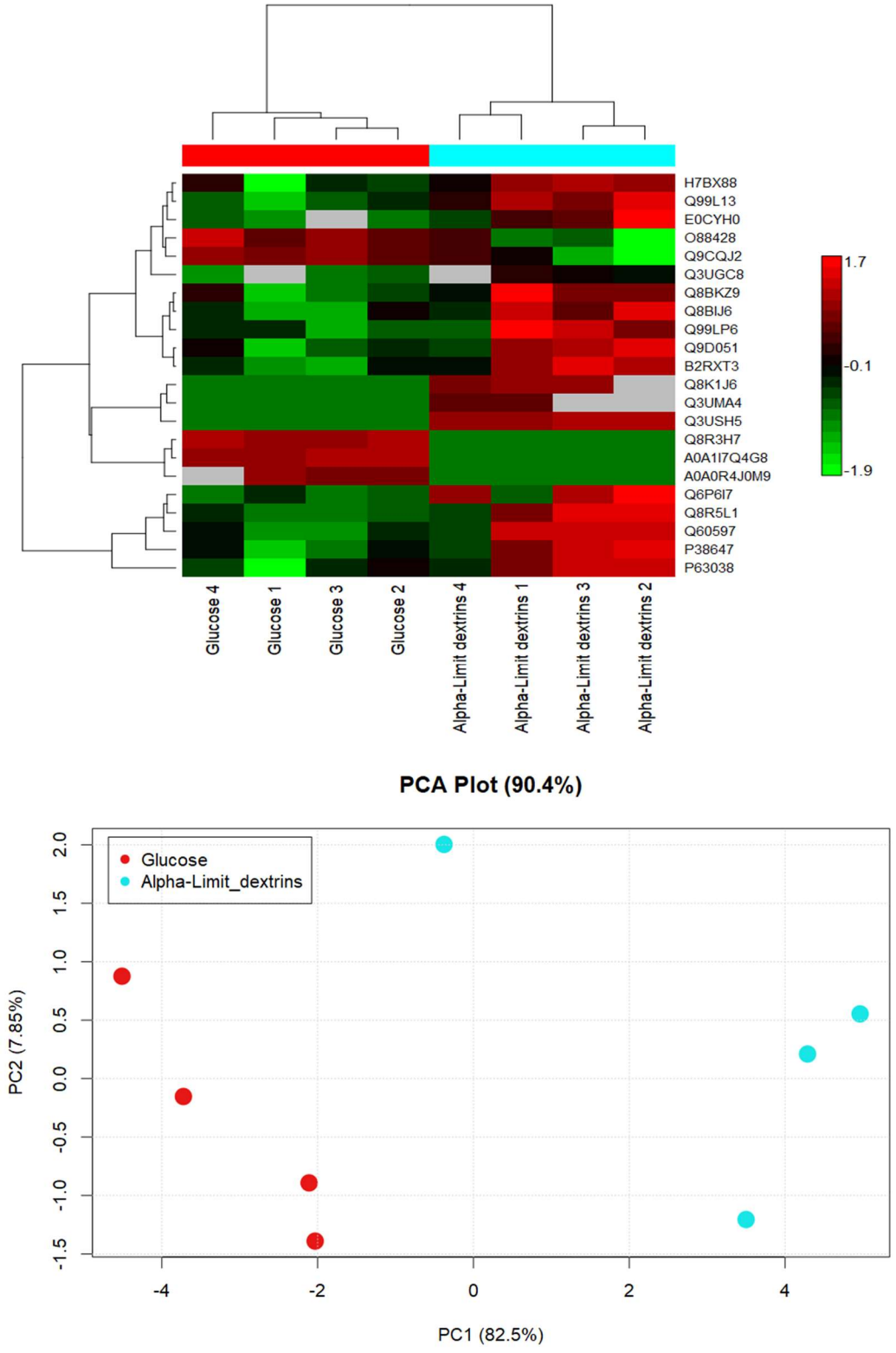

Figure 4.8 Heat map and PCA plot of identified proteins downregulated (< - 0.5) fold change and upregulated (> 0.5) fold change in STC-1 cells treated with 25 mM glucose compared to STC-1 cells treated with 2% α-limit dextrins.

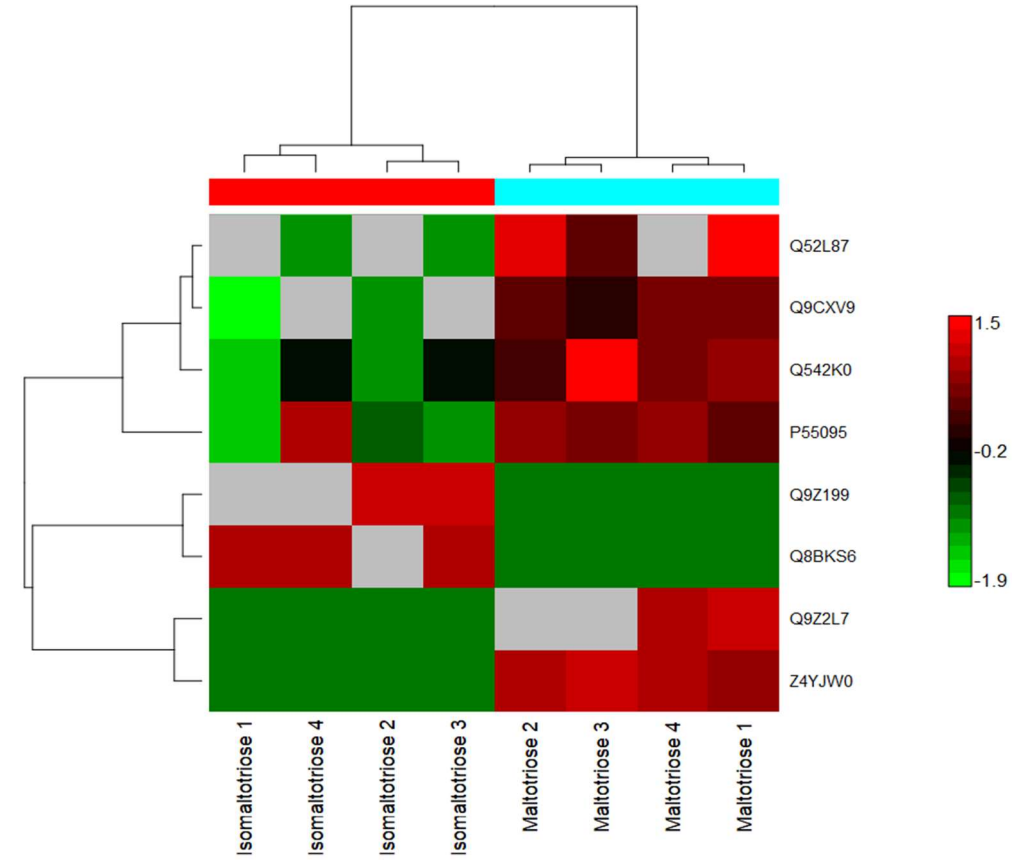

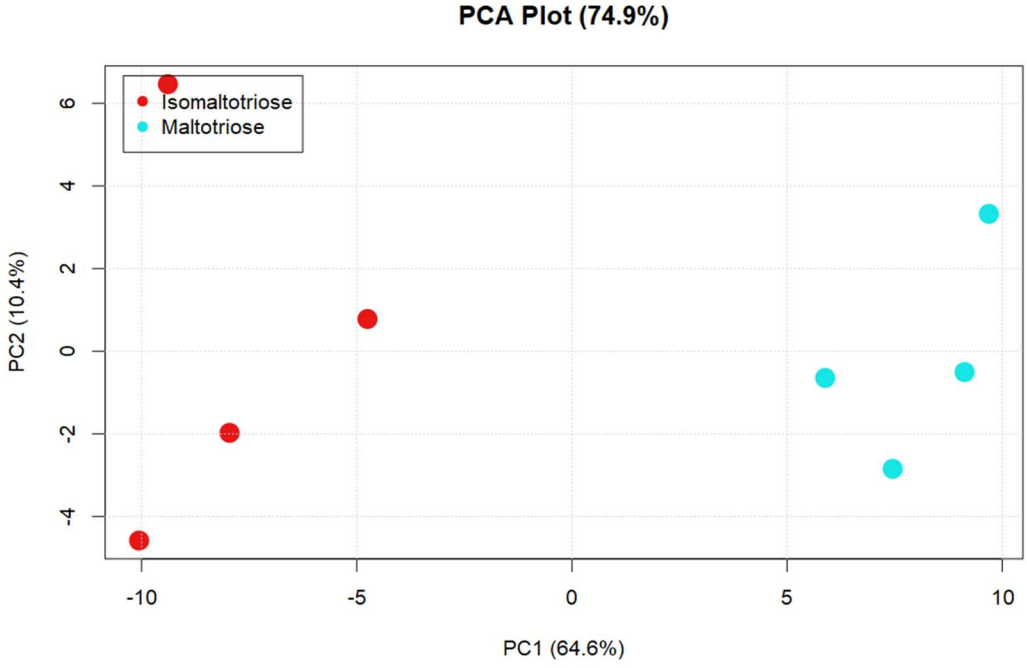

Figure 4.9 Heat map and PCA plot of identified proteins downregulated (< - 0.5) fold change and upregulated (> 0.5) fold change in STC-1 cells treated with 25 mM maltotriose compared to STC-1 cells treated with 25 mM isomaltotriose.

CHAPTER 5. THE ROLE OF SLOWLY DIGESTIBLE STARCH IN THE INTERVENTION AND THE PREVENTION OF OBESITY IN MICE

5.1 Abstract

α-Amylase digestion products of starch, maltooligosaccharides (MOS), were shown in Chapter II to stimulate L-cell secretion of anorexigenic peptides involved in glucose homeostasis, appetitive response and subsequent control of obesity. In a previous study from our laboratory, carbohydrate-based foods with slow digestion rate and locational digestion in the ileum had the beneficial effect of reducing food intake that was associated with stimulation of the gut-brain axis. Here we tested whether activation of the gut-brain axis using the same fabricated slowly digestible starch (SDS) microspheres would either increase weight loss of diet-induced obese (DIO) mice transferred to a low-fat diet or would reduce weight gain of lean mice placed on a high-fat diet. It was further hypothesized that the distal release of MOS by the digestion of SDS along the course of the small intestine contributes to the stimulation of the gut-brain axis. Alginate-entrapped starch microspheres with slow digesting rates were used to investigate the role of SDS in the intervention and prevention of obesity in C57BL/6J DIO and lean mice models over 12 weeks of feeding. Results showed that 20% SDS and pregelatinized starch in low-fat diets significantly improved weight loss, body fat reduction, and food intake reduction in DIO mice converted to low-fat diet for 12 weeks. Similarly, 15% SDS in high-fat diets showed significant reduction in weight gain rate and food intake in lean mice fed on 45% of calories high-fat diet. The intricate role of dietary carbohydrates on gut physiological response, related to satiety and food intake could be a new approach for food for health applications.

5.2 Introduction

Obesity is one of the most prevalent diseases in both developed and developing countries. In 2015~2016, the rate of obesity was 39.8% and affected about 93.3 million of US adults (CDC, 2018). Worldwide, obesity is predicted to increase to 573 million in 2030 from 396 million in 2005 [1]. It is reported that obesity is associated with a large spectrum of metabolic disorders including type II diabetes, hypertension, and cardiovascular diseases [2]. Approaches to combat obesity are many and have been extensively studied with a focus of diet and life style alterations. New approaches have been sought to tackle the problem of including using pharmaceutical agents, behavioral therapies, as well as surgery-based approaches such bariatric surgery [3]. Bariatric surgery has been the most effective treatment for the morbidly obese, however the surgery is still considered a radical procedure and expensive one and can have undesirable side effects. It is also impractical to the larger overweight population.

The Dietary Guidelines for Americans 2015-2020 (USDA) suggests that carbohydrates should provide 45-65% of total caloric intake [4]. The importance of the concept of carbohydrate quality relies on the fact that different carbohydrates show large variations in digestibility, sustainability, absorption rate, and glycemic index[5], [6]. Ludwig, 2002 showed that long-term consumption of high glycemic carbohydrates is detrimental to health [7]. Disrupting body glucose balance and excess energy storage contribute to this damage and ultimately can lead to the development of diabetes [8]. However, it was shown that when glucose is released in a slow rate over long period of time, health benefits were observed by decreasing the risk of developing diabetes and cardiovascular disease [9].

Starch is one of the major energy sources in the human diet that is digested in two phases. The first phase is by the salivary and pancreatic α-amylases to produce maltooligosaccharides (MOS) made up of linear oligomers and branched α-limit dextrins. The second phase is digestion

of the MOS to glucose by the small intestine brush border α-glucosidases, which is then absorbed by the intestinal cells. Starch is nutritionally classified by an in vitro test as rapidly digestible starch (RDS), slowly digestible starch (SDS), and resistant starch (RS) [10], and in the body is dependent on the rate of starch digestion in the small intestine, as well as the location where glucose delivery occurs [11]. RDS comprises the kind of starch that exists in most processed starchy foods. This portion of starch is quickly digested upon consumption and provide glucose in the duodenum and proximal jejunum. Contrarily, RS is resistant to digestion which allows it to reach the large intestine where it is fermented by the colonic microbiota. On the other hand, SDS is digested at a slower rate than RDS and provide extended or sustained glucose delivery [12].

One of the macronutrient stimuli of ileal brake induction and gastric emptying control are carbohydrates [13], and from a dietary approach is based on the capacity of SDS to digest into the distal small intestine to trigger the feedback inhibition mechanism [13]. In Chapter II of this thesis, MOS were shown to be a more strong and effective stimulator of GLP-1 secretion from enteroendocrine L-cells, which are an activator of the ileal brake, compared to glucose itself. Thus, the key requirement for the release MOS to the distal ileum is through a real and sustainable type of SDS.

The gastrointestinal tract responds to dietary nutrients to generate different satiety signals that regulate appetite and food intake [14], [15]. These signals are known to involve the central nervous system and the brain [16]. Within the brain, the hypothalamus specifically plays a central role in the gut-brain axis regulation of food intake and energy homeostasis [17], [18], [19] and [16]. One of the major hypothalamic nuclei regulating appetite signals is the arcuate nucleus [20]. This nucleus contains both the orexigenic neuropeptide Y (NPY) and agouti-related peptide (AgRP) neurons, as well as the anorexigenic pro-opiomelanocortin (POMC) and cocaine- and

amphetamine-regulated transcript (CART) containing neurons [21]. NPY and AgRP have been shown to play significant roles in energy homeostasis and satiety and appetite regulation [22], [23], [24].

The concept of the ileal brake and the ileal deposition of glucose is consistent with the fact the humans evolved on highly complex types of carbohydrates in general and slow digesting starch in particular. Glucose deposition in the ileum could be one of the key factors signaling the body adjust food motility and induce satiety. Conversely, the current prevalence of rapidly digestible carbohydrates in the form of sugars and highly processed starchy foods would not activate the ileal brake and gut-brain axis mechanisms and conceivably could be relevant to the prevalence of obesity and metabolic disorders associated with the Western diet. Additionally, the rate of starch digestion is the major determinant of starchy food glycemic response. It has been shown that rapidly digestible starch correlates to high glycemic index, whereas slowly digestible starch correlates to lower glycemic response [10],[25].

The long-term physiological and behavioral effect of high glycemic index carbohydrate diets in animal and humans is still controversial [26], [27]. In addition, different dietary factors have been shown to contributes to the overall effects of carbohydrates on gastric emptying, satiety and glucose balance. These factors include, the physical form of the diet, either solid or liquid form [28], particle size [29], as well as fiber content [30].

Activation of appetite-regulating gut hormones by carbohydrates was shown clearly in Chapter II cell culture studies and our rat study by Hasek *et al*., 2018 showed activation of the gut-brain axis by SDS in diet-induced obese rats [11]. Here, our interest was in the potential of SDS with ileal digestion in weight management. An animal model (mouse) was used study SDS and weight management and for inclusion of mechanisms related to carbohydrate sensation and

response. The study was designed to answer questions regarding physiological effects of dietary carbohydrate sensation in the intestinal epithelium and downstream consequences related to satiety induction and appetite suppression.

A technology small microspheres of starch entrapped within porous gelled alginate that hinder α-amylase access to starch was developed previously in our laboratory to produce experimental tool for slowly digestible starch delivery to the ileum [31]. The pores within the microspheres can be designed to be of different sizes to allow different rates of digestion. In the current study, body weight and food intake as long as body composition were monitored in mice being fed starch-entrapped microspheres in long-term consumption studies. In the first study, we tested the "intervention" effect of slowly digestible starch microspheres on weight reduction diet-induced obese mice. In the second study, we tested the "prevention" of consuming slowly digestible starch along with high fat diets in delaying weight gain through reducing food intake.

5.3 Materials and Methods

5.3.1 Preparation of Starch-Entrapped Microspheres

Starch-entrapped microspheres with a concentration of 0.75% sodium alginate were prepared in batches of 400 gm each to ensure complete and consistent mixing of the slurry. Sodium alginate (30 g) was dissolved in 3360 ml purified water. After complete solubility, 400 g starch was added with continuous mixing. The slurry was let to mix for 1-2 hours, then the mixture was dropped into a 2% calcium chloride bath through single 22-gauge needles. Microspheres were left in the calcium chloride bath for 3-4 hours, and then they were extensively washed with water and quickly washed with 70% ethanol to prevent the microspheres from sticking together. Microsphere were dried in a conventional oven at 42° C for 12 h. Gelatinization of the microspheres was

performed by boiling them in water for 20 min in a 1:10 starch to water ratio. Gelatinized microspheres were finally washed and freezed to -40° C before freeze-drying.

5.3.2 Diets

5.3.2.1 Intervention Study

Six experimental diets were used for this study. The standard high-fat diet TD.06414 adjusted calories diet (60/Fat) and low-fat diet TD.06416 adjusted calories diet (10/Fat) were purchased from Teklad Laboratory Animal Diets, Envigo (Madison, WI). The other four diets were formulated by incorporating different starch sources and levels into the low-fat control diet formulation (TD.06416). All the substitutions with the four formulated diets were made within the carbohydrate portion of the low-fat control diet without affecting protein or fat contents. The formulated diets were prepared to contain 40% pregelatinized starch (ULTRA-SPERSE A from Ingredion) (TD.170980), 40% raw corn starch (TD.171017), 20% starch-entrapped microspheres + 20% pregelatinized starch (TD.170981), and 40% starch-entrapped microspheres (TD.170982). Experimental diets were prepared at Teklad. The composition of the six experimental diets is shown in Table 5.1. The macronutrient composition of the experimental diets in % by weight is shown in Table 5.2. The composition of the experimental diets in % kcal is shown in Table 5.3. The starch-entrapped microspheres and the six experimental diets were tested for glucose release rate using *in vitro* starch digestion test. To perform the starch digestion test, 100 mg of grinded samples were mixed with sodium phosphate buffer (pH 6.9, 100 mM) and incubated in 37 °C water bath for 30 minutes. Then, enzyme mixture of pancreatin and amyloglucosidase was added and left for shaking at 160 rpm (time-zero). After 30 minutes and 60 minutes, 0.1 mL of the content was added to 0.9 mL absolute ethanol and centrifuged at 10,000 rpm for 3 minutes. Glucose concentrations were then measured in the digestion aliquots by the glucose oxidase/peroxidase

(GOPOD) method. Data of the *in vitro* starch digestion test performed on starch-entrapped microspheres and the six experimental diets are represented in Figure 5.1.

5.3.2.2 Prevention Study

Five experimental diets were used for this study. The standard high fat-diet TD.06415 adjusted calories diet (45/Fat) and low-fat diet TD.06416 adjusted calories diet (10/Fat) were purchased from Teklad. The other three diets were formulated by incorporating different starch sources and levels into the high-fat control diet (TD.06415). All the substitutions with the three formulated diets were made within the carbohydrate portion of the high-fat control diet without affecting protein or fat contents. The formulated diets were prepared to contain 15% pregelatinized starch (ULTRA-SPERSE A from Ingredion) (TD.170983), 15% starch-entrapped microspheres (TD.170984), and 30% starch-entrapped microspheres (TD.170985). Experimental diets were prepared by Teklad. The composition of the five experimental diets is shown in Table 5.4. The macronutrient composition of the experimental diets in % by weight is shown in Table 5.5. The composition of the experimental diets in % kcal is shown in Table 5.6.

The starch-entrapped microspheres and the five experimental diets were tested for glucose release rate using *in vitro* starch digestion test. Data of the *in vitro* starch digestion test performed on starch-entrapped microspheres and the five experimental diets are represented in Figure 5.17.

5.3.3 Animals

5.3.3.1 Intervention Study

All animal treatments were performed under protocol #1708001611, approved by the Purdue Animal Care and Use Committee (PACUC). Sixty 14-weeks-old male C57BL/6J Diet-Induced Obesity (60% DIO) mice were purchased from Jackson Laboratories (Bar Harbor, ME, USA) (JAX Stock #380050). Mice were maintained on a 12-hour light/dark cycle. Mice were kept

on ad libitum access to high-fat diet and water for three weeks for animal adaptation to the environments. Mice were divided into six experimental groups (n=10) where each group were maintained the following six diets: standard high-fat diet (TD.06414) (containing 60% of calories from fat), standard low-fat diet (TD.06416) (containing 10% of calories from fat), low-fat diet + RDS (TD.170980) (containing 10% of calories from fat + 40% pregelatinized starch), low-fat diet + raw corn starch (TD.171017) (containing 10% of calories from fat + 40% raw corn starch), low-fat diet + SDS (TD.170981) (containing 10% of calories from fat + 20% starch-entrapped microspheres), and low-fat diet + SDS (TD.170982) (containing 10% of calories from fat + 40% starch-entrapped microspheres). Mice were maintained on the experimental diets until age of week 12. To test the obesity intervention hypothesis, body weight and food intake were measured weekly.

5.3.3.2 Prevention Study

All animal treatments were performed under protocol #1708001611, approved by the Purdue Animal Care and Use Committee (PACUC). Seven-week-old male C57BL/6J mice were purchased from Jackson Laboratories (Bar Harbor, ME, USA) JAX Stock #380056. Mice were maintained on a 12-hour light/dark cycle and received water and chow diet. Mice were divided into five experimental groups (n=12) where each group was maintained on each of the following five diets: standard high-fat diet (TD.06415) (containing 45% of calories from fat), standard low-fat diet (TD.06416) (containing 10% of calories from fat), high-fat diet + DS (TD.170983) (containing 45% of calories from fat + 15% pregelatinized starch), high-fat diet + SDS (TD.170984) (containing 45% of calories from fat + 15% starch-entrapped microspheres), and high-fat diet + SDS (TD.170985) (containing 45% of calories from fat + 30% starch-entrapped

microspheres). Mice were maintained on these experimental diets until age of week 12. To test the obesity prevention hypothesis, body weight and food intake were measured weekly.

5.3.4 Body Weight and Food Intake

For each of the intervention and the prevention studies, mice body weight was recorded each week. Food intake was measured weekly by weighing the provided food at day 1 and weighing the remained food at day 8. All experimental diets that contained high fat content (45% or 60% calories from fat) were removed after one week of presence at room temperature to confirm freshness and uniform composition.

5.3.5 Body Composition

Body composition was monitored for mice in each of the two studies using two different methods: (1) Magnetic resonance imaging using EchoMRI™-100H for body composition of live moving small animals. EchoMRI provide information about the fat, lean and water portions of mice bodies, (2) Dual-energy X-ray absorptiometry (DEXA) using the Lunar PIXImus2 machine for body composition of animals under deep anesthesia. DEXA provide information about the fat and bone density of mice bodies. For DEXA scanning mice were anesthetized using VETAMAC isoflurane anesthesia machine at oxygen rates of 2 and isoflurane rate of 3. After anesthesia, mice eyes were protected using neomycin and polymyxinB sulfates, and Bacitracin zinc ophthalmic ointment. Data of body composition were analyzed using the LUNAR PIXImus2 2.10 software.

5.3.6 Euthanizing and Tissue Collection

At week 12 of the study phase, animals were euthanized using CO_2. Rapidly after euthanizing trunk blood was collected into EDTA-pre-coated syringes using cardiac puncture and blood was then transferred quickly into tubes containing EDTA, DPP IV inhibitor and aprotinin

(Millipore, Billerica, MA, USA) added at a dose of 10 µl/ml blood. Blood was centrifuged at 2000 rpm at 4°C for 15 min; and plasma was collected, aliquoted, flash-frozen in liquid nitrogen and stored at - 80°C until analyses (samples were not used for analyses in the current study and will be later analyzed). Liver from each mouse was isolated and freshly weighed before flash-freezing and storage at -80°C. Brains of all animals were harvested and frozen in liquid nitrogen and collected before being stored at -80°C (they were not used for analyses in the current study). The small intestine was collected from each mouse and rapidly put into modified Bouin's fixation buffer composed of 50% ethanol and 3% acetic acid in dH_2O [32] for overnight before getting ready to prepare histology sections.

5.3.7 Histology and Immunohistochemistry

Intestinal swiss-rolling was performed as described by Bialkowska *et al.*, 2016 [32]. The small intestine was washed two times with modified Bouin's fixative using a gavage needle. Using scissors, the small intestine was opened longitudinally along the mesenteric line. For some of the samples, the small intestine was cut into three equal sections following the stomach and immediately before the colon. The proximal segment was equivalent to the duodenum, the middle segment was equivalent to the jejunum, and the distal segment was equivalent to the ileum. For another portion of the samples, the whole small intestine was left one piece and used as it is for the Swiss role process. Each segment was Swiss rolled with the luminal side facing up and starting from the proximal side of the segment to the distal side. The resulting rolled segment was then transferred to 10% neutral-buffered formalin solution until sectioning. Immunohistochemistry was performed using the GLP-1 antibody (Anti-GLP1 antibody, ab22625) (Abcam, United Kingdom).

5.3.8 Statistical Analysis

Data were expressed as mean and standard error of the mean (Mean ± SEM). Body weight and food intake statistical analysis was performed using mixed model with repeated measures. Tukey's test has been used for pairwise comparison of treatments. For all other one-time point measurement data, mixed model has been used. The significance level of the test is $\alpha = 0.05$. Statistical analyses were conducted using SAS 9.4 (SAS Institute Inc., Cary, NC).

5.4 Results

5.4.1 Intervention Study

5.4.1.1 Body Weight

The average body weight of mice of the six experimental groups at baseline (and before the addition of experimental diets) was 44.1 ± 0.2 g. Mice in all groups at the baseline showed similar body composition identified by EchoMRI scanning with an average body fat percent of 30.4 ± 0.5 %, average lean body mass percent of 61.4 ± 0.5 % and average total water of 23.3 ± 0.2 g (Figure 5.2). After 5 weeks of adaptation using the same high-fat diet (60 % of calories from fat) used by Jackson Laboratories, diets were changed in five experimental groups to low-fat (10 % of calories from fat) diets with treatment diets containing RDS, SDS, and appropriate controls. Data of average body weight (g) of mice in six experimental groups throughout the study from week 1 to week 13 is shown in Figure 5.3. After one week of the addition of the five low-fat experimental diets, all treatment groups lost on average 19.5 % of their weight due to change from the high-fat to low-fat diet (from an average of 44.2 ± 0.2 g to 35.6 ± 0.87 g). The high-fat control group remained at a high body weight compared to low-fat treatment groups over the 13 weeks of observation. The body weight of 60 % high-fat control group was significantly higher (at $\alpha = 0.05$) compared to all other groups at $P = <0.0001$. Mice in the five low-fat diets showed gradual weight

loss form week 2 to week 5 ranging from an average of 35.6 ± 0.9 g for all mice in the five low-fat diets at week 2 to an average of 31.5 ± 0.8 g at week 5. The overall trend of body weight from week 2 to week 5 showed that the 40 % RCS group exhibited the lowest rate of weight loss among the five low-fat experimental groups followed by the 10 % low-fat control group. Diets containing 20 % and 40 % SDS microspheres showed a higher rate in weight loss between week 2 to week 5 compared to the control low-fat diet and the 40 % RCS diet. Unexpectedly, the highest effect of weight loss between week 2 to week 5 was observed in the 40 % pregelatinized starch group which was consistent with very low food intake in these three weeks (Figure 5.4). Body weight of all experimental groups in the following 8 weeks (between week 5 to week 13) exhibited a sustainable trend with a slight increase in average body weight by the end of week 13. Mice fed on 10 % low-fat control diet showed average body weight of 33.3 ± 0.4 at week 5 which increased by week 13 to 37.0 ± 0.9. Mice fed on 40 % RCS diet showed average body weight of 33.6 ± 0.9 at week 5 which increased by week 13 to 37.9 ± 1.2. Mice fed on 20 % PGS diet showed average body weight of 29.6 ± 0.6 at week 5 which increased by week 13 to 32.5 ± 0.4. Mice fed on 20 % SDS diet showed average body weight of 30.0±0.4 at week 5 which increased by week 13 to 31.9 ± 0.4. Mice fed on 40 % SDS diet showed average body weight of 31.2±0.7 at week 5 which increased by week 13 to 33.3 ± 0.7. Throughout the study, body weight of mice fed on SDS microsphere (20 % and 40 %) was lower compared to mice fed on 10 % low-fat control and 40 % RCS. The reduction in body weight of mice fed on 20 % PGS and 20 % SDS was statistically significant (at $\alpha = 0.05$) compared to mice fed on the 10 % low-fat control at $P = 0.0013$ and 0.0031, respectively. The reduction in body weight of mice fed on RCS and 40 % SDS was statistically insignificant (at $\alpha = 0.05$) compared to mice fed on the 10 % low-fat control at $P = 0.9857$ and 0.0921, respectively. Mice fed on RCS showed statistically significant (at $\alpha = 0.05$) higher body weight compared to 40

% PGS, 20 % SDS and 40 % SDS at $P = <0.0001$, <0.0001 and 0.0041, respectively. The reduction of body weight in 40 % PGS and 20 % SDS was statistically insignificant (at $\alpha = 0.05$) compared to each other or compared to the 40 % SDS group. Interestingly, average body weight of mice fed on 20% SDS microspheres was always lower than that of mice fed on the 40 % SDS microsphere diet.

5.4.1.2 Food Intake

Average daily food intake was estimated weekly starting from the experimental diet conversion. Data of average daily food intake (g/day) of mice in six experimental groups throughout the 12-weeks study is shown in Figure 5.4. Average daily food intake in the first week was higher in mice fed on the 60 % high-fat control diet (3.0 ± 0.1 g/day) compared to that of mice fed on the five 10 % low-fat diets. During the first week, mice in the low-fat control group and the 40% RCS group ate around 1.8 ± 0.3 and 1.8 ± 0.2 g/day, respectively, opposed to mice in the SDS microsphere groups that ate 0.6 ± 0.3 and 1.0 ± 0.3 g/day at the first week for 20 % SDS and 40 % SDS groups, respectively. Mice fed on the 40 % PGS diet ate around 0.5 ± 0.2 g/day in the first week. Although food intake levels in mice fed on the 60 % high-fat control remained sustainable throughout the 12 weeks of food intake measurement, food intake in other low-fat-based experimental groups showed a slight increase in food intake over time.

Mice fed on 10 % low-fat diet exhibited higher food intake over all other groups from week 2 and until the end of the study. The increase in daily food intake of mice fed on 10 % low-fat control was statistically significant (at $\alpha = 0.05$) compared to that of mice fed on 40 % PGS, 20 % SDS and 40 % SDS at $P = 0.0005$, 0.0002 and 0.0106, respectively. The increase in daily food intake of mice fed on 10 % low-fat control was not statistically significant (at $\alpha = 0.05$) compared to that of mice fed on RCS or 60 % high-fat control diet. Mice fed on 20 % SDS showed statistically

significant (at α = 0.05) reduction in daily food intake compared to mice fed on RCS at $P = 0.0044$. In addition, mice fed on 40 % PGS showed statistically significant (at α = 0.05) reduction in daily food intake compared to mice fed on RCS at $P = 0.0117$. Mice fed on 40 % RCS had statistically insignificant (at α = 0.05) higher food intake compared to mice fed on 40 % SDS throughout the study at $P = 0.1738$ and compared to mice fed on the 60 % high-fat control at $P = 0.8868$. Mice fed on 40 % PGS and 20 % SDS microsphere diets had the lowest food intake during the study, except for week 10 when mice fed on the 60 % high-fat control had a slight reduction in food intake.

5.4.1.3 Caloric Intake

Daily caloric intake was calculated by multiplying the daily food intake by the caloric equivalent (kcal/g) specific for each experimental diet. Data of average daily caloric intake (kcal/day) of mice in six experimental groups throughout the 12-weeks study is shown in Figure 5.5. As expected, mice fed on the 60 % high-fat control diet significantly consumed the highest caloric intake starting at week 1 (15.2 ± 0.6 kcal/day) and up to week 12 (16.1 ± 0.3 kcal/day) with an average of (15.4±0.4 kcal/day) throughout the study when compared to all other experimental groups at $P = <0.0001$. The daily caloric intake for this group was sustainable except for a small reduction at week 10. Except for week 1, where daily food intake was abnormally low, mice fed on the 10 % low-fat control and the 40 % RCS diets consumed higher caloric intake throughout the study (13.0 ± 0.5 and 12.3 ± 0.5 kcal/day, respectively), compared to mice fed on the 40 % PGS, 20 % SDS and 40% SDS diets (10.8 ± 0.5, 10.5 ± 0.4 and 10.8 ± 0.5 kcal/day, respectively).The increase in daily food intake of mice fed on 10 % low-fat control was statistically significant (at α = 0.05) compared to that of mice fed on 40 % PGS, 20 % SDS and 40 % SDS at $P = 0.0005$, 0.0002 and 0.0106, respectively. The increase in daily food intake of mice fed on 10%

low-fat control was not statistically significant (at α = 0.05) compared to that of mice fed on RCS or 60 % high-fat diet. Mice fed on 20 % SDS showed statistically significant (at α = 0.05) reduction in daily food intake compared to mice fed on RCS at $P = 0.0044$. Mice fed on 40 % PGS showed statistically significant (at α = 0.05) reduction in daily food intake compared to mice fed on RCS at $P = 0.0117$.

5.4.1.4 Body Composition

5.4.1.4.1 Dual-energy X-ray absorptiometry

Dual-energy X-ray absorptiometry (DEXA) scanning provided information about total tissue mass, fat percent, bone mineral density and bone mineral content of mice bodies throughout the study. DEXA scanning was used to monitor body composition at four-time points; week 2, week 6, week 10 and week 13 after diet conversion. Data of average total tissue mass (g) of mice in six experimental groups in the four-time points of scanning is shown in Figure 5.6. The increase in total tissue mass of mice fed on 60 % high-fat diet was significantly higher (at α = 0.05) than that of mice fed on all other experimental groups at $P = <0.0001$. In addition, total tissue mass of mice fed on RCS was significantly higher (at α = 0.05) than that of mice fed on 40 % PGS, 20 % SDS and 40% SDS diets at $P = <0.0001$, 0.0002 and 0.0177, respectively but didn't show significant difference compared to mice fed on 10 % low-fat control diet ($P = 0.9882$). Mice fed on the 10% low-fat control diet showed statistically significant (at α = 0.05) increase in total tissue mass compared to mice fed on 40% PGS and 20% SDS at $P = 0.001$ and 0.0047, respectively but didn't show statistically significant differences compared to mice fed on 40 % SDS diet. There were no statistical significant differences (at α = 0.05) in total tissue mass between mice fed on 40 % PGS, 20 % SDS and 40 % SDS diets when compared to each other.

Data of average body fat (%) of mice in six experimental groups in the four-time points of scanning is shown in Figure 5.7. As expected, mice fed on the 60 % high-fat control diet had the statistically significant (at $\alpha = 0.05$) highest body fat percent compared to all other groups until the end of the study at $P = <0.0001$. DEXA measurements obtained at week 2 (One week after dietary conversion) showed that all mice in experimental groups that converted into 10% low-fat control diets lost around 24% of their body fat in that first week. At week 2 (The first-time point), the average body fat (%) was 34.7 ± 2.1 %, 23.4 ± 2.2 %, 26.6 ± 2.4 %, 27.4 ± 2.9 %, 27.4 ± 2.5 % and 27.0 ± 3.0 % for mice fed on 60 % high-fat control, 10 % low-fat control, 40 % RCS, 40 % PGS, 20 % SDS and 40 % SDS diets, respectively. Among the five groups fed on low-fat diets, mice fed on 40% RCS showed the highest body fat percent from week 6 to week 13 (20.2 ± 2.3 % at week 6, 22.4 ± 2.2 % at week 10 and 24.3 ± 2.5 % at week 13). Mice fed on the 40 % PGS diet had body fat percent of 16.7 ± 1.1 % at week 6, 16.7±0.8 % at week 10 and 17.0 ± 0.9 % at week 13. Mice fed on the 20% SDS diet had body fat percent of 17.1 ± 0.7 % at week 6, 16.7 ± 0.6 % at week 10 and 16.5 ± 0.7 % at week 13. Mice fed on 40 % SDS diet had body fat percent of 17.3 ± 1.4 % at week 6, 17.1 ± 1.1 % at week 10 and 18.1 ± 1.3 % at week 13. No statistical differences in body fat percent (at $\alpha = 0.05$) were observed between mice fed on the five 10 % low-fat diets.

Data of average bone mineral densities (g/cm^2) of mice in six experimental groups in the four-time points of scanning is shown in Figure 5.8. Bone mineral densities at week 2 were similar in all experimental groups and was 0.06 ± 0.002, 0.07 ± 0.002, 0.07 ± 0.004, 0.07 ± 0.003, 0.07 ± 0.002 and 0.07 ± 0.003 g/cm^2 for mice fed on 60 % high-fat control, 10 % low-fat control, 40 % RCS, 40 % PGS, 20 % SDS and 40 % SDS diets, respectively. In all experimental groups, a trend of increasing bone mineral density was observed between week 10 and week 13. Among experimental groups, mice fed on the 60 % high-fat control had the lowest bone mineral density

at week 13 (0.068 ± 0.002 g/cm^2). The decrease in bone mineral density of mice fed on 60 % high-fat diet was statistically significant (at α = 0.05) compared to that of mice fed on 10 % low-fat control, 40 % RCS, 40 % PGS, 20 % SDS and 40 % SDS at *P* = 0.0409, 0.0132, 0.0337, 0.0164 and 0.0003, respectively. Mice fed on 40 % SDS diet had the highest bone mineral density (0.094 ±0.004 g/cm^2) by week 13 compared to all other group with significant difference (at α = 0.05) compared to the 60 % high-fat group (*P*= 0.0003) and statistically insignificant differences (at α = 0.05) when compare to other four 10 % low-fat diets. No statistical differences in bone mineral density (at α = 0.05) were observed between mice fed on the five 10 % low-fat diets.

Data of average bone mineral content (g) of mice in six experimental groups in the four-time points of scanning is shown in Figure 5.9. The same trend of bone mineral density (Figure 5.8) was observed for the bone mineral content. Bone mineral content at week 2 was similar in all experimental groups and was 0.61 ± 0.02, 0.65 ± 0.02, 0.72 ± 0.05, 0.72 ± 0.05, 0.66 ± 0.03 and 0.72 ± 0.05 g for mice fed on 60 % high-fat control, 10% low-fat control, 40 % RCS, 40 % PGS, 20 % SDS and 40 % SDS diets, respectively. Mice fed on the 60 % high-fat control showed the lowest bone mineral content (0.79 ± 0.04 g) at week 13, whereas mice fed on 40 % SDS diet had the highest bone mineral density (1.2 ± 0.06 g) at week 13. The decrease in bone mineral content of mice fed on 60 % high-fat diet was statistically significant (at α = 0.05) compared to that of mice fed on 10 % low-fat control, 40 % RCS, 40 % PGS, 20 % SDS and 40 % SDS at *P* = 0.0492, 0.0224, 0.0077, 0.0114 and <0.0001, respectively. No statistical differences in bone mineral content (at α = 0.05) were observed between mice fed on the five 10 % low-fat diets.

5.4.1.4.2 EchoMRI

Body composition was evaluated during the study using Echo - magnetic resonance imaging (EchoMRI) scanning. EchoMRI provides information about body fat, lean body mass,

and total water content. Figure 5.2 shows the baseline total body composition of mice in the six experimental groups of the intervention study before changing the 60 % high-fat adaptation diet to the different experimental diets. All mice in the experimental groups had similar average body fat percent of 30.4 ± 0.5 %, average lean mass percent of 61.4 ±0.5 % and average total water of 23.3 ± 0.2 g. After 8 weeks on the experimental diets, EchoMRI was used to monitor changes in body composition and results of body fat percent are shown in Figure 5.10. As expected, animals in the high-fat control diet retained their high average body fat percent (35.2 ± 1.8 %). Mice in other experimental groups lost more than 70.7 % of their body fat percent after conversion to low-fat diets. Mice fed on the 40 % RCS diet showed the highest body fat percent among the low-fat diets (14.6 ± 2.6 %), compared to body fat percent of the 10 % low-fat control group (10.6 ± 1.6 %), 40 % PGS group (8.2 ± 1.3 %), 20 % SDS group (8.9 ± 0.6 %) and 40 % SDS group (9.2 ± 1.2 %). The increase in body fat percent in mice fed on 60 % high-fat diet was statistically significant (at $\alpha = 0.05$) compared to that of mice fed on all other 10 % low-fat diets at $P = <0.0001$. At week 8, no statistical differences in body fat percent (at $\alpha = 0.05$) were observed between mice fed on the five 10 % low-fat diets.

Data of lean body mass percent (%) of mice in the different experimental groups is shown in Figure 5.11. The high-fat control diet showed the lowest average lean body mass percent (57.9 ± 1.5 %). The decrease in lean mass percent in mice fed on 60% high-fat diet was statistically significant (at $\alpha = 0.05$) compared to that of mice fed on all other 10% low-fat diets at $P = <0.0001$. All mice in other experimental groups had higher lean mass percent due to the conversion to low-fat diets. Lean body mass percent in mice fed on 10% low-fat diet was 81.4 ± 1.5% whereas lean body mass of mice fed on 40 % RCS, 40 % PGS, 20 % SDS and 40 % SDS diets were 77.2 ±

2.6%, 83.4 ± 1.3%, 82.3 ± 1.21% and 83.1 ± 1.5%, respectively. No statistical differences in lean body mass percent (at $\alpha = 0.05$) were observed between mice fed on the five 10% low-fat diets.

Data of total water mass (g) of mice in the different experimental groups is shown in Figure 5.12. Mice fed on the high-fat control diet showed total water mass of 24.8 ± 0.7 g. However, mice fed on 10% low-fat control, 40 % RCS, 40 % PGS, 20 % SDS, and 40 % SDS diets had total water mass of 24.4 ± 0.5, 23.8 ± 0.5, 22.0 ± 0.5, 21.3 ± 0.2 and 22.4 ± 0.4 g, respectively. The reduction in total water mass of mice fed on 20 % SDS was statistically significant (at $\alpha = 0.05$) compared to that of mice fed on 10 % low-fat control and mice fed on 60% high-fat control at $P = 0.0102$ and 0.0035, respectively. Similarly, the reduction in total water of mice fed on 40 % PGS was statistically significant (at $\alpha = 0.05$) compared to that of mice fed on 10 % low-fat control and mice fed on 60% high-fat control at $P = 0.0376$ and 0.0131, respectively.

5.4.1.5 Liver Weight

Liver weight (g) of mice in the six experimental groups by the end of the 13-week treatment phase is represented in Figure 5.13. Mice fed on the 60 % high-fat control diet had the highest liver weight (2.7 ± 0.31g) among experimental groups followed by mice fed on 40 % RCS diet (1.8 ± 0.14g). Mice fed on 10 % low-fat control diet had average liver weight of (1.7 ± 0.1 g), whereas, mice fed on 40 % PGS, 20 % SDS, and 40% SDS diets had the lowest average liver weight of 1.4 ± 0.08, 1.4 ± 0.06 and 1.4 ± 0.03 g, respectively. The increase in liver weight of mice fed on 60 % high-fat control diet was statistically significant (at $\alpha = 0.05$) compared to that of mice fed on 10% low-fat control, 40 % RCS, 40 % PGS, 20 % SDS and 40 % SDS at $P = 0.0046$, 0.0135, 0.0002, 0.0002 and 0.0003, respectively. No statistically significant differences (at $\alpha = 0.05$) in liver weight at $\alpha = 0.05$ were observed between mice fed on the five 10 % low-fat diets.

5.4.1.6 Immunohistochemistry of intestinal L-cells

Immunohistochemistry sections of the duodenum, jejunum and ileum of mice from each of the experimental groups are presented in Figure 5.14, Figure 5.15 and Figure 5.16, respectively. It is observed that L-cells are distributed evenly throughout the gastrointestinal tract.

5.4.2 Prevention Study

5.4.2.1 Body Weight

Data of average body weight (g) of mice in five experimental groups throughout the study from week 1 to week 13 is shown in Figure 5.18. Average body weight of mice in all experimental groups changed with treatments during the study period. Interestingly, mice fed on 15% SDS incorporated within 45 % high-fat diet showed body weight levels throughout the study close to that of mice fed on 10 % low-fat control diet. The average body weight of mice of the five experimental groups at the baseline point (and before the start of the experimental diets) was 24.3 ± 0.3 g. After 4 days of adaptation at the low-fat diet (10 % of calories from fat), diets were changed in four experimental groups to the high-fat (45 % of calories from fat) diets described above in the Material and Methods section. Over the treatment period (13 weeks), mice in all experimental groups increased in body weight. As expected, mice of the 45 % high-fat control group showed the highest rate in body weight increase starting from week 9 to week 13, finishing with an average body weight of 37.9 ± 1.0 g at week 13. Mice of the 10 % low-fat control group showed the lowest rate in body weight increase and ended up having an average body weight of 31.5 ± 1.1g at week 13. Average body weight of mice fed on the high-fat 15 % SDS diet at the end of the study (week 13) had an average body weight of 31.3 ± 0.9 g, equal to that of the 10% low-fat control group (31.5 ± 1.1 g). Interestingly, mice fed the 30% SDS/45% fat diet had the highest rate of body weight gain during the first 9 weeks of the study, though began reducing to 34.2 ± 1.0 g at the end

of the study and was lower than that of mice fed on the 45% high-fat control diet (37.9 ± 1.0 g) and the high-fat 15% PGS diet (35.8 ± 1.1 g) at week 13. The increase in the average body weight of 45 % high-fat control group was statistically significant (at $\alpha = 0.05$) compared to that of 10 % low-fat control group at $P = 0.0309$. Body weight of mice fed on 10 % low-fat control diet was lower than that of mice fed on 15 % PGS diet at $P = 0.0991$ and lower than that of mice fed on high-fat 30 % SDS diet at $P = 0.0576$.

5.4.2.2 Food Intake

Average daily food intake was estimated weekly starting from the experimental diet conversion. Data of average daily food intake (g/day) of mice in five experimental groups throughout the 12-weeks study is shown in Figure 5.19. Average daily food intake during the study period differed most notably with the 10% low-fat control group consistently consuming more than the 45% high-fat groups. Average daily food intake in the first week was higher in mice fed on the 10% low-fat control diet (2.9 ± 0.09 g/day) compared to that of mice fed on the four 45 % high-fat diets. During the first week, mice in the high-fat control, high-fat 15 % PGS, high-fat 15 % SDS and high-fat 30 % SDS groups ate 2.5 ± 0.03, 2.6 ± 0.08, 2.4 ± 0.08 and 2.7 ± 0.05 g/ day, respectively. Mice fed on 10% low-fat control diet showed the highest daily food intake throughout the study except for week 2 and 4, when mice in the 30% SDS group exhibited higher daily food intake. Mice in the 15% SDS microsphere group generally showed a trend of lower daily food intake, this being consistent with their lowest average body weight described in the previous section. The increase in daily food intake of mice fed on 10 % low-fat control was statistically significant (at $\alpha = 0.05$) compared to that of mice fed on 45 % high-fat control, high-fat 15 % PGS and high-fat 15 % SDS diets at $P = 0.0140$, 0.0103 and 0.0019, respectively. No statistically significant differences (at $\alpha = 0.05$) in daily food intake were observed between mice fed on high-

fat diets containing high-fat 15 % PGS, high-fat 15 % SDS or high-fat 30 % SDS when compared to each other.

5.4.2.3 Caloric Intake

Average daily caloric intake was estimated weekly starting from the experimental diet conversion. Data of average daily caloric intake (kcal/day) of mice in five experimental groups throughout the 12-weeks study is shown in Figure 5.20. The reduction in daily caloric intake of mice fed on 10% low-fat control was statistically significant (at $\alpha = 0.05$) compared to that of mice fed on 45 % high-fat control diet at $P = 0.0487$. No statistically significant differences (at $\alpha = 0.05$) in daily caloric intake were observed between mice fed on 10% low-fat diet compared to that of mice fed on high-fat diets containing high-fat 15 % PGS ($P = 0.0707$), high-fat 15% SDS ($P = 0.6112$) or high-fat 30 % SDS ($P = 0.1221$). No statistically significant differences in daily caloric intake were observed between mice fed on high-fat diets containing high-fat 15 % PGS, high-fat 15 % SDS or high-fat 30 % SDS when compared to each other.

5.4.2.4 Body Composition

5.4.2.4.1 Dual-energy X-ray absorptiometry

Dual-energy X-ray absorptiometry (DEXA) scanning provided information about total tissue mass, fat percent, bone mineral density and bone mineral content of mice bodies throughout the study. DEXA scanning was used to monitor body composition at two-time points; week 5 and week 12 after diet conversion. Data of average total tissue mass (g) of mice in five experimental groups in the two-time points of scanning is shown in Figure 5.21. The increase in total tissue mass of mice fed on 45 % high-fat diet (28.8 ± 0.65 g at week 5 and 37.1 ± 0.95 g at week 12) was significantly higher (at $\alpha = 0.05$) than that of mice fed on 10 % low-fat control diet (24.9 ± 0.60 g at week 5 and 30.5 ± 1.1 g at week 12) at $P = 0.0013$. In addition, total tissue mass of mice fed on

45% high-fat diet was significantly higher (at α = 0.05) than that of mice fed on high-fat 15% SDS (26.8 ± 0.75 g at week 5 and 30.0 ± 0.76 g at week 12) at P = 0.0056. Total tissue mass was significantly higher (at α = 0.05) in mice fed on high-fat 15 % PGS diet (28.2 ± 0.66 g at week 5 and 34.8 ± 1.13 g at week 12) compared to mice fed on 10 % low-fat control diet (24.9 ± 0.60 g at week 5 and 30.5 ± 1.1 g at week 12) at P = 0.0262. Moreover, total tissue mass was higher in mice fed on 15% PGS diet compared to mice fed on high-fat 15 % SDS diet at P = 0.0941 and was higher in mice fed on high-fat 30% SDS diet compared to mice fed on 10 % low-fat control diet at P = 0.0606.

Data of body fat percent (%) of mice in five experimental groups in the two-time points of scanning is shown in Figure 5.22. Data revealed that mice fed on the 45 % high-fat control diet gained the most body fat percent (20.4 ± 1.04% at week 5 and 29.2 ± 1.01% at week 12). Mice fed 15 % SDS microsphere diet and the 10 % low-fat control diet consistently showed both lower body fat percentage and a lower rate of increase. The increase in body fat (%) of mice fed on 45 % high-fat control diet was statistically significant (at α = 0.05) compared to that of mice fed 10 % low-fat control diet (16.2 ±1.17% at week 5 and 19.0 ± 1.73 % at week 12) and high-fat 15 % SDS diet (15.6 ± 0.84 % at week 5 and 17.8 ± 1.25 % at week 12) at P =0.0099 and 0.0035, respectively. Body fat percent was significantly higher (at α = 0.05) in mice fed on high-fat 15 % PGS (18.9 ± 1.52 % at week 5 and 26.6 ± 2.18 % at week 12) compared to mice fed on high-fat 15 % SDS at P = 0.0436. Interestingly, the high-fat 30 % SDS group at 5 weeks (20.17 ± 1.46 %) had already increased body fat content, but further rate of increase to week 12 (24.1 ± 1.56 %) was moderated similar to that observed for the high-fat 15 % SDS and the low-fat control groups. Body fat percent was higher in mice fed on high-fat 30 % SDS compared to mice fed on high-fat 15 % SDS at P = 0.0630. This went along with the lower food intake for the high-fat 15 % SDS microsphere group

as noted in Figure 5.19. The high-fat 15% PGS diet group had higher body fat and rate of increase similar to the 45 % high-fat control group.

Data of average bone mineral densities (g/cm^2) of mice in five experimental groups in the two-time points of scanning is shown in Figure 5.23. Although not statistically significant, mice fed on 45 % high-fat diet showed the highest bone mineral densities followed by mice fed on high-fat 15 % SDS diet. However, by week 12, mice fed on high-fat 30 % SDS diet showed the lowest bone mineral densities between groups. No statistical differences in bone mineral density at $\alpha = 0.05$ were observed between mice fed on any of the experimental diets based on Tukey's least squares means for treatment effect.

Data of average bone mineral content (g) of mice in five experimental groups in the two-time points of scanning is shown in Figure 5.24. Mice fed on the 10% low-fat control diet showed notable increase in bone mineral content from week 5 (0.56 ± 0.009) to week 12 (0.72 ± 0.034). Mice fed on high-fat 15% SDS diet (0.64 ± 0.023 g at week 5 and 0.72 ± 0.023 g at week 12) had the highest bone mineral content compared to 10% low-fat control at week 5 (0.56 ± 0.009), high-fat 15% PGS (0.59 ± 0.010 g at week 5 and 0.68 ± 0.018 at week 12), and high-fat 30% SDS (0.58 ± 0.018 at week 5 and 0.65 ± 0.015 at week 12) diets. No statistical differences in bone mineral content (at $\alpha = 0.05$) were observed between mice fed on any of the experimental diets based on Tukey's least squares means for treatment effect.

5.4.2.4.2 EchoMRI

Body composition was evaluated during the study using Echo-magnetic resonance imaging (EchoMRI) scanning. EchoMRI provides information about body fat, lean body mass, and total water content. Data of average body fat percent (%) of mice in five experimental groups at the end of week 12 of the study is shown in Figure 5.25. At the end of the study (week 12), mice fed on

high-fat 15 % SDS diet had the lowest average body fat percent (12.23 ± 1.41 %) compared to that of mice in the different high-fat experimental groups (25.91 ± 1.10 %, 21.38 ± 2.58 %, and 21.06 ± 1.76 % for mice fed on 45 % high-fat control, high-fat 15 % PGS, and high-fat 30 % SDS diets, respectively). The increase in body fat percent in mice fed on 45 % high-fat diet was statistically significant (at $\alpha = 0.05$) compared to that of mice fed on 10 % low-fat control at $P = 0.0069$ and mice fed on high-fat 15 % SDS diet at $P = 0.0012$. Body fat percent of mice fed on 15 % SDS was significantly (at $\alpha = 0.05$) lower than that of mice fed high-fat 15 % PGS at $P = 0.0486$ and was insignificantly lower than that of mice fed high-fat 30% SDS at $P = 0.0610$. Although not statistically significant, it is of interest that average body fat percent of mice fed on high-fat 15 % SDS diet (12.23 ± 1.41 %) (was even lower than that of mice fed on the 10 % low-fat control diet (14.32 ± 2.19 %) indicating a strong effect of the SDS microsphere in reducing fat deposition with long-term feeding of high fat diet.

Data of average lean body mass (%) of mice in five experimental groups at the end of week 12 of the study is shown in Figure 5.26. Lean body mass percent of mice differed among the experimental groups in accordance to body fat contents (Figure 5.25). Mice fed on the 45 % high-fat control diet showed the lowest average body lean mass percent (70.05 ± 1.02 %). All mice in the low-fat control group as well as other high-fat experimental groups had higher average lean body mass percent, though the same dietary fat content was consumed. The reduction in lean body mass percent in mice fed on 45 % high-fat control diet was statistically significant (at $\alpha = 0.05$) compared to that of mice fed on 10 % low-fat control diet (80.90 ± 2.05 %) at $P = 0.0100$ and mice fed on high-fat 15 % SDS diet (83.38 ± 1.39 %) at $P = 0.0012$. Average lean body mass percent of mice fed on high-fat 15 % SDS diet (83.38 ± 1.39 %) was significantly higher (at $\alpha = 0.05$) than that of mice fed high-fat 15 % PGS diet (74.35 ± 2.48 %) at $P = 0.0455$. Average lean body mass

percent of mice fed on high-fat 30 % SDS diet (75.21 ± 1.71 %) was insignificantly lower than that of mice fed 15 % SDS at $P = 0.0836$.

Data of average total water content (g) of mice in five experimental groups at the end of week 12 of the study is shown in Figure 5.27. Values of average water content were similar for the five experimental groups ranging from 21.56 ± 0.88 g in mice fed on the high-fat 15% SDS diet to 22.96 ± 0.44 g in mice fed on the 45% high-fat control diet. Average water content in mice fed on 10 % low-fat control, high-fat 15 % PGS, and high-fat 30 % SDS diets was 22.01 ± 0.49 g, 22.91 ± 0.41 g, and 22.03 ± 0.27 g, respectively. No statistical differences in total water content (g) were observed (at $\alpha = 0.05$) between mice fed on any of the experimental diets based on Tukey's least squares means for treatment effect.

5.4.2.5 Liver Weight

Liver weight (g) of mice in the five experimental groups by the end of the 13-week treatment phase is represented in Figure 5.28. Liver weight was somewhat lower in the high-fat 15 and 30 % SDS groups compared to the other treatment groups. A similar average liver weight was observed in mice fed on the 45 % high-fat control (1.44 ± 0.06 g), on the 10% low-fat control (1.43 ± 0.08 g), and on the high-fat 15 % PGS diets (1.39 ± 0.08 g). Mice fed the high-fat 15% and 30% SDS microspheres showed average liver weight of 1.29 ± 0.04 g and 1.28 ± 0.04 g, respectively. No statistical differences in liver weight were observed (at $\alpha = 0.05$) between mice fed on any of the experimental diets based on Tukey's least squares means for treatment effect.

5.4.2.6 Immunohistochemistry of intestinal L-cells

Immunohistochemistry sections of the duodenum, jejunum and ileum of mice from each of the five experimental groups are presented in Figure 5.29, Figure 5.30 and Figure 5.31

respectively. Similar to observation of the intervention study, it is observed that L-cells are evenly distributed throughout the gastrointestinal tract.

5.5 Discussion and Conclusions

A negative connotation of dietary carbohydrates has arisen in recent years with the increased prevalence of obesity and other metabolic diseases in developed, as well as urbanized developing, countries. The recommendation of the World Health Organization (WHO) to reduce overall carbohydrate intake, especially sugars and rapidly digestible starches, contributed further to this association [33], [34]. Recent national dietary guidelines have resulted in the development of new types of low carbohydrate diets that are suggested to provide acute health benefits such as weight loss and improved insulin sensitivity. However, a few recent studies suggested the association of long term consumption of low carbohydrate diets with chronic adverse health effects [35] ,such as deficiencies in water and electrolyte balance [36], [37], as well as the reduction in body glycolytic capacity [38],[39].

We think that humans evolved with the consumption of complex slowly digestible carbohydrates which facilitated an individual's satiation and a control of food intake. Therefore, the key characteristic influencing the physiological outcomes of carbohydrate consumption is its quality. The identification of the different aspects of carbohydrate quality is not clear. The term "carbohydrate quality" has been associated to glycemic index and dietary fiber content. However, other aspects of carbohydrate digestibility, such as digestion rate, locational digestion into the distal (ileal) small intestine, and sustained energy release could be of important in improving the overall outcome of carbohydrate consumption. The beneficial consequences of long-term consumption of slowly digestible starch have been reported [40].

In the current study, we showed that specific levels of SDS in mice diets promote reduction in body weight and altered food intake behavior in both obese and lean mice models. Results from Chapter II of this dissertation showed for the first time a prominent role of MOS in stimulating L-cell secretion of gut hormones, that was superior to glucose stimulation of these cells. In our laboratory group, Hasek *et al*., 2018 showed that carbohydrate-based foods with slow digestion rate and to the ileum had the beneficial effect of reducing food intake that was associated with stimulation of the gut-brain axis [11]. Here we tested whether activation of the gut-brain axis using the same fabricated SDS microspheres would either increase weight loss of DIO mice transferred from high-fat diet to a low-fat diet or would reduce weight gain of lean mice placed on a high-fat diet. It was further hypothesized that the distal release of MOS by the digestion of SDS along the course of the small intestine contributes to stimulation of the gut-brain axis and its downstream effects including food intake and weight management.

5.5.1 Intervention Study

The Intervention Study used diet-induced obese (DIO) male mice with prediabetic markers. Male C57BL/6J DIO mice at Jackson Laboratories were fed on D12492 60 kcal% fat diet between the ages of 6 and 30 weeks. It was shown that body weight of DIO mice growing at Jackson Laboratories starts to significantly deviate from that of the control lean group by week 17-19 [41]. By this time, DIO mice exhibited mild hyperglycemia, dyslipidemia, impaired glucose tolerance, and mildly elevated blood glucose levels [41]. Therefore, mice were obtained at week 14 of age and kept on the same high 60% high-fat diet for 5 weeks before the intervention of the diet (starting time of the study). One week after dietary intervention from the 60% high-fat diet to 10% low-fat diet with or without starch ingredients, mice in all low-fat groups lost between 19-20% of their body weight.

For the next three weeks, body weight showed a gradual reduction until week 5 where all experimental groups showed their lowest average body weight. Notably, mice fed on the 20% SDS diet showed significant reduction in body weight by the end of the study when compared to the low-fat control group at $P = 0.0031$, 40% raw corn starch group at $P = < 0.0001$, and the 60% high-fat control group at $P = < 0.0001$. Mice fed on the higher percentage of the SDS microspheres (40%), showed a significantly lower body weight only when compared to the 60 % high-fat control $P = < 0.0001$ and 40% RCS group at $P = 0.0040$.

The stronger effect was observed for daily food intake with the lower 20% SDS microsphere level compared the 40%. However, the average daily caloric intake was similar for the two groups, indicating that the slightly higher body weight in the 40% SDS group was not due to metabolic adaptation to caloric restriction [42]. Also, body weight and food intake of mice fed on the 40% PGS diet was reduced significantly compared to that of mice fed on 10 % low-fat control and mice fed on 40 % RCS and was similar to the SDS diets. As the PGS diet was included to represent a rapidly digestible starch, it is not clear why this diet was associated with a reduction in body weight similar to the 20% SDS microsphere diet.

Of interest, mice fed on 40% RCS had significantly higher body weight compared to mice in groups fed on 20% ($P = < 0.0001$) or 40% SDS ($P = 0.0041$) microsphere diets. These data are consistent with an increase of average daily intake (significant compared to 20% SDS diet and insignificant compared to 40% SDS diet) and caloric intake (significant compared to both 20% and 40% SDS diets) in this group. Perhaps this is related to the ability of mice to efficiently digest raw corn starch for energy production, as described previously in mice [43] and rats [44].

The conversion of diets in the five low-fat experimental groups from high-fat diet to low-fat diet significantly enhanced the bone metabolism in these groups as represented by the increase

of BMD and BMC. At the first time-point of DEXA analysis (at week 2), all groups showed higher BMD and BMC that become statistically significant by the end of the study (week 13). High-fat diets have been shown to reduce bone mineral density in rats [45]. In addition, a recent article from Devlin *et al*., 2018 showed metabolic dysfunction and bone loss in DIO C57BL/6J (B6) female mice indicating a reduction in skeletal acquisition in DIO mice [46]. Moreover, male TALLYHO/JngJ mice which developed early-onset of type II diabetes showed impaired skeletal acquisition and lower BMD that was correlated with increased leptin levels [47]. Leptin was previously shown to be inversely associated with BMD in lean and obese Danish males [48]. We expect that a reduction in circulating leptin levels due to the loss of body fat percent in these five low-fat groups is the main factor affecting the improvement in parameters of bone metabolism. Although not statistically significant, mice fed on 40% SDS diet had the highest BMD and BMC values starting from week 6 of feeding. While a few studies have shown a role of soluble non-digestible carbohydrates and resistant starch fermentation products in improving mineral absorption and bone mineral density [49], [50], no available information correlates digestible starches (rapid or slow) with increased mineral absorption and bone acquisition. We expect that the noted observations could be due to altered metabolic processes in response to the slow glucose release in this group or due to fermentation processes on starch arrived into the colon.

Xie *et al*., 2017 indicated that diets with higher amylose content cause gluconeogenesis downregulation, as well as less fat deposition in finishing pigs through stimulation of the insulin/PI3K/protein kinase B signaling pathway [51]. Here we observed reduction in average liver weight in mice fed on all of the 10% low-fat diet compared to the 60% high-fat diet, though the greatest reduction was in the lowest weight treatment groups (20 and 40% SDS microspheres diets, and 40% PGS diet). There was a correlative association between body weight reduction, and body

fat content and liver weight. The role of high dietary sucrose levels in the induction of *de novo* lipogenesis is well documented [52] and its potential to induce hepatic steatosis was reported [53]. Here, we hypothesize that the variations in liver weight between the low-fat groups are explained by the differences in RCS, PGS, and SDS microspheres in these diets, but due to the substitution of slowly digestible sources of starch that provide low glycemic response and sustainable glucose release. This is seen in comparison of liver weight of the 40% RCS with that of mice fed on more slowly digestible starches.

5.5.2 Prevention Study

In the Prevention Study, the ability of SDS materials to reduce food consumption and rate of weight gain was tested in young lean animals fed on a 45% high-fat-base diet for 12 weeks. The high fat content in the diet limited the ability of substituting more that 30% of dietary carbohydrates and slightly lower levels of SDS microspheres were incorporated at 15 and 30%, compared to the Intervention Study. Here, there was a clear trend of lower rate of weight gain in the 15% SDS microsphere group that ended up similar to the 10% low-fat control. Unlike the Intervention Study, mice fed on diet containing 15% PGS starch showed average body weight that was higher than that of mice 15% SDS microsphere diet ($P = 0.0512$). Consistent with the intervention study, the lower level (15%) of SDS microspheres had the higher effect of reducing body weight ($P = 0.0019$). In the Prevention Study, the 30% SDS microsphere diet showed higher/comparable average body weight in the first 9 weeks of the study to the 45% high-fat control, though then decreased to the final 12-week endpoint of the study. One of the major differences between the 30% SDS microsphere diet and all other diets in this study is the complete absence of sucrose in this diet. It could be possible that the absence of fast energy source and the relatively lower caloric intake (4.4 kcal/g) induced mice in this group to overeat in the first 7 weeks of the study. For the

last three weeks of the prevention study, body weight of the 30% SDS microsphere group started to reduce compared to the 45% high-fat control and the 15% PGS groups. Statistical analysis did not reveal significant differences in average liver weight between experimental groups, including the 10% low-fat control.

Immunohistochemistry of sections from different locations of the small intestine were performed using a specific GLP-1 antibody to examine the distribution of L-cells and any possible alteration in its distribution due to treatments. Interestingly, we observed an even and high distribution of L-cells throughout the small intestine starting from the proximal duodenum. This uniform and high distribution of L-cells throughout the small intestine suggest the importance of long locational-digesting carbohydrates in activating the gut-brain axis and ileal brake mechanism. The longer time required for the digestion of slowly digestible carbohydrates would allow for larger surface contact between starch digestion products and L-cells. No differences were observed in histological sections due to treatment but taken together with RNA sequencing data from Chapter III it may be reasonable to conclude that α-amylase degradation products (MOS) of starch in the small intestine interact with enteroendocrine L-cells to stimulate secretion of already existing cellular GLP-1 and OXM.

In regard to a food formulation strategy to design carbohydrate-based foods that activate the gut-brain axis to control appetite and manage weight, it may be that slowly digestible carbohydrates need only to digest as far distally as possible in the small intestine to activate enteroendocrine L-cells that line the intestine.

5.6 References

[1] T. Kelly, W. Yang, C. S. Chen, K. Reynolds, and J. He, “Global burden of obesity in 2005 and projections to 2030,” *Int. J. Obes.*, 2008.

[2] A. Must, J. Spadano, E. H. Coakley, A. E. Field, G. Colditz, and W. H. Dietz, “The Disease Burden Associated With Overweight and Obesity,” *JAMA*, vol. 282, no. 16, p. 1523, Oct. 1999.

[3] E. C. Mun, G. L. Blackburn, and J. B. Matthews, “Current status of medical and surgical therapy for obesity,” *Gastroenterology*, vol. 120, no. 3, pp. 669–681, Feb. 2001.

[4] Office of Disease Prevention and Health Promotion, “2015-2020 Dietary Guidelines for Americans,” 2015.

[5] D. J. Jenkins *et al.*, “Glycemic index of foods: a physiological basis for carbohydrate exchange,” *Am. J. Clin. Nutr.*, vol. 34, no. 3, pp. 362–366, Mar. 1981.

[6] K. N. Englyst, S. Vinoy, H. N. Englyst, and V. Lang, “Glycaemic index of cereal products explained by their content of rapidly and slowly available glucose,” *Br. J. Nutr.*, vol. 89, no. 03, p. 329, Mar. 2003.

[7] D. S. Ludwig, “The glycemic index: physiological mechanisms relating to obesity, diabetes, and cardiovascular disease.,” *JAMA*, vol. 287, no. 18, pp. 2414–23, May 2002.

[8] M. Brownlee, “Biochemistry and molecular cell biology of diabetic complications,” *Nature*, vol. 414, no. 6865, pp. 813–820, Dec. 2001.

[9] D. J. A. Jenkins *et al.*, “Glycemic index: overview of implications in health and disease.,” *Am. J. Clin. Nutr.*, vol. 76, no. 1, p. 266S–73S, Jul. 2002.

[10] H. N. Englyst, S. M. Kingman, and J. H. Cummings, “Classification and measurement of nutritionally important starch fractions.,” *Eur. J. Clin. Nutr.*, vol. 46 Suppl 2, pp. S33-50, Oct. 1992.

[11] L. Y. Hasek *et al.*, “Dietary Slowly Digestible Starch Triggers the Gut-Brain Axis in Obese Rats with Accompanied Reduced Food Intake,” *Mol. Nutr. Food Res.*, vol. 62, no. 5, p. 1700117, Mar. 2018.

[12] C. J. Seal *et al.*, “Postprandial carbohydrate metabolism in healthy subjects and those with type 2 diabetes fed starches with slow and rapid hydrolysis rates determined in vitro,” *Br. J. Nutr.*, vol. 90, no. 05, p. 853, Nov. 2003.

[13] F. Cisse, D. P. Erickson, A. M. R. Hayes, A. R. Opekun, B. L. Nichols, and B. R. Hamaker, “Traditional Malian Solid Foods Made from Sorghum and Millet Have Markedly Slower Gastric Emptying than Rice, Potato, or Pasta.,” *Nutrients*, vol. 10, no. 2, Jan. 2018.

[14] G. J. Schwartz, “The role of gastrointestinal vagal afferents in the control of food intake: current prospects,” *Nutrition*, vol. 16, no. 10, pp. 866–873, Oct. 2000.

[15] D. E. Cummings and J. Overduin, “Gastrointestinal regulation of food intake,” *J. Clin. Invest.*, vol. 117, 2007.

[16] S. S. Hussain and S. R. Bloom, “The regulation of food intake by the gut-brain axis: implications for obesity,” *Int. J. Obes.*, vol. 37, pp. 625–633, 2013.

[17] K. G. Murphy, W. S. Dhillo, and S. R. Bloom, “Gut Peptides in the Regulation of Food Intake and Energy Homeostasis,” 2006.

[18] A. P. Coll, I. S. Farooqi, and S. O’Rahilly, “The hormonal control of food intake.,” *Cell*, vol. 129, no. 2, pp. 251–62, Apr. 2007.

[19] M. W. Schwartz, “Central Nervous System Regulation of Food Intake,” *Obesity*, vol. 14, no. 2S, p. 1S–8S, Feb. 2006.

[20] A. C. Könner, T. Klöckener, and J. C. Brüning, “Control of energy homeostasis by insulin and leptin: Targeting the arcuate nucleus and beyond,” *Physiol. Behav.*, vol. 97, no. 5, pp. 632–638, Jul. 2009.

[21] R. Cone, M. Cowley, A. Butler, W. Fan, D. Marks, and M. Low, “The arcuate nucleus as a conduit for diverse signals relevant to energy homeostasis,” *Int. J. Obes.*, vol. 25, no. S5, pp. S63–S67, Dec. 2001.

[22] M. M. Hagan *et al.*, “Long-term orexigenic effects of AgRP-(83O132) involve mechanisms other than melanocortin receptor blockade,” 2000.

[23] L. Yang *et al.*, “Role of dorsomedial hypothalamic NPY in modulating food intake and energy balance.”

[24] H. Nakabayashi, M. Nishizawa, A. Nakagawa, R. Takeda, and A. Niijima, “Vagal hepatopancreatic reflex effect evoked by intraportal appearance of tGLP-1,” *Am. J. Physiol. Metab.*, vol. 271, no. 5, pp. E808–E813, Nov. 1996.

[25] K. N. Englyst, H. N. Englyst, G. J. Hudson, T. J. Cole, and J. H. Cummings, “Rapidly available glucose in foods: an in vitro measurement that reflects the glycemic response,” *Am. J. Clin. Nutr.*, vol. 69, no. 3, pp. 448–454, Mar. 1999.

[26] T. M. Wolever and C. Mehling, “Long-term effect of varying the source or amount of dietary carbohydrate on postprandial plasma glucose, insulin, triacylglycerol, and free fatty acid concentrations in subjects with impaired glucose tolerance,” *Am. J. Clin. Nutr.*, vol. 77, no. 3, pp. 612–621, Mar. 2003.

[27] J. McMillan-Price *et al.*, “Comparison of 4 Diets of Varying Glycemic Load on Weight Loss and Cardiovascular Risk Reduction in Overweight and Obese Young Adults,” *Arch. Intern. Med.*, vol. 166, no. 14, p. 1466, Jul. 2006.

[28] V. Ranawana and C. J. K. Henry, “Liquid and solid carbohydrate foods: comparative effects on glycemic and insulin responses, and satiety,” *Int. J. Food Sci. Nutr.*, vol. 62, no. 1, pp. 71–81, Feb. 2011.

[29] S. H. Holt and J. B. Miller, “Particle size, satiety and the glycaemic response.,” *Eur. J. Clin. Nutr.*, vol. 48, no. 7, pp. 496–502, Jul. 1994.

[30] B. Sloth *et al.*, “No difference in body weight decrease between a low-glycemic-index and a high-glycemic-index diet but reduced LDL cholesterol after 10-wk ad libitum intake of the low-glycemic-index diet,” *Am. J. Clin. Nutr.*, vol. 80, no. 2, pp. 337–347, Aug. 2004.

[31] M. Venkatachalam, M. R. Kushnick, G. Zhang, and B. R. Hamaker, “Starch-entrapped biopolymer microspheres as a novel approach to vary blood glucose profiles.,” *J. Am. Coll. Nutr.*, vol. 28, no. 5, pp. 583–90, Oct. 2009.

[32] A. B. Bialkowska, A. M. Ghaleb, M. O. Nandan, and V. W. Yang, “Improved Swiss-rolling Technique for Intestinal Tissue Preparation for Immunohistochemical and Immunofluorescent Analyses,” *J. Vis. Exp.*, no. 113, pp. e54161–e54161, Jul. 2016.

[33] WHO, “WHO | WHO calls on countries to reduce sugars intake among adults and children,” *WHO*, 2016.

[34] Food and Agriculture Organization of the United Nations. and I. Joint FAO/WHO Expert Consultation on Carbohydrates in Human Nutrition (1997 : Rome, *Carbohydrates in human nutrition : report of a joint FAO/WHO expert consultation, Rome, 14-18 April 1997.* World Health Organization, 1998.

[35] Ł. Czyżewska-Majchrzak, T. Grzelak, M. Kramkowska, K. Czyżewska, and H. Witmanowski, “The use of low-carbohydrate diet in type 2 diabetes-benefits and risks,” *Ann. Agric. Environ. Med.*, vol. 21, no. 2, pp. 320–326, 2014.

[36] S. T. Reddy, C.-Y. Wang, K. Sakhaee, L. Brinkley, and C. Y. C. Pak, “Effect of low-carbohydrate high-protein diets on acid-base balance, stone-forming propensity, and calcium metabolism,” *Am. J. Kidney Dis.*, vol. 40, no. 2, pp. 265–274, Aug. 2002.

[37] J. D. Carter, F. B. Vasey, and J. Valeriano, “The effect of a low-carbohydrate diet on bone turnover,” *Osteoporos. Int.*, vol. 17, no. 9, pp. 1398–1403, Sep. 2006.

[38] W. S. Yancy, M. K. Olsen, J. R. Guyton, R. P. Bakst, and E. C. Westman, “A low-carbohydrate, ketogenic diet versus a low-fat diet to treat obesity and hyperlipidemia: a randomized, controlled trial.,” *Ann. Intern. Med.*, vol. 140, no. 10, pp. 769–77, May 2004.

[39] S. A. Bilsborough and T. C. Crowe, “Low-carbohydrate diets: what are the potential short- and long-term health implications?,” *Asia Pac. J. Clin. Nutr.*, vol. 12, no. 4, pp. 396–404, 2003.

[40] S. Vinoy, M. Laville, and E. J. M. Feskens, “Slow-release carbohydrates: growing evidence on metabolic responses and public health interest. Summary of the symposium held at the 12th European Nutrition Conference (FENS 2015).,” *Food Nutr. Res.*, vol. 60, p. 31662, 2016.

[41] T. J. Laboratory, “Physiological Data Summary – Diet-Induced Obese (DIO) C57BL/6J (380050),” 2018. [Online]. Available: https://www.jax.org/jax-mice-and-services/strain-data-sheet-pages/phenotype-information-380050.

[42] L. M. Redman *et al.*, “Metabolic and Behavioral Compensations in Response to Caloric Restriction: Implications for the Maintenance of Weight Loss,” *PLoS One*, vol. 4, no. 2, p. e4377, Feb. 2009.

[43] K. Yamaki, T. Ide, Y. Takano-Ishikawa, and K. Shinohara, “Bioscience, Biotechnology, and Biochemistry Comparative Effects of Non-Gelatinized Corn and Rice Starches on the Life-Span of ICR Mice,” *Biosci. Biotechnol. Biochem.*, vol. 69, no. 1, pp. 13–18, 2014.

[44] L. A. Hildebrandt and J. A. Marlett, “Starch Bioavailability in the Upper Gastrointestinal Tract of Colectomized Rats,” *J. Nutr.*, vol. 121, no. 5, pp. 679–686, May 1991.

[45] M. Bielohuby *et al.*, “Short-term exposure to low-carbohydrate, high-fat diets induces low bone mineral density and reduces bone formation in rats,” *J. Bone Miner. Res.*, vol. 25, no. 2, pp. 275–284, Feb. 2010.

[46] M. J. Devlin *et al.*, “Differential effects of high fat diet and diet-induced obesity on skeletal acquisition in female C57BL/6J vs. FVB/NJ Mice,” *Bone Reports*, vol. 8, pp. 204–214, Jun. 2018.

[47] M. J. Devlin *et al.*, “Early-Onset Type 2 Diabetes Impairs Skeletal Acquisition in the Male TALLYHO/JngJ Mouse,” *Endocrinology*, vol. 155, no. 10, pp. 3806–3816, Oct. 2014.

[48] C. M. Morberg *et al.*, “Leptin and Bone Mineral Density: A Cross-Sectional Study in Obese and Nonobese Men,” *J. Clin. Endocrinol. Metab.*, vol. 88, no. 12, pp. 5795–5800, Dec. 2003.

[49] J. L. Greger, “Nondigestible Carbohydrates and Mineral Bioavailability,” *J. Nutr.*, vol. 129, no. 7, p. 1434S–1435S, Jul. 1999.

[50] K. E. Scholz-Ahrens and J. Schrezenmeir, “Inulin and Oligofructose and Mineral Metabolism: The Evidence from Animal Trials,” *J. Nutr.*, vol. 137, no. 11, p. 2513S–2523S, Nov. 2007.

[51] C. Xie, Y. Li, J. Li, L. Zhang, G. Zhou, and F. Gao, “Dietary starch types affect liver nutrient metabolism of finishing pigs,” *Br. J. Nutr.*, vol. 118, no. 05, pp. 353–359, Sep. 2017.

[52] H. Yamashita *et al.*, “A glucose-responsive transcription factor that regulates carbohydrate metabolism in the liver.,” *Proc. Natl. Acad. Sci. U. S. A.*, vol. 98, no. 16, pp. 9116–21, Jul. 2001.

[53] M. K. Pickens *et al.*, “Dietary sucrose is essential to the development of liver injury in the methionine-choline-deficient model of steatohepatitis.,” *J. Lipid Res.*, vol. 50, no. 10, pp. 2072–82, Oct. 2009.

Table 5.1 Composition of the experimental diets in g/kg.

	[1]HF	[2]LF	LF [3]RCS	LF [4]PGS	LF 20% [5]SDS	LF 40% SDS
g/kg						
Casein	265.0	210.0	210.0	210.0	210.0	210.0
L-Cystine	4.0	3.0	3.0	3.0	3.0	3.0
Corn Starch		280.0	400.0			
Pregelatinized starch				400.0	200.0	
Starch/Alginate microspheres (0.75%)					200.0	400.0
Maltodextrin	160.0	50.0	100.0	100.0	100.0	100.0
Sucrose	90.0	325.0	155.0	155.0	155.0	155.0
Lard	310.0	20.0	20.0	20.0	20.0	20.0
Soybean Oil	30.0	20.0	20.0	20.0	20.0	20.0
Cellulose	65.5	37.15	37.15	37.15	37.15	37.15
Mineral Mix, AIN-93G-MX (94046)	48.0	35.0	35.0	35.0	35.0	35.0
Calcium Phosphate, dibasic	3.4	2.0	2.0	2.0	2.0	2.0
Vitamin Mix, AIN-93-VX (94047)	21.0	15.0	15.0	15.0	15.0	15.0
Choline Bitartrate	3.0	2.75	2.75	2.75	2.75	2.75

*[1]LF: low-fat; [2]HF: high-fat; [3] RCS: raw waxy cornstarch, [4]PGS: pregelatinized waxy cornstarch; [5] SDS: slowly digestible starch [starch/Alginate microspheres (0.75%)].

Table 5.2 Macronutrient composition of the experimental diets in % by weight.

	[1]HF	[2]LF	LF [3]RCS	LF [4]PGS	LF 20% [5]SDS	LF 40% SDS
% by weight						
Protein	23.5	18.6	18.6	18.6	18.6	18.6
Carbohydrates	27.3	64.7	63.2	64.0	62.3	60.6
Fat	34.3	4.2	4.2	4.2	4.2	4.2

*[1] LF: low-fat; [2] HF: high-fat; [3] RCS: raw waxy cornstarch, [4] PGS: pregelatinized waxy cornstarch; [5] SDS: slowly digestible starch [starch/Alginate microspheres (0.75%)].

Table 5.3 Composition of the experimental diets in % kcal.

	[1]HF	[2]LF	LF [3]RCS	LF [4]PGS	LF 20% [5]SDS	LF 40% SDS
Kcal/g	5.1	3.7	3.7	3.7	3.6	3.5
% kcal						
Protein	18.3	20.0	20.3	20.2	20.6	21.0
Carbohydrates	21.4	69.8	69.3	69.5	69.0	68.3
Fat	60.3	10.2	10.4	10.3	10.5	10.7

*[1] LF: low-fat; [2] HF: high-fat; [3] RCS: raw waxy cornstarch, [4] PGS: pregelatinized waxy cornstarch; [5] SDS: slowly digestible starch [starch/Alginate microspheres (0.75%)].

Table 5.4 Composition of the experimental diets in g/kg.

	[1]LF	**[2]HF**	**HF [3]PGS**	**HF 15% [4]SDS**	**HF 30% SDS**
Casein	210.0	245.0	245.0	245.0	245.0
L-Cystine	3.0	3.5	3.5	3.5	3.5
Corn Starch	280.0	85.0			
Pregelatinized starch			150.0		
Starch/Alginate microspheres (0.75%)				150.0	300.0
Maltodextrin	50.0	115.0	100.0	100.0	100.0
Sucrose	325.0	200.0	150.0	150.0	
Lard	20.0	195.0	195.0	195.0	195.0
Soybean Oil	20.0	30.0	30.0	30.0	30.0
Cellulose	37.15	58.0	58.0	58.0	58.0
Mineral Mix, AIN-93G-MX (94046)	35.0	43.0	43.0	43.0	43.0
Calcium Phosphate, dibasic	2.0	3.4	3.4	3.4	3.4
Vitamin Mix, AIN-93-VX (94047)	15.0	19.0	19.0	19.0	19.0
Choline Bitartrate	2.75	3.0	3.0	3.0	3.0
Food Color	0.1	0.1	0.1	0.1	0.1

*[1] LF: low-fat (10% of calories from fat); [2] HF: high-fat (45% of calories from fat); [3] PGS: pregelatinized waxy cornstarch; [4] SDS: slowly digestible starch [starch/Alginate microspheres (0.75%)].

Table 5.5 Macronutrient composition of the experimental diets in % by weight.

	[1]LF	[2]HF	HF [3]PGS	HF 15% [4]SDS	HF 30% SDS
% by weight					
Protein	18.6	21.7	21.7	21.7	21.7
Carbohydrates	64.7	41.4	41.1	39.8	37.3
Fat	4.2	22.7	22.7	22.7	22.7

*[1] LF: low-fat (10% of calories from fat); [2] HF: high-fat (45% of calories from fat); [4] PGS: pregelatinized waxy cornstarch; [5] SDS: slowly digestible starch [starch/Alginate microspheres (0.75%)].

Table 5.6 Composition of the experimental diets in % kcal.

	[1]LF	[2]HF	HF [3]PGS	HF 15% [4]SDS	HF 30% SDS
Kcal/g	3.7	4.6	4.6	4.5	4.4
% kcal					
Protein	20.0	19.0	19.0	19.2	19.7
Carbohydrates	69.8	36.2	36.1	35.3	33.9
Fat	10.2	44.8	44.9	45.4	46.5

*[1] LF: low-fat (10% of calories from fat); [2] HF: high-fat (45% of calories from fat); [3] PGS: pregelatinized waxy cornstarch; [4] SDS: slowly digestible starch [starch/Alginate microspheres (0.75%)].

A

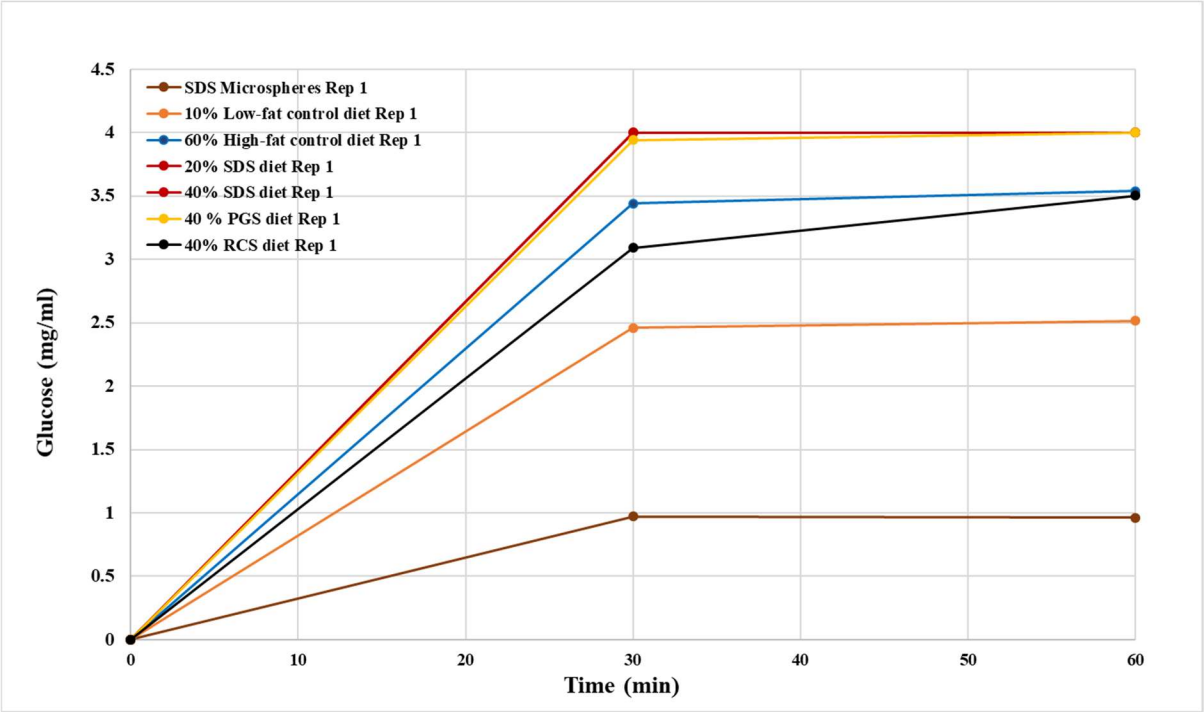

B

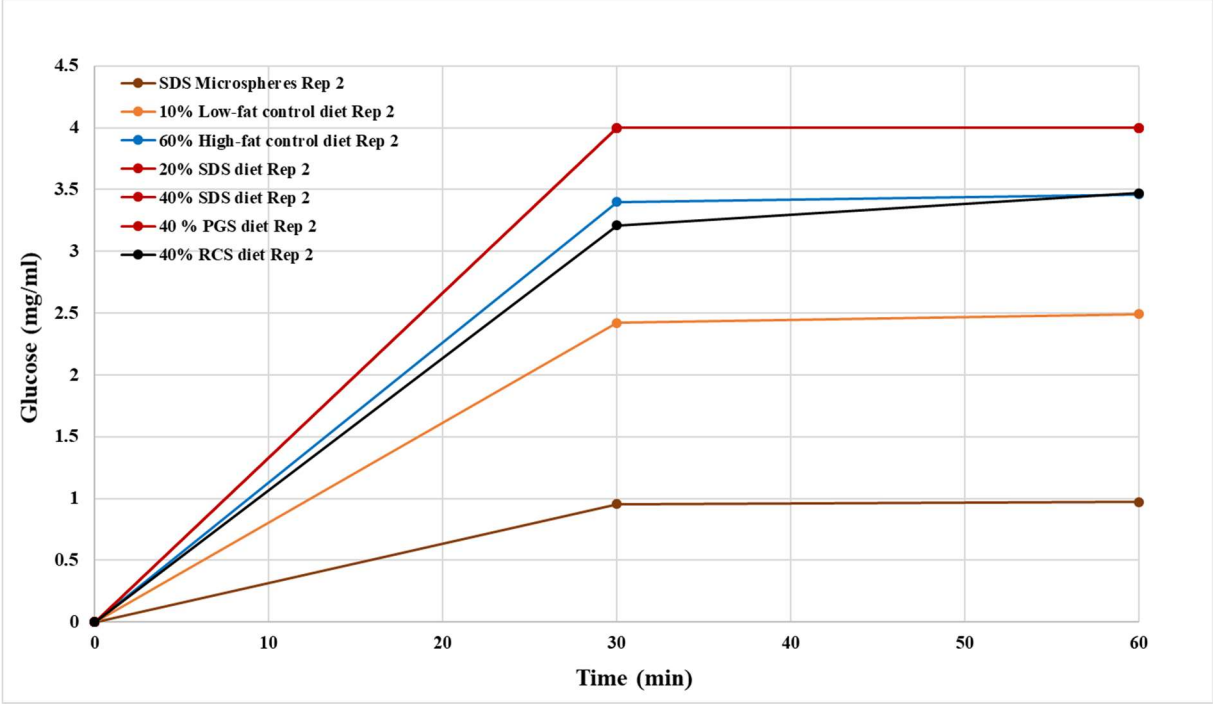

Figure 5.1 Release of reducing sugars from the slowly digestible starch-entrapped microspheres (SDS) and the six experimental diets used in the study **(Intervention Study)**. A and B are the result of digestion for 60 minutes for two independent replicates; A: replicate # 1, B: replicate #2. Diets that show the same values are grouped into one line with one color.

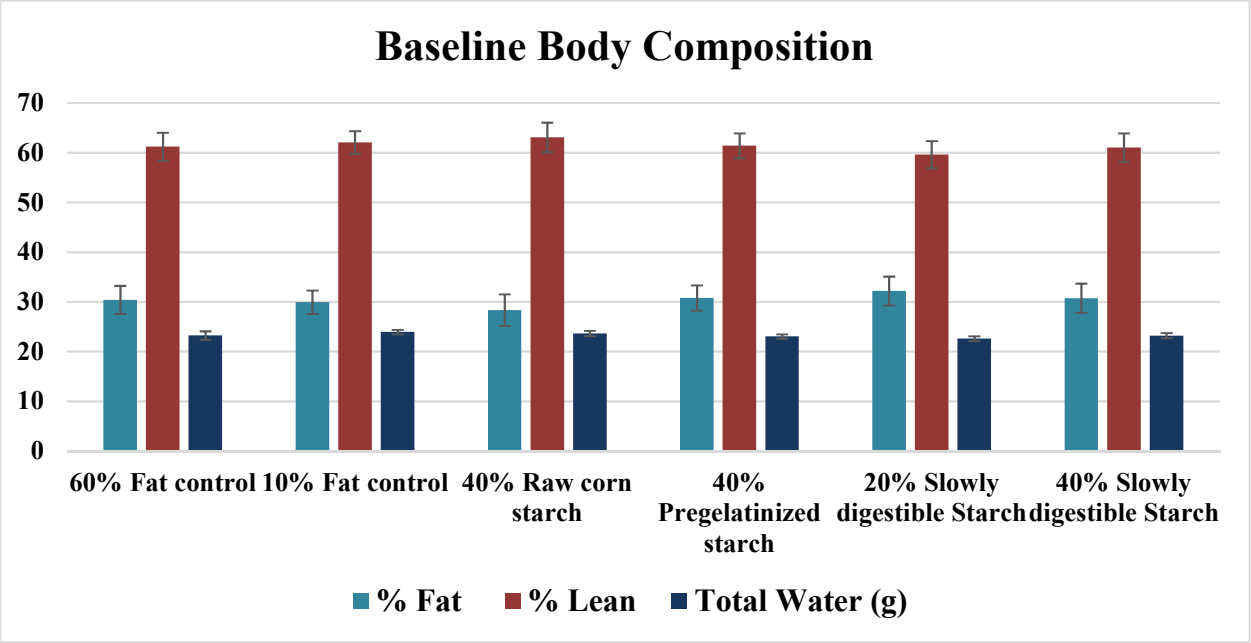

Figure 5.2 Average baseline body composition of mice in six experimental groups before treatment diet conversion **(Intervention Study)**. Body composition was evaluated using EchoMRI. Values denote group average (n=10) and bars represent standard error of the mean (Mean ± SEM). No statistical differences (at $\alpha = 0.05$) in body fat percent (% 30.4 ± 0.5), lean mass percent (% 61.4 ± 0.5) or total water (23.3 ± 0.2 g) were observed between mice at the beginning of the study (before treatment conversion).

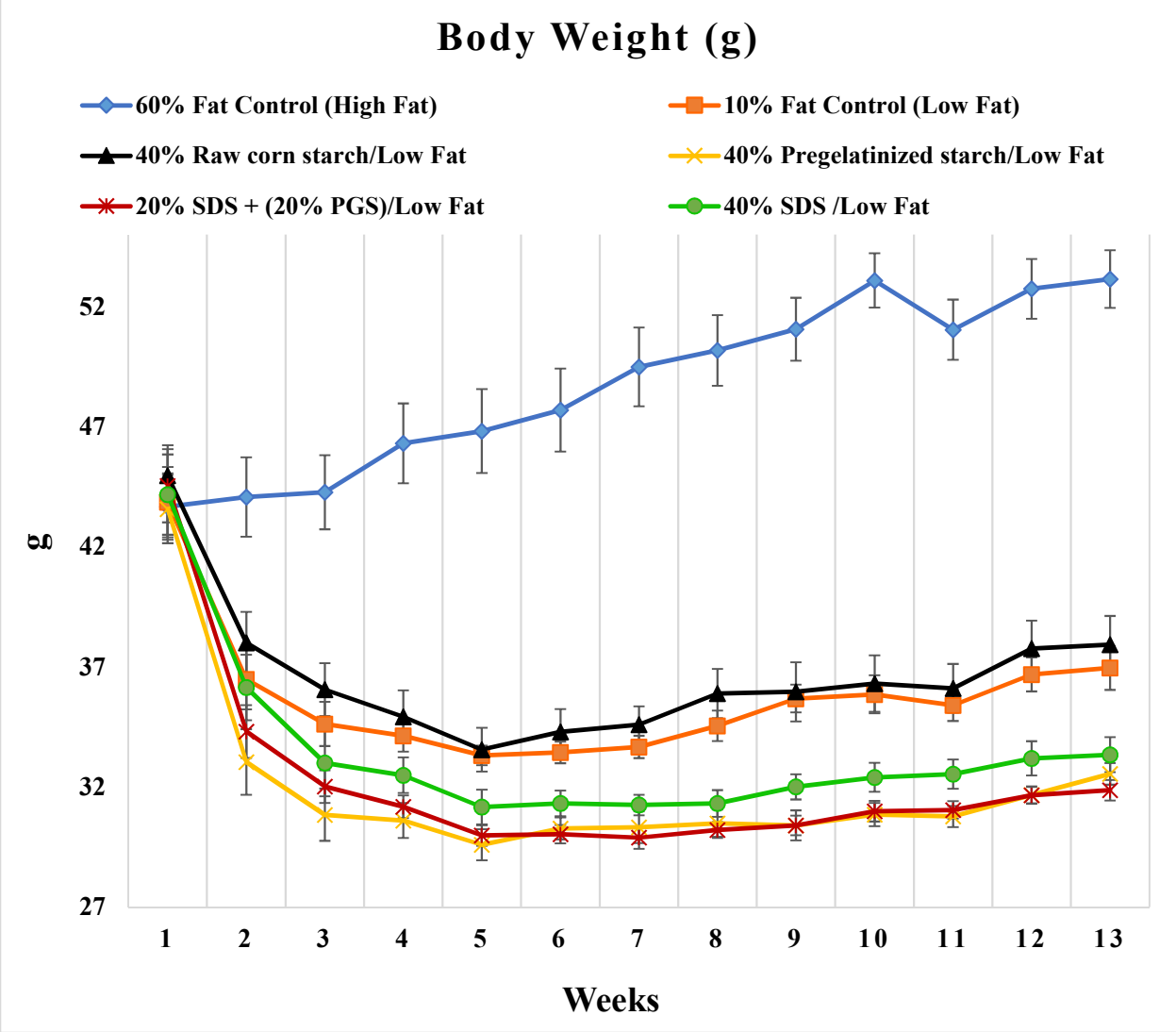

Figure 5.3: Average body weight (g) of mice in six experimental groups **(Intervention Study)** throughout the study from week 1 to week 13 (n=10). Values denote group average and bars represent standard error of the mean (Mean ± SEM). The increase in body weight of 60% high-fat control group was statistically significant (at α = 0.05) compared to all other groups at P = < 0.0001. The reduction in body weight of mice fed on 40 % PGS and 20 % SDS was statistically significant (at α = 0.05) compared to mice fed on the 10% low-fat control at P = 0.0013 and 0.0031, respectively. The reduction in body weight of mice fed on 40 % RCS and 40 % SDS was statistically insignificant (at α = 0.05) compared to mice fed on the 10% low-fat control at P = 0.9857 and 0.0921, respectively. Mice fed on 40 % RCS showed statistically significant (at α = 0.05) higher body weight compared to 40 % PGS, 20 % SDS and 40 % SDS at P= <0.0001, < 0.0001 and 0.0041, respectively. The reduction of body weight in 40 % PGS and 20 % SDS was statistically insignificant (at α = 0.05) compared to each other or compared to the 40 % SDS group.

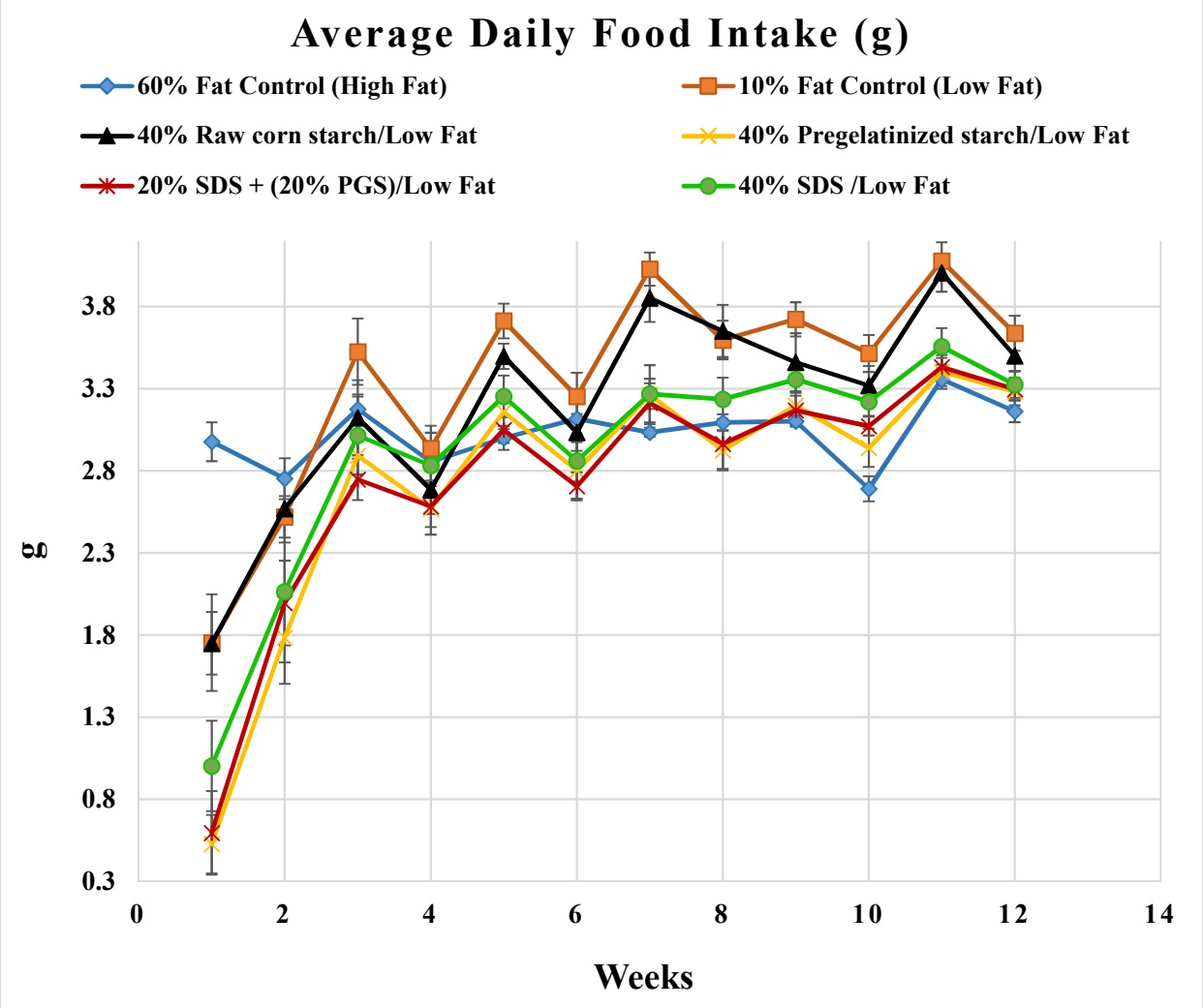

Figure 5.4 Average daily food intake (g) of mice in six experimental groups **(Intervention Study)** throughout the study from week 1 to week 12 (n=10). Values denote group average and bars represent standard error of the mean (Mean ± SEM). The increase in daily food intake of mice fed on 10 % low-fat control was statistically significant (at $\alpha = 0.05$) compared to that of mice fed on 40 % PGS, 20 % SDS and 40 % SDS at $P = 0.0005$, 0.0002 and 0.0106, respectively. The increase in daily food intake of mice fed on 10 % low-fat control was not statistically significant (at $\alpha = 0.05$) compared to that of mice fed on 40 % RCS or 60 % high-fat diet. Mice fed on 20 % SDS showed statistically significant (at $\alpha = 0.05$) reduction in daily food intake compared to mice fed on 40 % RCS at $P = 0.0044$. Mice fed on 40 % PGS showed statistically significant (at $\alpha = 0.05$) reduction in daily food intake compared to mice fed on 40 % RCS at $P = 0.0117$.

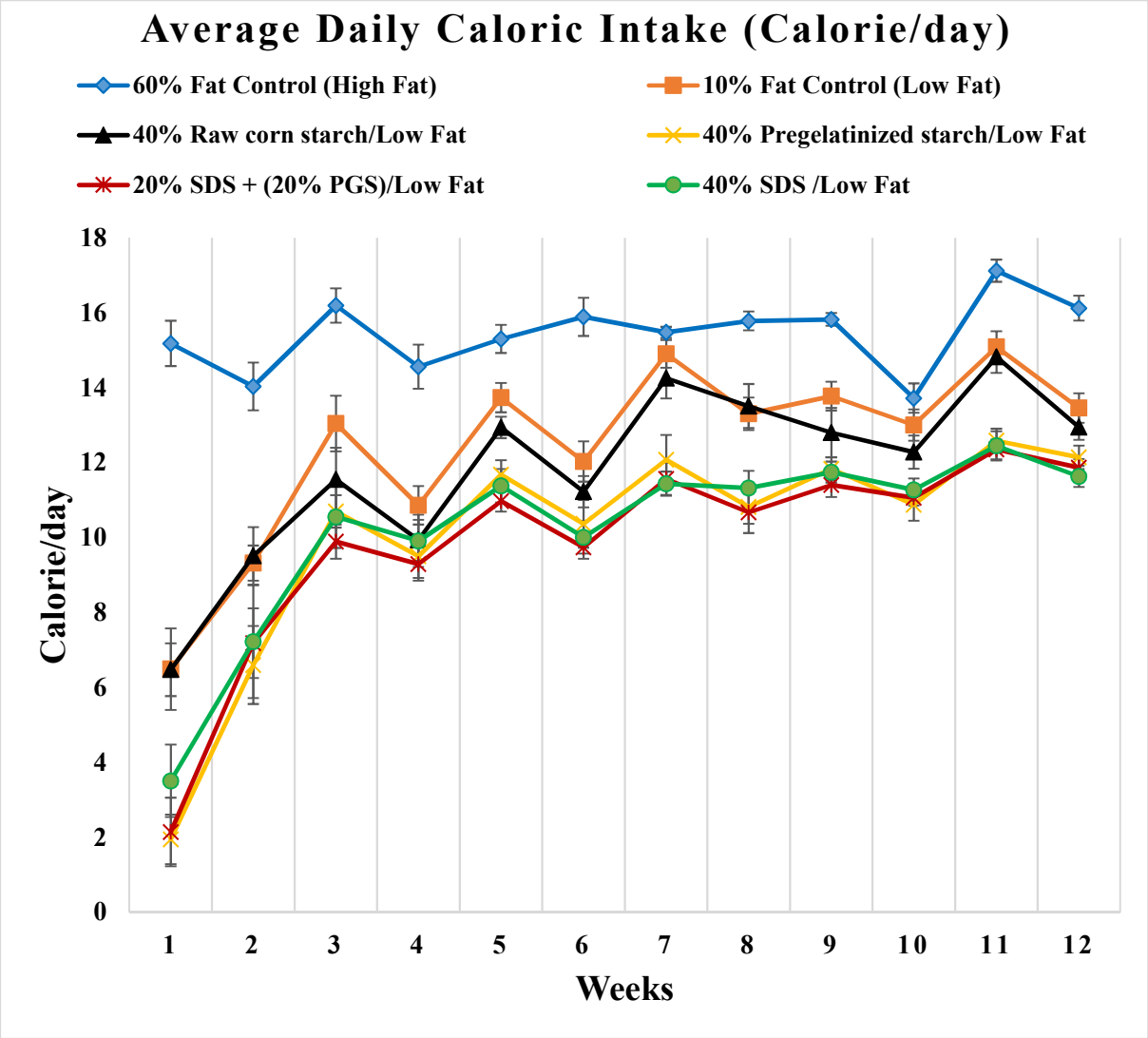

Figure 5.5 Average daily caloric intake (Calorie/day) of mice in six experimental groups **(Intervention Study)** from week 1 to week 12 throughout the study (n=10). Values denote group average and bars represent standard error of the mean (Mean ± SEM). The increase in daily caloric intake of mice fed on 60 % high-fat diet was statistically significant (at $\alpha = 0.05$) compared to that of mice fed on all other experimental groups at $P = < 0.0001$. Mice fed on 10 % low-fat control diet showed statistically significant (at $\alpha = 0.05$) higher daily caloric intake compared to mice fed on 40 % PGS, 20 % SDS or 40 % SDS diets at $P = 0.0003$, < 0.0001 and 0.0002, respectively but didn't show significant difference compared to mice fed on 40% RCS. Mice fed on 40 % RCS diet showed statistically significant (at $\alpha = 0.05$) higher daily caloric intake compared to mice fed on 40 % PGS, 20 % SDS and 40 % SDS diets at $P = 0.0097$, 0.0006 and 0.0051, respectively but didn't show significant difference compared to mice fed on 10 % low-fat control diet. There were no statistical significant differences (at $\alpha = 0.05$) in the daily caloric intake between mice fed on 40 % PGS, 20 % SDS and 40 % SDS diets.

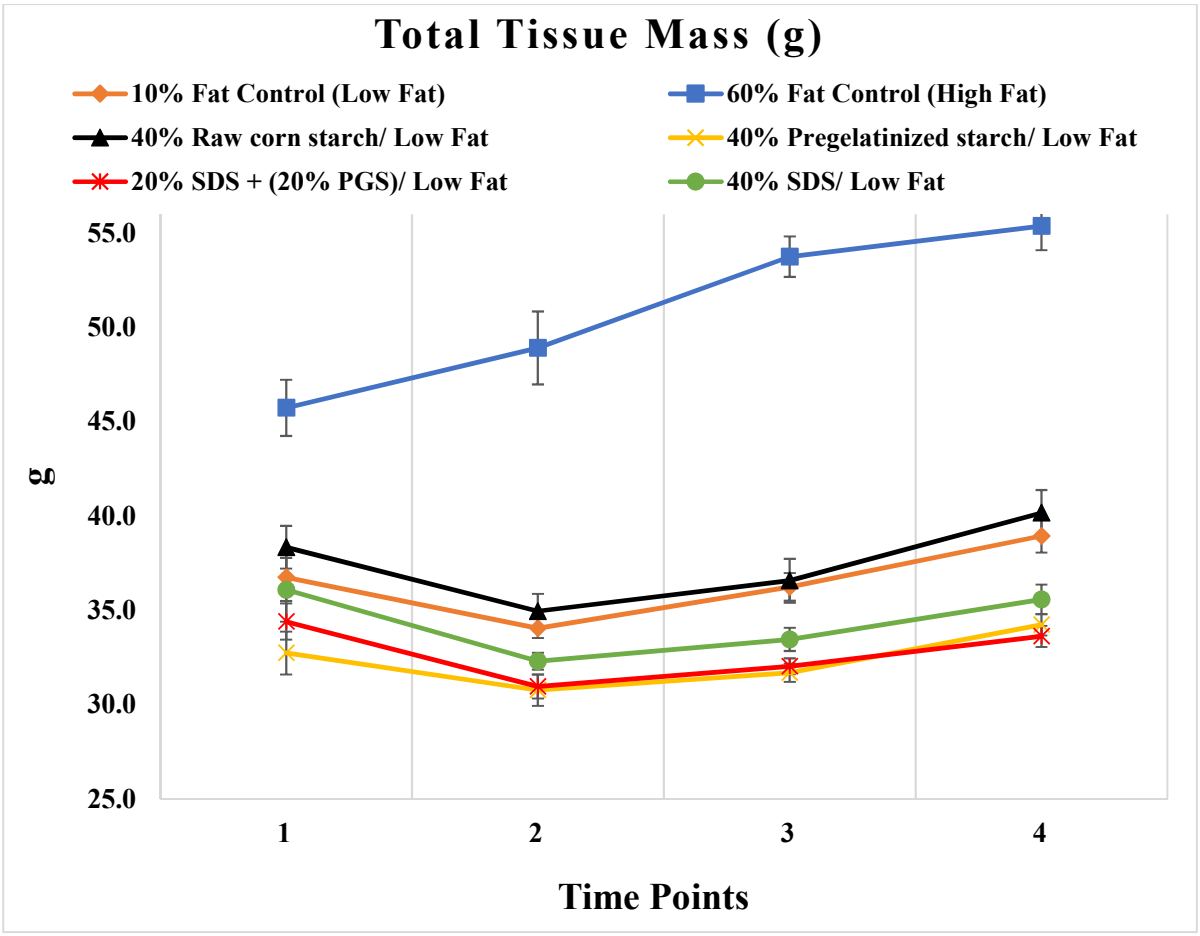

Figure 5.6 Total tissue mass (g) [DEXA] of mice in six experimental groups **(Intervention Study)** at four-time points throughout the study; 1: week 2, 2: week 6, 3: week 10 and 4: week 13. Values denote group average (n=10) and bars represent standard error of the mean (Mean ± SEM). The increase in total tissue mass of mice fed on 60 % high-fat diet was statistically significant (at α = 0.05) compared to that of mice fed on all other experimental groups at $P = < 0.0001$. The increase in total tissue mass of mice fed on 40 % RCS was statistically significant (at $\alpha = 0.05$) compared to mice fed on 40 % PGS, 20 % SDS and 40 % SDS diets at $P = < 0.0001$, 0.0002 and 0.0177, respectively but didn't show significant difference compared to mice fed on 10 % low-fat control diet. Mice fed on the 10% low-fat control diet showed statistically significant (at $\alpha = 0.05$) increase in total tissue mass compared to mice fed on 40 % PGS and 20 % SDS at $P = 0.001$ and 0.0047, respectively but didn't show statistical significant differences compared to mice fed on 40 % SDS. There were no statistical significant differences (at $\alpha = 0.05$) in total tissue mass between mice fed on 40 % PGS, 20 % SDS and 40 % SDS diets.

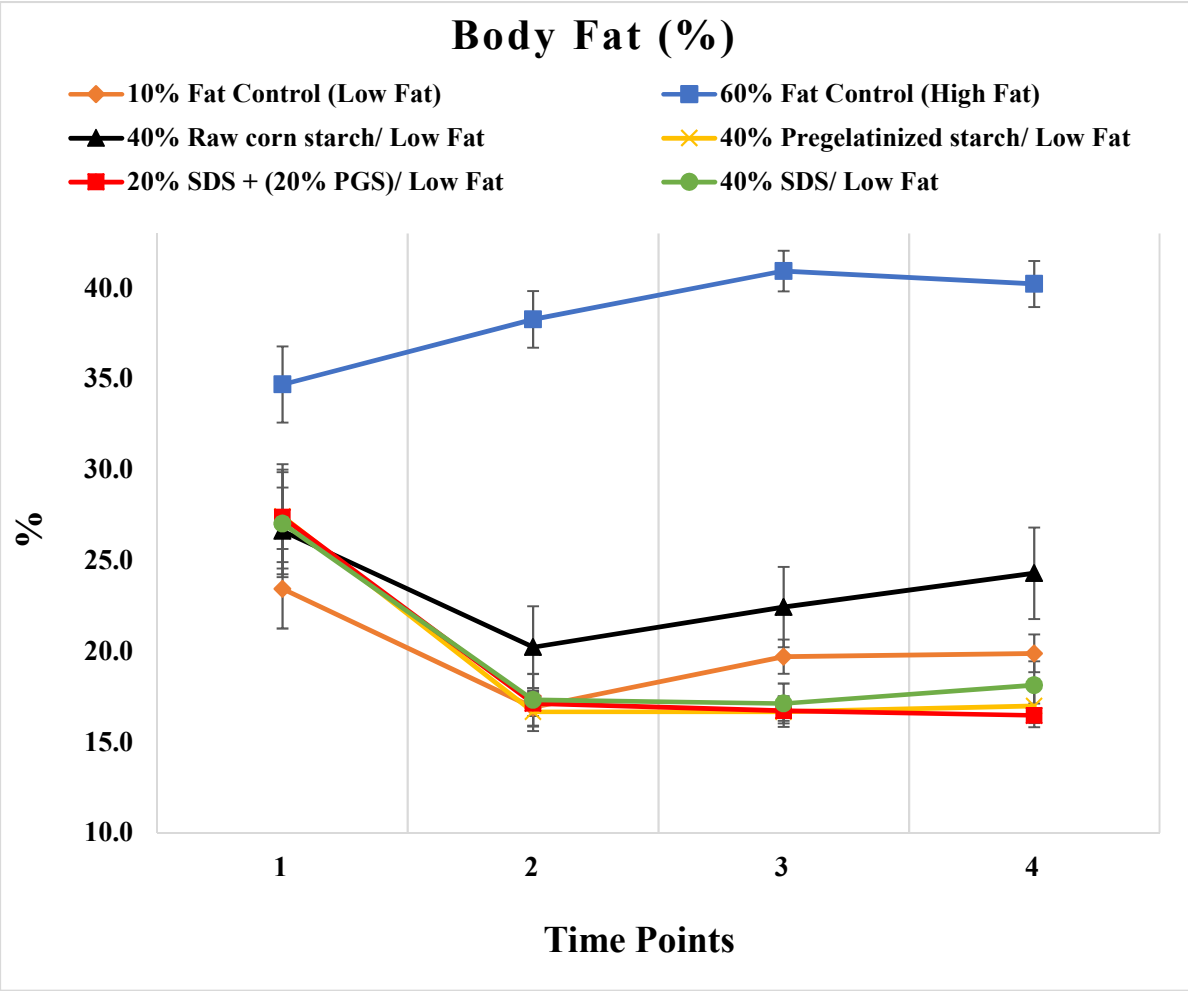

Figure 5.7 Average body fat percent (%) [DEXA] of mice in six experimental groups **(Intervention Study)** at four-time points throughout the study; 1: week 2, 2: week 6, 3: week 10 and 4: week 13. Values denote group average (n=10) and bars represent standard error of the mean (Mean ± SEM). The increase in body fat percent of mice fed on 60 % high-fat diet was statistically significant (at $\alpha = 0.05$) compared to that of mice fed on all other experimental groups at $P = < 0.0001$. No statistical differences in body fat percent (at $\alpha = 0.05$) were observed between mice fed on the five 10 % low-fat diets.

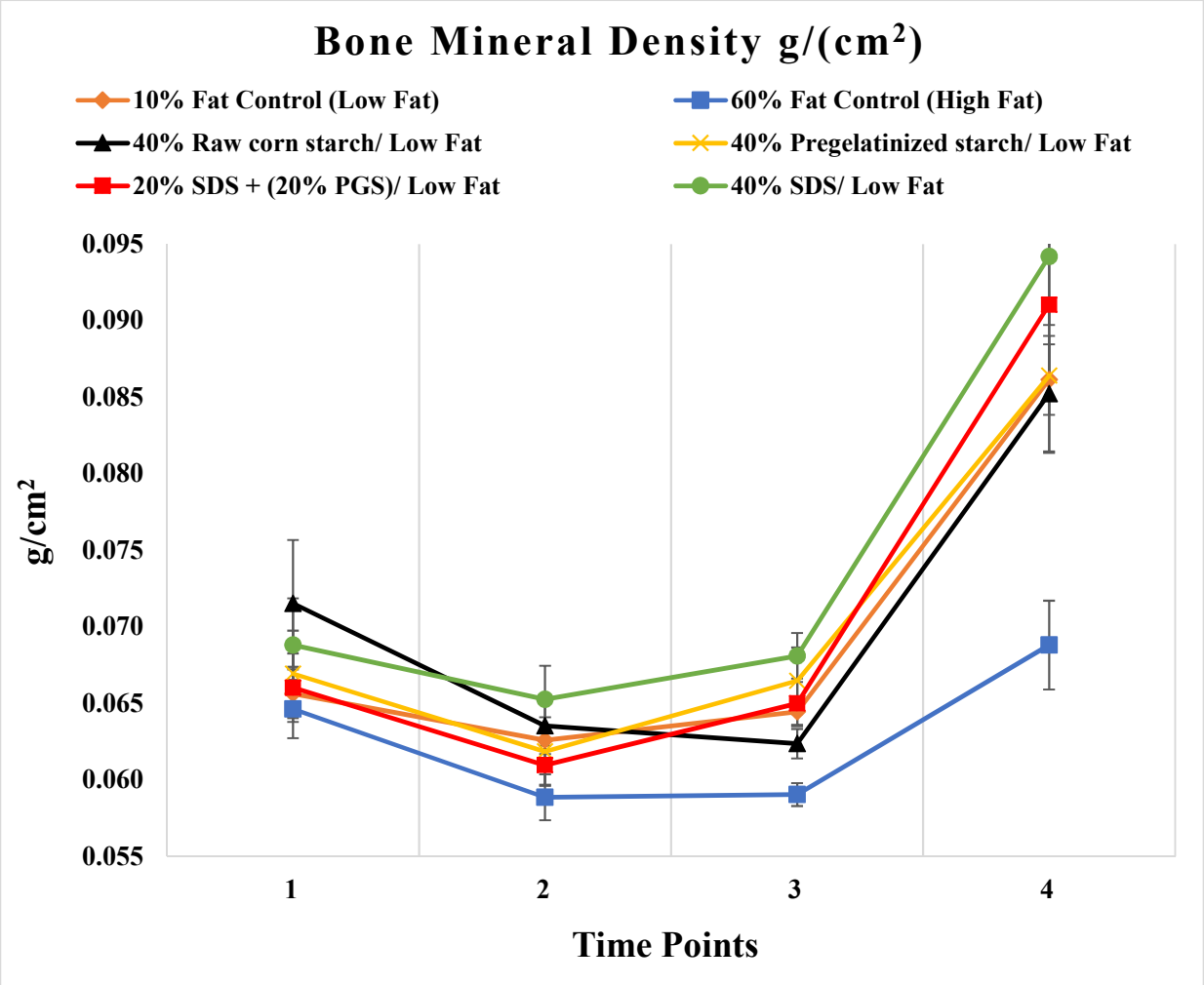

Figure 5.8 Bone mineral density (g/cm^2) [DEXA] of mice in six experimental groups **(Intervention Study)** at four-time points throughout the study; 1: week 2, 2: week 6, 3: week 10 and 4: week 13. Values denote group average (n=10) and bars represent standard error of the mean (Mean ± SEM). The decrease in bone mineral density of mice fed on 60 % high-fat diet was statistically significant (at $\alpha = 0.05$) compared to that of mice fed on 10 % low-fat control, 40 % RCS, 40 % PGS, 20 % SDS and 40 % SDS at $P = 0.0409$, 0.0132, 0.0337, 0.0164 and 0.0003, respectively. No statistical differences in bone mineral density (at $\alpha = 0.05$) were observed between mice fed on the five 10 % low-fat diets.

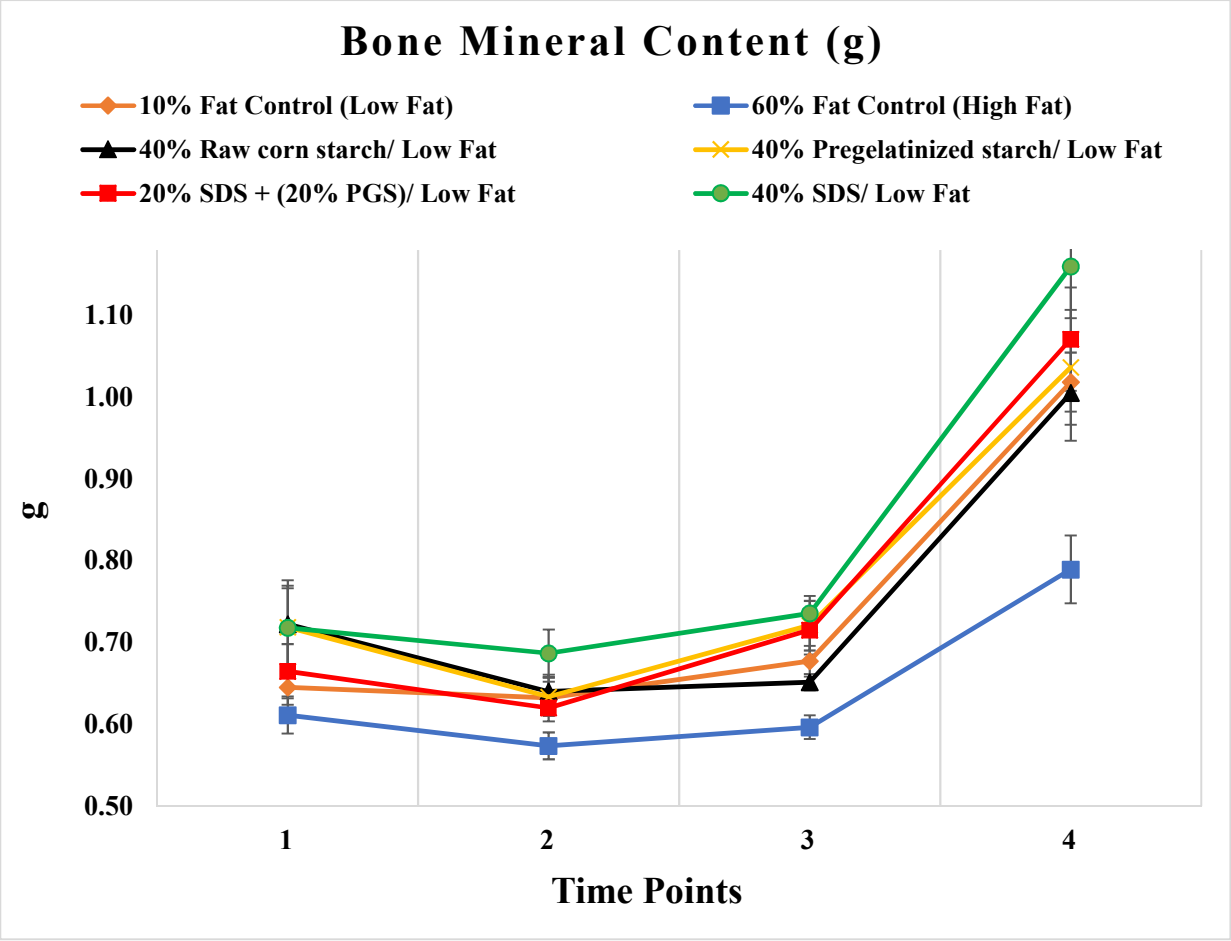

Figure 5.9 Bone mineral content (g) [DEXA] of mice in six experimental groups **(Intervention Study)** at four-time points throughout the study; 1: week 2, 2: week 6, 3: week 10 and 4: week 13. Values denote group average (n=10) and bars represent standard error of the mean (Mean ± SEM). The decrease in bone mineral content of mice fed on 60 % high-fat diet was statistically significant (at $\alpha = 0.05$) compared to that of mice fed on 10 % low-fat control, 40 % RCS, 40 % PGS, 20 % SDS and 40 % SDS at $P = 0.0492$, 0.0224, 0.0077, 0.0114 and <0.0001, respectively. No statistical differences in bone mineral content (at $\alpha = 0.05$) were observed between mice fed on the five 10 % low-fat diets.

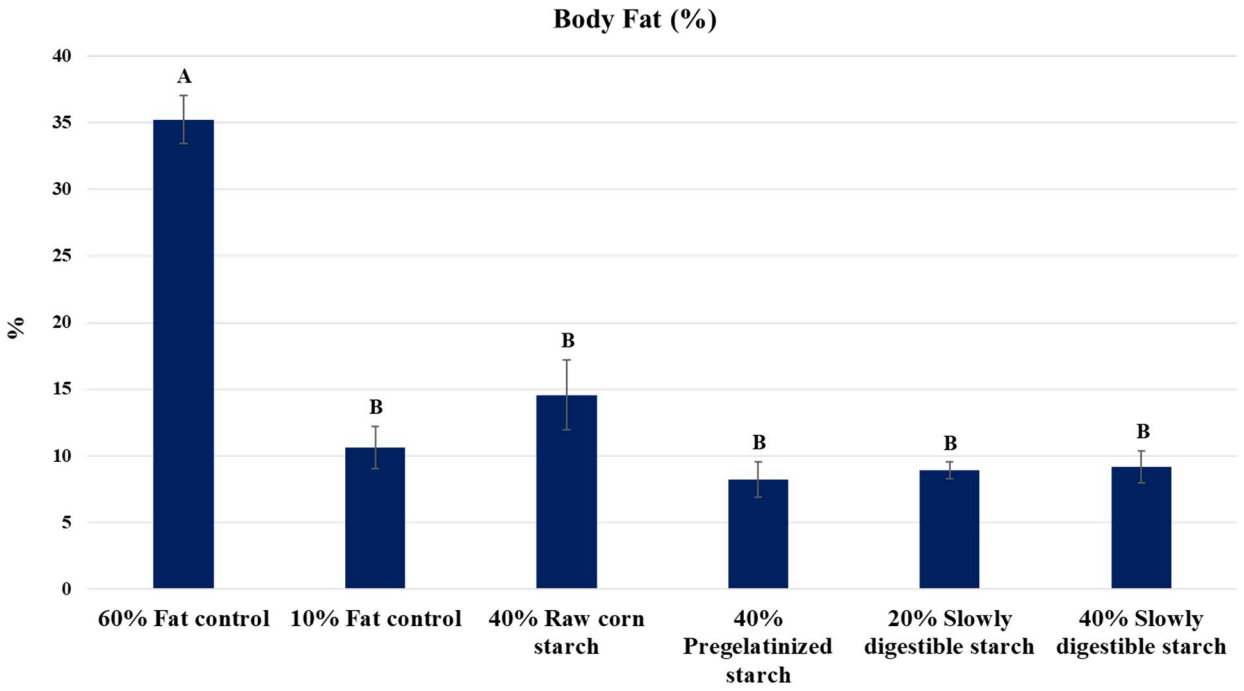

Figure 5.10 Average body fat percent (%) [EchoMRI] of mice in six experimental groups **(Intervention Study)** at week 8 after dietary conversion (n=10). Values denote group average (n=10) and bars represent standard error of the mean (Mean ± SEM). The increase in body fat percent in mice fed on 60 % high-fat diet was statistically significant (at $\alpha = 0.05$) compared to that of mice fed on all other 10 % low-fat diets at $P = < 0.0001$. No statistical differences in body fat percent (at $\alpha = 0.05$) were observed between mice fed on the five 10 % low-fat diets. Different letters denote statistically significant differences between treatments at $\alpha = 0.05$ based on Tukey's least squares means.

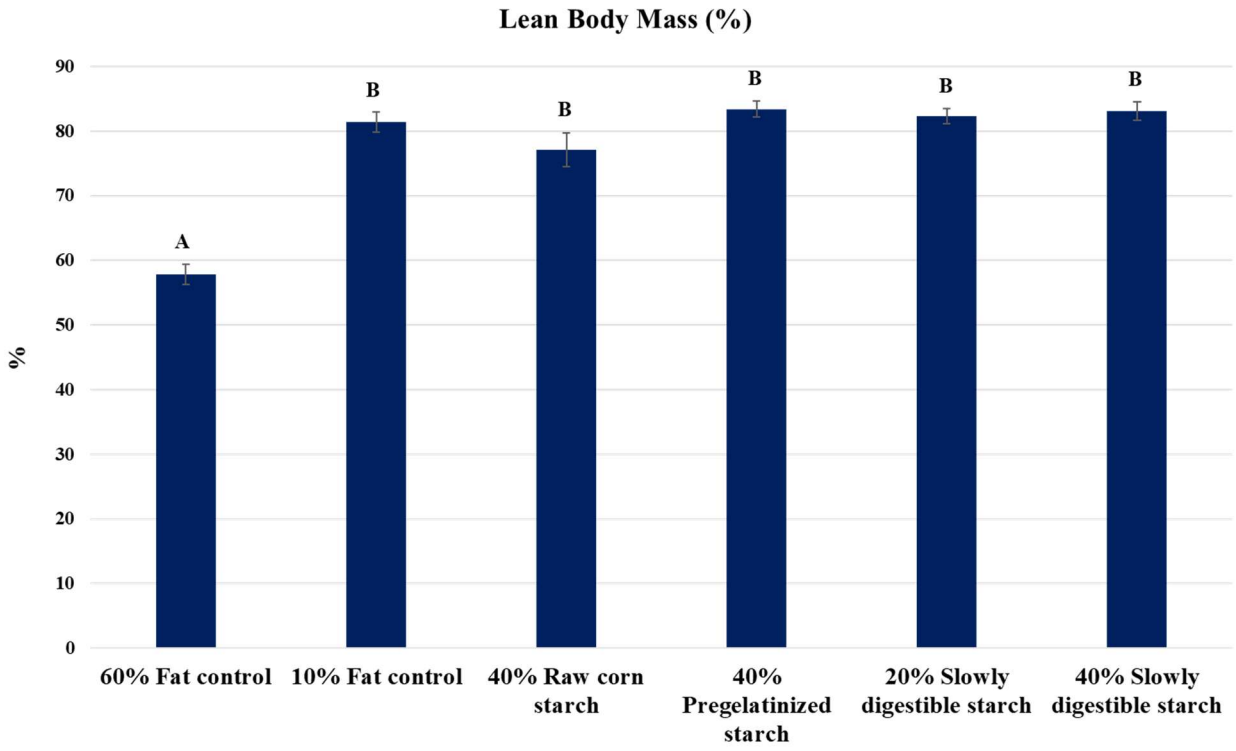

Figure 5.11 Average lean mass percent (%) [EchoMRI] of mice in six experimental groups **(Intervention Study)** at week 8 after dietary conversion. Values denote group average (n=10) and bars represent standard error of the mean (Mean ± SEM). The decrease in lean mass percent in mice fed on 60 % high-fat diet was statistically significant (at $\alpha = 0.05$) compared to that of mice fed on all other 10 % low-fat diets at $P = < 0.0001$. No statistical differences in lean mass percent (at $\alpha = 0.05$) were observed between mice fed on the five 10 % low-fat diets. Different letters denote statistically significant differences between treatments at $\alpha = 0.05$ based on Tukey's least squares means.

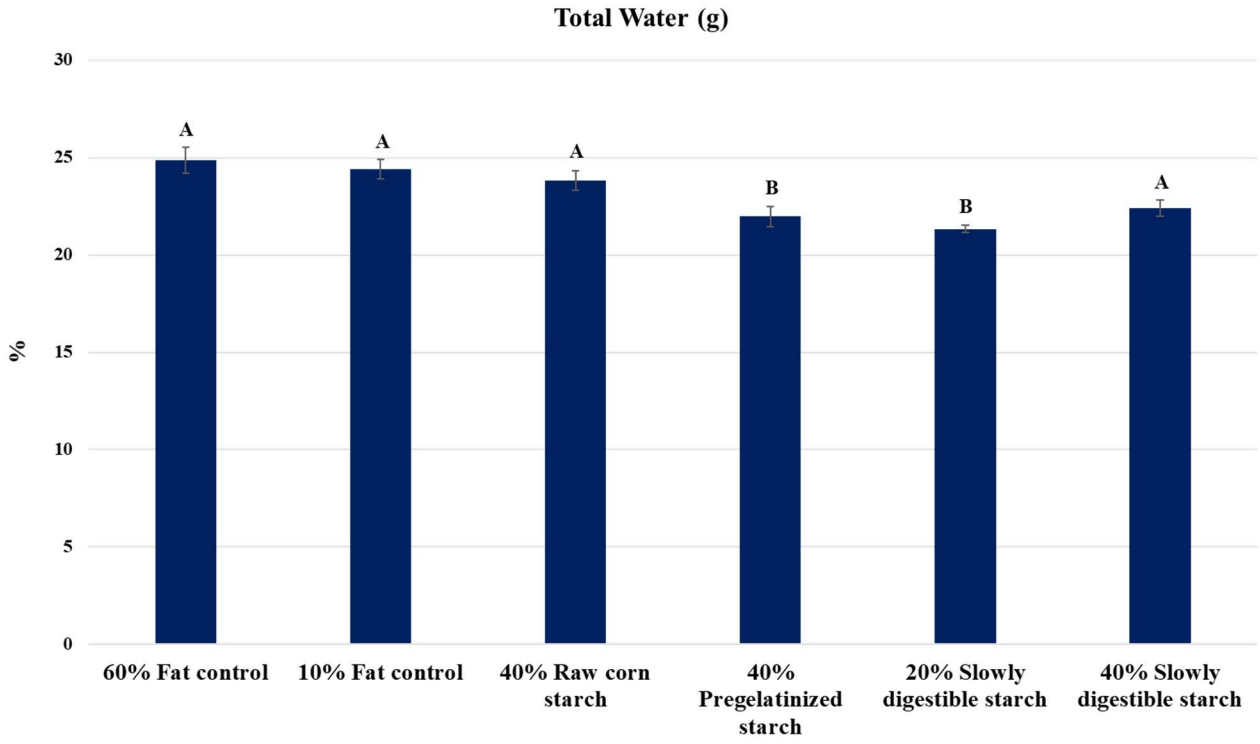

Figure 5.12 Average total water percent (%) [EchoMRI] of mice in six experimental groups **(Intervention Study)** at week 8 after dietary conversion. Values denote group average (n=10) and bars represent standard error of the mean (Mean ± SEM). The reduction in total water percent (%) of mice fed on 20 % SDS was statistically significant (at $\alpha = 0.05$) compared to that of mice fed on 10 % low-fat control and mice fed on 60 % high-fat control at $P = 0.0102$ and 0.0035, respectively. Similarly, the reduction in total water percent of mice fed on PGS was statistically significant (at $\alpha = 0.05$) compared to that of mice fed on 10 % low-fat control and mice fed on 60 % high-fat control at $P = 0.0376$ and 0.0131, respectively. Different letters denote statistically significant differences between treatments at $\alpha = 0.05$ based on Tukey's least squares means.

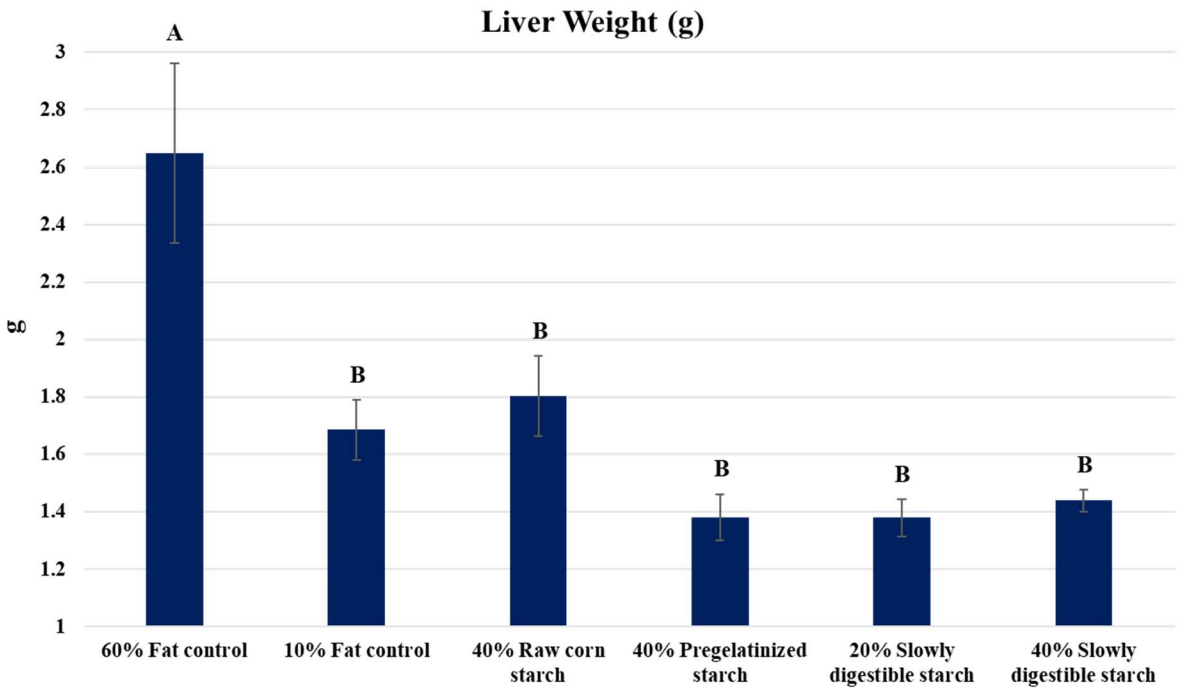

Figure 5.13 Liver weight (g) of mice in six experimental groups **(Intervention Study)** at the end of the study (week 13). Values denote group average (n=10) and bars represent standard error of the mean (Mean ± SEM). The increase in liver weight of mice fed on 60 % high-fat diet was statistically significant (at $\alpha = 0.05$) compared to that of mice fed on 10 % low-fat control, 40 % RCS, 40 % PGS, 20 % SDS and 40 % SDS at $P = 0.0046$, 0.0135, 0.0002, 0.0002 and 0.0003, respectively. No statistically significant differences (at $\alpha = 0.05$) in liver weight at $\alpha = 0.05$ were observed between mice fed on the five 10 % low-fat diets. Different letters denote statistically significant differences between treatments at $\alpha=0.05$ based on Tukey's least squares means for treatment effect.

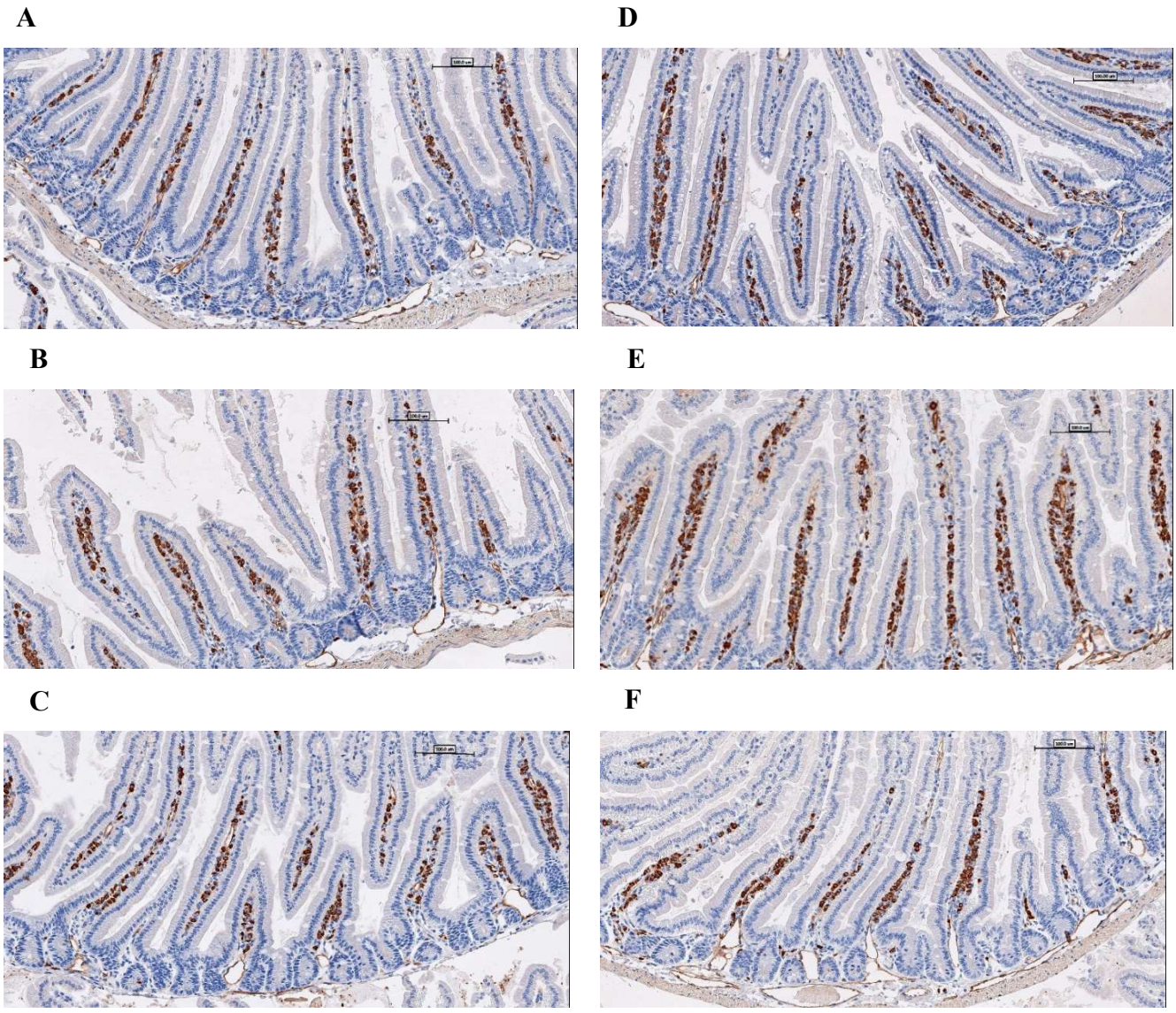

Figure 5.14 Immunohistochemistry sections of the mice **duodenum** from each experimental group **(Intervention Study)**. A: 10 % low-fat control group; B: 40 % RCS group; C: 40 % PGS group, D: 60 % high-fat control group; E: 20 % SDS group; F:40 % SDS group.

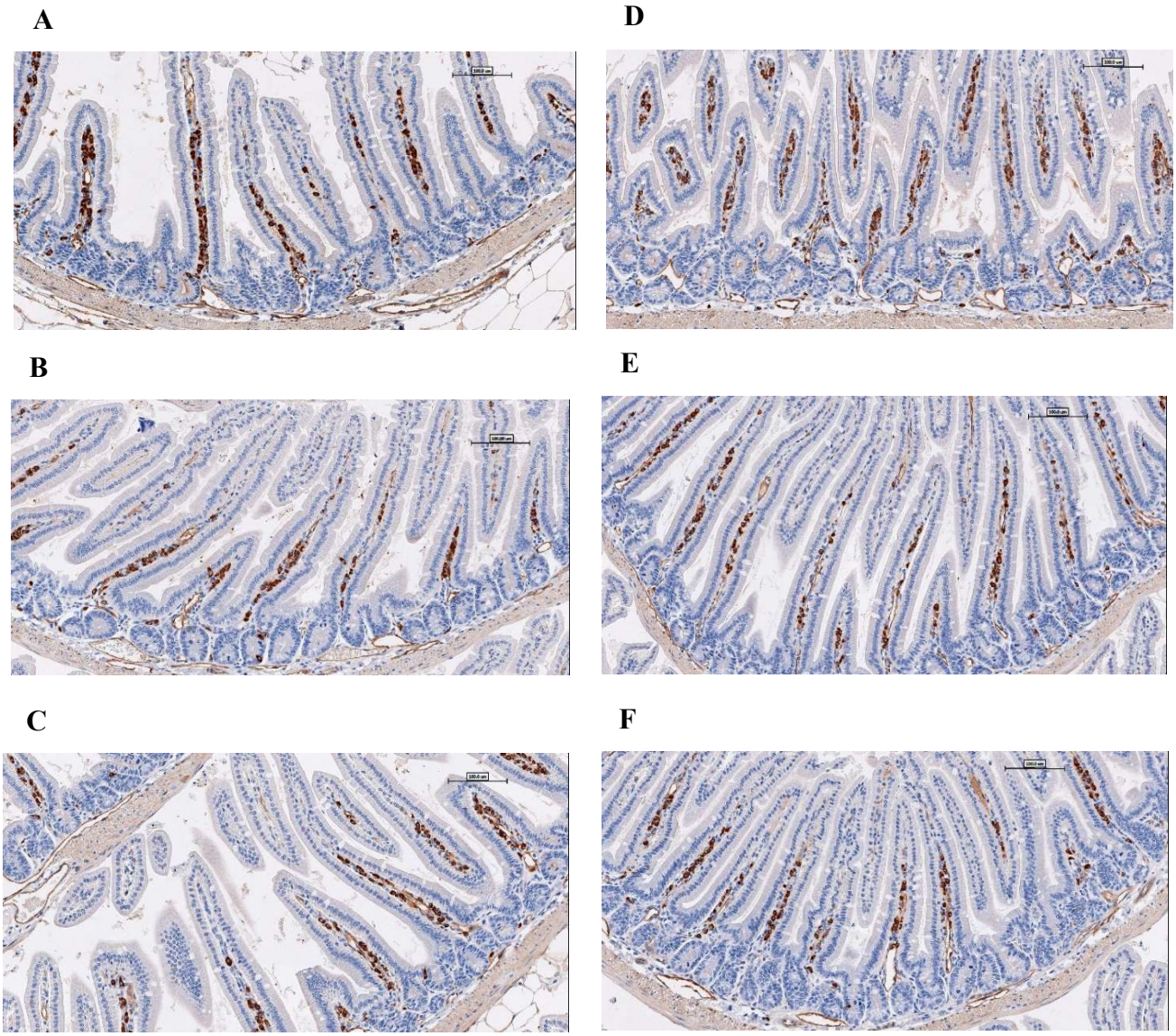

Figure 5.15 Immunohistochemistry sections of the mice **jejunum** from each experimental group **(Intervention Study)**. A: 10 % low-fat control group; B: 40 % RCS group; C: 40 % PGS group, D: 60 % high-fat control group; E: 20 % SDS group; F:40 % SDS group.

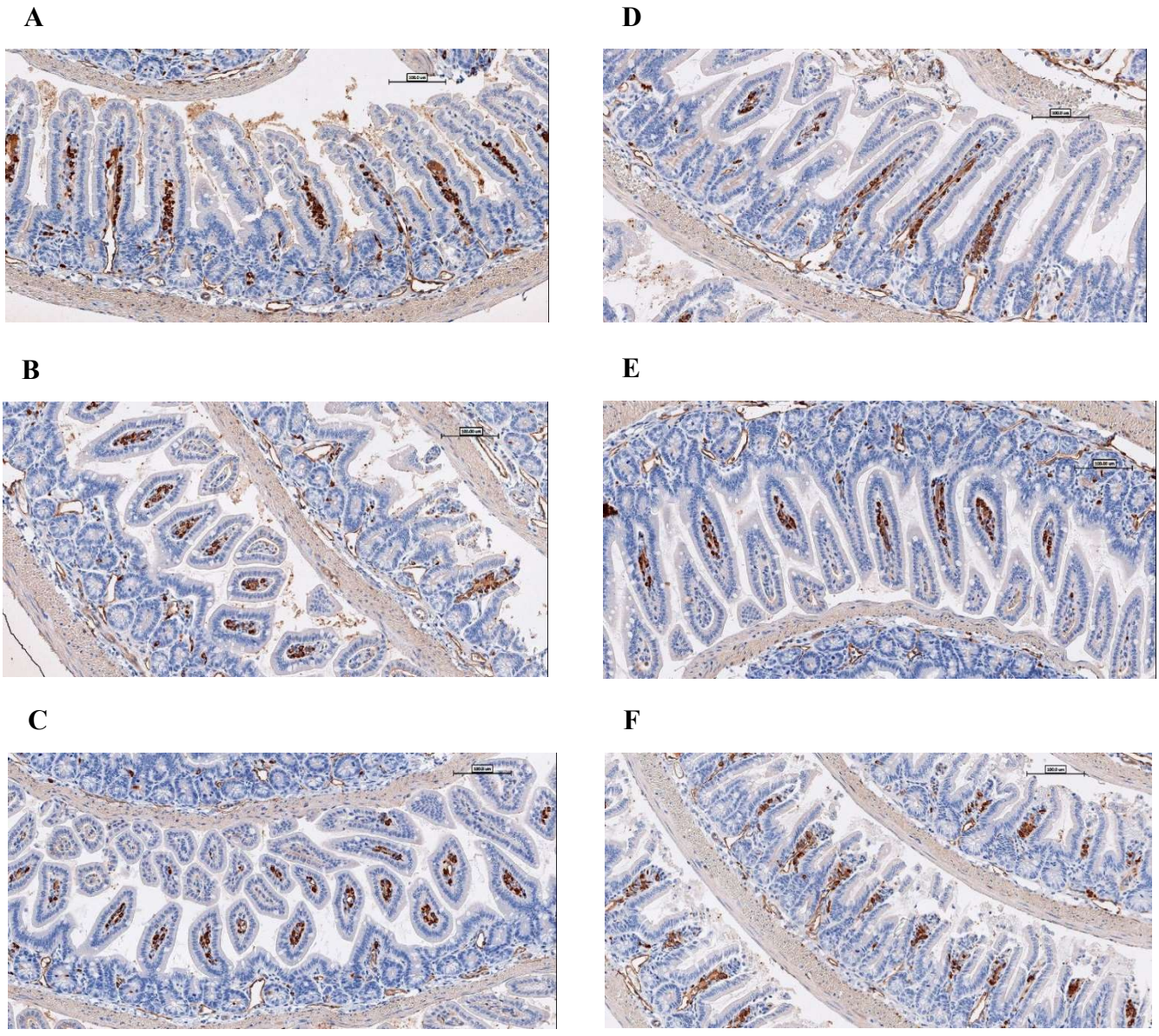

Figure 5.16 Immunohistochemistry sections of the mice **ileum** from each experimental group **(Intervention Study)**. A: 10 % low-fat control group; B: 40 % RCS group; C: 40 % PGS group, D: 60 % high-fat control group; E: 20 % SDS group; F:40 % SDS group.

A

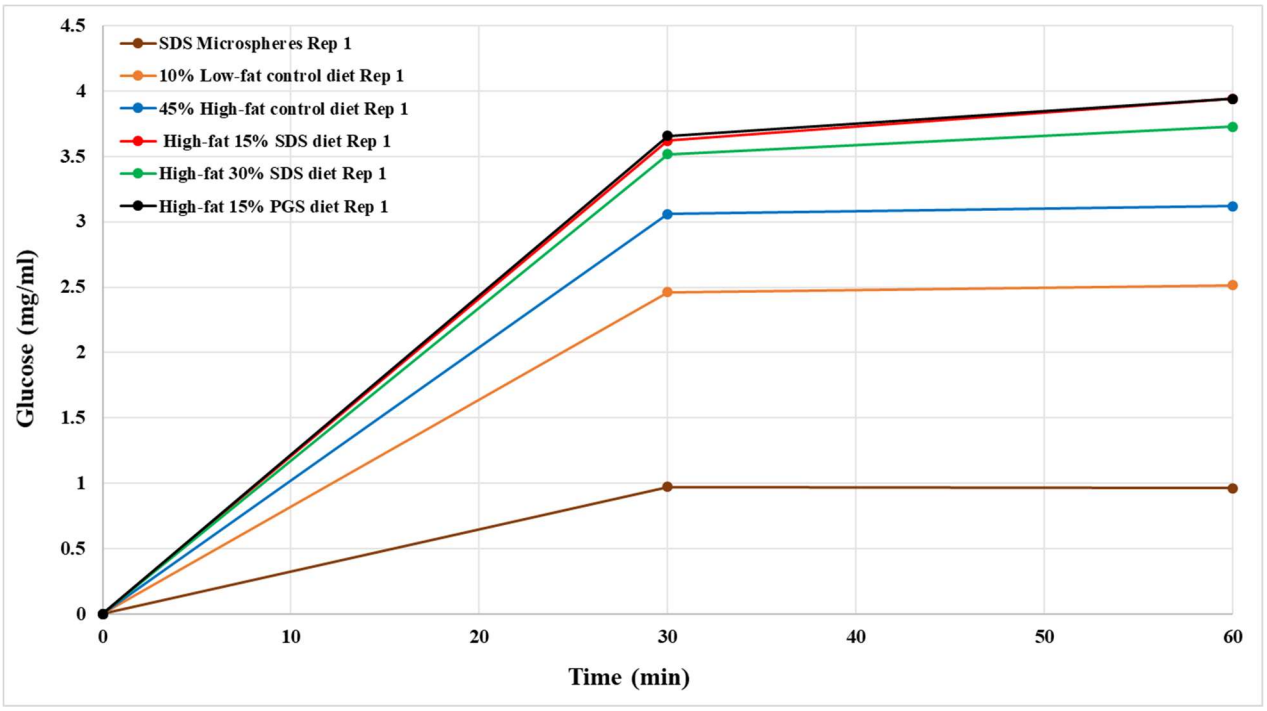

B

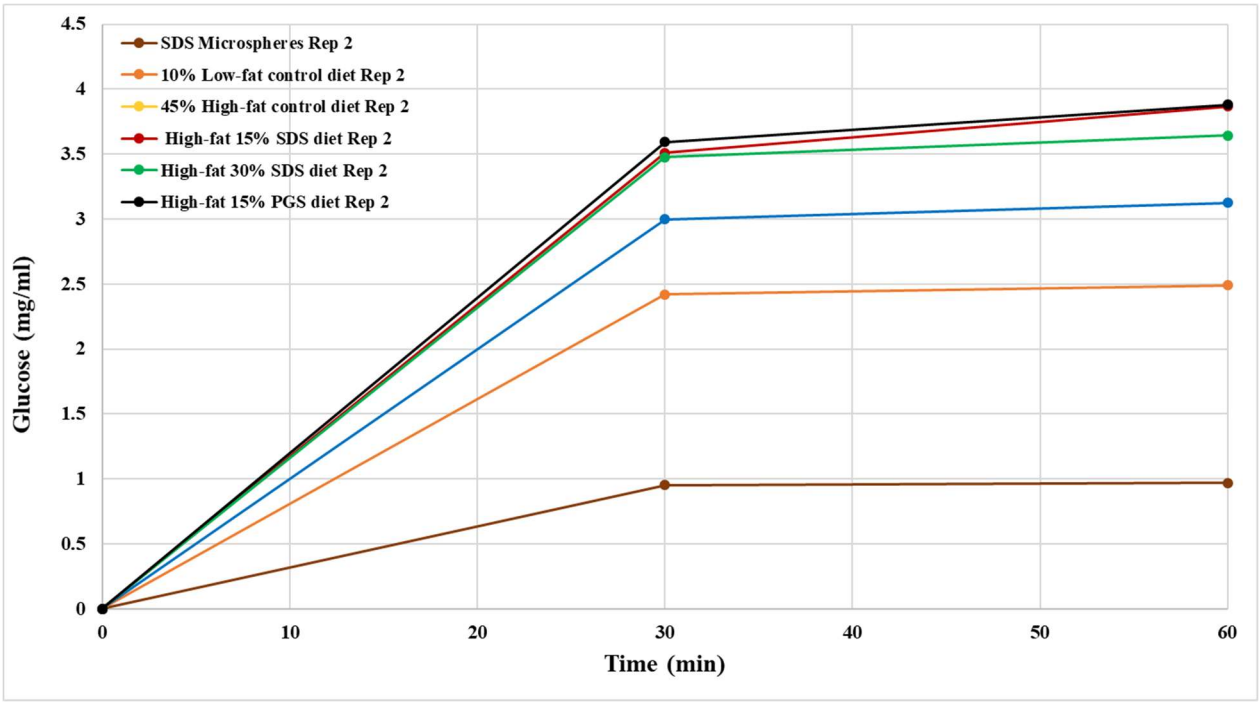

Figure 5.17 Release of reducing sugars from the slowly digestible starch-entrapped microspheres (SDS) and the five experimental diets used in the study **(Prevention Study)**. A and B are the result of digestion for 60 minutes for two independent replicates; A: replicate # 1, B: replicate #2.

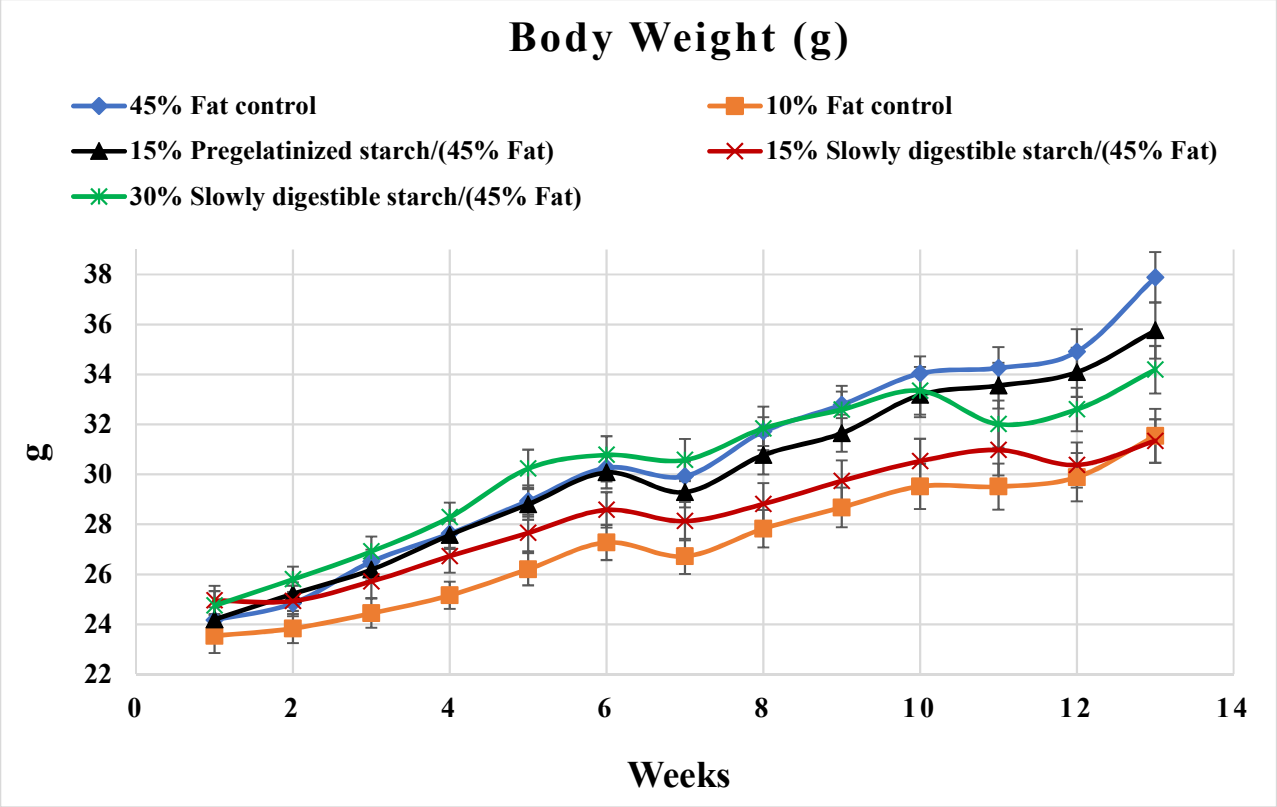

Figure 5.18 Average body weight (g) of mice in five experimental groups **(Prevention Study)** throughout the study from week 1 to week 13 (n=12). Values denote group average and bars represent standard error of the mean (Mean ± SEM). The increase in the average body weight of 45 % high-fat control group was statistically significant (at $\alpha = 0.05$) compared to that of 10 % low-fat control group at $P = 0.0309$. Body weight of mice fed on 10 % low-fat control diet was lower than that of mice fed on 15 % PGS diet at $P = 0.0991$ and lower than that of mice fed on 30 % SDS diet at $P = 0.0576$.

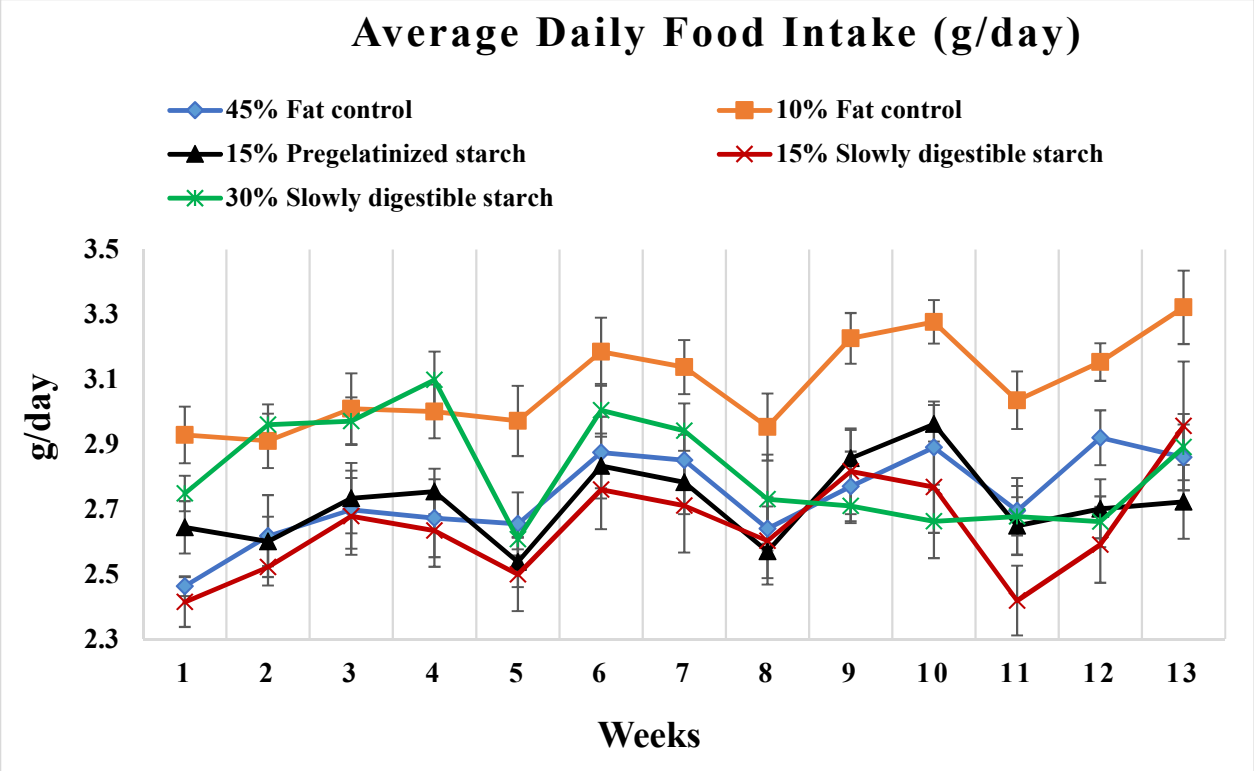

Figure 5.19 Average daily food intake (g) of mice in five experimental groups **(Prevention Study)** throughout the study from week 1 to week 13 (n=12). Values denote group average and bars represent standard error of the mean (Mean ± SEM). The increase in daily food intake of mice fed on 10 % low-fat control was statistically significant (at $\alpha = 0.05$) compared to that of mice fed on 45 % high-fat control, 15 % PGS and 15 % SDS diets at $P = 0.0140$, 0.0103 and 0.0019, respectively. No statistically significant differences (at $\alpha = 0.05$) in daily food intake were observed between mice fed on high-fat diets containing 15 % PGS, 15 % SDS or 30 % SDS when compared to each other.

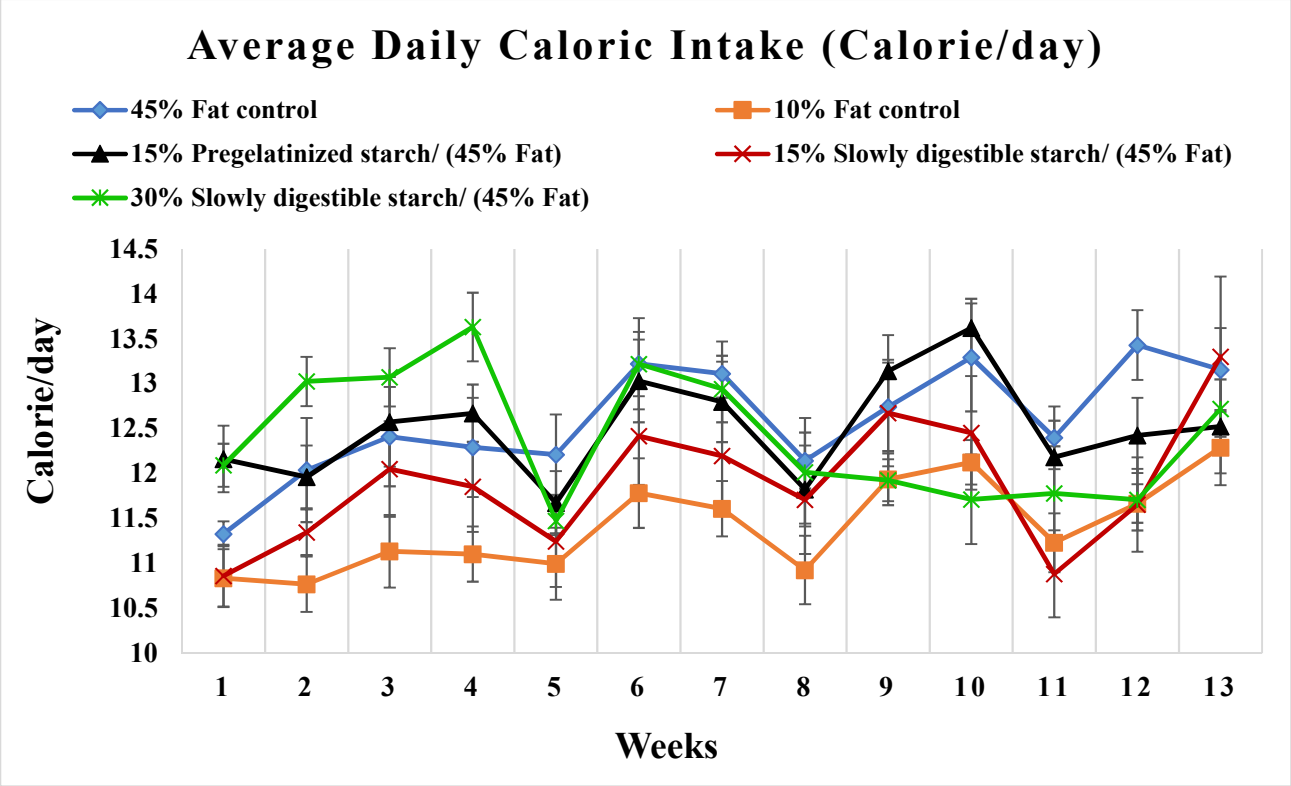

Figure 5.20 Average daily caloric intake (Calorie/day) of mice in five experimental groups **(Prevention Study)** throughout the study from week 1 to week 13 (n=12). Values denote group average and bars represent standard error of the mean (Mean ± SEM). The reduction in daily caloric intake of mice fed on 10 % low-fat control was statistically significant (at $\alpha = 0.05$) compared to that of mice fed on 45 % high-fat control diet at $P = 0.0487$. No statistically significant differences (at $\alpha = 0.05$) in daily caloric intake were observed between mice fed on 10 % low-fat diet compared to that of mice fed on high-fat diets containing 15 % PGS ($P = 0.0707$), 15 % SDS ($P = 0.6112$) or 30 % SDS ($P = 0.1221$). No statistically significant differences in daily caloric intake were observed between mice fed on high-fat diets containing 15 % PGS, 15 % SDS or 30 % SDS when compared to each other.

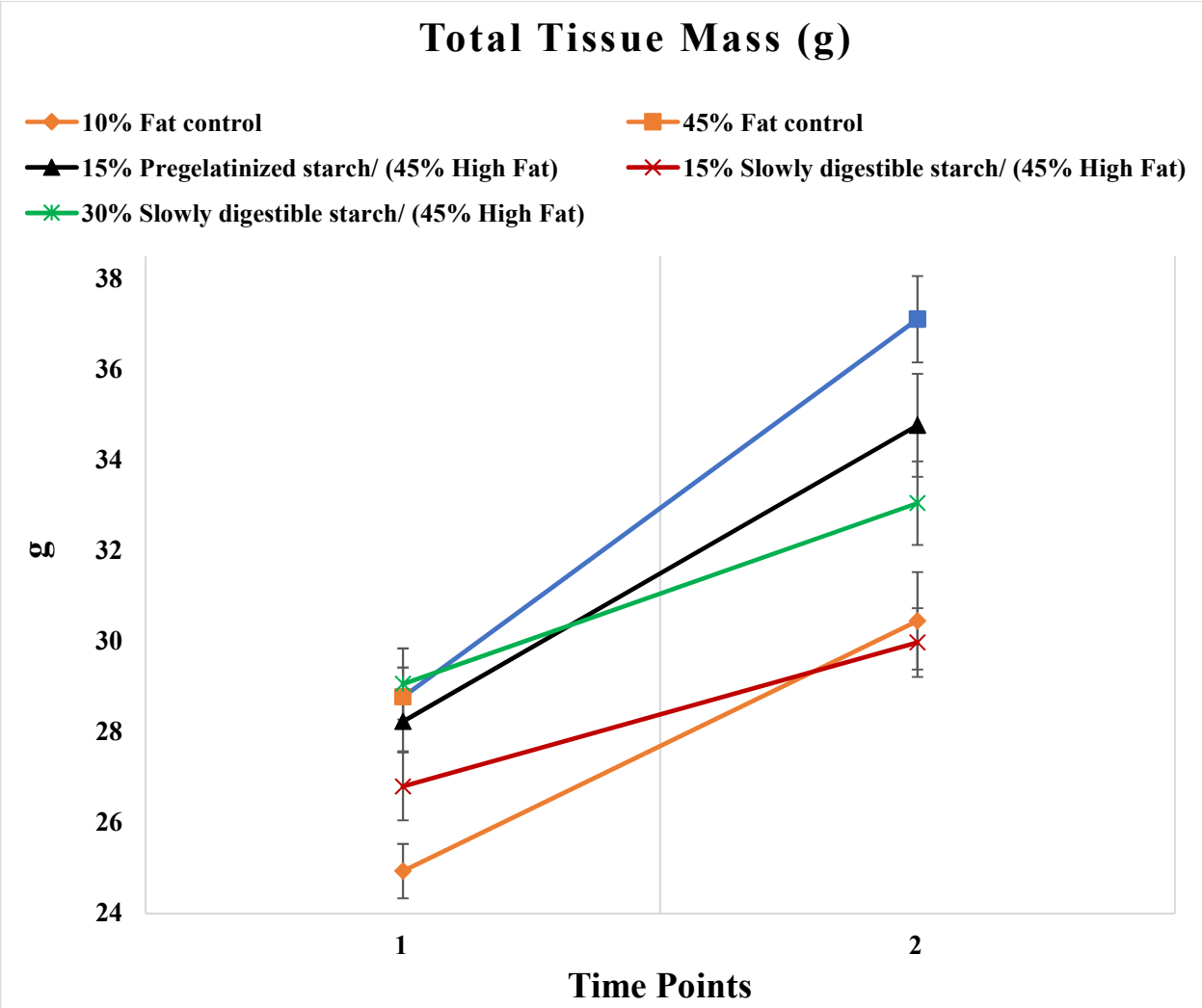

Figure 5.21 Total tissue mass (g) [DEXA] of mice in five experimental groups **(Prevention Study)** at two-time points throughout the study; 1: week 5 and 2: week 12. Values denote group average (n=12) and bars represent standard error of the mean (Mean ± SEM). The increase in total tissue mass (g) of mice fed on 45 % high-fat control diet was statistically significant (at $\alpha = 0.05$) compared to that of mice fed on 10 % low-fat control and 15 % SDS diets at $P = 0.0013$ and 0.0056, respectively. Total tissue mass was significantly higher (at $\alpha = 0.05$) in mice fed on 15% PGS diet compared to mice fed on 10 % low-fat control diet at $P = 0.0262$. Total tissue mass was higher in mice fed on 15 % PGS diet compared to mice fed on 15 % SDS diet at $P = 0.0941$. Total tissue mass was higher in mice fed on 30 % SDS diet compared to mice fed on 10 % low-fat control diet at $P = 0.0606$.

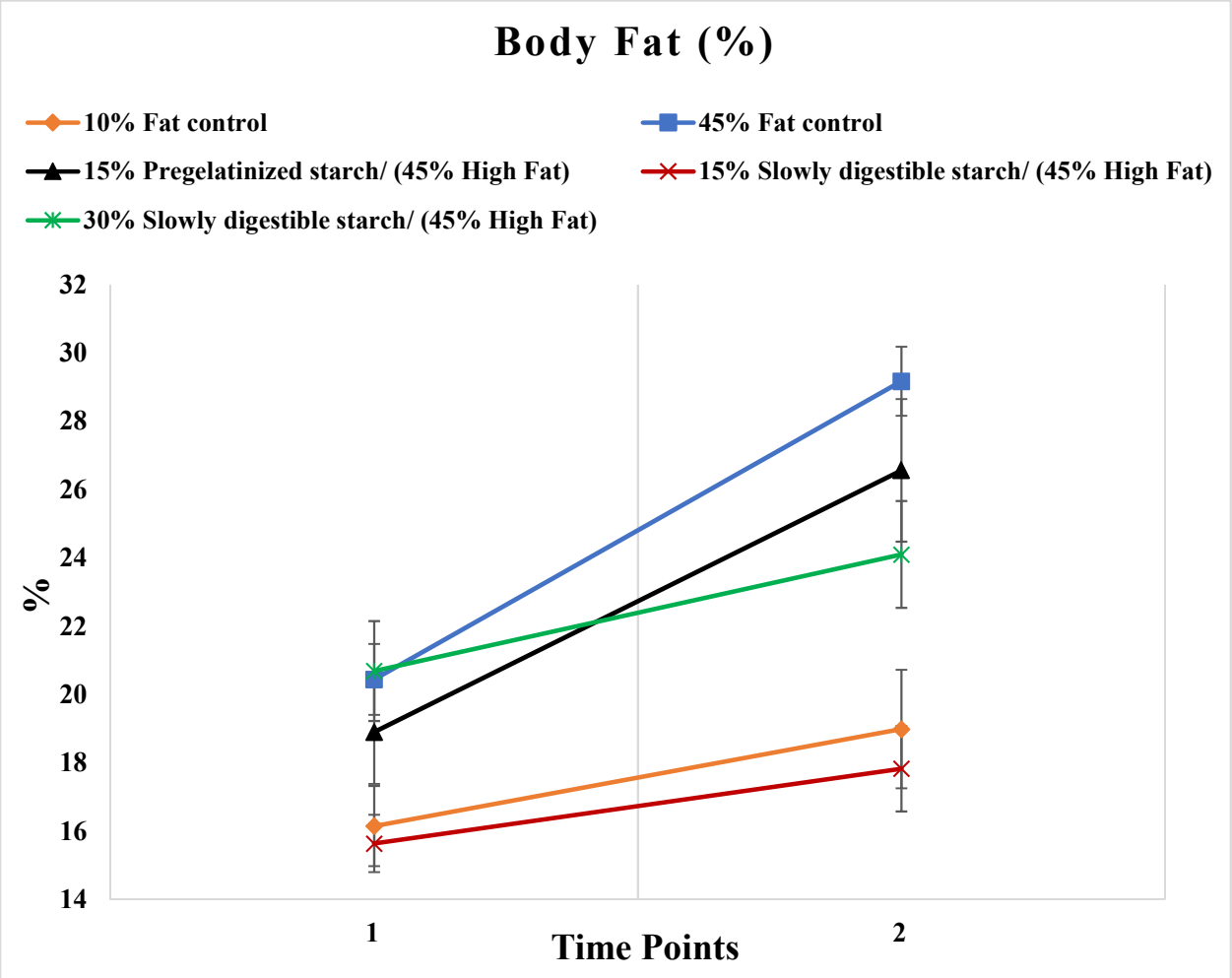

Figure 5.22 Average body fat (%) [DEXA] of mice in five experimental groups **(Prevention Study)** at two-time points throughout the study; 1: week 5 and 2: week 12. Values denote group average (n=12) and bars represent standard error of the mean (Mean ± SEM). The increase in body fat (%) of mice fed on 45 % high-fat control diet was statistically significant (at $\alpha = 0.05$) compared to that of mice fed 10 % low-fat control and 15% SDS diets at $P = 0.0099$ and 0.0035, respectively. Body fat percent was significantly higher (at $\alpha = 0.05$) in mice fed on 15 % PGS compared to mice fed on 15 % SDS at $P = 0.0436$. Body fat percent was higher in mice fed on 30 % SDS compared to mice fed on 15 % SDS at $P = 0.0630$.

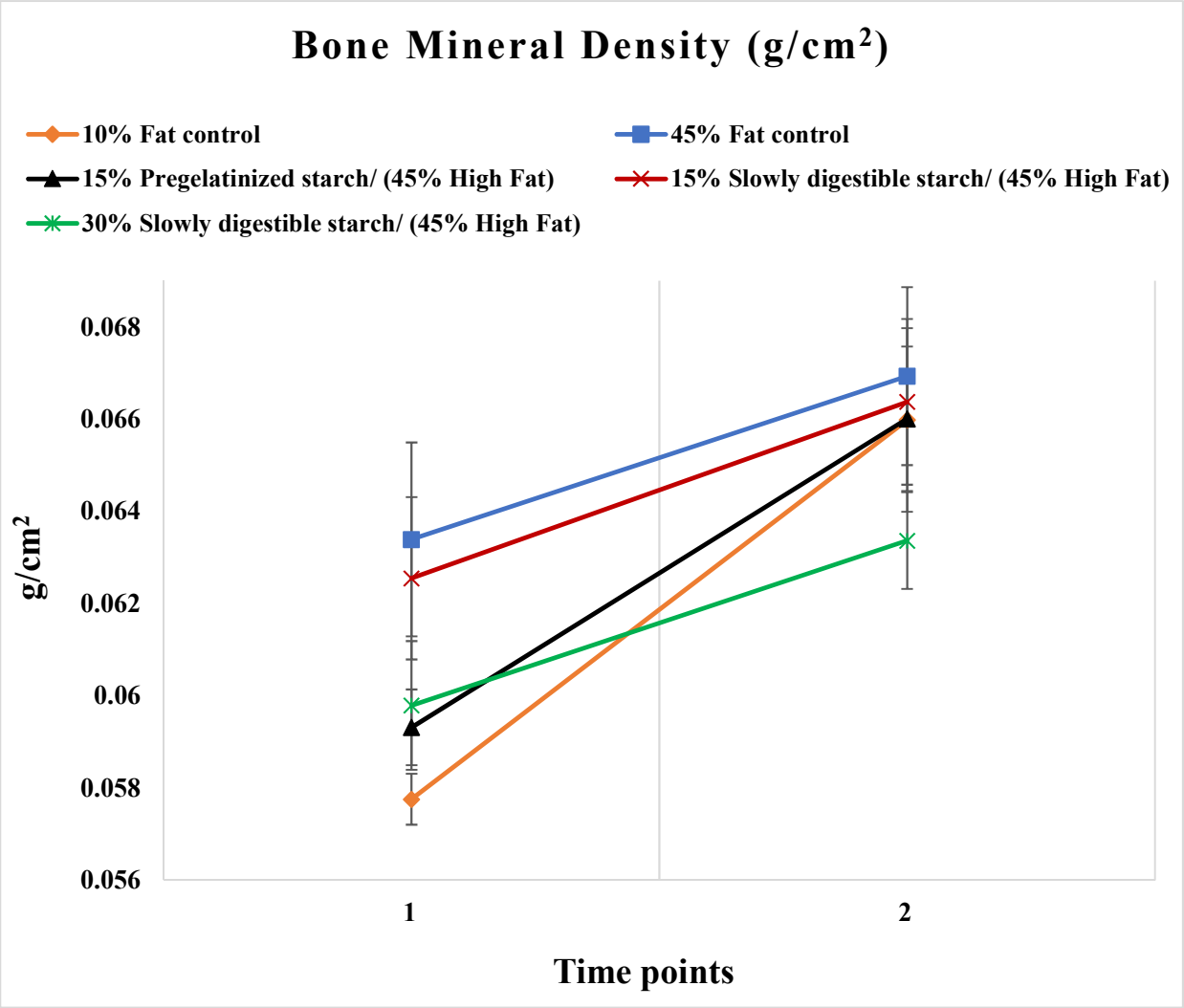

Figure 5.23 Bone mineral density (g/cm^2) [DEXA] of mice in five experimental groups **(Prevention Study)** at two-time points throughout the study; 1: week 5, 2: week 12. Values denote group average (n=12) and bars represent standard error of the mean (Mean ± SEM). No statistical differences in bone mineral density (g/cm^2) at $\alpha = 0.05$ were observed between mice fed on any of the experimental diets based on Tukey's least squares means for treatment effect.

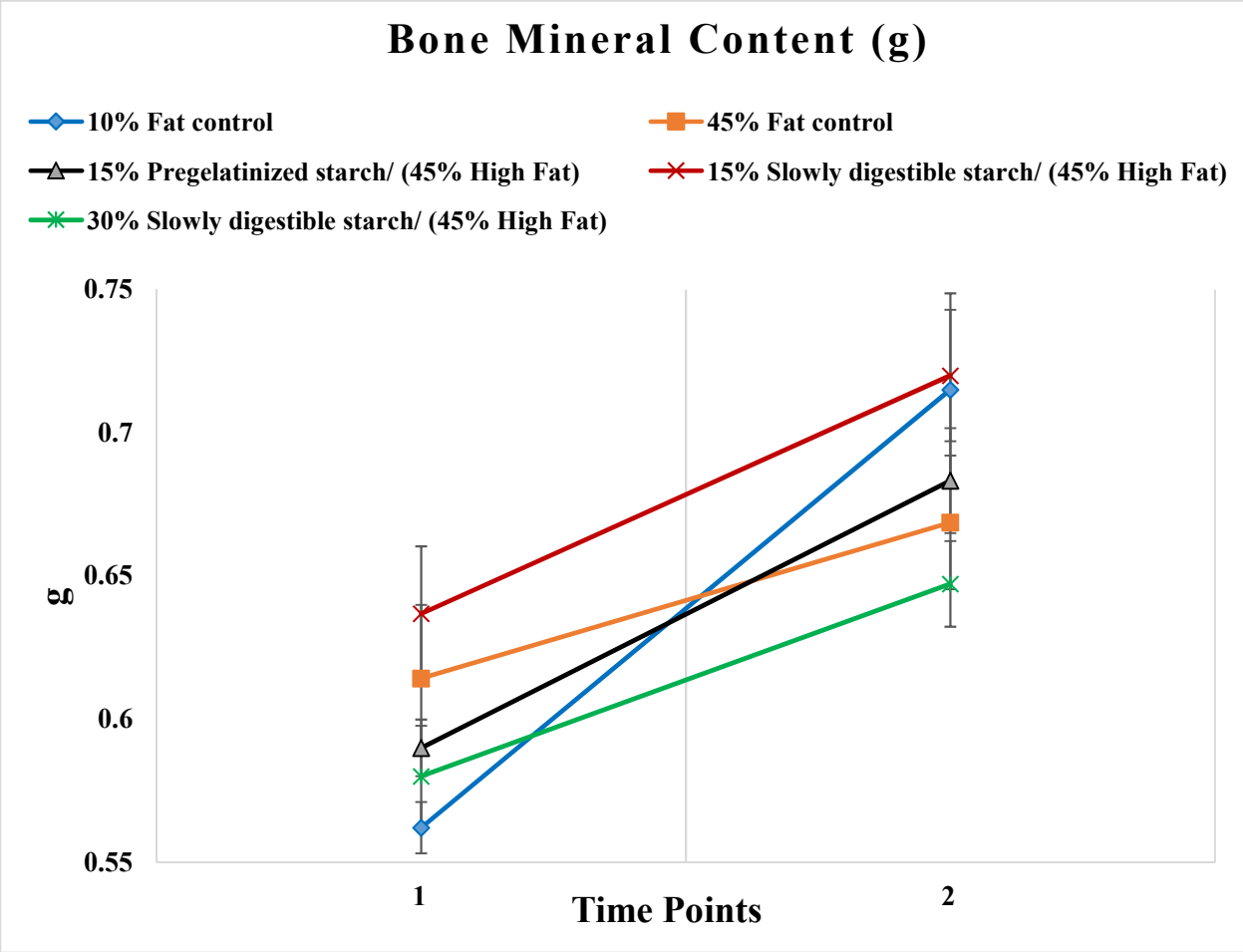

Figure 5.24 Bone mineral content (g) [DEXA] of mice in five experimental groups **(Prevention Study)** at two-time points throughout the study; 1: week 5, 2: week 12. Values denote group average (n=12) and bars represent standard error of the mean (Mean ± SEM). No statistical differences in bone mineral content (g) at $\alpha = 0.05$ were observed between mice fed on any of the experimental diets based on Tukey's least squares means for treatment effect.

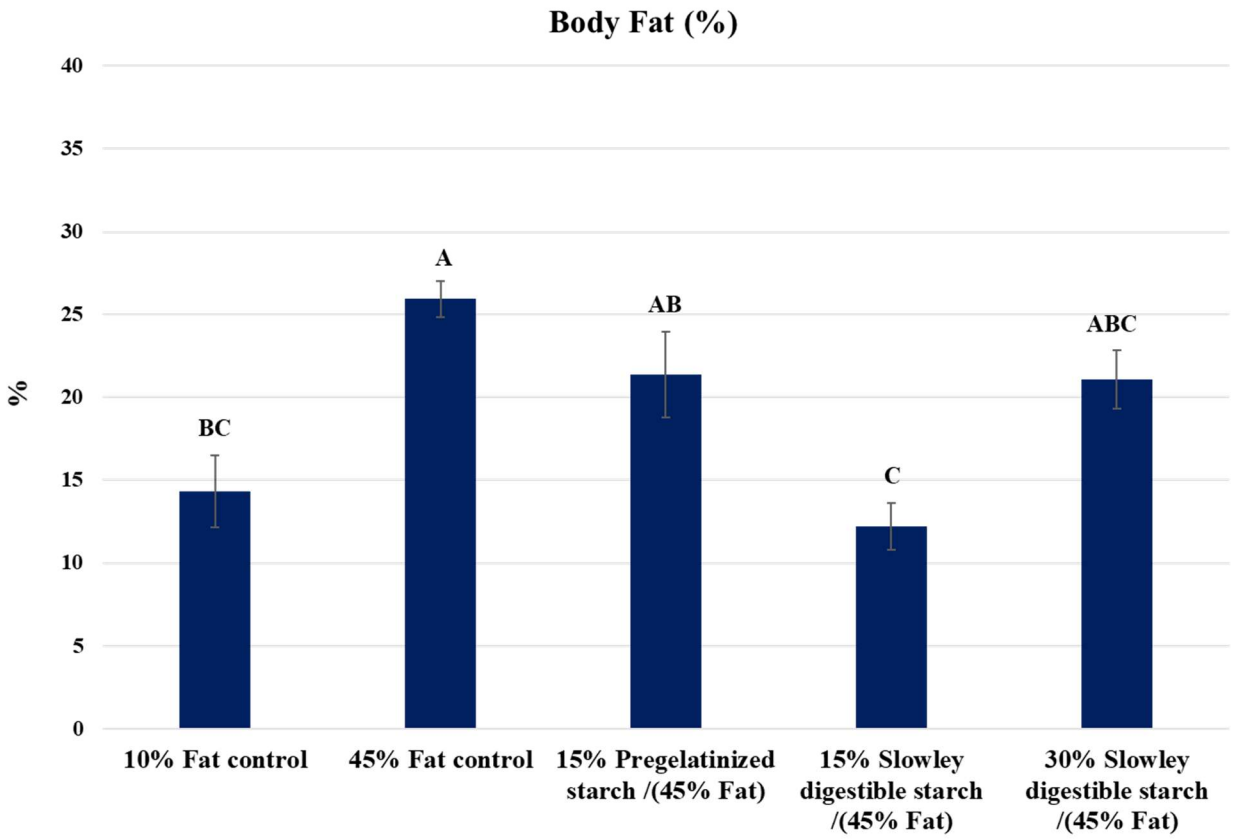

Figure 5.25 Body fat (%) [EchoMRI] of mice in five experimental groups **(Prevention Study)** at the end of the study (week 13). Values denote group average (n=12) and bars represent standard error of the mean (Mean ± SEM). The increase in body fat percent in mice fed on 45 % high-fat diet was statistically significant (at $\alpha = 0.05$) compared to that of mice fed on 10% low-fat control at $P = 0.0069$ and mice fed on 15 % SDS diet at $P = 0.0012$. Body fat (%) of mice fed on 15 % SDS was significantly (at $\alpha = 0.05$) lower than that of mice fed 15 % PGS at $P = 0.0486$. Body fat (%) of mice fed on 15 % SDS was lower than that of mice fed 30 % SDS at $P = 0.0610$. Different letters denote statistically significant differences between treatments at $\alpha=0.05$ based on Tukey's least squares means.

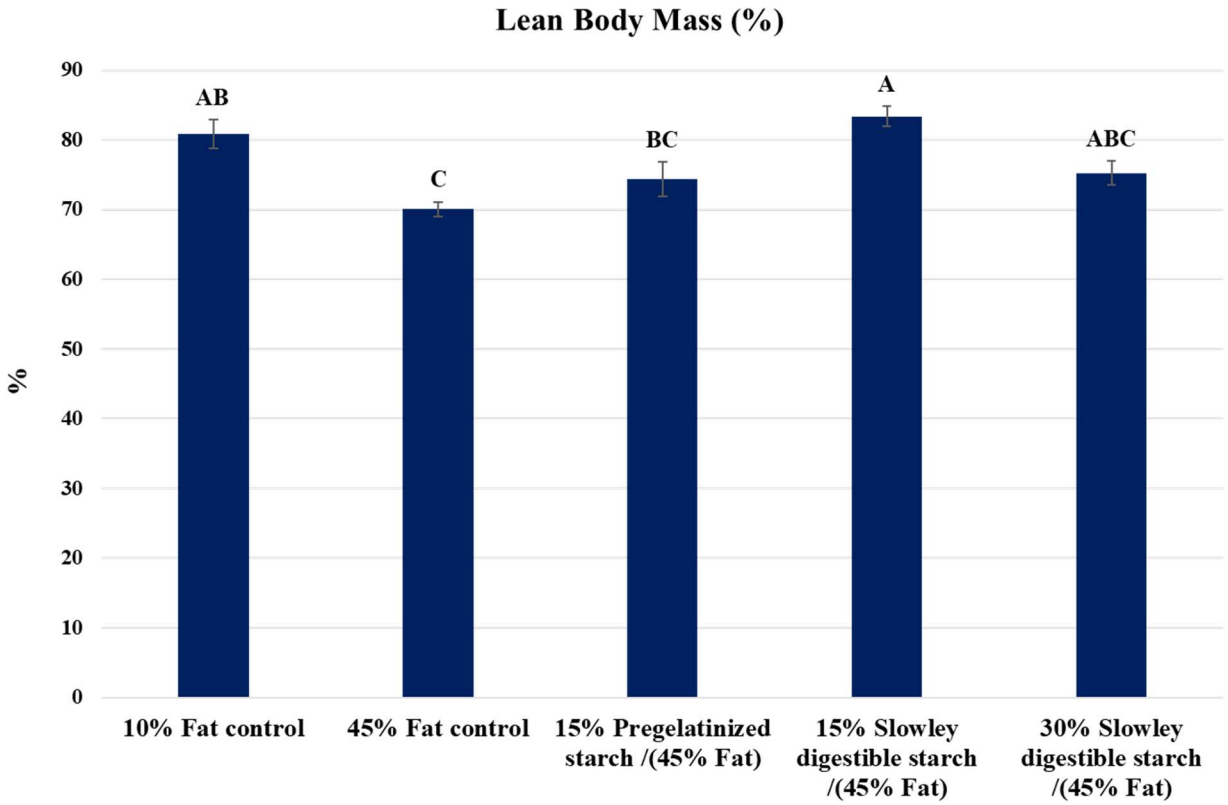

Figure 5.26 Lean body mass (%) [EchoMRI] of mice in five experimental groups **(Prevention Study)** at the end of the study (week 13). Values denote group average (n=12) and bars represent standard error of the mean (Mean ± SEM). The reduction in lean body mass percent in mice fed on 45 % high-fat diet was statistically significant (at $\alpha = 0.05$) compared to that of mice fed on 10 % low-fat control at $P = 0.0100$ and mice fed on 15% SDS diet at $P = 0.0012$. Lean body mass (%) of mice fed on 15 % SDS was significantly higher (at $\alpha = 0.05$) than that of mice fed 15 % PGS at $P = 0.0455$. Lean body mass (%) of mice fed on 30 % SDS was lower than that of mice fed 15 % SDS at $P = 0.0836$. Different letters denote statistically significant differences between treatments at $\alpha=0.05$ based on Tukey's least squares means.

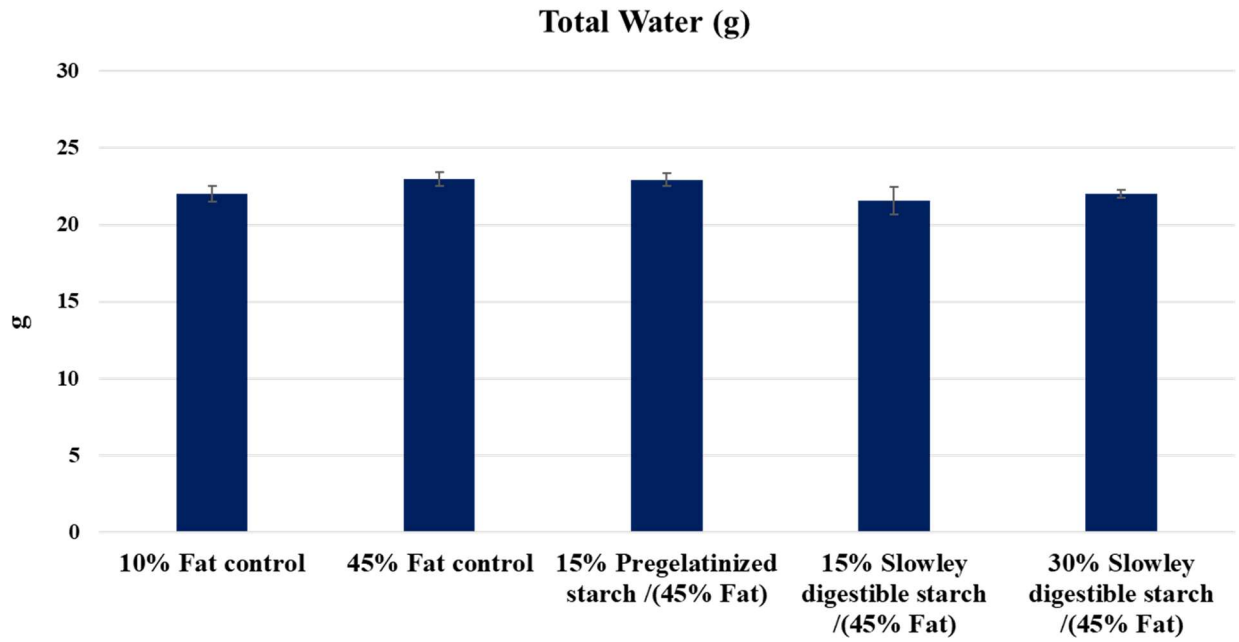

Figure 5.27 Total water (%) [EchoMRI]of mice in five experimental groups **(Prevention Study)** at the end of the study (week 13). Values denote group average (n=12) and bars represent standard error of the mean (Mean ± SEM). No statistical differences in total water (%) at $\alpha = 0.05$ were observed between mice fed on any of the experimental diets based on Tukey's least squares means for treatment effect.

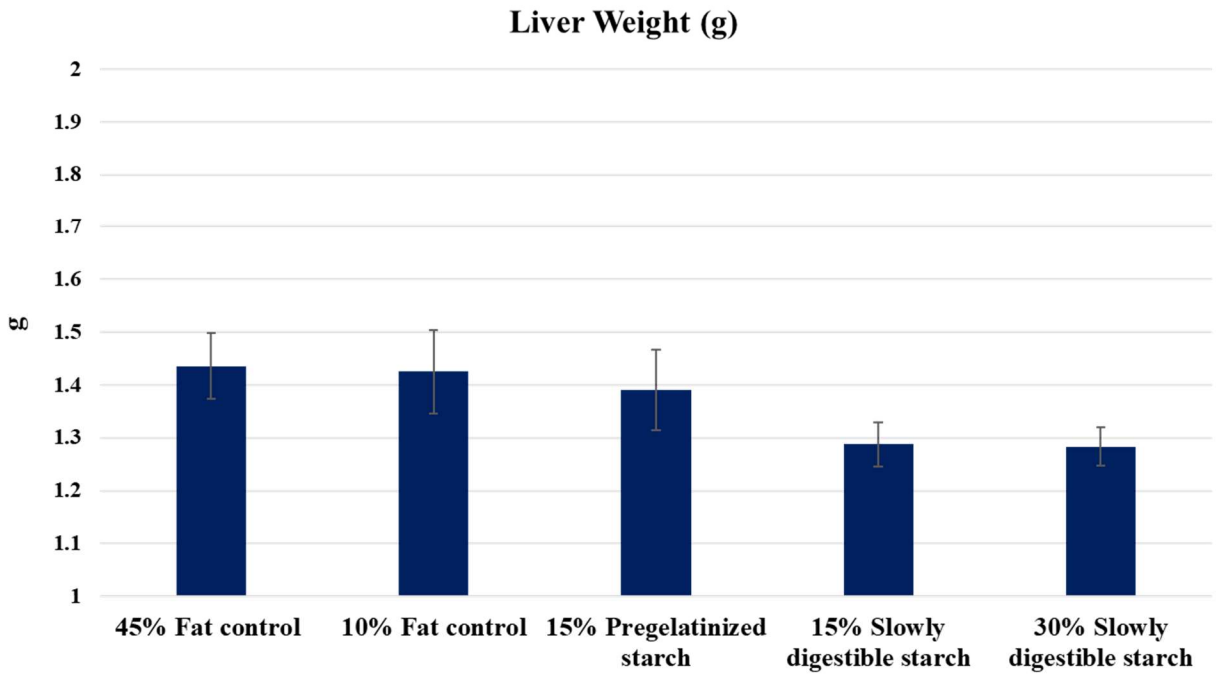

Figure 5.28 Liver weight (g) of mice in five experimental groups **(Prevention Study)** at the end of the study (week 13). Values denote group average (n=12) and bars represent standard error of the mean (Mean ± SEM). No statistical differences in liver weight at $\alpha = 0.05$ were observed between mice fed on any of the experimental diets based on Tukey's least squares means for treatment effect.

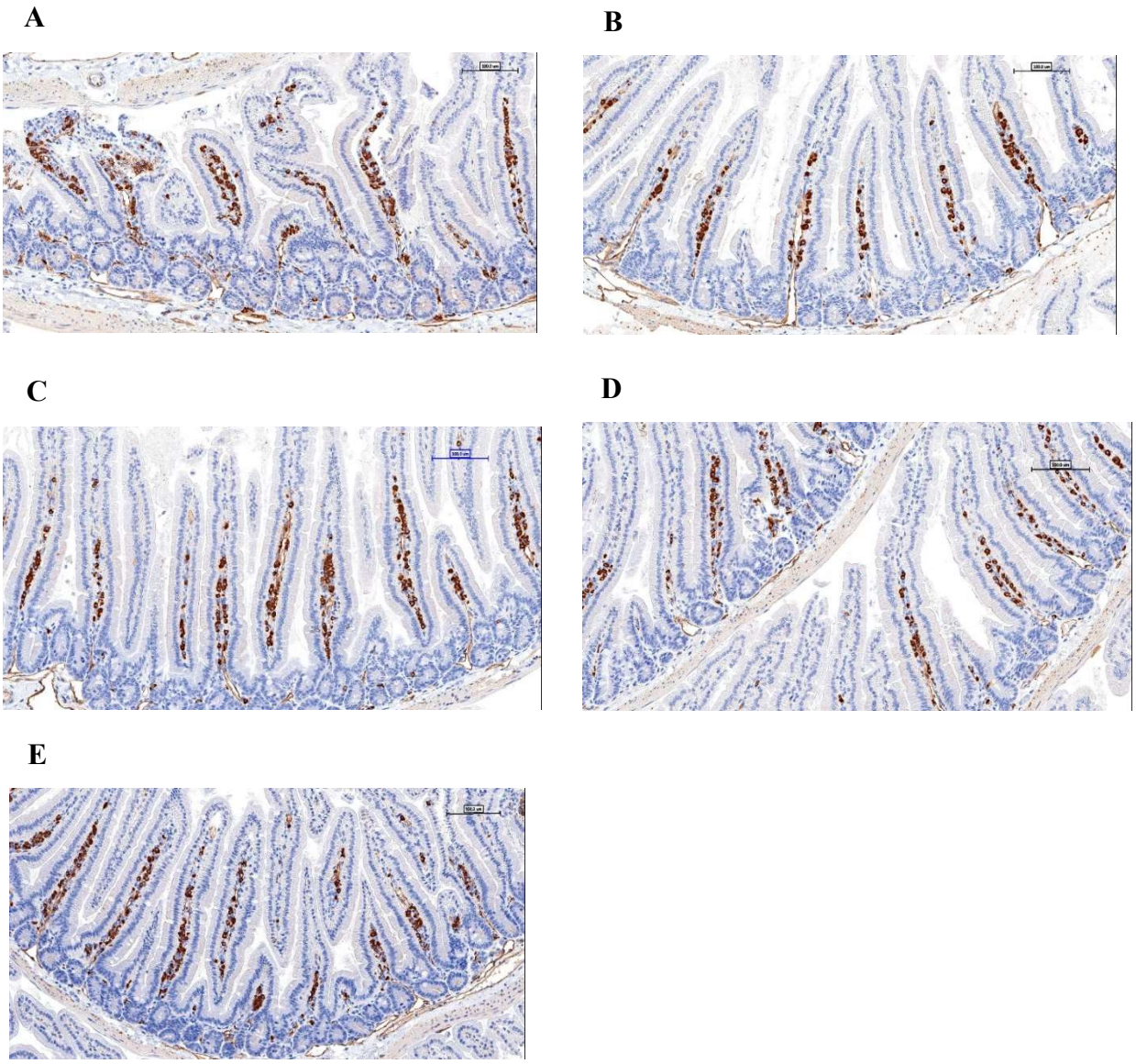

Figure 5.29 Immunohistochemistry sections of the mice **duodenum** from each experimental group **(Prevention Study)**. A: 10% low-fat control group; B: 45 % high-fat control group; C: 15 % PGS group, D: 15 % SDS group; E:30 % SDS group.

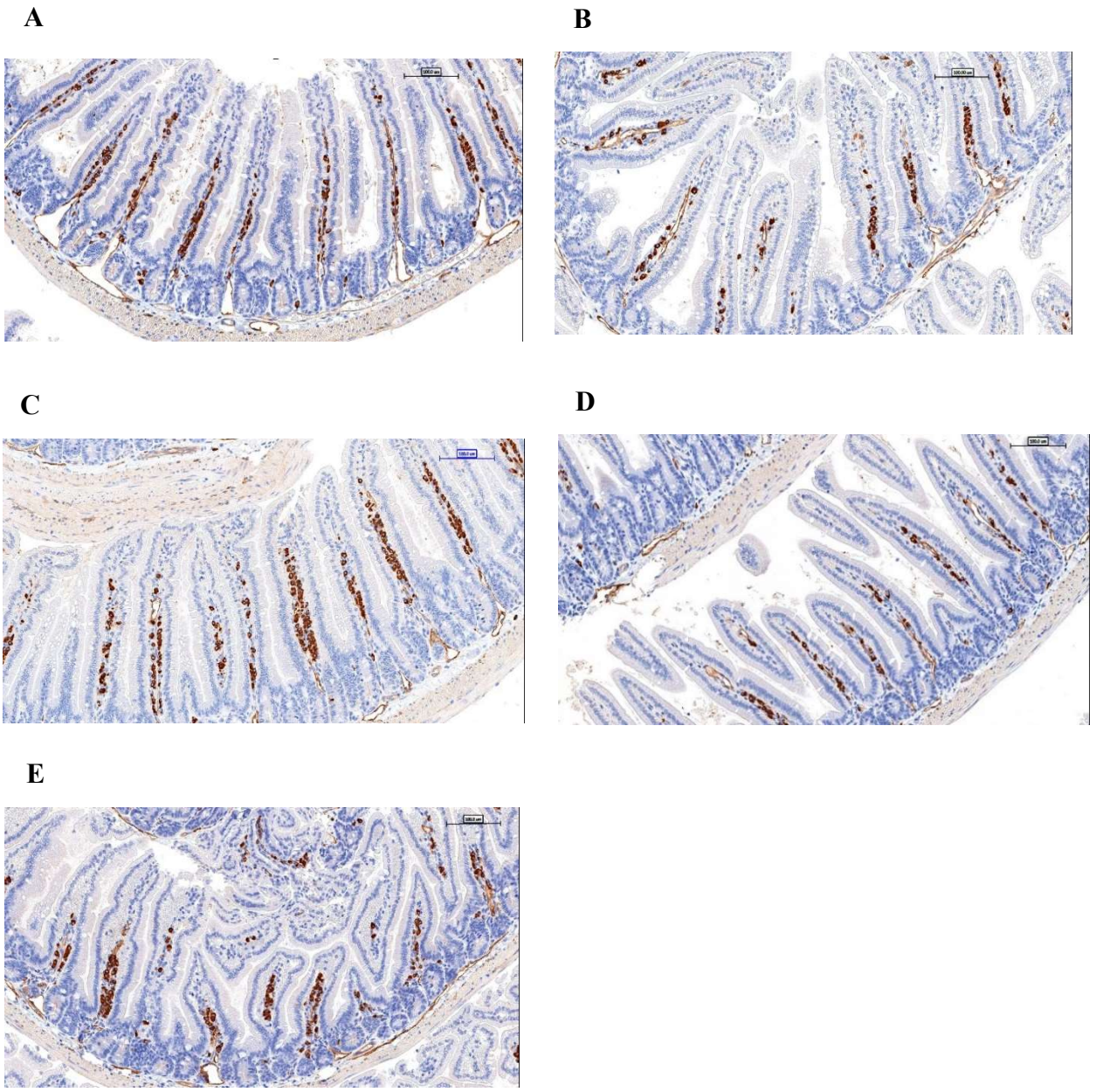

Figure 5.30 Immunohistochemistry sections of the mice **jejunum** from each experimental group **(Prevention Study)**. A: 10 % low-fat control group; B: 45 % high-fat control group; C: 15 % PGS group, D: 15 % SDS group; E:30 % SDS group.

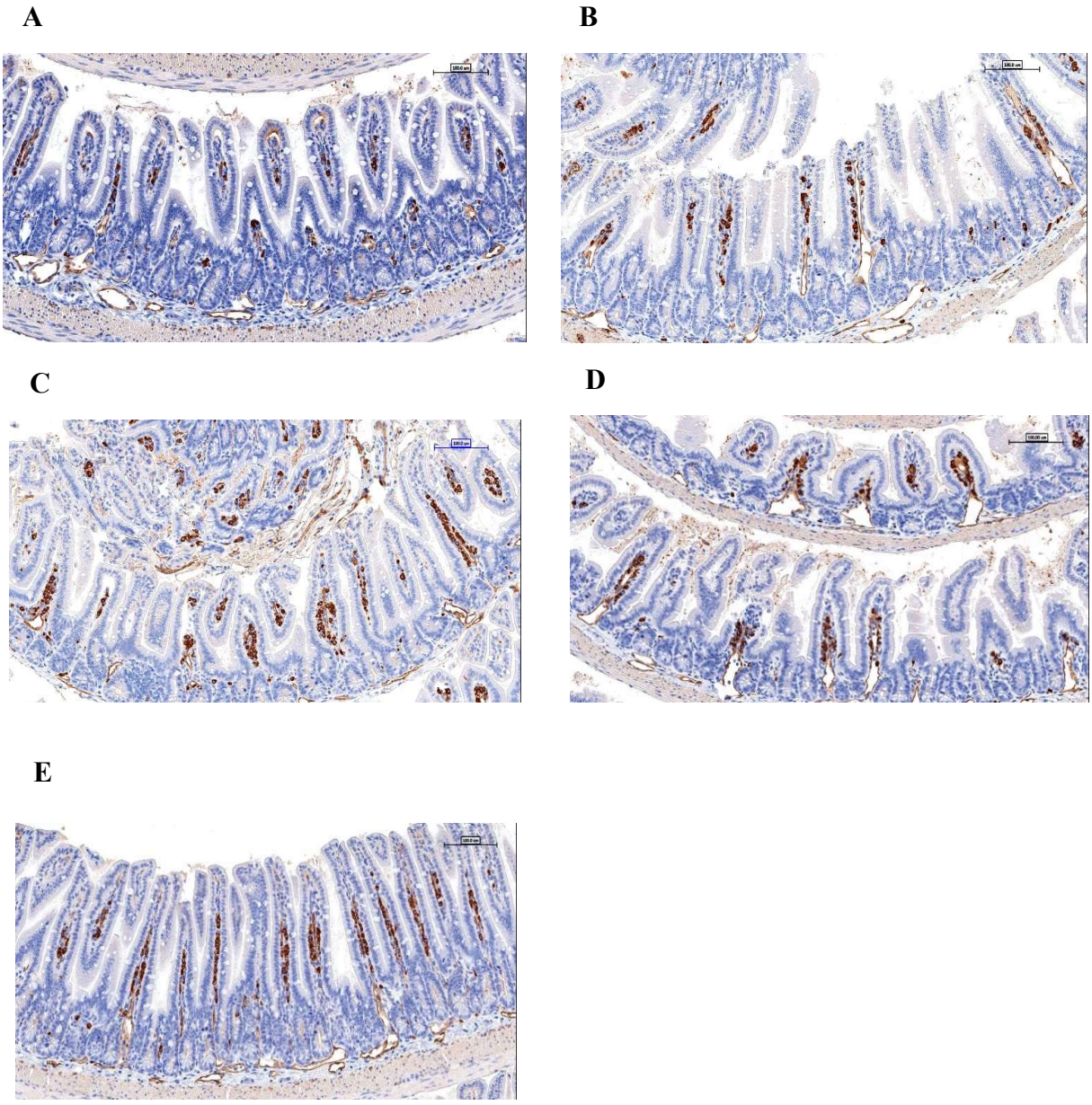

Figure 5.31 Immunohistochemistry sections of the mice **ileum** from each experimental group **(Prevention Study)**. A: 10 % low-fat control group; B: 45 % high-fat control group; C: 15 % PGS group, D: 15 % SDS group; E:30 % SDS group.

CHAPTER 6. CONCLUSIONS AND FUTURE DIRECTIONS

6.1 Conclusions

The hormonal assay study, represented in Chapter II of this dissertation, provides new insights into carbohydrate sensing in the gut and reports for the first-time unique stimulatory effects of α-amylase digestion products of starch (MOS, DP 2-5) in triggering enteroendocrine L-cells. MOS significantly affected L-cell sensitivity and anorexigenic gut hormone productivity, especially with the proglucagon gene products GLP-1 and OXM in mouse and human L-cell models, respectively. These effects on the proglucagon gene products were superior to known effects of one of the SCFA fiber fermentation products, propionate. On the other hand, MOS did not show strong enhancement of PYY release, whereas propionate showed the strongest stimulation. These findings suggest that L-cell models could possess selective stimulatory mechanisms where larger MOS are highly stimulating toward the release of the proglucagon gene products, GLP-1 (in case of STC-1 cells) and OXM (in case of NCI-H716 cells), whereas SCFA are highly stimulating toward PYY release (in case of STC-1 cells). In addition, we recommend that MOS exhibit their effects through the induction of exocytosis of GLP-1- or OXM-containing vesicles and not through a positive regulation of the proglucagon gene expression. These data suggest that MOS induce higher secretion, but not higher synthesis, of the proglucagon gene products (mainly GLP 1 and OXM). Finally, we observed a protective effect of MOS on the Caco-2 intestinal monolayer, where MOS somewhat improved barrier function as measured by TEER.

Transcriptome analysis, represented in Chapter III of this dissertation, revealed several putative target genes that may have a role in enteroendocrine L-cells in mediating the chemosensation and subsequent release of gut hormones, and barrier function, when exposed to the α-amylase degradation products of dietary starch (MOS, and here maltotriose in particular). In addition, this

is the first study that provides transcriptomic analysis of the STC-1 cell line model and the first study on transcriptomic analysis of cells treated with a carbohydrate that is exposed to them from the digestive process in the lumen of the small intestine. Several genes were significantly upregulated with maltotriose treatment that are associated with chemosensation, cytoplasmic vesicle secretion, and cellular tight junctions. These relate to maltotriose activation of L-cells, as shown in Chapter II, that result in GLP-1 and OXM secretion and improvement in barrier function of the Caco-2 cell monolayer.

Data from global proteomic profiling, represented in Chapter IV of this dissertation, supported the previously suggested hypothesis that MOS exhibit a stimulation effect on L-cells through the induction of secretion and not synthesis of the proglucagon gene. Cells treated with isomaltotriose and maltotetraose (representing other products of α-amylase degradation of starch) showed lower levels of the proglucagon protein products (GLP-1 and OXM peptides) compared to cells treated with glucose. This observation supports our suggestion that MOS stimulate the secretion of GLP-1 and OXM and not the synthesis of the proglucagon gene products. In this case, we would expect a significant reduction of the cellular concentrations of these peptides inside the cells, as a result of secreting the majority of peptides into the culture media. Also, such observation was not observed in the case of PYY indicating that MOS are not a selective stimulator for PYY. This was supported by the hormone secretion data showing MOS stimulated secretion on GLP-1 and OXM, but not PYY which was stimulated by propionate. Global proteomic profiling revealed several target proteins that are significantly regulated by different MOS. Maltose treatment showed induction in α-mannosidase levels consistent with increase in α-glucosidase levels, previously observed in the Caco-2 cell model after maltose treatment [1]. In addition, maltotriose boosted the

integrin-mediated pathway indicating a possible target for an adhesion receptor for extracellular matrix sensation. Moreover, the Wnt signaling pathway was enhanced in maltose-treated cells. Although the triggering of appetite-regulating gut hormones by carbohydrates was shown clearly in cell culture studies, *in vivo* data was needed to examine whether the data translates to the animal. Also, animal studies (in this case, mice) allows for inclusion of other important factors in studying the effect of slowly digestible carbohydrates on the intestinal epithelium such as adjacent enterocytes to the enteroendocrine L-cells, mucus layers, and immune cells, which together contribute to the overall mechanism of carbohydrate sensation and response. The animal studies presented in Chapter V provided data which support the beneficial effects of slowly digestible starch, which we consider the available food-based source for MOS delivery into the distal small intestine. Using an obesity intervention strategy of DIO mice and obesity prevention in lean healthy mice we were able to answer questions regarding the physiological effects of dietary complex carbohydrate that could be exhibited through sensation in the intestinal epithelium and downstream consequences related to satiety induction, appetite suppression, and weight management. Switching the diet from 60% high-fat diet to 10% fat-low diet initiated fast loss of 19.5% of body weight in the first week of the study. We reported that raw corn starch (RCS) was well-utilized by diet-induced obese (DIO) C57BL/6 mice, whereas the RCS group showed higher body weight, body fat percent, and daily food intake than the other low-fat diet treatment groups. The formulated 20% SDS microsphere and the pregelatinized starch (PGS) low-fat diet treatment groups showed faster weight loss rate and reduced body fat percent compared to other low-fat groups. Although used in the study of Hasek *et al*., 2018 as rapidly digestible starch [2], PGS diet showed an unexpected behavior in contrast to our hypothesis, though digestion data showed a fast digestion rate of the PGS diet. Because PGS in the Prevention Study did not less weight gain than

the 15% SDS microspheres, it was not clear why PGS did not cause less weight loss in the Invervention Study.

One of the interesting findings of the Intervention Study was the observation that L-cells were evenly and thoroughly distributed throughout the small intestine. This is contrary to a common view that these enteroendocrine cells are in greater abundance in the distal small intestine and colon. The Prevention Study showed that high-fat 15% SDS in the diet was successfully in preventing DIO in mice fed on 45% of calories from fat (high-fat diet). Importantly, mice fed on high-fat 15% SDS diet showed average body fat percent comparable or lower than mice fed on the low-fat diet (10%). In the Prevention Study, PGS behaved as previously indicated by Hasek *et al*., 2018, suggesting important effects of the diet context and mice background physiology in the behavior of the use of PGS. Similar to obese mice, L-cells were evenly and thoroughly distributed throughout the small intestine of the lean mice.

6.2 Future Directions

More studies are required to understand the mechanism through which L-cells react to MOS, as well as different effectors and regulators involved in these processes. First, more molecular-based assays should be used to further confirm that SGLT-1, GLUT2, and sweet taste receptor are not involved in the L-cell sensation process of MOS, and that there is another chemosensing entity on the apical surface of the cells. Functional assays could be the next step in the objective of identifying the putative receptor or sensor that is involved in this sensation process. Another important objective, would be understanding the proposed selective stimulation differentiating between the release of the proglucagon gene products versus the release of the PYY gene product. The suggestion that MOS stimulates the secretion and not the synthesis of GLP-1 and OXM

requires validation by a different type of experiment such as the investigation of the different regulators of the secretion process.

The use of dietary carbohydrates to achieve a gut physiological response that relates to satiety and food intake could be a new approach for food for health applications. It is conceivable that bioactive carbohydrates could be designed to confer physiological outcomes relevant to obesity reduction and type II diabetes treatment.

The transcriptomic analysis presented in Chapter III provides ground work for further investigations to elucidate cellular mechanisms related to the potential beneficial outcomes that could be revealed by longer, sustainable, and distal delivery of α-amylase starch degradation products and the downstream outcomes to manage food intake and control obesity. Maltotriose is usually the second most abundant product of α-amylase digestion of starch after maltose (around 30%) which makes the investigation and deep analysis of the 181 differentially expressed genes altered between glucose and maltotriose an important target for understanding the proposed sensing mechanism of MOS. For example, genes included in oxidative stress and Wnt signaling pathways are of interest as well as the eight tight junction proteins that are enhanced with maltotriose treatment. Moreover, functional assays measuring *de novo* glucose uptake, insulin signaling, and other metabolic parameters may provide insights into the consequences of MOS sensation by L-cells in other relevant signaling pathways.

The global proteomic profiling, presented in Chapter IV of this dissertation, is a foundation for more studies seeking the elucidation of the sensing mechanism in the intestinal lumen and the role of MOS in L-cell biology and metabolic disorders. Hormonal assays on GLP-1, OXM, and PYY is an important next step to validate the proteomic analysis data and to confirm the secretion hypothesis. In addition, isomaltotriose should be considered for future hormonal assay as the

proteomic data suggest that the stimulation effect of isomaltotriose may be superior to that of maltotriose. Although proteomic data of differential proteins in cells treated with α-limit dextrins did not reveal targets related to proglucagon proteins, we think that hormonal assays should be used to investigate the secretion triggering capabilities of α-limit dextrins on L-cells.

Regarding *in vivo* studies, more investigations are required to understand the current outcomes of the obesity intervention and prevention studies of this thesis. Blood plasma samples were collected every 2-weeks throughout the 12-week feeding period in both studies. Parameters related to glucose levels, incretin response (GLP-1 and glucose-dependent insulinotropic peptide (GIP)), OXM, PYY, CCK, ghrelin, insulin and leptin will be measured in all time points of the study to correlate the results with body weight and food intake outcomes. In addition, relative gene expression of gut-brain axis regulatory neuropeptides, especially the orexigenic peptides: neuropeptides Y (NPY), agouti-related peptide (AgRP), melanin-concentrating hormone (MCH) and the anorexigenic peptides: proopiomelanocortin (POMC), cocaine-and amphetamine-regulated transcript (CART), and corticotropin-releasing hormone (CRH) will be measured from the collected hypothalamus samples. Liver fat deposition patterns will be investigated by performing liver histological sections. Moreover, one of our research interests is to understand the possible influences of the different diets used in both the intervention and prevention studies in altering the microbial communities of mice fed on these diets. For this purpose, frozen freshly-collected feces of mice from both studies were collected and will be analyzed for gut microbial communities using 16S rRNA sequencing. Additionally, the behavior of PGS as a rapidly digestible starch source in different diet contexts and with different mice physiological backgrounds will be further investigated. Finally, deeper investigation to understand L-cell reactivity to experimental diets is recommended.

6.3 References

[1] M. Chegeni, M. Amiri, B. L. Nichols, H. Y. Naim, and B. R. Hamaker, “Dietary starch breakdown product sensing [1] M. Chegeni, M. Amiri, B. L. Nichols, H. Y. Naim, and B. R. Hamaker, ‘Dietary starch breakdown product sensing mobilizes and apically activates α-glucosidases in small intestinal enterocytes,’ FASEB J., vol. 32,” *FASEB J.*, vol. 32, no. 7, pp. 3903–3911, Jul. 2018.

[2] L. Y. Hasek *et al.*, “Dietary Slowly Digestible Starch Triggers the Gut-Brain Axis in Obese Rats with Accompanied Reduced Food Intake,” *Mol. Nutr. Food Res.*, vol. 62, no. 5, p. 1700117, Mar. 2018.